

BEAMFORMING SCHEMES FOR NEXT GENERATION WIRELESS
COMMUNICATION SYSTEMS

by

Yangwen Liang

M.A.Sc., The University of British Columbia, 2006

B.Eng., McMaster University, 2004

A THESIS SUBMITTED IN PARTIAL FULFILLMENT OF
THE REQUIREMENTS FOR THE DEGREE OF

DOCTOR OF PHILOSOPHY

in

The Faculty of Graduate Studies

(Electrical and Computer Engineering)

THE UNIVERSITY OF BRITISH COLUMBIA
(Vancouver)

October 2011

© Yangwen Liang, 2011

Abstract

Multiple-input multiple-output (MIMO) and relaying are two promising techniques which will be employed in next generation wireless communication systems. Transmit beamforming (BF) and receive combining are simple yet popular methods for performance enhancement for MIMO and/or relaying. This thesis investigates several BF schemes for MIMO and relaying systems.

For systems combining MIMO and orthogonal frequency division multiplexing (MIMO-OFDM) technology, we propose a novel time-domain BF (TD-BF) scheme which uses cyclic BF filters (C-BFFs). Both perfect and partial channel state information at the transmitter are considered. The C-BFFs are optimized for maximum average mutual information per sub-carrier and minimum average uncoded bit error rate. We show that TD-BF has a more favorable performance/feedback rate trade-off than previously proposed frequency-domain BF schemes.

Secondly, BF for one-way cooperative networks with multiple multi-antenna amplify-and-forward relays in frequency-nonselective channels is considered. The source BF vector and the amplify-and-forward BF matrices at the relays are optimized for maximization of the signal-to-interference-plus-noise ratio (SINR) at the destination under three different power constraints. We show the benefits of having multiple antennas at the source and/or multiple multi-antenna relays.

Subsequently, we investigate filter-and-forward BF (FF-BF) for one-way relay networks in frequency-selective channels. For the processing at the destination, we investi-

gate two different cases: a simple slicer, and a linear equalizer (LE) or a decision–feedback equalizer (DFE). For both cases, we optimize the FF–BF matrix filters at the relays for maximization of the SINR under a transmit power constraint, and for the first case we consider additionally optimization of the FF–BF matrix filters for minimization of the total transmit power under a quality of service constraint.

Leveraging results from one–way relaying, we also investigate FF–BF for two–way relay networks. For the simple slicer case, we show that the optimization problems are convex. For the LE/DFE case, we establish an upper and an achievable lower bound for an SINR max–min problem.

Preface

Chapters 2–5 are based on work conducted at UBC by myself under the supervision of Professor Robert Schober. In addition, the research in Chapters 2, 4, and 5 was performed in collaboration with Professor Wolfgang Gerstacker from the University of Erlangen–Nuremberg. For the work in Chapters 4 and 5, I also collaborated with Dr. Aissa Ikhlef, a postdoctoral fellow in Professor Robert Schober’s group at the University of British Columbia. For all chapters, I conducted the paper survey on related topics, formulated the problems, proposed problem solutions, and performed the analysis and the simulations of the considered communication systems. Professor Robert Schober, Professor Wolfgang Gerstacker, and Dr. Aissa Ikhlef provided valuable feedback on my manuscript drafts.

Three papers related to Chapter 2 have been published:

- Y. Liang, R. Schober, and W. Gerstacker, “Time–Domain Transmit Beamforming for MIMO–OFDM Systems with Finite Rate Feedback”. *IEEE Transactions on Communications*, 57(9): 2828–2838, Sept. 2009.
- Y. Liang, R. Schober, and W. Gerstacker, “Time–Domain Transmit Beamforming for MIMO–OFDM Systems”. In *Proceedings of the IEEE Global Telecommunications Conference (GLOBECOM)*, Washington DC, USA, Nov. 2007.
- Y. Liang, R. Schober, and W. Gerstacker, “Minimum BER Transmit Beamforming for MIMO–OFDM Systems with Finite Rate Feedback”. In *Proceedings of the IEEE International Conference on Communications (ICC)*, Beijing, China, May 2008.

Four papers related to Chapter 3 have been published:

- Y. Liang and R. Schober, “Cooperative Amplify-and-Forward Beamforming with Multiple Multi-Antenna Relays”. *IEEE Transactions on Communications*, 59(9): 2605–2615, Sept. 2011.
- Y. Liang and R. Schober, “Cooperative Amplify-and-Forward Beamforming for OFDM Systems with Multiple Relays”. In *Proceedings of the IEEE International Conference on Communications (ICC)*, Dresden, Germany, Jun. 2009.
- Y. Liang and R. Schober, “Cooperative Amplify-and-Forward Beamforming with Multi-Antenna Source and Relays” (**invited paper**). In *Proceedings of the Third International Workshop on Computational Advances in Multi-Sensor Adaptive Processing (CAMSAP)*, Aruba, Dec. 2009.
- Y. Liang and R. Schober, “Amplify-and-Forward Multi-Antenna Beamforming with Joint Source-Relay Power Constraint”. In *Proceedings of the IEEE Vehicular Technology Conference (VTC)*, Ottawa, Canada, Sept. 2010.

Three papers related to Chapter 4 have been published:

- Y. Liang, A. Ikhlef, W. Gerstacker, and R. Schober, “Cooperative Filter-and-Forward Beamforming with Equalization for Frequency-Selective Channels”. *IEEE Trans. on Wireless Commun.*, 10(1): 228–239, Jan. 2011.
- Y. Liang, A. Ikhlef, W. Gerstacker, and R. Schober, “Filter-and-Forward Beamforming with Multiple Multi-Antenna Relays for Frequency-Selective Channels” (**invited paper**). In *Proceedings of the International ICST Conference on Communications and Networking in China (Chinacom)*, Aug. 2010.

- Y. Liang, A. Ikhlef, W. Gerstacker, and R. Schober, “Cooperative Filter–and–Forward Beamforming with Equalization for Frequency–Selective Channels”. In *Proceedings of the IEEE Global Telecommunications Conference (GLOBECOM)*, Miami, USA, Dec. 2010.

Two papers related to Chapter 5 have been accepted/published, and one paper is under preparation for submission:

- Y. Liang, A. Ikhlef, W. Gerstacker, and R. Schober, “Two–Way Filter–and–Forward Beamforming for Frequency–Selective Channels”. Accepted by the *IEEE Transactions on Wireless Communications*, Oct. 2011.
- Y. Liang, A. Ikhlef, W. Gerstacker, and R. Schober, “Cooperative Two–Way Filter–and–Forward Beamforming for Frequency–Selective Channels”. In *Proceedings of the IEEE International Conference on Communications (ICC)*, Kyoto, Japan, Jan. 2011.
- Y. Liang, A. Ikhlef, W. Gerstacker, and R. Schober, “Two–Way Filter–and–Forward Beamforming with Multiple Multi–Antenna Relays for Frequency–Selective Channels”. In preparation, Oct. 2011.

Table of Contents

Abstract	ii
Preface	iv
Table of Contents	vii
List of Tables	xii
List of Figures	xiv
List of Abbreviations	xxiii
Notation	xxvii
Acknowledgments	xxix
Dedication	xxxii
1 Introduction	1
1.1 Beamforming for MIMO Systems	1
1.2 Cooperative Relay Network	4
1.3 Two-Way Cooperative Relay Network	7
1.4 Contributions of the Thesis	9
1.5 Organization of the Thesis	10

2	Time-Domain Transmit Beamforming for MIMO-OFDM Systems . . .	14
2.1	Introduction	14
2.2	System Model	16
2.2.1	Transmitter Processing for TD-BF	16
2.2.2	MIMO Channel	18
2.2.3	Receiver Processing	18
2.2.4	Feedback Channel	20
2.3	Maximum AMI Criterion	20
2.3.1	Formulation of the Optimization Problem	20
2.3.2	Solution of the Optimization Problem for $L_g = N_c$	21
2.3.3	Solution of the Optimization Problem for $L_g < N_c$	23
2.4	Minimum BER Criterion	26
2.4.1	Formulation of the Optimization Problems	27
2.4.2	Solution of the Optimization Problems for $L_g = N_c$	28
2.4.3	Solution of the Optimization Problems for $L_g < N_c$	29
2.5	Finite-Rate Feedback and Comparison	32
2.5.1	Finite-Rate Feedback Case	32
2.5.2	Comparison with FD-BF	33
2.6	Simulation Results	35
2.6.1	Simulation Parameters	36
2.6.2	Maximum AMI Criterion	36
2.6.3	Minimum BER Criterion	39
2.6.4	Comparison of Maximum AMI and Minimum BER Criteria	44
2.7	Conclusions	45

3	Cooperative AF–BF with Multiple Multi–Antenna Relays	46
3.1	Introduction	46
3.2	System Model and Optimization Problem	49
3.2.1	System Model	50
3.2.2	Formulation of the Optimization Problem	51
3.3	Optimal AF–BF Matrices	53
3.3.1	AF–BF with Individual Power Constraints for Relays	53
3.3.2	AF–BF with Joint Power Constraint for Relays	57
3.3.3	AF–BF with Joint Power Constraint for Source and Relays	58
3.3.4	Comparison of the Solutions for the Different Constraints	59
3.4	Optimal BF Vector at the Source	60
3.4.1	AF–BF with Individual Power Constraints for Relays	60
3.4.2	AF–BF with Joint Power Constraint for Relays	62
3.4.3	AF–BF with Joint Power Constraint for Source and Relays	65
3.4.4	Comparison of the Solutions and CSI Feedback Requirements	67
3.5	Simulation Results	69
3.5.1	Comparison of Source BF Vector Optimization Methods	69
3.5.2	Impact of Network Parameters on Performance	74
3.5.3	Impact of Power Constraints on Performance	76
3.6	Conclusions	80
 4	 Cooperative FF–BF with Multiple Multi–Antenna Relays	 81
4.1	Introduction	81
4.2	System Model	84
4.2.1	FF–BF at Relays	84
4.2.2	Processing at Destination	86

Table of Contents

4.2.3	Feedback Channel	87
4.3	FIR FF–BF without Equalization	87
4.3.1	SINR Maximization Under Relay Power Constraint	90
4.3.2	Relay Power Minimization Under SINR Constraint	91
4.3.3	SINR Maximization Under Source–Relay Power Constraint	92
4.3.4	Source–Relay Power Minimization Under SINR Constraint	93
4.4	FF–BF with Equalization	94
4.4.1	Optimal IIR FF–BF with Equalization	94
4.4.2	Optimal FIR FF–BF with Equalization	104
4.5	Simulation Results	109
4.5.1	FF–BF without Equalization	110
4.5.2	FF–BF with Equalization	115
4.6	Conclusions	123
5	Two–Way FF–BF with Multiple Single Antenna Relays	125
5.1	Introduction	125
5.2	System Model	126
5.2.1	FF–BF at Relays	128
5.2.2	Transceiver Processing	129
5.3	FIR FF–BF without Equalization	130
5.3.1	Max–min Criterion Under Relay Power Constraint	133
5.3.2	Relay Power Minimization Under SINR Constraints	135
5.4	FF–BF with Equalization	136
5.4.1	Optimal IIR FF–BF with Equalization	137
5.4.2	FIR FF–BF Filter Optimization	143
5.5	Simulations	145

Table of Contents

5.5.1	Relay Power Minimization for FF–BF without Equalization	145
5.5.2	Max–min SINR Optimization for FF–BF with and without Equal- ization	148
5.5.3	Max–min SINR vs. Minimum Sum MSE Optimization for FF–BF with ZF–LE	150
5.5.4	Impact of Number of Relays N_R	151
5.5.5	BER Performance for Fading Channels	153
5.6	Conclusions	155
6	Summary of Thesis and Future Research Topics	157
6.1	Summary of Results	157
6.2	Future Work	159
6.2.1	Two–way Relaying with Multiple Multi–antenna Relays	160
6.2.2	Cooperative Communications for Multi–user Systems	161
6.2.3	Synchronization for Cooperative Communications	161
6.2.4	Cooperative Communications for Cognitive Radio	162
	Bibliography	163

List of Tables

2.1	Calculation of the optimum C-BFFs \mathbf{g} for the maximum AMI and the minimum average BER criterion using a GA, respectively. Termination constant ϵ has a small value (e.g. $\epsilon = 10^{-4}$). i denotes the iteration and δ_i is the adaptation step size necessary for the GA.	26
2.2	Feedback Requirements for TD-BF, ideal FD-BF, and FD-BF with modified spherical (MS), Grassmannian (GS), and geodesic (GD) interpolation.	34
3.1	Gradient algorithm for calculation of source BF vector $\hat{\mathbf{g}}$ for individual and joint relay power constraints. The definitions of $\hat{\mathbf{g}}$ and the gradient grad_k depend on the power constraint, cf. Section 3.4. Termination constant ϵ has a small value (e.g. $\epsilon = 10^{-5}$). k denotes the iteration index and a_k is the adaptation step size chosen through a backtracking line search [1].	62
3.2	Gradient algorithm for calculation of source BF vector \mathbf{g} and power allocation for joint source-relay power constraint. Termination constant ϵ has a small value (e.g. $\epsilon = 10^{-5}$). k denotes the iteration index and a_k is the adaptation step size chosen through a backtracking line search [1].	67

4.1	Numerical algorithm for finding the optimum power allocation $p(f)$ for IIR FF–BF filters at the relays. $X = \text{DFE}$, $X = \text{LE}$, and $X = \text{MF}$ for DFE, LE, and an MF receiver, respectively. Termination constant ϵ and frequency spacing Δf have small values (e.g. $\epsilon = 10^{-5}$, $\Delta f = 10^{-5}$). i denotes the iteration index.	104
4.2	Gradient algorithm (GA) for calculation of near-optimal FIR FF–BF filter vector \mathbf{a} . Termination constant ϵ has a small value (e.g. $\epsilon = 10^{-5}$). i denotes the iteration index and δ_i is the adaptation step size chosen through a backtracking line search [1].	108

List of Figures

1.1	Different relaying protocols. (a) decode-and-forward (DF) relaying protocol, and (b) amplify-and-forward (AF) protocol. x_s : signal broadcasted from the source, x_r : signal transmitted from the relay, \hat{x}_s : regenerated signal after decoding, TS_x : time slot x , and a : scaling factor.	5
1.2	Different two-way relaying protocols. (a) Bidirectional one-way relaying protocol, (b) Time Division Broadcast (TDBC) protocol, and (c) Multiple Access Broadcast (MABC) protocol. s_1 : signal transmitted from transceiver 1 (TC1), s_2 : signal transmitted from transceiver 2 (TC2), and $f(s_1, s_2)$: processed version of the received signals.	8
2.1	MIMO-OFDM system with TD-BF. P/S: Parallel-to-serial conversion. S/P: Serial-to-parallel conversion. CE: Channel estimation.	17
2.2	AMI of TD-BF (AMI criterion), MS-FD-BF [2], and GD-FD-BF [3] with perfect CSI. $N_T = 2$, $N_R = 1$, $N_c = 512$, and IEEE 802.11n Channel Model B. For comparison the AMIs for ideal FD-BF and single-input single-output (SISO) transmission ($N_T = 1$, $N_R = 1$) are also shown.	37
2.3	AMI of TD-BF (AMI criterion) vs. number of feedback bits B per channel update. $N_T = 2$, $N_R = 1$, $N_c = 512$, $E_s/N_0 = 10$ dB, and IEEE 802.11n Channel Model B. For comparison the AMIs for GD-FD-BF with codebooks from [4] are also shown.	38

2.4	BER of coded MIMO–OFDM system with TD–BF (AMI criterion), MS–FD–BF [2], and GD–FD–BF [3]. Perfect CSI and finite–rate feedback, $N_T = 2$, $N_R = 1$, $N_c = 512$, $R_c = 1/2$, and IEEE 802.11n Channel Model B. For comparison the BERs for ideal FD–BF and SISO transmission ($N_T = 1$, $N_R = 1$) are also shown.	40
2.5	Average BER of uncoded MIMO–OFDM system with TD–BF. Minimum average BER criterion (solid lines) and max–min criterion (dashed lines), perfect CSI, $N_T = 2$, $N_R = 1$, $N_c = 512$, and IEEE 802.11n Channel Model B. For comparison the BERs for ideal FD–BF and SISO transmission ($N_T = 1$, $N_R = 1$) are also shown.	41
2.6	Average BER of uncoded MIMO–OFDM system with TD–BF (average BER criterion) vs. number of feedback bits B per channel update. GA was used for C–BFF optimization. $N_T = 2$, $N_R = 1$, $N_c = 512$, $E_b/N_0 = 10$ dB, and IEEE 802.11n Channel Model B.	42
2.7	Average BER of uncoded and coded MIMO–OFDM system with TD–BF (average BER criterion). GA was used for C–BFF optimization and $L_g = 2$ is valid for all curves shown. Perfect CSI (bold lines) and finite–rate feedback channel, $N_T = 2$, $N_R = 1$, $N_c = 512$, and IEEE 802.11n Channel Model B.	43
2.8	Average BER of uncoded and coded MIMO–OFDM system employing TD–BF with perfect CSI. Average BER criterion (dashed lines) and AMI criterion (solid lines), $N_T = 3$, $N_R = 1$, $N_c = 512$, and IEEE 802.11n Channel Model B.	44

3.1	Cooperative network with one multi-antenna source, multiple multi-antenna relays, and one single-antenna destination. g_i , $1 \leq i \leq N_T$, denotes the i th element of source BF vector \mathbf{g} . $n_{i,\mu}$, $1 \leq \mu \leq M_i$, is the μ th element of noise vector $\mathbf{n}_{1,i}$ at relay i , $1 \leq i \leq N_R$	49
3.2	Locations of source, destination, and relays in simulation.	70
3.3	CDF of the instantaneous SINR for AF-BF with <i>joint relay power constraint (PC)</i> and one relay located at (a) and (e), respectively. Results for different optimization methods for the source BF vector for multiple relays are shown and compared with relay selection. A path-loss exponent of 3, $N_T = 2$, and $d = 1$ are assumed.	71
3.4	CDF of the instantaneous SINR for AF-BF with <i>joint source-relay power constraint (PC)</i> and N_R relays. Results for different optimization methods for the source BF vector for multiple relays are shown and compared with relay selection. A path-loss exponent of 3, $N_T = 2$, and $d = 1$ are assumed. The relays are located at (a) and (e) for $N_R = 2$, (a)-(e) for $N_R = 5$, and (a)-(e) with 2 relays at each location for $N_R = 10$	72
3.5	CDF of the instantaneous SINR for AF-BF with <i>individual relay power constraints (PCs)</i> and $N_R = 5$ single-antenna relays at locations (a)-(e). Results for different optimization methods for the source BF vector for multiple relays are shown and compared with relay selection. A path-loss exponent of 3 and $d = 1$ are assumed.	73

3.6	Average SINR vs. distance d for AF–BF with <i>joint relay power constraint (PC)</i> and different numbers of antennas N_T at the source. A path–loss exponent of 3 is assumed. For comparison the SNR without relaying for a source transmit power of $P = 2$ and the SINR for relay selection are also shown.	75
3.7	Average SINR vs. distance d for AF–BF with <i>individual relay power constraints (PCs)</i> and different numbers of antennas N_T at the source. A path–loss exponent of 3 is assumed. For comparison the SNR without relaying for a source transmit power of $P = 2$ and the SINR for relay selection are also shown.	76
3.8	Average SINR vs. distance d for AF–BF with <i>joint source–relay power constraint (PC)</i> and different numbers of relays and different numbers of relay antennas. A path–loss exponent of 3 is assumed. For comparison the SNR without relaying for a source transmit power of $P = 2$ and the SINR for relay selection are also shown.	77
3.9	Average mutual information (AMI) in (bits/s/Hz) vs. distance d for two different network setups and different power constraints (PCs). The relays are in locations (a) and (e) for $N_R = 2$ and (a)–(e) for $N_R = 5$. The proposed gradient methods are used for computation of the source BF vector \mathbf{g} . A path–loss exponent of 4 is assumed. For comparison the average mutual information without relaying for a source transmit power of $P = 2$ and the average mutual information for relay selection are also shown.	78

3.10	Average BER vs. σ_d^2/σ_n^2 for two different network setups and different power constraints. The relays are in locations (a) and (e) for $N_R = 2$ and (a)–(e) for $N_R = 5$. The proposed gradient methods are used for computation of the source BF vector \mathbf{g} . A path-loss exponent of 3 and $d = 1$ are assumed. AF–BF: 16–QAM. Direct transmission: QPSK, source transmit power $P = 2$.	79
4.1	Cooperative network with one single-antenna source, multiple multi-antenna relay nodes, and one single-antenna destination. EQ is the equalizer at the destination. $\hat{s}[k]$ are estimated symbols after the equalizer or slicer.	85
4.2	Locations of source, destination, and relays in simulation.	110
4.3	Average SINR vs. decision delay k_0 for FIR FF–BF without equalization (EQ) at the destination. The FF–BF filters were optimized for SINR maximization under <i>joint relay power constraint</i> . Exponentially decaying channel power delay profile with $L_g = L_h = 5$, $d = 1$, $N_R = 5$, $M_z = 1$, $z \in \{1, 2, \dots, 5\}$ and $\gamma_g = \gamma_h = 10$ dB.	111
4.4	Average SINR vs. distance d for FIR FF–BF without equalization (EQ) at the destination. The FF–BF matrix filters were optimized for a <i>joint relay power constraint</i> . Exponentially decaying channel power delay profile with $\sigma_t = 2$ and $L_g = L_h = 5$, and $\gamma_g = \gamma_h = 10$ dB. Results for direct transmission with transmit power $P = 2$ at the source are also included. . .	112
4.5	Average SINR vs. distance d for FIR FF–BF without equalization (EQ) at the destination. The FF–BF matrix filters were optimized for a <i>joint source-relay power constraint</i> . Exponentially decaying channel power delay profile with $\sigma_t = 2$ and $L_g = L_h = 5$, and $\gamma_g = \gamma_h = 10$ dB. Results for direct transmission with transmit power $P = 2$ at the source are also included. . .	113

4.6	Total average source and relay transmit power vs. required SINR γ for FIR FF–BF without equalization (EQ) at the destination for <i>relay power minimization</i> and <i>joint source–relay power minimization</i> . Exponentially decaying power delay profile with $\sigma_t = 2$ and $L_g = L_h = 5$, $d = 1$, and $\gamma_g = \gamma_h = 10$ dB.	114
4.7	Feasibility probability vs. required SINR γ for FIR FF–BF without equalization (EQ) at the destination for <i>relay power minimization</i> and <i>joint source–relay power minimization</i> . Exponentially decaying power delay profile with $\sigma_t = 2$ and $L_g = L_h = 5$, $d = 1$, and $\gamma_g = \gamma_h = 10$ dB.	115
4.8	SINR vs. iteration number i of GA given in Table 4.2 for FIR FF–BF with MMSE–DFE at the destination. $\gamma_g = \gamma_h = 10$ dB, $L_g = L_h = 5$, and $\bar{g}_{1,z}[k] = \bar{h}_{1,z}[k] = 1/\sqrt{5}$, $0 \leq k < 5$, $1 \leq z \leq 5$. $N_R = 5$ relays with $M_z = 1$, $1 \leq z \leq N_R$, at locations (a)–(e), respectively. For comparison the SINR for IIR FF–BF is also shown.	116
4.9	Frequency responses of IIR FF–BF filters for $\gamma_g = \gamma_h = 10$ dB, $N_R = 1$ single antenna relay, $L_g = L_h = 2$, and $\bar{g}_{1,1}[k] = \bar{h}_{1,1}[k] = 1/\sqrt{2}$, $k \in \{0, 1\}$. For comparison the frequency response of the test channel is also shown.	118
4.10	Frequency responses of IIR FF–BF filter and FIR FF–BF filters of various lengths for MMSE–DFE at the receiver. All channel parameters are identical to those in Fig. 4.9.	119

4.11	Average SINR vs. distance d for FF–BF with MMSE–LE, MMSE–DFE, and an MF receiver at the destination. $N_R = 2$ relays with $M_1 = 2$ and $M_2 = 3$, exponentially decaying power delay profile with $\sigma_t = 2$ and $L_g = L_h = 5$, and $\gamma_g = \gamma_h = 10$ dB. For comparison the SINRs of FF–BF without (w/o) equalization (EQ) at the destination and without relaying are also shown, respectively.	120
4.12	Average SINR vs. decay parameter σ_t for FF–BF with MMSE–LE, MMSE–DFE, and an MF receiver at the destination. $N_R = 2$ relays with $M_1 = 2$ and $M_2 = 3$, distance $d = 1$, exponentially decaying power delay profile with $L_g = L_h = 5$, and $\gamma_g = \gamma_h = 10$ dB. For comparison the SINRs of FF–BF without (w/o) equalization (EQ) at the destination and without relaying are also shown, respectively.	121
4.13	Average BER of BPSK vs. transmit SNR γ for FF–BF with MMSE–LE, MMSE–DFE, and an MF receiver at the destination. Exponentially decaying power delay profile with $\sigma_t = 2$ and $L_g = L_h = 5$. For comparison the BER of FF–BF without (w/o) equalization (EQ) at the destination is also shown.	122
5.1	Cooperative two–way network with two transceiver nodes and N_R relay nodes. EQ is the equalizer at the transceivers. $\hat{s}_1[k]$ and $\hat{s}_2[k]$ are estimated received symbols at TC2 and TC1, respectively.	127
5.2	Locations of TC1, TC2, and the relays in the simulations.	146

5.3	Total average relay transmit power vs. required SINRs γ_1 and γ_2 for FIR FF–BF without equalization at the transceivers. The FF–BF filters were optimized for minimization of the relay transmit power. Exponentially decaying power delay profile with $\sigma_t = 2$, $L_g = L_h = 5$, $d = 1$, $N_R = 5$, and $\gamma_g = \gamma_h = 10$ dB.	146
5.4	Feasibility probability vs. required SINRs γ_1 and γ_2 for FIR FF–BF without equalization at the transceivers. The FF–BF filters were optimized for minimization of the relay transmit power. Exponentially decaying power delay profile with $\sigma_t = 2$, $L_g = L_h = 5$, $d = 1$, $N_R = 5$, and $\gamma_g = \gamma_h = 10$ dB. . .	147
5.5	Average worst–case SINR at the transceivers vs. distance d for FF–BF with/without equalization at the transceivers. The FF–BF filters were optimized for maximization of the minimum transceiver SINR. Exponentially decaying channel power delay profile with $\sigma_t = 2$, $L_g = L_h = 5$, $d = 1$, $N_R = 5$, and $\gamma_g = \gamma_h = 10$ dB.	148
5.6	Average SINR at transceivers vs. distance d for FF–BF with/without equalization (EQ) at the transceivers. The FF–BF filters were optimized for maximization of the minimum transceiver SINR. Exponentially decaying channel power delay profile with $\sigma_t = 2$, $L_g = L_h = 5$, $d = 1$, $N_R = 5$, and $\gamma_g = \gamma_h = 10$ dB.	149
5.7	Average SINR at transceivers vs. distance d for FF–BF with ZF–LE at the transceivers. Exponentially decaying channel power delay profile with $\sigma_t = 2$, $L_g = L_h = 5$, $d = 1$, $N_R = 5$, and $\gamma_g = \gamma_h = 10$ dB.	151

5.8	Average SINR vs. number of relays N_R for FF–BF with MMSE–DFE, ZF–LE, MF, and slicer (no equalizer) receivers at the transceivers. Exponentially decaying power delay profile with $\sigma_t = 2$, $L_g = L_h = 5$, $d = 1$, and $\gamma_g = \gamma_h = 10$ dB.	152
5.9	Average BER of BPSK vs. transmit SINR γ for FF–BF with MMSE–DFE, MF, and slicer receiver at the transceivers. BERs for FIR FF–BF with EQ and IIR FF–BF with MMSE–DFE were generated using the FF–BF filters from the achievable lower bound of the max–min criterion. Exponentially decaying power delay profile with $\sigma_t = 2$, $L_g = L_h = 5$, $N_R = 5$, and $d = 1$	154
5.10	Average BER of BPSK vs. transmit SINR γ for FF–BF with ZF–LE and MF receiver at the transceivers. For the min–max criterion, BERs were generated using the FF–BF filters from the achievable lower bound. Exponentially decaying power delay profile with $\sigma_t = 2$, $L_g = L_h = 5$, $N_R = 5$, and $d = 1$	155

List of Abbreviations

3GPP	3rd Generation Partnership Project
4G	The Fourth Generation
AF	Amplify-and-Forward
AMI	Average Mutual Information
AWGN	Additive White Gaussian Noise
BER	Bit Error Rate
BF	Beamforming
BICM	Bit Interleaved Coded Modulation
BPSK	Binary Phase Shift Keying
C-BFF	Cyclic Beamforming Filter
CC	Convolutional Code
CDF	Cumulative Distribution Function
CIR	Channel Impulse Response
CP	Cyclic Prefix
CSI	Channel State Information
CSIT	CSI at the Transmitter
DF	Decode-and-Forward
DFE	Decision-Feedback Equalizer
DFT	Discrete Fourier Transform
DSTC	Distributed Space-Time Coding

List of Abbreviations

EDGE	Enhanced Data Rates for GSM Evolution
EQ	Equalization
FCC	Federal Communications Commission
FEC	Forward Error Correction
FF-BF	Filter-and-Forward Beamforming
FD	Frequency Domain
FFT	Fast Fourier Transform
FIR	Finite Impulse Response
GA	Gradient Algorithm
GD	Geodesic
GS	Grassmannian
GSM	Global System for Mobile Communications
GVQ	Global Vector Quantization
IDFT	Inverse Discrete Fourier Transform
IEEE	Institute of Electrical and Electronic Engineers
IFFT	Inverse Fast Fourier Transform
i.i.d.	Independent and Identically Distributed
IIR	Infinite Impulse Response
ISI	Inter-Symbol Interference
LE	Linear Equalizer
LTE	(3GPP) Long Term Evolution
MABC	Multiple Access Broadcast
MF	Matched Filter
MIMO	Multiple-Input Multiple-Output
MLSE	Maximum Likelihood Sequence Estimation

List of Abbreviations

MMSE	Minimum Mean Square Error
MS	Modified Spherical
MSE	Mean Square Error
NP-hard	Non-Deterministic Polynomial-Time Hard
OFDM	Orthogonal Frequency Division Multiplexing
OFDMA	Orthogonal Frequency Division Multiple Access
PC	Power Constraint
QAM	Quadrature Amplitude Modulation
QOQC	Quadratic Objective Quadratic Constraint
QoS	Quality of Service
QPSK	Quaternary Phase Shift Keying
SDP	Semidefinite Programming
SINR	Signal-to-Interference-plus-Noise Ratio
SISO	Single-Input Single-Output
SIMO	Single-Input Multiple-Output
SOCP	Second-Order Cone Programming
SM	Spatial Multiplexing
SNR	Signal-to-Noise Ratio
STBC	Space-Time Block Code
STTC	Space-Time Trellis Code
TC	Transceiver
TD	Time Domain
TDBC	Time Division Broadcast
WiMAX	Worldwide Interoperability for Microwave Access
WLAN	Wireless Local Area Network

List of Abbreviations

ZF Zero Forcing

Notation

$(\cdot)^T$	Transpose
$(\cdot)^H$	Hermitian transpose
$(\cdot)^*$	Complex conjugate
$\mathbf{0}_X$	All-zero column vector of length X
\mathbf{I}_X	$X \times X$ identity matrix
$[\mathbf{X}]_{ij}$	Element of matrix \mathbf{X} in row i and column j
$\det(\cdot)$	Matrix determinant
$\text{diag}\{x_1, \dots, x_N\}$	Diagonal matrix with x_1, \dots, x_N on the main diagonal
$\text{diag}\{\mathbf{X}_1, \dots, \mathbf{X}_N\}$	Block diagonal matrix with $\mathbf{X}_1, \dots, \mathbf{X}_N$ on the main diagonal
$\Re\{\cdot\}$	Real part of a complex number
$\Im\{\cdot\}$	Imaginary part of a complex number
$ \cdot $	Absolute value of a complex number
$\ \cdot\ _2$	Euclidean norm
$\ \cdot\ _F$	Frobenius norm
$\lambda_{\max}(\cdot)$	Maximum eigenvalue of a matrix
$\lambda_i(\cdot)$	i th eigenvector of a matrix
$\text{vec}(\cdot)$	Vectorization of a matrix (stacking the columns of \cdot on top of each other)
$\text{trace}(\cdot)$	Trace of a matrix
x^+	$\max(0, x)$
\otimes	Kronecker product

Notation

\oplus	Kronecker sum
$*$	Discrete-time convolution
$\mathcal{E}\{\cdot\}$	Statistical expectation
$\mathcal{F}\{x[k]\}$	Fourier transform of discrete-time signal $x[k]$, i.e. $\sum_{k=-\infty}^{\infty} x[k]e^{-j2\pi fk}$
$Q(\cdot)$	Gaussian Q-function [5]
$\mathbf{A} \succeq \mathbf{B}$	$\mathbf{A} - \mathbf{B}$ is positive semidefinite

Acknowledgments

It is a long journey for each Ph.D. degree. I am lucky that I am not walking all the way alone by myself. Without support from a large number of people, this work would have not been done.

First, I would like to express my deep and sincere gratitude to my advisor, Professor Robert Schober, for his support and invaluable advice during my Ph.D. study. As a profound and distinguished professor, Dr. Schober sets an example of being a great researcher. The knowledge and training I got from him benefit me then, now and forever. I am much indebted for his patience and encouragement over the years. Without his support and guidance, this thesis would not be possible. I also would like to express my gratitude to Professor Wolfgang Gerstaecker and Dr. Aissa Ikhlef for many stimulating and helpful discussions on the work we have done together.

Also, I greatly thank the members of my doctoral committee, Dr. Vijay Bhargava, Dr. Vikram Krishnamurthy, Dr. Lutz Lampe, Dr. Victor Leung, and Dr. Vincent Wong for the time and effort in evaluating my work and providing valuable feedback and suggestions. Many thanks go to the members of the Communications Theory Group for all the fruitful discussions, group meetings, and feedback at many points.

Last but not least, I owe my deepest gratitude to my lovely wife, Yifan Tian, for her love, understanding, patience and encouragement. I thank my parents, Guosong Liang and Qinjun Li, from the bottom of my heart for their love and inspiration from thousands of miles away. Special thanks are owed to my parents-in-law, Wendong Tian and Zhichun

Acknowledgments

Dong, for their understanding and encouragement.

Financial support from the Natural Sciences and Engineering Research Council of Canada (NSERC), the University of British Columbia, the Killam Trusts, IEEE Canada, the IEEE Communications Society, and the China Scholarship Council (CSC) is gratefully acknowledged.

Dedication

To My Family

Chapter 1

Introduction

Higher data rates, more reliable communication, and higher number of users are the main driving forces for physical layer advancement for next generation wireless communication systems. Multiple-input-multiple-output (MIMO) schemes, orthogonal frequency division multiplexing (OFDM), and relaying schemes are some of the enabling techniques to achieve all the aforementioned objectives. Hence, we will provide a brief overview of some related techniques in this chapter.

This chapter is organized as follows. In Section 1.1, we briefly review beamforming (BF) for MIMO wireless systems. In Section 1.2, we discuss one-way relaying protocols, and in Section 1.3, we introduce two-way relaying protocols. We briefly outline the contributions made in this thesis in Section 1.4, and the thesis organization is given in Section 1.5.

1.1 Beamforming for MIMO Systems

In the past two decades, the application of multiple antennas at both the transmitter and the receiver has attracted considerable interest within both academia and industry as a means of providing significant performance gains over conventional single antenna based solutions [6]–[8]. These MIMO systems enable a spatial diversity gain, a spatial multiplexing gain, or both, leading to high performance next generation wireless communication systems.

Spatial diversity is achieved by sending the data signal over multiple independent fading

paths in space (different transmit antennas) and by utilizing appropriate combining techniques at the receiver. Several schemes have been proposed to exploit the spatial diversity gain. For example, space–time block codes (STBC) [9, 10] and space–time trellis codes (STTC) [11] are well–known transmit diversity techniques, which lead to improved link reliability. Spatial multiplexing techniques yield a system capacity increase by transmitting independent and separately encoded data streams from the multiple transmit antennas in parallel over the spatial channels. The maximum number of data streams the system can support is limited by the minimum of the number of transmit and the number of receive antennas. Several schemes have been proposed to exploit the spatial multiplexing gain. Examples include the vertical Bell Labs layered space–time (V–BLAST) [12] and the diagonal Bell Labs layered space–time (D–BLAST) [13] schemes.

The aforementioned techniques to achieve a spatial diversity gain or a spatial multiplexing gain are based on the so–called open–loop configuration, where only the receiver has knowledge of the communication channel. Recent research shows that system performance can be further enhanced by so–called closed–loop MIMO techniques, where the transmitter also knows the channel. By exploiting channel state information (CSI) at the transmitter, transmit BF and receiver combining can be used to exploit the spatial diversity gain offered by MIMO systems to mitigate the effects of fading in wireless communications, cf. e.g. [14] and reference therein. In practical systems, ideal BF is not possible since the amount of information that can be fed back from the receiver to the transmitter is limited. Therefore, BF for quantized CSI and finite–rate feedback channels has recently received considerable attention [15]–[19].

To avoid complex equalization at the receiver, MIMO is often combined with OFDM which converts broadband frequency–selective channels into a number of parallel narrow–band frequency–flat channels [20]. In such a MIMO–OFDM system, spatial multiplexing,

space–time coding, and other signal processing algorithms are usually employed in order to approach the MIMO channel capacity. MIMO–OFDM has been adopted in various recent standards such as IEEE 802.11 (WLAN) [21], IEEE 802.16 (Worldwide Interoperability for Microwave Access (WiMAX) standard) [22], and Long Term Evolution (LTE) [23]. Transmit BF techniques proposed for narrowband channels can be easily extended to broadband MIMO–OFDM systems by applying independent BF in each sub–carrier [24, 25]. However, the obvious drawback of this approach is that the amount of CSI data that has to be fed back from the receiver to the transmitter is prohibitively large for practical OFDM systems with moderate–to–large number of sub–carriers N_c (e.g. $N_c \geq 64$). Since the fading gains as well as the corresponding BF vectors are correlated across OFDM sub–carriers, in [2] it was proposed to reduce the amount of feedback by only feeding back the BF vectors for a small number of sub–carriers. The remaining BF vectors are obtained by modified spherical interpolation. This approach significantly reduces the required amount of feedback at the expense of some loss in performance. The required number of feedback bits of this frequency–domain BF (FD–BF) scheme can be further reduced by post–processing of the feedback bits [26] and/or by adopting improved interpolator designs such as Grassmannian interpolators [27] or geodesic interpolators [3]. However, fundamentally for all of these FD–BF schemes the required amount of feedback to achieve a certain performance is tied to the number of OFDM sub–carriers. This may be problematic in OFDM systems with a large number of sub–carriers and stringent limits on the affordable amount of feedback. Therefore, this motivates us to propose a novel time–domain (TD) approach to BF in MIMO–OFDM systems in Chapter 2.

1.2 Cooperative Relay Network

Multiple-antenna processing is a promising approach to improve the capacity and reliability of next generation communication systems as pointed out in the previous section. However, such technique requires that multiple antennas are separated by at least one-half of the wavelength of the transmitted signal from each other to obtain low correlation between the spatial channels. This requirement fundamentally limits the possibility of having multiple antennas on small communication devices. It has been recently shown that the performance of a wireless communication network can also be enhanced by relaying, which leads to an improved network coverage, throughput, and transmission reliability [28]–[31]. Indeed, relay networks can mimic MIMO systems and introduce spatial diversity in a distributed fashion. As a result, cooperative and relay communications have been one of the most widely studied topics in communications over the past few years.

The two most important relay protocols in the literature are amplify-and-forward (AF) relaying and decode-and-forward (DF) relaying [30, 31]. An illustration of the half-duplex AF and DF protocols is given in Fig. 1.1. In both protocols, cooperative transmissions are initiated by having the source broadcasts its signal to both the relays and the destination. If the AF protocol is employed, each relay performs linear processing on the received signal and forwards the resulting signal directly to the destination without performing decoding. On the other hand, if the DF protocol is employed, each relay will decode and regenerate a new signal to the destination in the subsequent time slot. Thereby, AF relaying is generally believed to be less complex. At the destination, for AF relaying, signals from both the source and the relays are combined to provide better detection performance. If no direct link between the source and the destination is available, only signals from the relays will be used for detection.

AF spatial multiplexing (AF-SM) relaying for single-relay networks with multiple an-

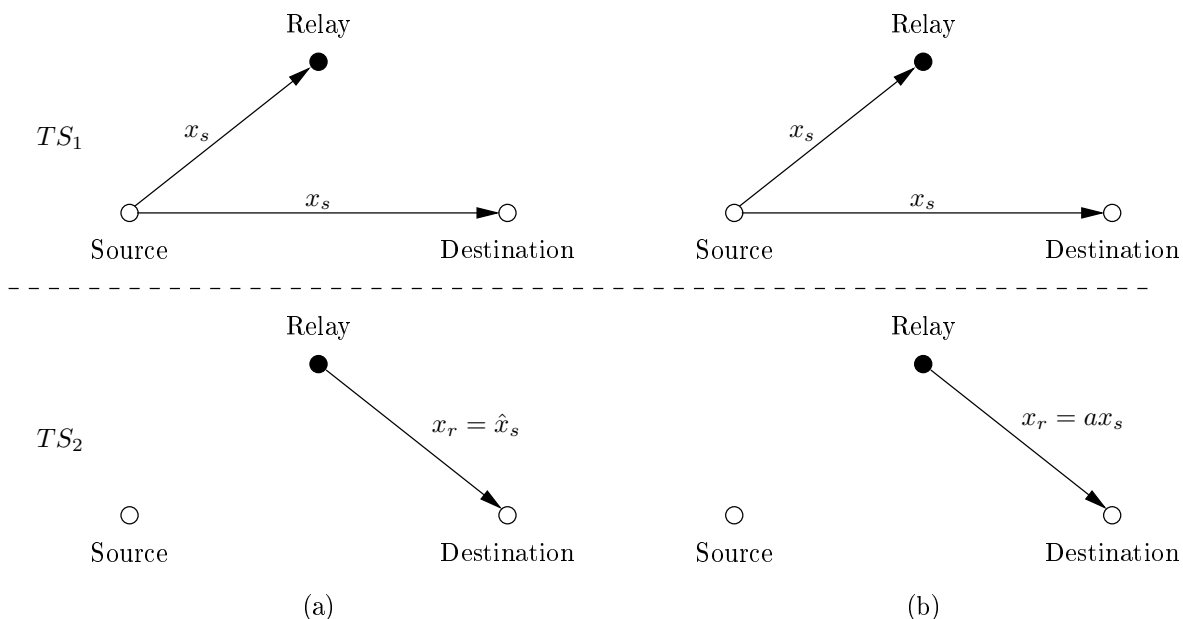


Figure 1.1: Different relaying protocols. (a) decode-and-forward (DF) relaying protocol, and (b) amplify-and-forward (AF) protocol. x_s : signal broadcasted from the source, x_r : signal transmitted from the relay, \hat{x}_s : regenerated signal after decoding, TS_x : time slot x , and a : scaling factor.

tennas at the source, the relay, and the destination was discussed in [32]–[34]. However, in downlink transmission the destination node can often support only a single antenna. In this case, BF is an efficient and popular approach to exploit the spatial diversity offered by the channel. AF–BF for wireless relay networks was considered in [35]–[44] and references therein. In particular, AF–BF for networks with one single-antenna source and multiple single-antenna relays was considered in [35, 36, 40, 41] and [39, 42] under a joint power constraint for all relays and individual relay power constraints, respectively. Since both the source and the relays were assumed to have only one antenna, respectively, the resulting signal-to-interference-noise ratio (SINR) maximization problem at the destination involved only the optimization of one scalar BF gain for each relay. In contrast, in [37, 38], AF–BF for a network with a single relay and multiple antennas at the relay and the source was investigated and closed-form solutions for the BF vector at the source and

the AF–BF matrix at the relay were provided. Furthermore, in [43, 44], the performance of AF–BF with multiple antennas at the source and one single–antenna relay was investigated. However, in practice, a relay network may comprise multiple relays and both the relays and the source may have multiple antennas. The extension of the results provided in those aforementioned paper to this general case is not straightforward. This problem will be discussed in details in Chapter 3.

The combination of relaying and OFDM has also attracted a lot of attention recently. Relaying for wideband OFDM–based cooperative networks is investigated in [45]–[48]. In [45], a relay network with one transmitter–receiver pair and a single AF relay is considered and all three nodes are equipped with multiple antennas. A power allocation scheme which maximizes the instantaneous rate of the network is proposed for this scenario. Linear filtering for relay networks with one relay node was introduced in [46]. In [49], a time–domain AF–BF scheme for cooperative OFDM networks with multiple relays is proposed.

As mentioned above, BF for cooperative networks with single–carrier transmission over frequency–nonselective channels and multi–carrier transmission over frequency–selective channels has been studied extensively in the literature. In contrast, the literature on BF (and other relay processing techniques as well) for single–carrier transmission over frequency–selective channels is very sparse. Nevertheless, wireless channels are typically frequency selective and multi–carrier modulation is not applicable in still evolving legacy systems such as Global System for Mobile Communications (GSM) and Enhanced Data Rates for GSM Evolution (EDGE) whose standard is still being further extended, and wireless sensor networks, for which the cost and power consumption of the highly linear power amplifiers required for OFDM may be prohibitive. To compensate for the effect of frequency–selective channels, filter–and–forward (FF) beamforming (FF–BF) for frequency–selective channels is proposed in [50]. However, in [50], only a simple slicer was

employed at the destination requiring the FF–BF filters at the relays to equalize both the source–relay and the relay–destination channels. This motivates us to consider the case if a simple linear equalization (LE) or decision–feedback equalization (DFE) is performed at the destination in Chapter 3.

In recent years, cooperative communication and relay technologies have gradually made their way into wireless standards, such as IEEE 802.16j [51] (an amendment to IEEE 802.16e mobile WiMAX standard), and LTE–Advanced [52]. The goal of utilizing cooperative communications in both standards is to increase the data rates available to cell–edge users and to increase coverage at a given data rate.

1.3 Two–Way Cooperative Relay Network

Most of the published results on distributed beamforming consider a one–way relaying protocol where the relays cooperate with each other to deliver the signals transmitted from a source (or several sources) to a destination (or several destinations). In two–way relaying, the relays cooperate with each other to establish reliable bidirectional communication between two transceivers [53, 54]. The capacity and achievable rate region for two–way relaying protocols have been studied in [55, 56] and references therein. The choice between one–way and two–way relaying mainly depends on the application. One–way relaying is of interest for unidirectional communication, whereas two–way relaying is preferable for bidirectional communication.

Various protocols for two–way relaying exist in the literature. The most common two–way relaying protocols are the bidirectional one–way relaying protocol, the time division broadcast (TDBC) protocol, and the multiple access broadcast (MABC) protocol. To achieve bidirectional communication between two transceivers, a straightforward approach is to employ two successive one–way relaying operations, as shown in Fig. 1.2 (a). However,

60], a two-way relay network with single multi-antenna relays is considered, whereas [58] considered a network with multiple single antenna relays. However, all the aforementioned papers consider frequency-nonselective channels. This motivates us to investigate two-way relaying schemes for frequency-selective channels in Chapter 5.

1.4 Contributions of the Thesis

This thesis considers BF schemes for performance enhancement that may find application in several current or upcoming wireless communication standards. The main contributions of this thesis are as follows.

1. We propose a novel time-domain approach to BF in MIMO-OFDM systems. The proposed time-domain BF scheme employs cyclic BF filters. Simulation results confirm the excellent performance of the proposed scheme and show that time-domain BF has a more favorable performance/feedback rate trade-off than previously proposed frequency-domain BF schemes.
2. We propose BF schemes for cooperative networks with one multi-antenna source, multiple multi-antenna AF relays, and one single-antenna destination. For a given BF vector at the source, we find the optimal AF-BF matrices at the relays for each of the three considered power constraints, namely individual relay power constraint, joint relay power constraint and joint source-relay power constraint. Several numerical methods for finding the optimal source BF vectors are also proposed.
3. We investigate FF-BF for one-way relay networks employing single-carrier transmission over frequency-selective channels. We consider two cases for the receive processing at the destinations: (1) a slicer and (2) LE/DFE. For both cases, we optimize the FF-BF filters for maximization of the SINR under a transmit power constraint.

In addition, for case (1), we also optimize the FF–BF filters for minimization of the transmit power under a QoS constraint, respectively. We find closed–form/near–optimal solutions for the IIR and FIR FF–BF matrix filters at the relays.

4. Drawing from the findings on one–way relaying, we investigate FF–BF for two–way relay networks with multiple single–antenna relays. We consider two cases for the receive processing at the transceivers: (1) a slicer and (2) LE/DFE. For both cases, we optimize the FF–BF filters at the relays for an SINR balancing objective under a relay transmit power constraint. Additionally, for case (1) we also consider the optimization of the FF–BF filters for minimization of the total transmit power subject to two QoS constraints to guarantee a certain level of performance. For case (1), we show that the optimization problems are convex. For case (2), we provide an upper bound and an achievable lower bound for the optimization problem, and our results show that the gap between both bounds is small.

1.5 Organization of the Thesis

In the following, we provide a brief overview of the remainder of this thesis.

In Chapter 2, we propose a novel single–data stream, time–domain BF scheme for MIMO–OFDM systems which uses cyclic BF filters (C–BFFs). Assuming perfect CSI at the transmitter, the C–BFFs are optimized for two different criteria, namely, maximum average mutual information (AMI) per sub–carrier and minimum average uncoded bit error rate (BER). If the C–BFF length L_g is equal to the number of sub–carriers N_c , closed–form solutions to both optimization problems exist. For the practically relevant case $L_g < N_c$ we present numerical methods for calculation of the optimum C–BFFs for both criteria. Using a global vector quantization (GVQ) approach, the C–BFFs are quantized

for practical finite-rate feedback channels. Simulation results for typical IEEE 802.11n channels confirm the excellent performance of the proposed scheme and show that TD-BF has a more favorable performance/feedback rate trade-off than previously proposed FD-BF schemes.

In Chapter 3, we consider BF for cooperative networks with one multi-antenna source, multiple multi-antenna AF relays, and one single-antenna destination. The source BF vector and the AF-BF matrices at the relays are optimized for maximization of the SINR at the destination under three different power constraints. In particular, we consider individual relay power constraints, a joint relay power constraint, and a joint power constraint for the source and the relays. We solve the associated optimization problems in two stages. In the first stage, we find the optimal AF-BF matrices for a given BF vector at the source. For the cases of individual and joint relay power constraints, closed-form solutions for the AF-BF matrices are provided, respectively. Furthermore, for the case of a joint source-relay power constraint, the direction of the AF-BF matrices is derived in closed form and an efficient numerical algorithm for the power allocation between the source and the relays is provided. In the second stage, the optimal source BF vectors are computed. Thereby, we show that for the joint relay and the joint source-relay power constraints, the resulting problem can be transformed into a non-convex polynomial programming problem which allows for an exact solution for small scale networks. For large scale networks and networks with individual relay power constraints, we propose efficient suboptimal optimization methods for the source BF vector. Simulation results show the benefits of having multiple antennas at the source and/or multiple multi-antenna relays and illustrate the performance differences introduced by the three different power constraints.

In Chapter 4, we investigate FF-BF for relay networks employing single-carrier transmission over frequency-selective channels. In contrast to prior work, which concentrated

on multiple single-antenna relay nodes, we consider networks employing multiple multi-antenna relay nodes. For the processing at the destination, we investigate two different cases: (1) a simple slicer without equalization and (2) a LE or a DFE. For both cases, we optimize the FF-BF matrix filters at the relays for maximization of the SINR under a transmit power constraint, and for the first case we consider additionally optimization of the FF-BF matrix filters for minimization of the total transmit power under a quality of service (QoS) constraint. For the first case, we obtain closed-form solutions for the optimal FIR FF-BF matrix filters, whereas for the second case, we provide the optimal solution for IIR FF-BF matrix filters, and an efficient gradient algorithm for recursive calculation of near-optimal FIR FF-BF matrix filters. Our simulation results reveal that for a given total number of antennas in the network, a small number of multiple-antenna relays can achieve significant performance gains over a large number single-antenna relays.

In Chapter 5, we consider FF-BF for two-way relay networks employing single-carrier transmission over frequency-selective channels. We adopt the MABC protocol for two-way relaying with single-antenna relays is assumed. Similar to the one-way relaying with FF-BF, the relay nodes filter the received signal using FIR or IIR filters. For the processing at the transceivers, we investigate two different cases: (1) a simple slicer without equalization and (2) LE/DFE. For the first case, we optimize FIR FF-BF filters, respectively, for maximization of the minimum transceiver SINR subject to a relay transmit power constraint and for minimization of the total relay transmit power subject to two QoS constraints to guarantee a certain level of performance. We show that both problems can be transformed into a convex second-order cone programming (SOCP) problem, which can be efficiently solved using standard tools. For the second case, we optimize IIR and FIR FF-BF filters for max-min optimization of the SINR, and for transceivers with zero-forcing LE, also for minimization of the sum MSE at the equalizer outputs of both transceivers. Leveraging

results from FF–BF for one–way relaying, we establish an upper and an achievable lower bound for the max–min problem and an exact solution for the sum MSE problem. Since the gap between the upper and the lower bound for the max–min problem is small, a close–to–optimal solution is obtained. Our simulation results reveal that the performance of FF–BF without equalization at the transceivers crucially depends on the slicer decision delay and transceivers with slicers can closely approach the performance of transceivers with equalizers provided that the FF–BF filters are sufficiently long and a sufficient number of relays is deployed.

Finally, Chapter 6 summarizes the contributions of this thesis and outlines areas of future research.

Chapter 2

Time–Domain Transmit Beamforming for MIMO–OFDM Systems

2.1 Introduction

As pointed out in Chapter 1, transmit BF and receiver combining are simple yet efficient techniques for exploiting the benefits of MIMO–OFDM systems [14]. Several FD–BF with CSI feedback reduction schemes have been proposed in recent publications, e.g. [2, 3, 26, 27]. With the observation that the fading gains as well as the corresponding BF vectors are correlated across OFDM sub–carriers, [2] proposed to reduce the amount of feedback by only feeding back the BF vectors for a small number of so–called pilot sub–carriers. The remaining BF vectors are obtained by modified spherical interpolation. This approach significantly reduces the required amount of feedback at the expense of some loss in performance. The required number of feedback bits of this FD–BF scheme can be further reduced by post–processing of the feedback bits [26] and/or by adopting improved interpolator designs such as Grassmannian interpolators [27] or geodesic interpolators [3]. However, fundamentally for all of these FD–BF schemes the required amount of feedback to achieve a certain performance is tied to the number of OFDM sub–carriers.

In this chapter, we propose a novel TD approach to BF in MIMO–OFDM systems¹.

¹In this chapter, we only consider single–stream BF which is sometimes also referred to as maximal–ratio transmission. We note, however, that the concept of TD–BF can also be extended to multi–stream BF which is also referred to as spatial multiplexing.

The motivation for considering a TD approach is that the fading correlations in the FD, which are exploited for interpolation in [2, 3, 27], have their origin in the TD. These correlations are due to the fact that the number of sub-carriers is typically much larger than the number of non-zero channel impulse response (CIR) coefficients. Therefore, tackling the problem directly in the TD is a natural choice. The proposed TD-BF scheme employs C-BFFs of length $L_g \leq N_c$. The C-BFFs are optimized for maximization of the AMI and for minimization of the average uncoded BER, respectively. While other C-BFF optimization criteria are certainly possible (e.g., maximum cut-off rate, minimum coded BER), the adopted criteria can be considered as extreme cases in the sense that they cater to systems using very powerful (ideally capacity-achieving) forward error correction (FEC) coding (AMI criterion) and systems with weak or no FEC coding (uncoded BER criterion), respectively. For perfect CSI both criteria lead to (different) nonlinear eigenvalue problems for the C-BFF coefficient vectors, and we show that closed-form solutions to both problems exist for $L_g = N_c$. However, for the practically more interesting case of $L_g < N_c$, a closed-form solution does not exist for either problem, and we provide efficient numerical methods for calculation of the C-BFFs. Furthermore, for the case of a finite-rate feedback channel we draw from the findings in [61, 62] and propose a global vector quantization (GVQ) algorithm for maximum AMI and minimum BER codebook design, respectively. This chapter also provides a detailed comparison between TD-BF and FD-BF [2, 3, 27].

We note that TD pre-processing for MIMO-OFDM has been considered in different contexts before. For example, TD-BF schemes with one scalar BF weight per antenna (as opposed to C-BFFs) have been proposed to reduce the number of inverse discrete Fourier transforms (IDFTs) required at the transmitter of MIMO-OFDM systems, cf. e.g. [63] and references therein. Similarly, cyclic delay diversity, which is a simple form of space-time coding, cf. e.g. [64, 65], may be viewed as a TD MIMO-OFDM pre-processing technique.

Furthermore, BF with *linear* BFFs has been considered for *single-carrier* transmission over frequency-selective channels and DFE at the receiver in [62]. However, the concept of employing C-BFFs for (limited feedback) BF in MIMO-OFDM systems is novel and has not been considered before.

The remainder of this chapter is organized as follows. In Section 2.2, the considered system model is presented. The optimization of the C-BFFs for maximization of the AMI and minimization of the average BER is discussed in Sections 2.3 and 2.4, respectively. In Section 2.5, a GVQ algorithm for finite-rate feedback TD-BF and a detailed comparison between TD-BF and FD-BF are presented. Simulation results are provided in Section 2.6, and some conclusions are drawn in Section 2.7.

2.2 System Model

We consider a MIMO-OFDM system with N_T transmit antennas, N_R receive antennas, and N_c OFDM sub-carriers. The block diagram of the discrete-time overall transmission system in equivalent complex baseband representation is shown in Fig. 2.1. In the next four subsections, we introduce the models for the transmitter, the channel, the receiver, and the feedback channel.

2.2.1 Transmitter Processing for TD-BF

The modulated symbols $D[n]$, $0 \leq n < N_c$, are taken from a scalar symbol alphabet \mathcal{A} and have variance $\sigma_D^2 = \mathcal{E}\{|D[n]|^2\} = 1$. The transmit symbol vector $\mathbf{x} \triangleq [x[0] \ x[1] \ \dots \ x[N_c - 1]]^T$ after the IDFT operation can be represented as

$$\mathbf{x} \triangleq \mathbf{W}\mathbf{D}, \tag{2.1}$$

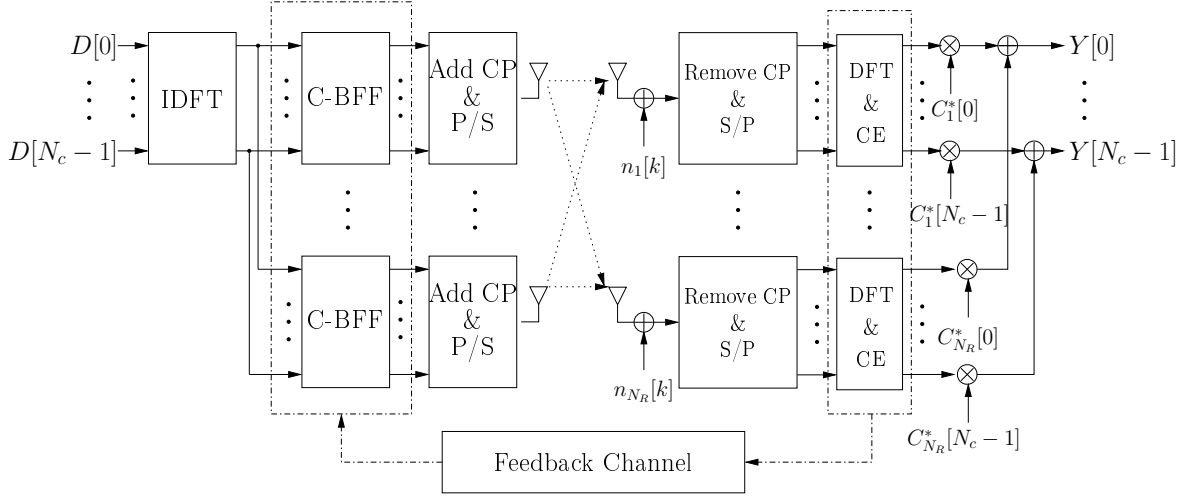


Figure 2.1: MIMO-OFDM system with TD-BF. P/S: Parallel-to-serial conversion. S/P: Serial-to-parallel conversion. CE: Channel estimation.

where $\mathbf{D} \triangleq [D[0] \ D[1] \ \dots \ D[N_c - 1]]^T$ and \mathbf{W} is the unitary IDFT matrix [66], i.e., $x[k] = \frac{1}{\sqrt{N_c}} \sum_{n=0}^{N_c-1} D[n] e^{j2\pi nk/N_c}$.

At transmit antenna n_t sequence $x[k]$ is filtered with a C-BFF with impulse response $g_{n_t}[k]$, $0 \leq k < L_g$, $1 \leq n_t \leq N_T$, of length $L_g \leq N_c$. The resulting OFDM symbol after cyclic filtering is given by

$$\mathbf{s}_{n_t} = \tilde{\mathbf{G}}_{n_t} \mathbf{x}, \quad (2.2)$$

where $\tilde{\mathbf{G}}_{n_t}$ is an $N_c \times N_c$ column-circulant matrix with first column $[\mathbf{g}_{n_t}^T \ \mathbf{0}_{N_c-L_g}^T]^T$, $\mathbf{g}_{n_t} \triangleq [g_{n_t}[0] \ g_{n_t}[1] \ \dots \ g_{n_t}[L_g - 1]]^T$. We note that in practice the cyclic filtering in (2.2) can be implemented using the following three simple steps:

1. Add a cyclic prefix (CP) of length $L_g - 1$ to \mathbf{x} to generate $\bar{\mathbf{x}} \triangleq [x[N_c - L_g + 1] \ \dots \ x[N_c - 1] \ \mathbf{x}^T]^T$.
2. Pass the elements of $\bar{\mathbf{x}}$ through a *linear* filter with coefficients $g_{n_t}[k]$, $0 \leq k < L_g$, to generate $\bar{\mathbf{s}}_{n_t} \triangleq [\bar{s}_{n_t}[0] \ \bar{s}_{n_t}[1] \ \dots \ \bar{s}_{n_t}[N_c + L_g - 2]]^T$, where $\bar{s}_{n_t}[k] = \sum_{\kappa=0}^{L_g-1} g_{n_t}[\kappa] \bar{x}[k - \kappa]$ and $\bar{x}[k]$, $0 \leq k < N_c + L_g - 1$, are the elements of $\bar{\mathbf{x}}$ and $\bar{x}[k] = 0$ for $k < 0$.

3. Remove the CP from $\bar{\mathbf{s}}_{n_t}$ to obtain $\mathbf{s}_{n_t} = [\bar{\mathbf{s}}_{n_t}[L_g - 1] \dots \bar{\mathbf{s}}_{n_t}[N_c + L_g - 2]]^T$.

After cyclic filtering a CP is added to \mathbf{s}_{n_t} . We assume that the CP length is not smaller than $L - 1$, where L is the length of the CIR. We note that due to the cyclic structure of $\bar{\mathbf{G}}_{n_t}$, TD-BF does not affect the length requirements of the CP, i.e., the required CP length for TD-BF is identical to that for single-antenna transmission.

2.2.2 MIMO Channel

We model the wireless channel as a frequency-selective and spatially correlated MIMO channel. The spatial correlations may be introduced by insufficient antenna spacing. The channel between transmit antenna n_t and receive antenna n_r is characterized by its impulse response $h_{n_t n_r}[l]$, $0 \leq l < L$. Note that the impulse response coefficients for a given transmit/receive antenna pair are also generally mutually correlated due to transmit and receive filtering. As is typically done in the BF literature, e.g. [15]–[19], [2, 3, 27], we assume that the transmitted data is organized in frames. The channel remains constant during each frame but changes randomly between frames (block fading model).

2.2.3 Receiver Processing

TD-BF does not affect the processing at the receiver, i.e., standard OFDM receiver processing is applied. After CP removal the discrete-time received signal at receive antenna n_r , $1 \leq n_r \leq N_R$, can be modeled as

$$\mathbf{r}_{n_r} = \sum_{n_t=1}^{N_T} \bar{\mathbf{H}}_{n_t n_r} \bar{\mathbf{G}}_{n_t} \mathbf{x} + \mathbf{n}_{n_r}, \quad (2.3)$$

where $\bar{\mathbf{H}}_{n_t n_r}$ is an $N_c \times N_c$ column-circulant matrix with first column $[h_{n_t n_r}[0] \dots h_{n_t n_r}[L-1] \mathbf{0}_{N_c-L}^T]^T$ and \mathbf{n}_{n_r} is an additive white Gaussian noise (AWGN) vector whose entries

$n_{n_r}[k]$, $0 \leq k < N_c$, are independent and identically distributed (i.i.d.) with zero mean and variance σ_n^2 .

After DFT we obtain at antenna n_r

$$\mathbf{R}_{n_r} = \mathbf{W}^H \mathbf{r}_{n_r} = \sum_{n_t=1}^{N_T} \mathbf{H}_{n_t n_r} \mathbf{G}_{n_t} \mathbf{D} + \mathbf{N}_{n_r}, \quad (2.4)$$

where $\mathbf{H}_{n_t n_r} \triangleq \mathbf{W}^H \bar{\mathbf{H}}_{n_t n_r} \mathbf{W} = \text{diag}\{H_{n_t n_r}[0] \dots H_{n_t n_r}[N_c - 1]\}$, $\mathbf{G}_{n_t} \triangleq \mathbf{W}^H \bar{\mathbf{G}}_{n_t} \mathbf{W} = \text{diag}\{G_{n_t}[0] \dots G_{n_t}[N_c - 1]\}$, and $\mathbf{N}_{n_r} \triangleq \mathbf{W}^H \mathbf{n}_{n_r} = [N_{n_r}[0] \dots N_{n_r}[N_c - 1]]^T$. The $N_{n_r}[n]$, $0 \leq n < N_c$, are i.i.d. AWGN samples with variance σ_n^2 . The FD channel gains $H_{n_t n_r}[n]$ and the C-BFF gains $G_{n_t}[n]$ are given by

$$H_{n_t n_r}[n] \triangleq \sum_{l=0}^{L-1} h_{n_t n_r}[l] e^{-j2\pi n l / N_c}, \quad (2.5)$$

$$G_{n_t}[n] \triangleq \sum_{l=0}^{L_g-1} g_{n_t}[l] e^{-j2\pi n l / N_c}. \quad (2.6)$$

Considering now the n th sub-carrier and assuming an N_R -dimensional receive combining vector $\mathbf{C}[n] \triangleq [C_1[n] \dots C_{N_R}[n]]^T$, with (2.4) the combined received signal can be expressed as

$$Y[n] = \mathbf{C}^H[n] \mathbf{H}[n] \mathbf{G}[n] \mathbf{D}[n] + \mathbf{C}^H[n] \mathbf{N}[n], \quad 0 \leq n < N_c, \quad (2.7)$$

where $N_R \times N_T$ matrix $\mathbf{H}[n]$ contains $H_{n_t n_r}[n]$ in row n_r and column n_t , $\mathbf{G}[n] \triangleq [G_1[n] \dots G_{N_T}[n]]^T$, and $\mathbf{N}[n] \triangleq [N_1[n] \dots N_{N_R}[n]]^T$. In this chapter, we assume that the receiver has perfect knowledge of $\mathbf{H}[n]$, $0 \leq n < N_c$. In this case, the combining vector $\mathbf{C}[n]$ that maximizes the SNR of $Y[n]$ is given by $\mathbf{C}[n] = \mathbf{H}[n] \mathbf{G}[n]$ (maximal-ratio combining).

2.2.4 Feedback Channel

We assume that a feedback channel from the receiver to the transmitter is available, cf. Fig. 2.1. In the idealized case, where the feedback channel has infinite capacity, the receiver sends the unquantized C-BFF vector \mathbf{g} , $\mathbf{g} \triangleq [\mathbf{g}_1^T \dots \mathbf{g}_{N_T}^T]^T$, to the transmitter (perfect CSI case). In the more realistic case, where the feedback channel can only support the transmission of B bits per channel update, the receiver and the transmitter have to agree on a pre-designed C-BFF vector codebook $\mathcal{G} \triangleq \{\hat{\mathbf{g}}_1, \hat{\mathbf{g}}_2, \dots, \hat{\mathbf{g}}_N\}$ of size $N = 2^B$, where $\hat{\mathbf{g}}_n$ is an $N_T L_g$ -dimensional vector. For a given channel vector $\mathbf{h} \triangleq [h_{11}[0] \ h_{11}[1] \ \dots \ h_{11}[L-1] \ h_{21}[0] \ \dots \ h_{N_T N_R}[L-1]]^T$ the receiver determines the address n of the codeword (C-BFF vector) $\hat{\mathbf{g}}_n \in \mathcal{G}$, $1 \leq n \leq N$, which maximizes the prescribed optimality criterion (maximum AMI or minimum BER). Subsequently, index n is sent to the transmitter which then utilizes $\mathbf{g} = \hat{\mathbf{g}}_n$ for BF. Similar to [2, 3, 27] we assume that the feedback channel is error-free and has zero delay.

2.3 Maximum AMI Criterion

In this section, we optimize the C-BFFs for maximization of the AMI per sub-carrier. After rigorously formulating the optimization problem, we present a closed-form solution for $L_g = N_c$ and numerical methods for computation of the optimum C-BFFs for $L_g < N_c$.

2.3.1 Formulation of the Optimization Problem

Assuming i.i.d. Gaussian input symbols $D[\cdot]$, the mutual information (in bit/s/Hz) of the n th sub-carrier is given by [66]

$$C[n] = \log_2(1 + \text{SNR}[n]). \quad (2.8)$$

For maximal-ratio combining the SNR of the n th sub-carrier can be obtained from (2.7)

as

$$\text{SNR}[n] = \frac{1}{\sigma_n^2} \mathbf{G}^H[n] \mathbf{H}^H[n] \mathbf{H}[n] \mathbf{G}[n]. \quad (2.9)$$

We note that $\mathbf{G}[n]$ can be expressed as

$$\mathbf{G}[n] = \mathbf{F}[n] \mathbf{g}, \quad (2.10)$$

where the n_t th row of $N_T \times N_T L_g$ matrix $\mathbf{F}[n]$ is given by $[\mathbf{0}_{(n_t-1)L_g}^T \mathbf{f}^T[n] \mathbf{0}_{(N_T-n_t)L_g}^T]$, $1 \leq n_t \leq N_T$, with $\mathbf{f}[n] \triangleq [1 e^{-j2\pi n/N_c} \dots e^{-j2\pi(L_g-1)n/N_c}]^T$. Therefore, the AMI per sub-carrier depends on \mathbf{g} and is given by $C = \frac{1}{N_c} \sum_{n=0}^{N_c-1} C[n]$. The optimization problem can now be formulated as

$$\max_{\mathbf{g}} \sum_{n=0}^{N_c-1} C[n] \quad (2.11)$$

$$\text{s.t.} \quad \mathbf{g}^H \mathbf{g} = 1, \quad (2.12)$$

where (2.12) is a transmit power constraint.

2.3.2 Solution of the Optimization Problem for $L_g = N_c$

Although in practice $L_g \ll N_c$ is desirable to minimize the amount of feedback, it is insightful to first consider $L_g = N_c$ since in this case a closed-form solution to the optimization problem in (2.11), (2.12) exists. In addition, the solution for $L_g = N_c$ serves as a performance upper bound for the practically relevant case $L_g < N_c$. For $L_g = N_c$ matrix $\mathbf{F} \triangleq [\mathbf{F}^T[0] \dots \mathbf{F}^T[N_c-1]]^T$ is invertible, and for a given $\mathbf{G} \triangleq [\mathbf{G}^T[0] \dots \mathbf{G}^T[N_c-1]]^T$ the

C-BFF vector \mathbf{g} can be obtained from

$$\mathbf{g} = \mathbf{F}^{-1}\mathbf{G}, \quad (2.13)$$

cf. (2.10). This means (2.11) and (2.12) are equivalent to

$$\max_{\mathbf{G}} \quad \sum_{n=0}^{N_c-1} \log_2 \left(1 + \frac{1}{\sigma_n^2} \mathbf{G}^H[n] \mathbf{H}^H[n] \mathbf{H}[n] \mathbf{G}[n] \right) \quad (2.14)$$

$$\text{s.t.} \quad \mathbf{G}^H \mathbf{G} = N_c. \quad (2.15)$$

The solution to this equivalent problem can be obtained as

$$\mathbf{G}[n] = \alpha[n] \mathbf{E}_{\max}[n], \quad 0 \leq n < N_c, \quad (2.16)$$

where $\mathbf{E}_{\max}[n]$ is that eigenvector of matrix $\mathbf{H}^H[n] \mathbf{H}[n]$ which corresponds to the maximum eigenvalue $\lambda_{\max}[n]$, and $\alpha[n]$ is obtained from

$$\alpha[n] = \sqrt{N_c \sigma_n^2 \left(\frac{1}{\lambda} - \frac{1}{N_c \lambda_{\max}[n]} \right)^+}, \quad (2.17)$$

where $x^+ \triangleq \max(0, x)$ and λ is the solution to the waterfilling equation

$$\sigma_n^2 \sum_{n=0}^{N_c-1} \left(\frac{1}{\lambda} - \frac{1}{N_c \lambda_{\max}[n]} \right)^+ = 1. \quad (2.18)$$

Once $\mathbf{G}[n]$, $0 \leq n < N_c$, has been calculated, the optimum \mathbf{g} can be obtained from (2.13). Therefore, in this case, TD-BF is equivalent to ideal FD-BF with waterfilling which is not surprising since for $L_g = N_c$ there are as many degrees of freedom in the TD as there are in the FD.

2.3.3 Solution of the Optimization Problem for $L_g < N_c$

For $L_g < N_c$ the $N_T N_c \times N_T L_g$ matrix \mathbf{F} is not invertible, i.e., (2.11) and (2.14) are not equivalent anymore². For convenience we rewrite (2.11), (2.12) as

$$\max_{\mathbf{g}} \quad \sum_{n=0}^{N_c-1} \log_2 \left(1 + \frac{1}{\sigma_n^2} \mathbf{g}^H \mathbf{M}[n] \mathbf{g} \right) \quad (2.19)$$

$$\text{s.t.} \quad \mathbf{g}^H \mathbf{g} = 1 \quad (2.20)$$

with $N_T L_g \times N_T L_g$ matrix $\mathbf{M}[n] \triangleq \mathbf{F}^H[n] \mathbf{H}^H[n] \mathbf{H}[n] \mathbf{F}[n]$. Unfortunately, the objective function in (2.19) is not a concave function, i.e., (2.19), (2.20) is not a convex optimization problem. In fact, (2.19) and (2.20) are equivalent to the maximization of a product of Rayleigh coefficients

$$\tilde{L}(\mathbf{g}) \triangleq \prod_{n=0}^{N_c-1} \frac{\mathbf{g}^H (\sigma_n^2 \mathbf{I}_{N_T L_g} + \mathbf{M}[n]) \mathbf{g}}{\mathbf{g}^H \mathbf{g}}, \quad (2.21)$$

which is a well-known difficult mathematical problem that is not well understood for $N_c > 1$, cf. e.g. [67, 68].

In the remainder of this subsection, we will first consider a relaxation of (2.19), (2.20) to find a suboptimum solution and then provide a numerical algorithm for calculation of the optimum C-BFF vector.

1) *Relaxation of the Optimization Problem:* A popular approach for solving non-convex optimization problems is to transform the original non-convex problem into a convex one by relaxing the constraints [1]. This leads in general to a suboptimum (but often close-to-optimum) solution for the original problem. For the problem at hand we may define a

²Note that pseudo inverse can be used as an alternative way to find the optimal \mathbf{g} in this case. However, we found that the resulting performance is not comparable with the performance from the algorithm introduced in this section.

matrix $\mathbf{S} \triangleq \mathbf{g}\mathbf{g}^H$ and rewrite (2.19), (2.20) as

$$\max_{\mathbf{S}} \sum_{n=0}^{N_c-1} \log_2 \det \left(\mathbf{I}_{N_R} + \frac{1}{\sigma_n^2} \mathbf{H}[n] \mathbf{F}[n] \mathbf{S} \mathbf{F}^H[n] \mathbf{H}^H[n] \right) \quad (2.22)$$

$$\text{s.t.} \quad \text{trace}\{\mathbf{S}\} \leq 1, \quad (2.23)$$

$$\mathbf{S} \succeq 0, \quad (2.24)$$

$$\text{rank}\{\mathbf{S}\} = 1, \quad (2.25)$$

where $\mathbf{S} \succeq 0$ means that \mathbf{S} is a positive-semidefinite matrix. It is easy to show that equality is satisfied in (2.23) when \mathbf{S} is optimal. The equivalent optimization problem in (2.22)–(2.25) is still non-convex due to the rank condition in (2.25) but can be relaxed to a convex problem by dropping this rank condition. The resulting relaxed problem is a convex semidefinite programming (SDP) problem which can be solved with standard algorithms, cf. [1]. If the \mathbf{S} found by this procedure has rank one, the corresponding \mathbf{g} is also the solution to the original, non-convex problem. On the other hand, if the optimum \mathbf{S} does not have rank one, the eigenvector of \mathbf{S} corresponding to its maximum eigenvalue can be used as (suboptimum) approximate solution to the original non-convex problem.

Unfortunately, the amount of time to solve the relaxed optimization problem strongly depends on N_c , and for medium numbers of sub-carriers (e.g. $N_c \geq 64$) standard optimization software (e.g. “yalmip” and “SeDuMi”) takes a very long time to find the optimum \mathbf{S} . Therefore, this relaxation approach is most useful for the practically less relevant case when the number of sub-carriers is small (e.g. $N_c < 64$).

2) *Gradient Algorithm:* The Lagrangian of (2.19), (2.20) can be formulated as

$$L(\mathbf{g}) = \sum_{n=0}^{N_c-1} \log_2 \left(1 + \frac{1}{\sigma_n^2} \mathbf{g}^H \mathbf{M}[n] \mathbf{g} \right) - \mu \mathbf{g}^H \mathbf{g}, \quad (2.26)$$

where μ denotes the Lagrange multiplier. The optimum C-BFF vector has to fulfill

$\partial L(\mathbf{g})/\partial \mathbf{g}^* = \mathbf{0}_{N_T L_g}$, which leads to the non-linear eigenvalue problem

$$\left[\sum_{n=0}^{N_c-1} \frac{\mathbf{M}[n]}{\sigma_n^2 + \mathbf{g}^H \mathbf{M}[n] \mathbf{g}} \right] \mathbf{g} = \mu \mathbf{g}. \quad (2.27)$$

For very low SNRs (i.e., $\sigma_n^2 \rightarrow \infty$) the optimum C-BFF vector can be obtained from (2.27) as the unit-norm eigenvector of $\sum_{n=0}^{N_c-1} \mathbf{M}[n]$ which corresponds to the maximum eigenvalue of that matrix, i.e., a closed-form solution exists for this special case. Unfortunately, the low SNR solution for \mathbf{g} does not yield a good performance for finite, practically relevant SNRs. Therefore, we provide in Table 2.1 a gradient algorithm (GA) for optimization problem (2.19), (2.20). Since the considered problem (2.19), (2.20) is not a convex optimization problem, we cannot guarantee that the GA will converge to the globally optimum solution. However, if the step size δ_i is chosen appropriately, the GA will converge to a local optimum, cf. e.g. [69] for guidelines on the choice of step sizes for GAs. To which local optimum the GA converges, generally depends on the initial vector \mathbf{g}_0 . For the problem at hand, our simulations have shown that the choice of the initial vector \mathbf{g}_0 is not critical and the GA always achieved very similar AMI values for different random \mathbf{g}_0 . Furthermore, for those cases where the relaxation method discussed in 1) found the solution to the original problem (2.19), (2.20), i.e., \mathbf{S} had rank one, the solution found with the GA achieved the same AMI.

We note that the speed of convergence of the GA depends on the adaptation step size δ_i . For the results shown in Section 2.6, we have adopted the *backtracking line search* procedure outlined in [69, p. 41], which optimizes the step size δ_i in each iteration. Thereby, starting from an initial value $\delta_i = \bar{\delta} > 0$ the step size is gradually reduced as $\delta_i \leftarrow \rho \delta_i$ with contraction factor $\rho \in (0, 1)$ until the so-called *Armijo condition* with constant c is fulfilled [69, p. 41]. We found that for the problem at hand, the GA in Table 2.1 with backtracking line search ($c = 0.49$, $\rho = 0.9$, and $\bar{\delta} = 1$) typically terminates after around 100 iterations

Table 2.1: Calculation of the optimum C-BFFs \mathbf{g} for the maximum AMI and the minimum average BER criterion using a GA, respectively. Termination constant ϵ has a small value (e.g. $\epsilon = 10^{-4}$). i denotes the iteration and δ_i is the adaptation step size necessary for the GA.

1	Let $i = 0$ and initialize the C-BFF vector with some \mathbf{g}_0 fulfilling $\mathbf{g}_0^H \mathbf{g}_0 = 1$.
2	Update the C-BFF vector: AMI: $\tilde{\mathbf{g}}_{i+1} = \mathbf{g}_i + \delta_i \left[\sum_{n=0}^{N_c-1} \frac{\mathbf{M}[n]}{\sigma_n^2 + \mathbf{g}_i^H \mathbf{M}[n] \mathbf{g}_i} \right] \mathbf{g}_i$ BER: $\tilde{\mathbf{g}}_{i+1} = \mathbf{g}_i + \delta_i \left[\sum_{n=0}^{N_c-1} \exp\left(-\frac{c_2}{\sigma_n^2} \mathbf{g}_i^H \mathbf{M}[n] \mathbf{g}_i\right) \mathbf{M}[n] \right] \mathbf{g}_i$
3	Normalize the C-BFF: $\mathbf{g}_{i+1} = \frac{\tilde{\mathbf{g}}_{i+1}}{\sqrt{\tilde{\mathbf{g}}_{i+1}^H \tilde{\mathbf{g}}_{i+1}}}$
4	If $1 - \mathbf{g}_{i+1}^H \mathbf{g}_i < \epsilon$, goto Step 5, otherwise increment $i \rightarrow i + 1$ and goto Step 2.
5	\mathbf{g}_{i+1} is the desired C-BFF vector.

if the termination constant (defined in Table 2.1) is set to $\epsilon = 10^{-4}$. However, in practice, the speed of convergence of the GA is not critical, since in the realistic finite-rate feedback case, the GA is only used to find the C-BFF codebook, which is done off-line.

2.4 Minimum BER Criterion

The main criterion considered for C-BFF optimization in this section is the BER averaged over all sub-carriers. However, we will also consider the minimization of the maximum sub-carrier BER for optimization of the C-BFFs. Besides the additional insight that this second BER criterion offers, it also provides a useful starting point for numerical computation of the minimum average BER C-BFF filters, cf. Section 2.4.3.

2.4.1 Formulation of the Optimization Problems

While closed-form expressions for the BER or/and symbol error rate exist for most regular signal constellations such as M -ary quadrature amplitude modulation (M -QAM) and M -ary phase-shift keying (M -PSK), these expressions are quite involved which is not desirable for C-BFF optimization. Therefore, we adopt here the simple yet accurate BER approximations from [70], which allow us to express the approximate BER of the n th sub-carrier as

$$\text{BER}[n] \approx c_1 \exp(-c_2 \text{SNR}[n]), \quad (2.28)$$

where the n th sub-carrier SNR is defined in (2.9) and c_1 and c_2 are modulation dependent constants. For example, for square M -QAM we have $c_1 = 0.2$ and $c_2 \triangleq 3/[2(M-1)]$ [70]. Throughout this chapter we assume that all sub-carriers use the same modulation scheme.

1) *Average BER Criterion:* The (approximate) average BER is given by $\text{BER} = \frac{1}{N_c} \sum_{n=0}^{N_c-1} \text{BER}[n]$. Consequently, the minimum average BER optimization problem can be formulated as

$$\min_{\mathbf{g}} \sum_{n=0}^{N_c-1} \text{BER}[n] \quad (2.29)$$

$$\text{s.t.} \quad \mathbf{g}^H \mathbf{g} = 1. \quad (2.30)$$

2) *Max-Min Criterion:* Since the exponential function is monotonic, we observe from (2.28) that minimizing the maximum sub-carrier BER is equivalent to maximizing the minimum sub-carrier SNR. The resulting max-min problem becomes

$$\max_{\mathbf{g}} \min_{\forall n} \text{SNR}[n] \quad (2.31)$$

$$\text{s.t.} \quad \mathbf{g}^H \mathbf{g} = 1. \quad (2.32)$$

Since for high SNR, the maximum sub-carrier BER dominates the average BER, we expect that in this case both optimization criteria lead to similar performances.

2.4.2 Solution of the Optimization Problems for $L_g = N_c$

For the solution of the optimization problem we exploit again the fact that for $L_g = N_c$ matrix \mathbf{F} is invertible, i.e., for a given \mathbf{G} the C-BFF vector \mathbf{g} can be obtained from (2.13).

1) *Average BER Criterion:* Eq. (2.13) implies that (2.29) and (2.30) are equivalent to

$$\min_{\mathbf{G}} \sum_{n=0}^{N_c-1} \exp\left(-\frac{c_2}{\sigma_n^2} \mathbf{G}^H[n] \mathbf{H}^H[n] \mathbf{H}[n] \mathbf{G}[n]\right) \quad (2.33)$$

$$\text{s.t.} \quad \mathbf{G}^H \mathbf{G} = N_c. \quad (2.34)$$

Formulating (2.33) and (2.34) as a Lagrangian, it can be shown that the optimum $\mathbf{G}[n]$ is again proportional to $\mathbf{E}_{\max}[n]$, i.e., (2.16) is still valid. However, now $\alpha[n]$ in (2.16) is given by

$$\alpha[n] = \sqrt{\frac{\sigma_n^2}{c_2 \lambda_{\max}[n]} \left[\ln\left(\frac{\lambda_{\max}[n]}{\lambda}\right) \right]^+}, \quad (2.35)$$

where λ is the solution to the waterfilling problem

$$\frac{\sigma_n^2}{c_2 N_c} \sum_{n=0}^{N_c-1} \left[\frac{\ln(\lambda_{\max}[n]/\lambda)}{\lambda_{\max}[n]} \right]^+ = 1. \quad (2.36)$$

For high SNR, i.e., $\sigma_n^2 \ll 1$, $\lambda_{\max}[n] > \lambda$, $0 \leq n < N_c$, holds and the sub-carrier BER can be calculated as $\text{BER}[n] = c_1 \lambda / \lambda_{\max}[n]$, where $\lambda = \exp([\sum_{n=0}^{N_c-1} (\ln(\lambda_{\max}[n]) / \lambda_{\max}[n]) - c_2 N_c / \sigma_n^2] / [\sum_{n=0}^{N_c-1} 1 / \lambda_{\max}[n]])$, cf. (2.9), (2.28), (2.35), and (2.36). This means for high SNR the sub-carrier BER is inversely proportional to the maximum sub-carrier eigenvalue $\lambda_{\max}[n]$.

2) *Max-Min Criterion:* Exploiting (2.13) also for the max-min criterion, it can be shown that the optimum solution has again the general form given by (2.16) with

$$\alpha[n] = \left(\frac{\lambda_{\max}[n]}{N_c} \sum_{n=0}^{N_c-1} \frac{1}{\lambda_{\max}[n]} \right)^{-\frac{1}{2}}. \quad (2.37)$$

This means that for the max-min criterion and $L_g = N_c$ all sub-carrier SNRs are equal to $\text{SNR}[n] = N_c / (\sigma_n^2 \sum_{n=0}^{N_c-1} 1 / \lambda_{\max}[n])$. Therefore, in contrast to the minimum average BER solution, for the max-min solution all sub-carriers have identical BERs.

2.4.3 Solution of the Optimization Problems for $L_g < N_c$

Since \mathbf{F} is not invertible for $L_g < N_c$, we present alternative approaches for solving the BER optimization problems in this subsection.

1) *Average BER Criterion:* For convenience we rewrite (2.29), (2.30) as

$$\min_{\mathbf{g}} \sum_{n=0}^{N_c-1} \exp \left(-\frac{c_2}{\sigma_n^2} \mathbf{g}^H \mathbf{M}[n] \mathbf{g} \right) \quad (2.38)$$

$$\text{s.t.} \quad \mathbf{g}^H \mathbf{g} = 1, \quad (2.39)$$

where $\mathbf{M}[n]$ was defined in Section 2.3. Unfortunately, the objective function in (2.38) is not a convex function, i.e., (2.38), (2.39) is not a convex optimization problem. Therefore, similar to Section 2.3.3, we first pursue a relaxation approach to find a suboptimum solution

to the problem. In particular, letting again $\mathbf{S} = \mathbf{g}\mathbf{g}^H$ we can rewrite (2.38), (2.39) as

$$\min_{\mathbf{S}} \sum_{n=0}^{N_c-1} \exp\left(-\frac{c_2}{\sigma_n^2} \text{trace}(\mathbf{H}[n]\mathbf{F}[n]\mathbf{S}\mathbf{F}^H[n]\mathbf{H}^H[n])\right) \quad (2.40)$$

$$\text{s.t.} \quad \text{trace}\{\mathbf{S}\} \leq 1, \quad (2.41)$$

$$\mathbf{S} \succeq 0, \quad (2.42)$$

$$\text{rank}\{\mathbf{S}\} = 1. \quad (2.43)$$

The equivalent optimization problem (2.40)–(2.43) is still non-convex due to the rank condition in (2.43) but can be relaxed to a convex SDP problem by dropping this rank condition. The resulting convex problem has similar properties as the relaxed convex problem in the AMI case. In particular, a (possibly suboptimum) solution to the original minimum BER problem is given by that eigenvector of the optimum \mathbf{S} which corresponds to its maximum eigenvalue. Furthermore, the complexity of the relaxed problem again strongly depends on N_c , and becomes prohibitive for a moderate number of sub-carriers (e.g. $N_c \geq 64$).

2) *Max-Min Criterion:* For the max-min criterion, we may rewrite (2.31), (2.32) as

$$\max_{\mathbf{g}} \min_{\forall n} \mathbf{g}^H \mathbf{M}[n] \mathbf{g} \quad (2.44)$$

$$\text{s.t.} \quad \mathbf{g}^H \mathbf{g} = 1, \quad (2.45)$$

which constitutes a quadratic objective quadratic constraint (QOQC) NP-hard problem [71]. This problem can be restated in equivalent form as [71]

$$\max \quad t \tag{2.46}$$

$$\text{s.t.} \quad \text{trace}\{\mathbf{S}\} \leq 1, \tag{2.47}$$

$$\text{trace}\{\mathbf{M}[n]\mathbf{S}\} \geq t, \quad \forall n, \tag{2.48}$$

$$\mathbf{S} \succeq 0, \tag{2.49}$$

$$\text{rank}\{\mathbf{S}\} = 1. \tag{2.50}$$

By dropping the rank condition (2.50) the optimization problem (2.46)–(2.50) can be relaxed to an SDP problem. Unlike the SDP problems for the maximum AMI and the minimum average BER criteria, the complexity of the SDP problem (2.46)–(2.49) is dominated by L_g and not by N_c . Since we are mainly interested in the case where $L_g \ll N_c$, the relaxed problem for the max–min criterion can be solved even for large N_c (e.g. $N_c \geq 256$) using standard software (e.g. “SeDuMi”).

3) *Gradient Algorithm:* Unfortunately, for both relaxed optimization problems presented in this section the resulting \mathbf{S} has a high rank most of the time, and the dominant eigenvector of \mathbf{S} is a suboptimum solution which may entail a significant performance degradation. However, a GA may be used to recursively improve the initial C-BFF vector found through relaxation. In Table 2.1, we provide the GA for the average BER criterion since this is our primary BER-related criterion. However, if the average BER SDP problem (2.40)–(2.42) cannot be solved since the number of sub-carriers N_c is too large, we use the solution found for the max–min SDP problem (2.46)–(2.49) for initialization of the GA. In this context, we note that the initial vector \mathbf{g}_0 seems to have a larger impact on the quality of the solution found by the GA for the minimum BER criterion than for the max-

imum AMI criterion discussed in Section 2.3. Nevertheless, for the speed of convergence of the GA for the minimum BER criterion, similar statements hold as for the GA for the maximum AMI criterion.

2.5 Finite-Rate Feedback and Comparison

In this section, we briefly discuss codebook design for finite-rate feedback channels based on the GVQ algorithm in [62]. Furthermore, we also compare TD-BF with interpolation-based FD-BF [2, 3, 27].

2.5.1 Finite-Rate Feedback Case

Vector quantization can be used to design a codebook \mathcal{G} of size N for the finite-rate feedback channel case, cf. Section 2.2.4. Here, we adopt the GVQ algorithm introduced in [62]. For this purpose a set $\mathcal{H} \triangleq \{\mathbf{h}_1, \mathbf{h}_2, \dots, \mathbf{h}_T\}$ of T channel vectors \mathbf{h}_n is generated. Thereby, the $N_T N_R L$ -dimensional vector \mathbf{h}_n contains the CIR coefficients of all $N_T N_R$ CIRs of the n th MIMO channel realization. For each of these channel realizations the corresponding C-BFF vector $\mathbf{g} = \bar{\mathbf{g}}_n$ is generated using the GA for the maximum AMI criterion or the GA for the minimum BER criterion, cf. Table 2.1, yielding the set $\mathcal{G}_T \triangleq \{\bar{\mathbf{g}}_1, \bar{\mathbf{g}}_2, \dots, \bar{\mathbf{g}}_T\}$. The vector quantizer can then be represented as a function $\mathcal{Q}: \mathcal{G}_T \rightarrow \mathcal{G}$. Ideally, this function is optimized for minimization of the *mean quantization error*

$$\text{MQE} \triangleq \frac{1}{T} \sum_{i=1}^T d(\mathcal{Q}(\bar{\mathbf{g}}_i), \bar{\mathbf{g}}_i), \quad (2.51)$$

where $d(\hat{\mathbf{g}}_m, \bar{\mathbf{g}}_i)$ denotes the distortion caused by quantizing $\bar{\mathbf{g}}_i \in \mathcal{G}_T$ to $\hat{\mathbf{g}}_m \in \mathcal{G}$. The distortion measure depends on the optimization criterion and is given by

$$d(\hat{\mathbf{g}}_m, \bar{\mathbf{g}}_i) \triangleq - \sum_{n=0}^{N_c-1} \log_2 (1 + \text{SNR}_{(\hat{\mathbf{g}}_m, \mathbf{h}_i)}[n]) \quad (2.52)$$

and

$$d(\hat{\mathbf{g}}_m, \bar{\mathbf{g}}_i) \triangleq \sum_{n=0}^{N_c-1} \exp(-c_2 \text{SNR}_{(\hat{\mathbf{g}}_m, \mathbf{h}_i)}[n]) \quad (2.53)$$

for the maximum AMI and the minimum BER criterion, respectively. Here, $\text{SNR}_{(\hat{\mathbf{g}}_m, \mathbf{h}_i)}[n]$ is defined in (2.9) and the subscripts indicate that $\mathbf{G}[n]$ and $\mathbf{H}[n]$ have to be calculated for $\hat{\mathbf{g}}_m$ and \mathbf{h}_i , respectively. With this definition for the distortion measure the GVQ algorithm given in [62, Section IV] can be straightforwardly applied to find \mathcal{G} . We omit here further details and refer the interested reader to [61, 62] and references therein.

Once the off-line optimization of the codebook is completed, \mathcal{G} is conveyed to the transmitter and the receiver. For a given channel realization \mathbf{h} the receiver selects that C-BFF $\hat{\mathbf{g}}_m \in \mathcal{G}$ which minimizes the distortion measure (2.52) [AMI criterion] or (2.53) [BER criterion] and feeds back the corresponding index to the transmitter.

2.5.2 Comparison with FD-BF

We compare TD-BF with FD-BF in terms of feedback requirements and computational complexity.

1) *Feedback Requirements:* The required number of complex feedback symbols S for TD-BF, interpolation-based FD-BF with modified spherical (MS-FD-BF) [2], Grassmannian (GS-FD-BF) [27], and geodesic (GD-FD-BF) [3] interpolation, and ideal FD-BF are summarized in Table 2.2, where K denotes the cluster size in interpolation-based FD-BF [2], i.e., N_c/K is the number of sub-carriers for which CSI is assumed to be available at the

Table 2.2: Feedback Requirements for TD-BF, ideal FD-BF, and FD-BF with modified spherical (MS), Grassmannian (GS), and geodesic (GD) interpolation.

BF Scheme	Number of Complex Feedback Symbols per Frame
Ideal FD-BF	$S = N_c N_T$
MS-FD-BF [2]	$S = \frac{N_c}{K} (N_T + 1)$
GS-FD-BF [27] and GD-FD-BF [3]	$S = \frac{N_c}{K} N_T$
Proposed TD-BF	$S = N_T L_g$

transmitter. We will use S to compare the feedback requirements of TD-BF and FD-BF in Section 2.6.

2) *Computational Complexity:* The calculation of the C-BFFs and the GVQ-based codebook design for the proposed TD-BF scheme are more involved than the calculation of the BF weights and the codebook design method adopted in [2, 3, 27] for FD-BF, respectively. However, in practice, codebook design is done very infrequently. In fact, if the statistical properties of the MIMO channel do not change (as is typically the case in downlink scenarios), the codebook has to be designed only once. Therefore, in practice, the computational effort for C-BFF calculation and codebook design can be neglected. The interpolation of BF weights in FD-BF has to be done in every frame. The interpolation complexity is generally proportional to N_c but strongly depends on the interpolator used. For example, modified spherical interpolation requires a grid search whereas Grassmannian and geodesic interpolation do not. Assuming a codebook of size N selecting the beamformer index at the receiver requires evaluation of N and NN_c/K distortion measures for TD-BF and interpolation-based FD-BF, respectively. However, a fair quantitative comparison of the associated complexities is difficult since the required N to achieve a similar performance may be very different in both cases.

Similar to [63] we assume that the inverse IDFTs and the BF itself dominate the complexities of TD-BF and FD-BF. As is customary in the literature, we adopt the required

number of complex multiplications as measure for complexity and assume that the (I)DFT is implemented as a (inverse) fast Fourier transform ((I)FFT). Following [2] we assume that one (I)FFT operation requires $N_c \log_2(N_c)/2$ complex multiplications. Therefore, since FD-BF requires N_T IFFT operations and $N_T N_c$ complex multiplications for BF, a total of

$$M_{\text{FD}} = \frac{N_T N_c}{2} \log_2(N_c) + N_T N_c \quad (2.54)$$

complex multiplications are obtained. In contrast, assuming a straightforward TD implementation of convolution,

$$M_{\text{TD}} = \frac{N_c}{2} \log_2(N_c) + L_g N_T N_c \quad (2.55)$$

complex multiplications are required for TD-BF. A comparison of M_{FD} and M_{TD} shows that the complexity of TD-BF is lower than that of FD-BF if

$$L_g < \frac{N_T - 1}{2N_T} \log_2(N_c) + 1. \quad (2.56)$$

For example, assuming $N_c = 512$ sub-carriers and $N_T = 2$, $3 \leq N_T < 9$, and $N_T \geq 9$ TD-BF requires a lower complexity than FD-BF for $L_g \leq 3$, $L_g \leq 4$, and $L_g \leq 5$, respectively. Our results in Section 2.6 show that generally a high performance can be achieved with these small values of L_g .

2.6 Simulation Results

In this section, we present simulation results for the AMI and the BER of MIMO-OFDM with TD-BF. Besides the uncoded BER, we also consider the BER of a coded system employing the popular bit interleaved coded modulation (BICM) concept, since the com-

bination of BICM and OFDM has been adopted in various recent standards, cf. e.g. [20]. However, first we briefly discuss the parameters used in our simulations.

2.6.1 Simulation Parameters

Throughout this section we consider a MIMO-OFDM system with $N_T = 2$ or $N_T = 3$ transmit antennas, $N_R = 1$ receive antenna, and $N_c = 512$ OFDM sub-carriers. If BICM is employed, the data bits are encoded with the quasi-standard $(171, 133)_8$ convolutional code of rate $R_c = 1/2$, possibly punctured, interleaved, and Gray mapped to the data symbols $D[\cdot]$ [20, 25]. At the receiver standard Viterbi soft decoding is applied. For all BER results 16-QAM was used. For practical relevance we adopted for our simulations the IEEE 802.11n Channel Model B with $L = 9$ assuming a carrier frequency of 2.5 GHz and a transmit antenna spacing of $\lambda_0/2$, where λ_0 is the wavelength [72]. All simulation results were averaged over 100,000 independent channel realizations. For $L_g < N_c$ the C-BFF vectors were calculated with the algorithms given in Table 2.1. The all-ones vector and the solution of the relaxed max-min problem were used for initialization of the GAs for the maximum AMI and the minimum BER criterion, respectively. For $L_g = N_c$ (equivalent to ideal FD-BF) the closed-form solutions for the C-BFF provided in Sections 2.3.2 and 2.4.2 were used. For the finite-rate feedback case the C-BFF vector codebook was generated with the GVQ algorithm discussed in Section 2.5.1 based on a training set of $T = 1000$ independent channel realizations.

2.6.2 Maximum AMI Criterion

We first consider TD-BF with AMI-optimized C-BFFs and compare its performance with that of MS-FD-BF [2] and GD-FD-BF [3], respectively. We note that in [2] an AMI criterion is used for interpolator optimization, whereas the interpolator optimization in [3]

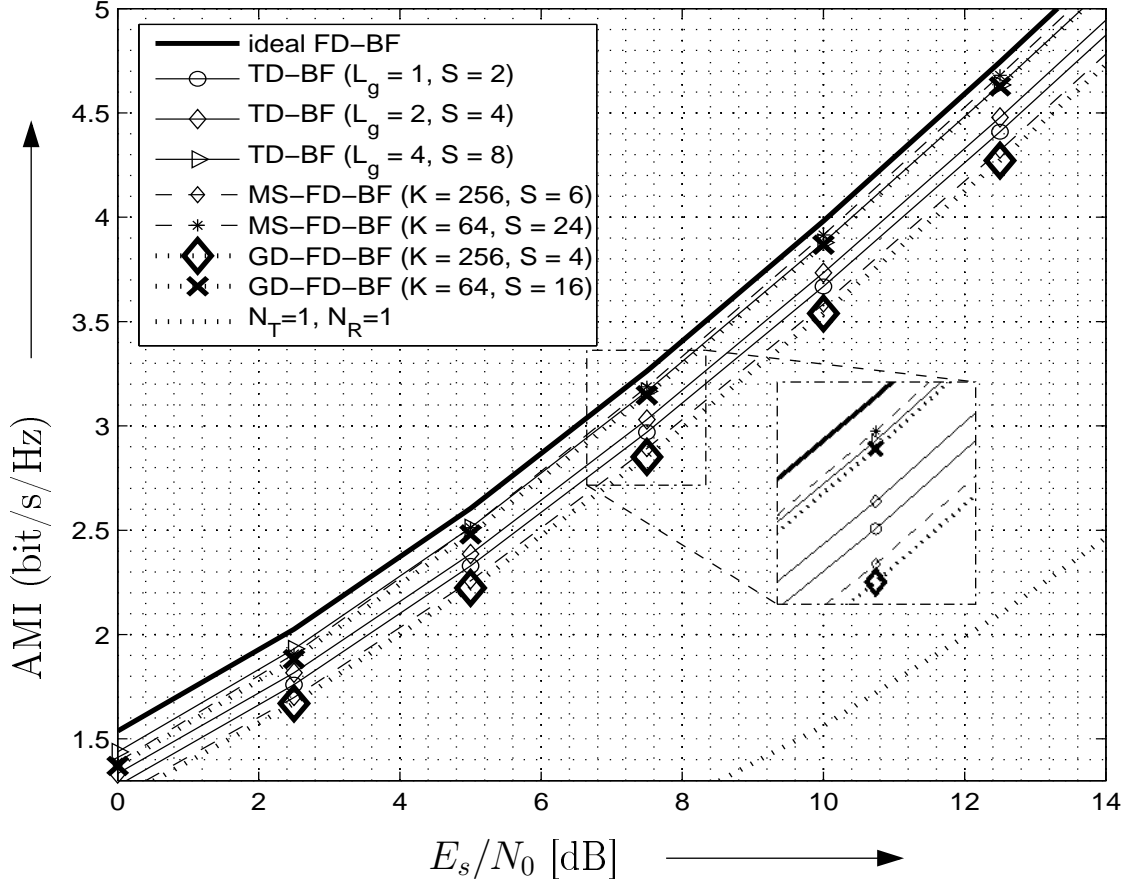


Figure 2.2: AMI of TD-BF (AMI criterion), MS-FD-BF [2], and GD-FD-BF [3] with perfect CSI. $N_T = 2$, $N_R = 1$, $N_c = 512$, and IEEE 802.11n Channel Model B. For comparison the AMIs for ideal FD-BF and single-input single-output (SISO) transmission ($N_T = 1$, $N_R = 1$) are also shown.

is not directly tied to the AMI or BER. Throughout this subsection $N_T = 2$ is valid.

Fig. 2.2 shows the AMI per sub-carrier vs. E_s/N_0 (E_s : energy per received symbol, N_0 : power spectral density of underlying continuous-time passband noise process) for the proposed TD-BF, MS-FD-BF, and GD-FD-BF for the case of perfect CSI at the transmitter. To facilitate a fair comparison between TD-BF with C-BFFs of length L_g and FD-BF with cluster size K , we have included in the legend of Fig. 2.2 the respective required number of complex feedback symbols S , cf. Table 2.2. As can be observed, TD-

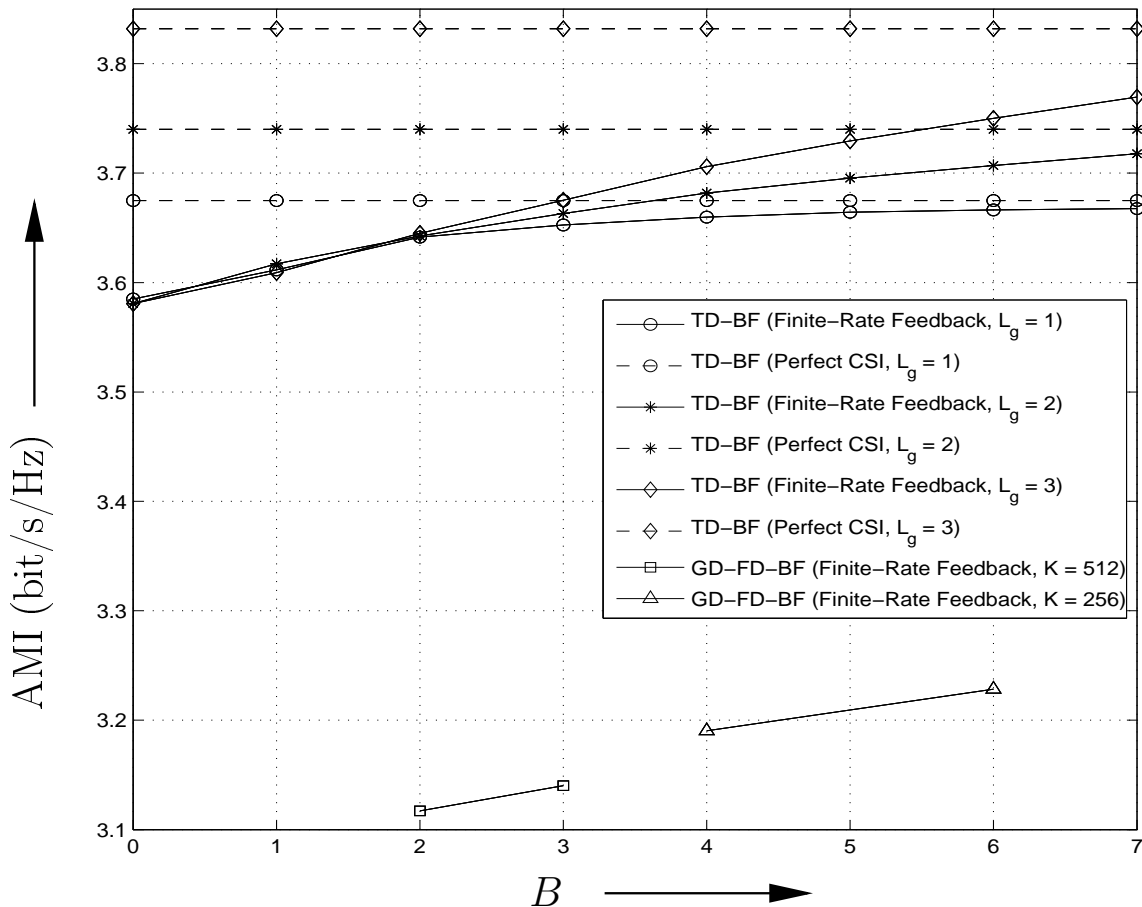


Figure 2.3: AMI of TD-BF (AMI criterion) vs. number of feedback bits B per channel update. $N_T = 2$, $N_R = 1$, $N_c = 512$, $E_s/N_0 = 10$ dB, and IEEE 802.11n Channel Model B. For comparison the AMIs for GD-FD-BF with codebooks from [4] are also shown.

BF provides a better performance/feedback trade-off than interpolation-based FD-BF. For example, TD-BF with $S = 2$ ($L_g = 1$) outperforms MS-FD-BF and GD-FD-BF with $S = 6$ ($K = 256$) and $S = 4$ ($K = 256$), respectively. MS-FD-BF with $S = 24$ ($K = 64$) is necessary to outperform TD-BF with $S = 8$ ($L_g = 4$) which performs only less than 0.5 dB worse than ideal FD-BF.

In Fig. 2.3, we consider the AMI of TD-BF with finite-rate feedback channel as a

function of the number of feedback bits B (solid lines) for an SNR of $E_s/N_0 = 10$ dB. For comparison, Fig. 2.3 also contains the AMI for TD-BF with perfect CSI (dashed lines) and the AMIs for GD-FD-BF with the best known codebooks from [4] and $K = 512$ and $K = 256$. For $B = 0$ the codebook has just one entry and no feedback is required. As can be observed from Fig. 2.3, finite-rate feedback TD-BF approaches the performance of the perfect CSI case as B increases. Furthermore, as expected, the number of feedback bits required to approach the perfect CSI case increases with increasing L_g . The performance of the GD-FD-BF scheme is significantly worse than that of the TD-BF scheme for the same number of feedback bits. From further simulations we have observed that GD-FD-BF requires more than $B = 80$ feedback bits to achieve the same performance as TD-BF with 7 feedback bits and $L_g = 3$.

Fig. 2.4 shows the BERs of a coded MIMO-OFDM system ($R_c = 1/2$) employing TD-BF, MS-FD-BF, and GD-FD-BF vs. E_b/N_0 , where E_b denotes the average energy per information bit. Both perfect CSI and finite-rate feedback are considered. With perfect CSI at the transmitter, at a BER of 10^{-4} the performance of TD-BF with $S = 6$ is about 0.8 dB and 0.77 dB worse than that of MS-FD-BF with $S = 48$ and GD-FD-BF with $S = 64$, respectively. However, in case of finite-rate feedback the performance of TD-BF with $B = 7$ is slightly better than that of GD-FD-BF with $B = 64$ and MS-FD-BF with $B = 80$, where we adopted the codebooks from [4] for GD-FD-BF and MS-FD-BF, respectively.

2.6.3 Minimum BER Criterion

Now, we shift our attention to TD-BF with BER-optimized C-BFFs. $N_T = 2$ is still valid.

Assuming perfect CSI we show in Fig. 2.5 the average BERs for the average BER criterion and the max-min criterion, respectively. As expected, for $L_g = N_c$ (ideal FD-

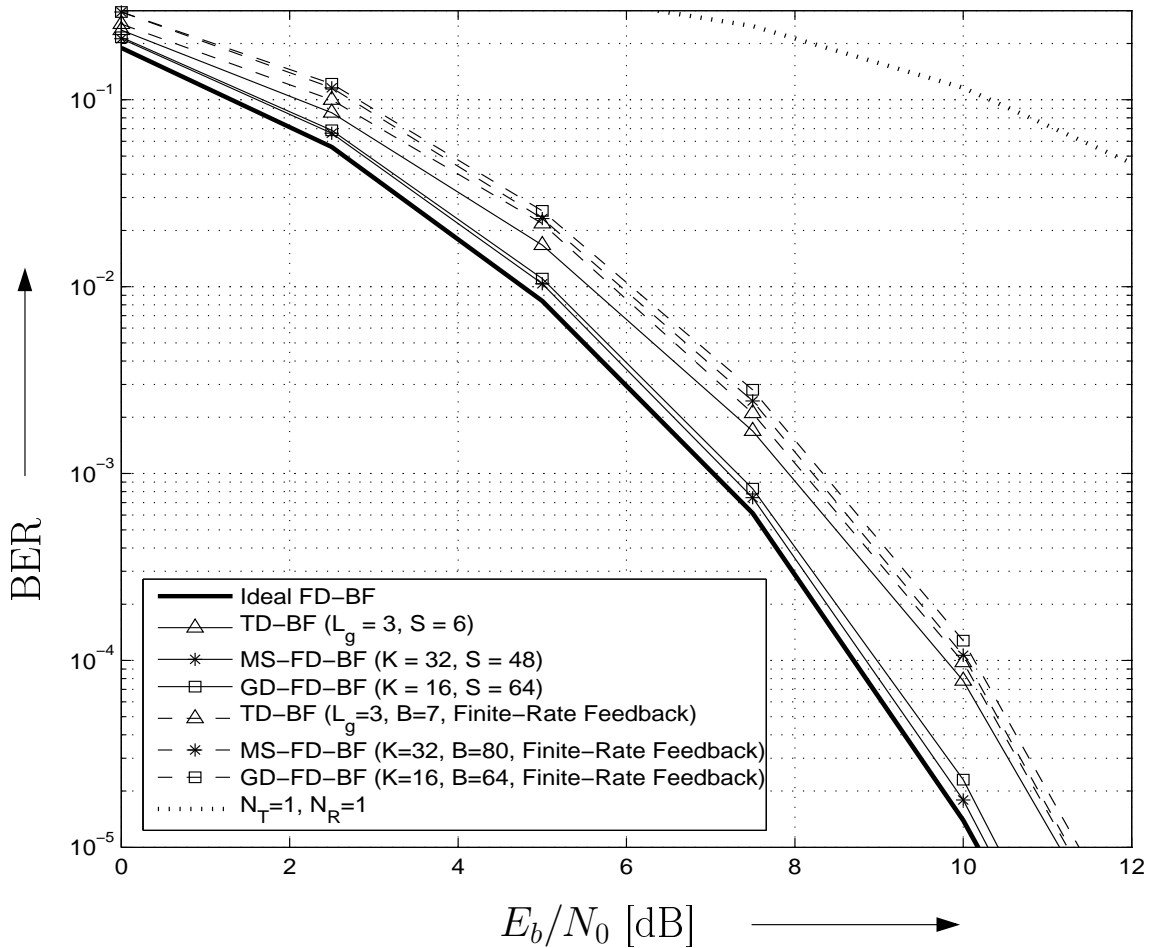


Figure 2.4: BER of coded MIMO-OFDM system with TD-BF (AMI criterion), MS-FD-BF [2], and GD-FD-BF [3]. Perfect CSI and finite-rate feedback, $N_T = 2$, $N_R = 1$, $N_c = 512$, $R_c = 1/2$, and IEEE 802.11n Channel Model B. For comparison the BERs for ideal FD-BF and SISO transmission ($N_T = 1$, $N_R = 1$) are also shown.

BF) the average BER criterion leads to a lower average BER than the max-min criterion. However, the difference between both criteria is less than 1 dB at $\text{BER} = 10^{-3}$. For $L_g = 1$ and $L_g = 5$ we show the average BER obtained for the relaxed max-min criterion. As can be observed the performance is quite poor in this case and a comparison with single-antenna transmission ($N_T = 1$) suggests that the diversity offered by the second antenna

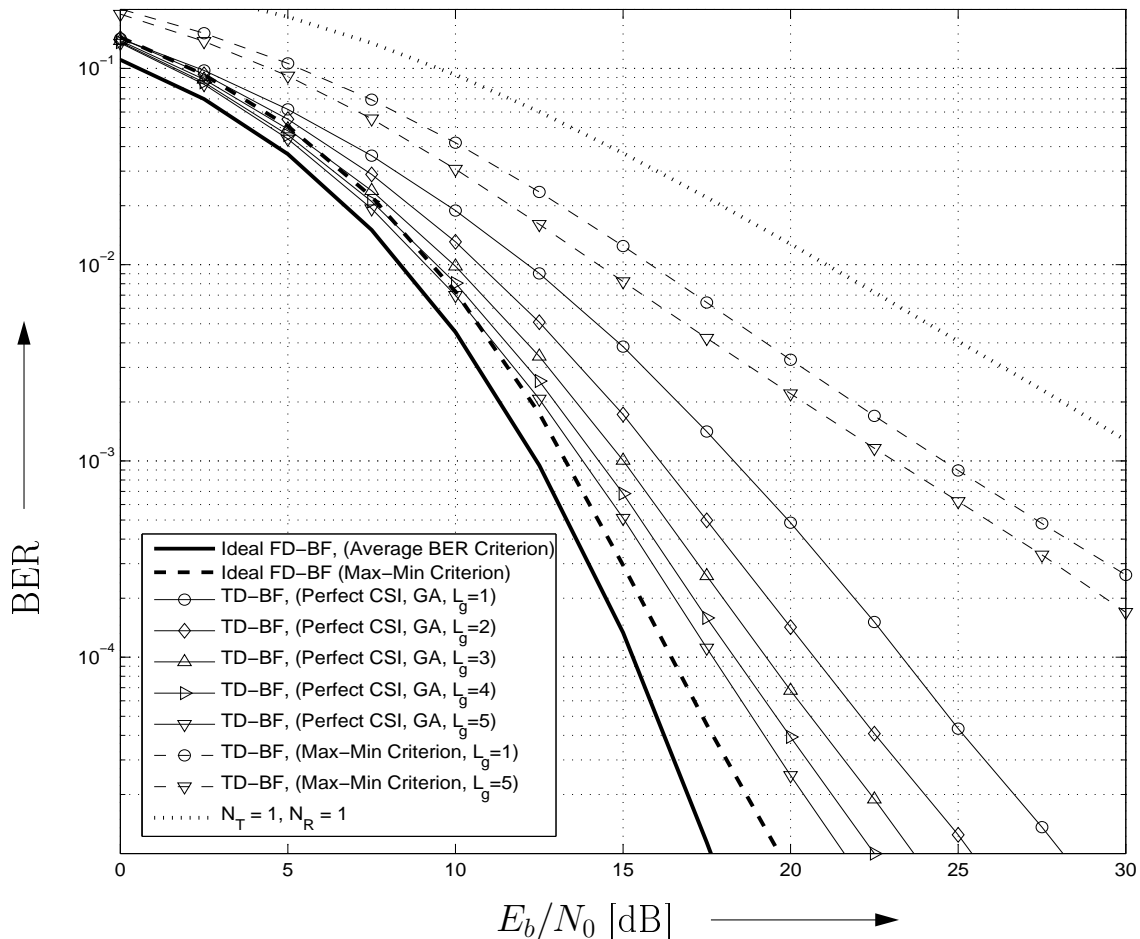


Figure 2.5: Average BER of uncoded MIMO-OFDM system with TD-BF. Minimum average BER criterion (solid lines) and max-min criterion (dashed lines), perfect CSI, $N_T = 2$, $N_R = 1$, $N_c = 512$, and IEEE 802.11n Channel Model B. For comparison the BERs for ideal FD-BF and SISO transmission ($N_T = 1$, $N_R = 1$) are also shown.

is not exploited. However, Fig. 2.5 clearly shows that this diversity can be exploited if the GA is used to improve the relaxed max-min solution. In this case, the BER approaches the BER of the limiting $L_g = N_c$ case as L_g increases. For example, for $L_g = 5$ the performance loss compared to $L_g = N_c = 512$ is less than 1.5 dB at $\text{BER} = 10^{-3}$.

In Fig. 2.6, we investigate the effect of a finite-rate feedback channel on the average BER. In particular, we show the average BER as a function of the number of feedback bits B

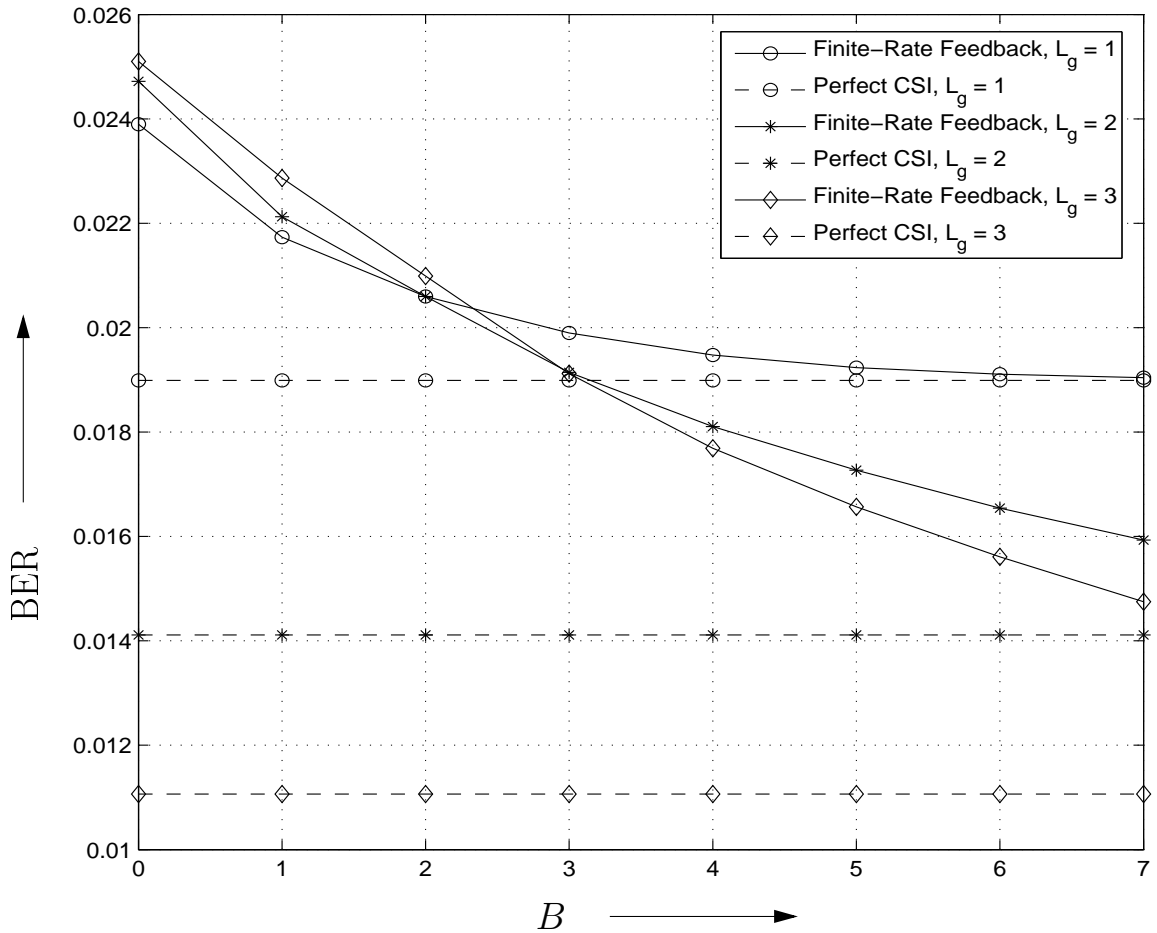


Figure 2.6: Average BER of uncoded MIMO-OFDM system with TD-BF (average BER criterion) vs. number of feedback bits B per channel update. GA was used for C-BFF optimization. $N_T = 2$, $N_R = 1$, $N_c = 512$, $E_b/N_0 = 10$ dB, and IEEE 802.11n Channel Model B.

(solid lines) for an SNR of $E_b/N_0 = 10$ dB. For comparison, Fig. 2.6 also contains the BERs for perfect CSI (dashed lines). As can be observed, finite-rate feedback BF approaches the performance of the perfect CSI case as B increases. Furthermore, as expected, the number of feedback bits required to approach the perfect CSI case increases with increasing L_g . Therefore, smaller L_g are preferable if only few feedback bits can be afforded.

In Fig. 2.7 we show the average BER for uncoded and coded ($R_c = 1/2$) transmission

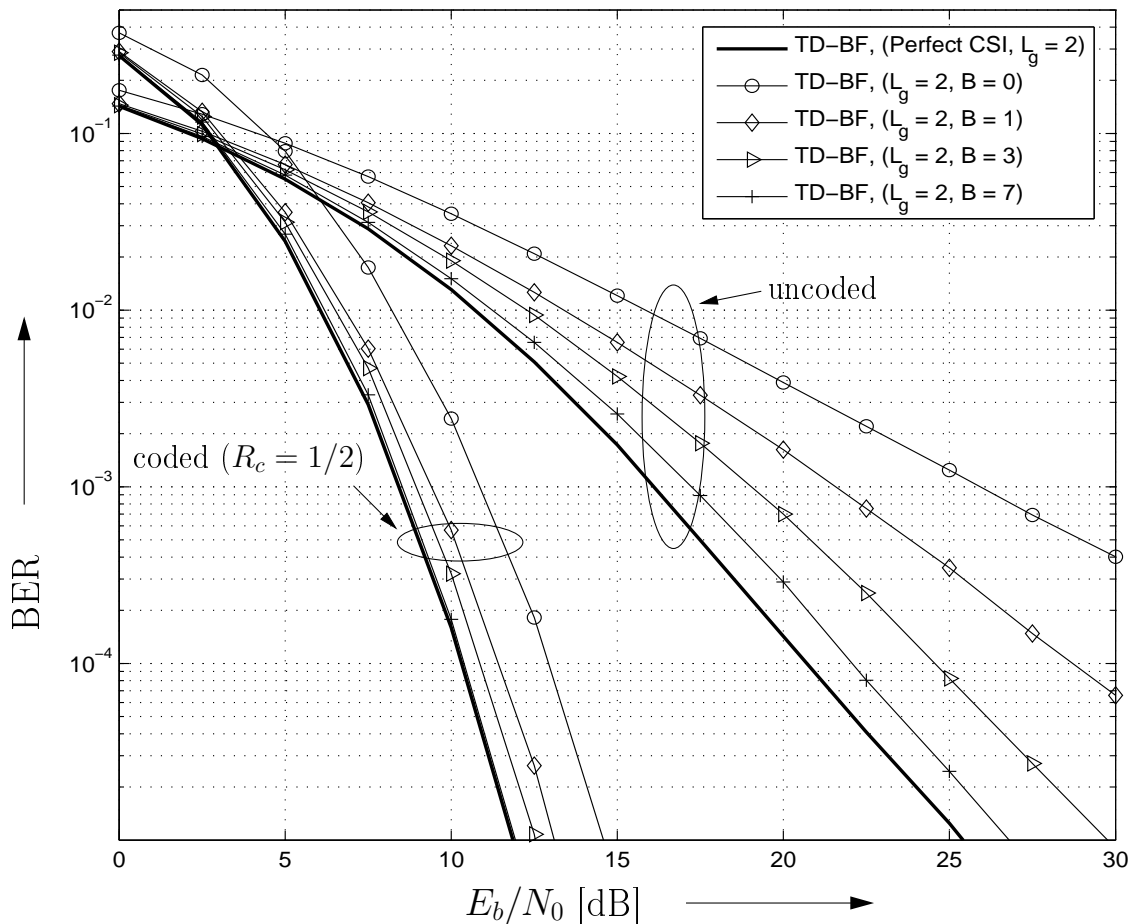


Figure 2.7: Average BER of uncoded and coded MIMO-OFDM system with TD-BF (average BER criterion). GA was used for C-BFF optimization and $L_g = 2$ is valid for all curves shown. Perfect CSI (bold lines) and finite-rate feedback channel, $N_T = 2$, $N_R = 1$, $N_c = 512$, and IEEE 802.11n Channel Model B.

with finite-rate feedback TD-BF and TD-BF with perfect CSI, respectively. C-BFFs of length $L_g = 2$ were used in all cases and the C-BFF vector codebook was optimized for $E_b/N_0 = 10$ dB. Interestingly, for coded transmission significantly fewer feedback bits are required to approach the performance of the perfect CSI case than for uncoded transmission. For example, for $\text{BER} = 10^{-4}$ and $B = 3$ feedback bits the performance loss compared to perfect CSI is 0.45 dB and 3.8 dB for coded and uncoded transmission, respectively.

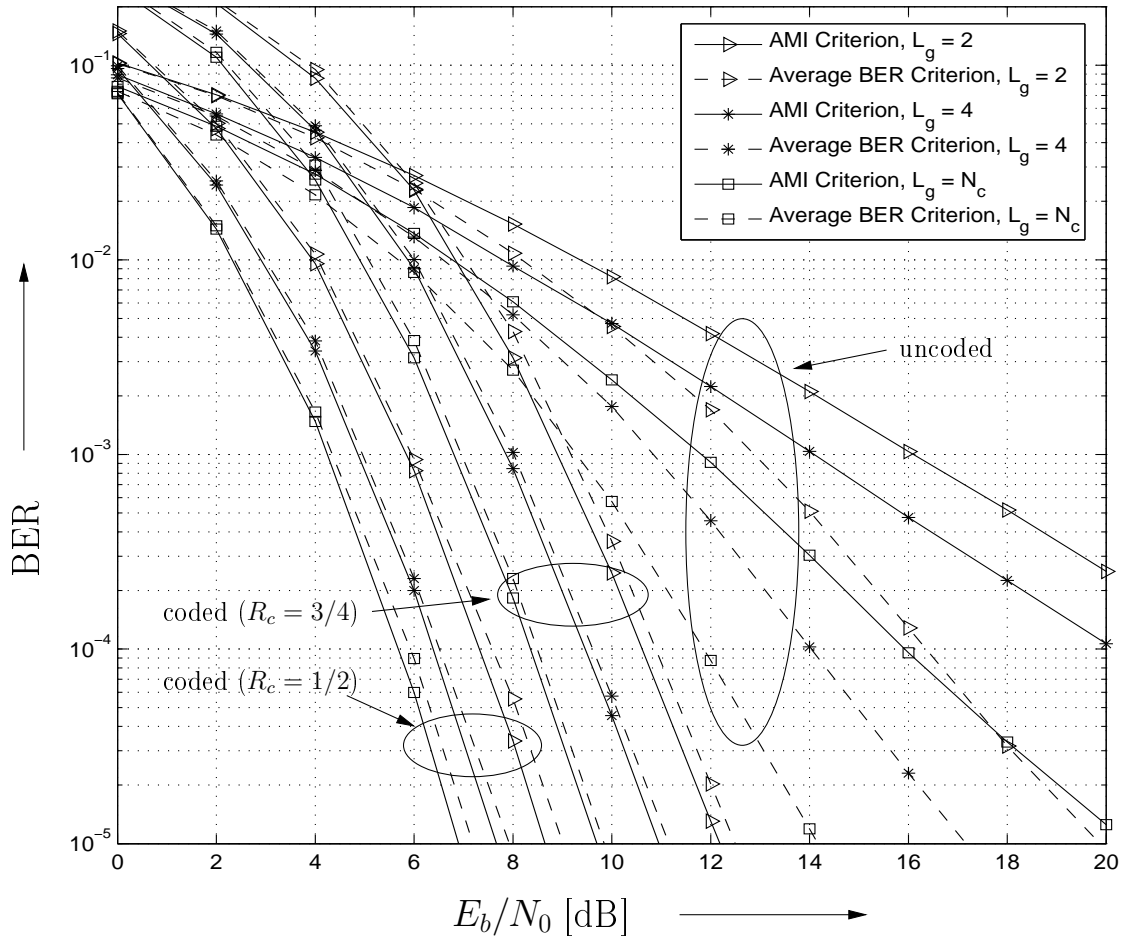


Figure 2.8: Average BER of uncoded and coded MIMO-OFDM system employing TD-BF with perfect CSI. Average BER criterion (dashed lines) and AMI criterion (solid lines), $N_T = 3$, $N_R = 1$, $N_c = 512$, and IEEE 802.11n Channel Model B.

2.6.4 Comparison of Maximum AMI and Minimum BER

Criteria

In Fig. 2.8, we compare the average BERs of uncoded and coded MIMO-OFDM systems employing minimum average BER (dashed lines) and maximum AMI (solid lines) TD-BF, respectively. We assume perfect CSI, $N_T = 3$, $L_g = 2, 4$, and N_c (ideal FD-BF). As one would expect, for uncoded transmission the minimum average BER criterion yields a

significantly better performance than the maximum AMI criterion. However, although the employed convolutional codes are by no means capacity achieving, for the coded case the maximum AMI criterion yields a lower BER than the minimum average BER criterion.

2.7 Conclusions

In this chapter, we have proposed a novel TD approach to BF in MIMO-OFDM systems. The C-BFFs have been optimized for maximization of the AMI and minimization of the BER, respectively, and efficient algorithms for recursive calculation of the optimum C-BFFs have been provided for both criteria. In contrast to existing FD-BF schemes, for TD-BF the number of complex feedback symbols to be conveyed to the transmitter is independent from the number of OFDM sub-carriers. For the case of a finite-rate feedback channel a GVQ algorithm has been introduced for codebook design. Simulation results for the IEEE 802.11n Channel Model B have confirmed the excellent performance of TD-BF and have shown that TD-BF achieves a more favorable performance/feedback rate trade-off than FD-BF.

Chapter 3

Cooperative Amplify-and-Forward Beamforming with Multiple Multi-Antenna Relays

3.1 Introduction

In the previous chapter, we have introduced a novel TD-BF scheme for direct point-to-point transmission. Starting from this chapter, we consider BF schemes for cooperative relay networks. Since the AF protocol is generally believed to be less complex than the DF protocol, we will consider AF in all the remaining chapters.

Recently, AF-BF for wireless relay networks was considered in [35]–[44] and [73]. AF-BF for networks with one single-antenna source and multiple single-antenna relays was considered in [39, 42] for individual relay power constraints, [35, 36, 40, 41] for a joint power constraint for all relays, and [73] for and a joint power constraint for the source and all relays, respectively. Since both the source and the relays were assumed to have only one antenna, respectively, the resulting SINR maximization problem at the destination involved only the optimization of one scalar BF gain for each relay. In contrast, in [37, 38], AF-BF for a network with a single relay and multiple antennas at the relay and the source was investigated and closed-form solutions for the BF vector at the source and the AF-BF

matrix at the relay were provided. Furthermore, in [43, 44], the performance of AF–BF with multiple antennas at the source and one single–antenna relay was investigated. We note that in practice a relay network may comprise multiple relays *and* both the relays and the source may have multiple antennas. The extension of the results in the aforementioned papers to this general case is not straightforward as it results in complex non–convex optimization problems for the AF–BF matrices at the relays and the BF vector at the source. We note that multiple multi–antenna relays were considered in [74]. However, in [74], DF relaying was assumed and the source had only a single antenna.

In this chapter, we consider AF–BF for networks with one multi–antenna source (e.g. a base station), multiple multi–antenna relays, and one single–antenna destination (e.g. a mobile phone). The SINR at the destination is adopted as performance criterion and the BF vector at the source and the AF–BF matrices at the relays are optimized under three different power constraints. In particular, we consider the cases of individual relay power constraints, a joint power constraint for all relays, and a joint source–relay power constraint. This chapter makes the following contributions:

- For a given BF vector at the source, we find the optimal AF–BF matrices at the relays for each of the three considered power constraints. In particular, we provide closed–form solutions for the AF–BF matrices for the individual and joint relay power constraints, respectively. For the joint source–relay power constraint, we derive the direction of the AF–BF matrices in closed form and provide a simple numerical method for finding the optimal power allocation for the source and the relays. In case of a single relay, this power allocation is given in closed form.
- For the joint relay and the joint source–relay power constraints, we show that the optimization problem for the source BF vector can be converted into a polynomial programming problem. Although this problem is non–convex, it can be efficiently

solved with the GloptiPoly or SOSTOOLS software tools [75, 76] for small scale networks (e.g. two antennas at the source and two relays with arbitrary numbers of antennas). For large scale networks and networks with individual relay power constraints, we provide efficient suboptimal methods for computation of the optimal source BF vector.

- To implement the proposed AF–BF scheme, the source node has to acquire the channel state information of all source–relay channels and the Euclidean norm of each relay–destination channel vector for computation of the optimal source BF vector. In contrast, for all considered power constraints, the relays have to know only their own source–relay and relay–destination channels if the source feeds back one complex scalar to each relay (individual power constraints), one complex scalar to all relays (joint relay power constraint), or one complex and one real scalar to all relays (joint source–relay power constraint).
- Our simulation results confirm that the proposed suboptimal optimization methods for the source BF vector achieve a close-to-optimal performance. Furthermore, our results show that increasing the number of antennas at the source is highly beneficial if the source–relay channels have a lower SNR than the relay–destination channels. In contrast, increasing the number of relays or the number of relay antennas is always beneficial.

The remainder of this chapter is organized as follows. In Section 3.2, the considered system model is presented and the proposed optimization problem is rigorously formulated. The optimization of the AF–BF matrices for maximization of the SINR for a given BF vector at the source is discussed in Section 3.3. In Section 3.4, the optimization of the source BF vector is investigated. Simulation results are provided in Section 3.5, and some conclusions are drawn in Section 3.6.

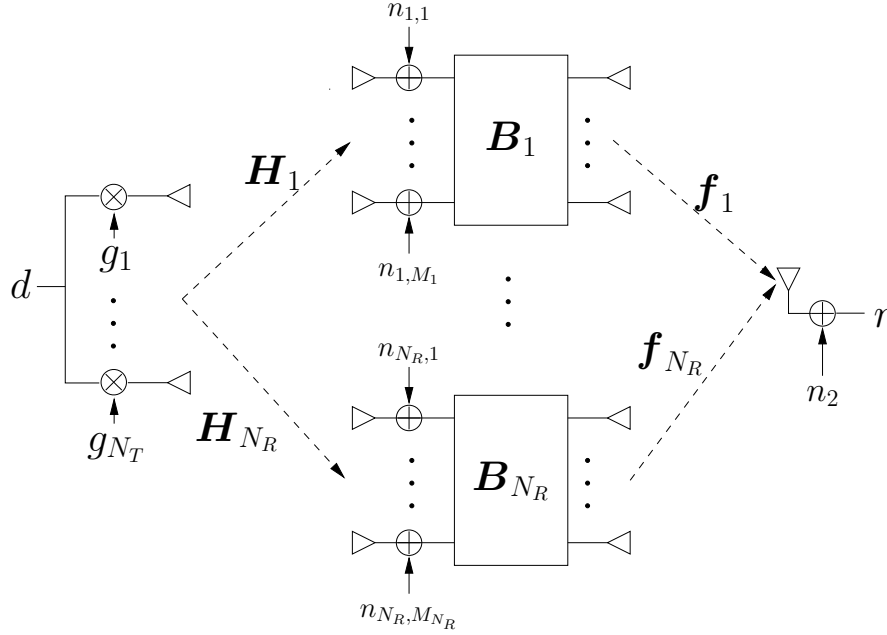


Figure 3.1: Cooperative network with one multi–antenna source, multiple multi–antenna relays, and one single–antenna destination. g_i , $1 \leq i \leq N_T$, denotes the i th element of source BF vector \mathbf{g} . $n_{i,\mu}$, $1 \leq \mu \leq M_i$, is the μ th element of noise vector $\mathbf{n}_{1,i}$ at relay i , $1 \leq i \leq N_R$.

3.2 System Model and Optimization Problem

We consider the downlink of a relay network with one source node, N_R relays, and one destination node. A block diagram of the discrete–time overall transmission system in equivalent complex baseband representation is shown in Fig. 3.1. We assume that N_T , M_i , and one antennas are available at the source (e.g. base station or access point), relay i , $1 \leq i \leq N_R$, and the destination (e.g. mobile phone), respectively. As usual, transmission is organized in two intervals. In the first transmission interval, the source node sends a data packet to the relays, which forward this packet to the destination node in the second transmission interval. We assume that there is no direct link between the source node and the destination node.

3.2.1 System Model

In the first transmission interval, the source transmits the elements of N_T -dimensional vector,

$$\mathbf{x} = \mathbf{g} d, \quad (3.1)$$

over its N_T antennas, where \mathbf{g} denotes the N_T -dimensional BF vector, and d is the modulated symbol taken from a scalar symbol alphabet \mathcal{A} with variance $\sigma_d^2 \triangleq \mathcal{E}\{|d|^2\} = 1$. The signal received at the M_i antennas of relay i , $1 \leq i \leq N_R$, can be modeled as

$$\mathbf{q}_i = \mathbf{H}_i \mathbf{x} + \mathbf{n}_{1,i}, \quad (3.2)$$

where $[\mathbf{H}_i]_{\mu\nu}$, $1 \leq \mu \leq M_i$, $1 \leq \nu \leq N_T$, is the channel gain between antenna ν of the source and antenna μ of relay i , and the elements of vector $\mathbf{n}_{1,i}$ represent AWGN with variance σ_1^2 .

In the second transmission interval, relay i transmits the μ th element of vector

$$\mathbf{s}_i = \mathbf{B}_i \mathbf{q}_i \quad (3.3)$$

over antenna μ , $1 \leq \mu \leq M_i$, where \mathbf{B}_i is an $M_i \times M_i$ AF-BF matrix. The received signal at the destination node is given by

$$r = \sum_{i=1}^{N_R} \mathbf{f}_i^T \mathbf{s}_i + n_2, \quad (3.4)$$

where the μ th element of M_i -dimensional vector \mathbf{f}_i is the channel gain between antenna μ , $1 \leq \mu \leq M_i$, of relay i and the destination node, and n_2 is AWGN with variance σ_2^2 .

Combining (3.1)–(3.4), the received signal at the destination node can be expressed as

$$r = \sum_{i=1}^{N_R} \mathbf{f}_i^T \mathbf{B}_i \mathbf{H}_i \mathbf{g} d + \sum_{i=1}^{N_R} \mathbf{f}_i^T \mathbf{B}_i \mathbf{n}_{1,i} + n_2 = \mathbf{f}^T \mathbf{B}_D \mathbf{H} \mathbf{g} d + \mathbf{f}^T \mathbf{B}_D \mathbf{n}_1 + n_2, \quad (3.5)$$

with relay–destination channel vector $\mathbf{f} \triangleq [\mathbf{f}_1^T \dots \mathbf{f}_{N_R}^T]^T$, AF–BF block diagonal matrix $\mathbf{B}_D \triangleq \text{diag}\{\mathbf{B}_1, \dots, \mathbf{B}_{N_R}\}$, $(\sum_{i=1}^{N_R} M_i) \times N_T$ source–relay channel matrix $\mathbf{H} \triangleq [\mathbf{H}_1^T \dots \mathbf{H}_{N_R}^T]^T$, and relay noise vector $\mathbf{n}_1 \triangleq [\mathbf{n}_{1,1}^T \dots \mathbf{n}_{1,N_R}^T]^T$.

3.2.2 Formulation of the Optimization Problem

From (3.5) the SINR at the destination node can be obtained as

$$\text{SINR} = \frac{|\mathbf{f}^T \mathbf{B}_D \mathbf{H} \mathbf{g}|^2}{\|\mathbf{f}^T \mathbf{B}_D\|_2^2 \sigma_1^2 + \sigma_2^2}. \quad (3.6)$$

The design problem considered in this chapter is the optimization of the BF vector \mathbf{g} at the source and the AF–BF matrices \mathbf{B}_i , $1 \leq i \leq N_R$, at the relays for maximization of the SINR at the destination node while constraining the power emitted by the source and the relays. Formally, the resulting optimization problem can be formulated as follows:

$$\max_{\mathbf{g}, \mathbf{B}_i, 1 \leq i \leq N_R} \quad \text{SINR} \quad (3.7a)$$

$$\text{s.t.} \quad \text{Power Constraints} \quad (3.7b)$$

For the power constraints, we consider three different scenarios:

Constraint I (Individual Power Constraints for Relays): If the transmit power of the

source and each relay is limited, the power constraints are given by

$$\|\mathbf{g}\|_2^2 \leq P_1, \quad (3.8a)$$

$$\|\mathbf{B}_i \mathbf{H}_i \mathbf{g}\|_2^2 + \sigma_1^2 \|\mathbf{B}_i\|_F^2 \leq P_{2,i}, \quad 1 \leq i \leq N_R, \quad (3.8b)$$

where P_1 and $P_{2,i}$ denote the maximum transmit powers of the source and relay i , respectively.

Constraint II (Joint Power Constraint for Relays): As an alternative to the individual relay power constraint, we may impose a joint relay power constraint resulting in

$$\|\mathbf{g}\|_2^2 \leq P_1, \quad (3.9a)$$

$$\sum_{i=1}^{N_R} (\|\mathbf{B}_i \mathbf{H}_i \mathbf{g}\|_2^2 + \sigma_1^2 \|\mathbf{B}_i\|_F^2) \leq P_2, \quad (3.9b)$$

where P_1 and P_2 denote the maximum transmit powers of the source and all relays, respectively.

Constraint III (Joint Power Constraint for Source and Relays): Finally, we may impose a joint power constraint on the source and the relays, which leads to

$$\|\mathbf{g}\|_2^2 + \sum_{i=1}^{N_R} (\|\mathbf{B}_i \mathbf{H}_i \mathbf{g}\|_2^2 + \sigma_1^2 \|\mathbf{B}_i\|_F^2) \leq P, \quad (3.10)$$

where P is the maximum total transmit power. Since Constraint I is more restrictive than Constraint II and Constraint II is more restrictive than Constraint III, we expect Constraint I to result in the lowest SINR in (3.7a) and Constraint III in the highest SINR among the three sets of constraints if the maximum overall power budget is the same, i.e., $P = P_1 + P_2$ and $P_2 = \sum_{i=1}^{N_R} P_{2,i}$.

In the next two sections, we will solve problem (3.7) for the three different constraints

in (3.8)–(3.10).

3.3 Optimal AF–BF Matrices

It is convenient to solve problem (3.7) in two steps. In Subsections 3.3.1–3.3.3, we determine the optimal AF–BF matrices \mathbf{B}_i , $1 \leq i \leq N_R$, for a given BF vector \mathbf{g} at the source under the three considered power constraints. The obtained solutions are compared in Subsection 3.3.4. The optimization of the BF vector will be tackled in Section 3.4. For the following, it is convenient to define vector $\mathbf{u}_i \triangleq \mathbf{H}_i \mathbf{g}$, $1 \leq i \leq N_R$.

3.3.1 AF–BF with Individual Power Constraints for Relays

Combining (3.7) and (3.8) we obtain the optimization problem

$$\max_{\mathbf{B}_i, 1 \leq i \leq N_R} \frac{\left| \sum_{i=1}^{N_R} \mathbf{f}_i^T \mathbf{B}_i \mathbf{u}_i \right|^2}{\sigma_1^2 \sum_{i=1}^{N_R} \mathbf{f}_i^T \mathbf{B}_i \mathbf{B}_i^H \mathbf{f}_i + \sigma_2^2} \quad (3.11a)$$

$$\text{s.t.} \quad \mathbf{u}_i^H \mathbf{B}_i^H \mathbf{B}_i \mathbf{u}_i + \sigma_1^2 \|\mathbf{B}_i\|_F^2 \leq P_{2,i}, \quad 1 \leq i \leq N_R, \quad (3.11b)$$

where we have ignored the source power constraint (3.8a) since \mathbf{g} is assumed to be fixed.

Next, we introduce the definitions $\mathbf{w}_i \triangleq \mathbf{u}_i^* \otimes \mathbf{f}_i^*$, $\mathbf{b}_i \triangleq \text{vec}\{\mathbf{B}_i\}$, $\mathbf{T}_i \triangleq \mathbf{I}_{M_i} \otimes \mathbf{f}_i^T$, and $\mathbf{Q}_i \triangleq \mathbf{u}_i^T \otimes \mathbf{I}_{M_i}$. With these definitions, we can rewrite problem (3.11) in equivalent form as

$$\max_{\mathbf{b}_i, 1 \leq i \leq N_R} \frac{\left| \sum_{i=1}^{N_R} \mathbf{w}_i^H \mathbf{b}_i \right|^2}{\sigma_1^2 \sum_{i=1}^{N_R} \mathbf{b}_i^H \mathbf{T}_i^H \mathbf{T}_i \mathbf{b}_i + \sigma_2^2} \quad (3.12a)$$

$$\text{s.t.} \quad \mathbf{b}_i^H \left(\mathbf{Q}_i^H \mathbf{Q}_i + \sigma_1^2 \mathbf{I}_{M_i^2} \right) \mathbf{b}_i \leq P_{2,i}, \quad 1 \leq i \leq N_R. \quad (3.12b)$$

For the next step, we introduce matrix \mathbf{J}_i , which is obtained from matrix $\mathbf{Q}_i^H \mathbf{Q}_i + \sigma_1^2 \mathbf{I}_{M_i^2} \triangleq \mathbf{J}_i^H \mathbf{J}_i$ via Cholesky decomposition, and vector $\mathbf{y}_i \triangleq \mathbf{J}_i \mathbf{b}_i$. Vector \mathbf{y}_i can be represented as $\mathbf{y}_i \triangleq \sqrt{\tilde{P}_{2,i}} \mathbf{x}_i$, where $\tilde{P}_{2,i} = \|\mathbf{y}_i\|_2^2$ and \mathbf{x}_i is a unit norm vector. Now, we can restate problem (3.12) as

$$\max_{\tilde{P}_{2,i}, \mathbf{x}_i, 1 \leq i \leq N_R} \frac{\left| \sum_{i=1}^{N_R} \sqrt{\tilde{P}_{2,i}} \mathbf{w}_i^H \mathbf{J}_i^{-1} \mathbf{x}_i \right|^2}{\sum_{i=1}^{N_R} \mathbf{x}_i^H \left(\sigma_1^2 \tilde{P}_{2,i} \mathbf{J}_i^{-H} \mathbf{T}_i^H \mathbf{T}_i \mathbf{J}_i^{-1} + \frac{\sigma_2^2}{N_R} \mathbf{I}_{M_i^2} \right) \mathbf{x}_i} \quad (3.13a)$$

$$\text{s.t.} \quad \|\mathbf{x}_i\|_2^2 = 1, \quad \tilde{P}_{2,i} \leq P_{2,i}, \quad 1 \leq i \leq N_R. \quad (3.13b)$$

Assuming that the powers $\tilde{P}_{2,i}$, $1 \leq i \leq N_R$, are fixed, we can find direction vectors \mathbf{x}_i , $1 \leq i \leq N_R$, that maximize (3.13a) by differentiating the objective function with respect to \mathbf{x}_i and by accounting for the constraint $\|\mathbf{x}_i\|_2^2 = 1$ by using Lagrange multipliers. After some algebraic manipulations, this leads to

$$\mathbf{x}_i = \alpha_i \left(\mathbf{J}_i^{-H} \mathbf{T}_i^H \mathbf{T}_i \mathbf{J}_i^{-1} + \beta_i \mathbf{I}_{M_i^2} \right)^{-1} \mathbf{J}_i^{-H} \mathbf{w}_i, \quad (3.14)$$

where α_i and β_i are complex and positive real constants, respectively, whose exact value is not important for the final result as will be shown in the following. In particular, using the definitions of \mathbf{J}_i , \mathbf{T}_i , and \mathbf{w}_i in (3.14), we obtain

$$\begin{aligned} \mathbf{x}_i &= \alpha_i \mathbf{J}_i \left(\mathbf{T}_i^H \mathbf{T}_i + \beta_i (\mathbf{Q}_i^H \mathbf{Q}_i + \sigma_1^2 \mathbf{I}_{M_i^2}) \right)^{-1} \mathbf{w}_i \\ &= \alpha_i \mathbf{J}_i \left((\mathbf{I}_{M_i} \otimes \mathbf{f}_i^T)^H (\mathbf{I}_{M_i} \otimes \mathbf{f}_i^T) + \beta_i (\mathbf{u}_i^T \otimes \mathbf{I}_{M_i})^H (\mathbf{u}_i^T \otimes \mathbf{I}_{M_i}) + \sigma_1^2 \beta_i \mathbf{I}_{M_i^2} \right)^{-1} \mathbf{w}_i \\ &= \alpha_i \mathbf{J}_i \left((\mathbf{I}_{M_i} \otimes \mathbf{f}_i^* \mathbf{f}_i^T) + (\beta_i (\mathbf{u}_i^* \mathbf{u}_i^T + \sigma_1^2 \mathbf{I}_{M_i}) \otimes \mathbf{I}_{M_i}) \right)^{-1} (\mathbf{u}_i^* \otimes \mathbf{f}_i^*), \end{aligned} \quad (3.15)$$

where we have used the identity $(\mathbf{A} \otimes \mathbf{B})(\mathbf{C} \otimes \mathbf{D}) = \mathbf{AC} \otimes \mathbf{BD}$ [77]. \mathbf{x}_i can be further simplified by introducing the Kronecker sum $(\mathbf{A} \otimes \mathbf{I}_M) + (\mathbf{I}_M \otimes \mathbf{B}) = \mathbf{A} \oplus \mathbf{B}$ in (3.15) and

exploiting the relation [78]

$$(\mathbf{M} \oplus \mathbf{N})^{-1} = \sum_{i=1}^M \sum_{j=1}^M \frac{(\mathbf{m}_i \otimes \mathbf{n}_j)(\bar{\mathbf{m}}_i \otimes \bar{\mathbf{n}}_j)^H}{\lambda_i(\mathbf{M}) + \lambda_j(\mathbf{N})}, \quad (3.16)$$

where \mathbf{m}_i , \mathbf{n}_i , $\bar{\mathbf{m}}_i$, and $\bar{\mathbf{n}}_i$ denote the eigenvectors of $M \times M$ matrices \mathbf{M} , \mathbf{N} , \mathbf{M}^H , and \mathbf{N}^H , respectively. This leads to

$$\begin{aligned} \mathbf{x}_i &= \alpha_i \mathbf{J}_i (\beta_i (\mathbf{u}_i^* \mathbf{u}_i^T + \sigma_1^2 \mathbf{I}_{M_i}) \oplus \mathbf{f}_i^* \mathbf{f}_i^T)^{-1} (\mathbf{u}_i^* \otimes \mathbf{f}_i^*) \\ &= \alpha_i \mathbf{J}_i \frac{\left(\frac{\mathbf{u}_i^*}{\|\mathbf{u}_i\|_2} \otimes \frac{\mathbf{f}_i^*}{\|\mathbf{f}_i\|_2} \right) \left(\frac{\mathbf{u}_i^*}{\|\mathbf{u}_i\|_2} \otimes \frac{\mathbf{f}_i^*}{\|\mathbf{f}_i\|_2} \right)^H}{\|\mathbf{f}_i\|_2^2 + \beta_i (\|\mathbf{u}_i\|_2^2 + \sigma_1^2)} (\mathbf{u}_i^* \otimes \mathbf{f}_i^*) \\ &= \frac{\alpha_i}{\|\mathbf{f}_i\|_2^2 + \beta_i (\|\mathbf{u}_i\|_2^2 + \sigma_1^2)} \mathbf{J}_i (\mathbf{u}_i^* \otimes \mathbf{f}_i^*). \end{aligned} \quad (3.17)$$

Exploiting (3.17) along with $\mathbf{b}_i = \sqrt{\tilde{P}_{2,i}} \mathbf{J}_i^{-1} \mathbf{x}_i$, we obtain for the AF-BF matrix \mathbf{B}_i the expression

$$\mathbf{B}_i = c_i \mathbf{f}_i^* \mathbf{u}_i^H, \quad 1 \leq i \leq N_R, \quad (3.18)$$

where complex scalar c_i has to be optimized taking into account the per-relay power constraint. Eq. (3.18) reveals that under a per-relay power constraint eigenbeamforming with respect to the source-relay and the relay-source channel is optimal. For the special case where the source and all relays have only a single antenna, i.e., \mathbf{f}_i and \mathbf{u}_i are scalars, this result has already been derived in [39].

Substituting (3.18) into problem (3.11), it is obvious that all c_i have to have the same phase θ to achieve the maximum SINR, i.e., $c_i = |c_i| e^{j\theta}$. The resulting optimization

problem is given by

$$\max_{|c_i|} \frac{\left(\sum_{i=1}^{N_R} |c_i| \|\mathbf{f}_i\|_2 \|\mathbf{u}_i\|_2\right)^2}{\sigma_1^2 \sum_{i=1}^{N_R} |c_i|^2 \|\mathbf{f}_i\|_2^2 + \sigma_2^2} \quad (3.19a)$$

$$\text{s.t.} \quad |c_i| \leq \sqrt{\frac{P_{2,i}}{\|\mathbf{u}_i\|_2^2 + \sigma_1^2}}, \quad 1 \leq i \leq N_R. \quad (3.19b)$$

Problem (3.19) is equivalent to the power allocation problem for relaying with multiple single–antenna relays, which was solved in [39]. For completeness, we provide the solution here using the notation of this chapter. Define

$$\phi_i = \frac{\|\mathbf{u}_i\|_2 \sqrt{\|\mathbf{u}_i\|_2^2 + \sigma_1^2}}{\sqrt{P_{2,i}} \|\mathbf{f}_i\|_2} \quad (3.20)$$

and sort ϕ_i in descending order $\phi_{\tau_1} \geq \phi_{\tau_2} \geq \dots \geq \phi_{\tau_{N_R}}$, where $(\tau_1, \dots, \tau_{N_R})$ is an ordering of $(1, \dots, N_R)$. The optimal solution to problem (3.19) is given by [39]

$$c_i = \begin{cases} \sqrt{\frac{P_{2,i}}{\|\mathbf{u}_i\|_2^2 + \sigma_1^2}} e^{j\theta}, & i = \tau_1, \dots, \tau_j, \\ \kappa_j \frac{\|\mathbf{u}_i\|_2}{\|\mathbf{f}_i\|_2} e^{j\theta}, & i = \tau_{j+1}, \dots, \tau_{N_R}, \end{cases} \quad (3.21)$$

where

$$\kappa_j \triangleq \frac{\sigma_2^2 + \sigma_1^2 \sum_{m=1}^j \frac{P_{2,\tau_m} \|\mathbf{f}_{\tau_m}\|_2^2}{\|\mathbf{u}_{\tau_m}\|_2^2 + \sigma_1^2}}{\sigma_2^2 \sum_{m=1}^j \frac{\sqrt{P_{2,\tau_m}} \|\mathbf{f}_{\tau_m}\|_2 \|\mathbf{u}_{\tau_m}\|_2}{\sqrt{\|\mathbf{u}_{\tau_m}\|_2^2 + \sigma_1^2}}} \quad (3.22)$$

and j is the smallest index such that $\kappa_j < \phi_{\tau_{j+1}}^{-1}$.

For a given source BF vector \mathbf{g} , (3.18) and (3.21) fully specify the optimal AF–BF matrices for multiple multi–antenna relays with individual relay power constraints.

3.3.2 AF–BF with Joint Power Constraint for Relays

Considering (3.13) and taking into account the differences between constraints (3.8) and (3.9), the optimization problem for the joint relay power constraint can be rewritten as

$$\max_{\tilde{P}_2, \mathbf{y}} \frac{\mathbf{y}^H \mathbf{J}^{-H} \mathbf{w} \mathbf{w}^H \mathbf{J}^{-1} \mathbf{y}}{\mathbf{y}^H \left(\sigma_1^2 \mathbf{J}^{-H} \mathbf{T}^H \mathbf{T} \mathbf{J}^{-1} + \sigma_2^2 / \tilde{P}_2 \mathbf{I}_M \right) \mathbf{y}} \quad (3.23a)$$

$$\text{s.t.} \quad \|\mathbf{y}\|_2^2 \leq P_2, \quad (3.23b)$$

where $\|\mathbf{y}\|_2^2 = \tilde{P}_2 \leq P_2$, $\mathbf{y} \triangleq \mathbf{J} \mathbf{b}$, $\mathbf{b} = [\mathbf{b}_1^T \dots \mathbf{b}_{N_R}^T]^T$, $\mathbf{J} \triangleq \text{diag}\{\mathbf{J}_1, \dots, \mathbf{J}_{N_R}\}$, $\mathbf{T} \triangleq \text{diag}\{\mathbf{T}_1, \dots, \mathbf{T}_{N_R}\}$, and $M \triangleq \sum_{i=1}^{N_R} M_i^2$. We observe from (3.23a) that the maximum is achieved for $\tilde{P}_2 = P_2$, i.e., the inequality in (3.23b) can be replaced by an equality. Thus, problem (3.23) reduces to a generalized eigenvalue problem. Consequently, the solution to problem (3.23) is given by [77]

$$\mathbf{y} = c \left(\sigma_1^2 \mathbf{J}^{-H} \mathbf{T}^H \mathbf{T} \mathbf{J}^{-1} + \frac{\sigma_2^2}{P_2} \mathbf{I}_M \right)^{-1} \mathbf{J}^{-H} \mathbf{w}, \quad (3.24)$$

where c is a complex scaling factor. Using similar operations as in (3.15)–(3.17) and $\mathbf{b} = \mathbf{J}^{-1} \mathbf{y}$ we obtain for the optimal BF matrix for AF relays with a joint power constraint

$$\mathbf{B}_i = c s_i \mathbf{f}_i^* \mathbf{u}_i^H, \quad 1 \leq i \leq N_R, \quad (3.25)$$

where

$$s_i \triangleq \frac{P_2}{P_2 \|\mathbf{f}_i\|_2^2 \sigma_1^2 + \|\mathbf{u}_i\|_2^2 \sigma_2^2 + \sigma_1^2 \sigma_2^2}, \quad 1 \leq i \leq N_R, \quad (3.26)$$

$$c \triangleq \left(\sum_{i=1}^{N_R} \frac{P_2 \|\mathbf{f}_i\|_2^2 \|\mathbf{u}_i\|_2^2 (\|\mathbf{u}_i\|_2^2 + \sigma_1^2)}{(P_2 \|\mathbf{f}_i\|_2^2 \sigma_1^2 + \|\mathbf{u}_i\|_2^2 \sigma_2^2 + \sigma_1^2 \sigma_2^2)^2} \right)^{-1/2} e^{j\theta} \quad (3.27)$$

with arbitrary phase θ . We note that the proposed solution for the AF–BF matrix includes the result in [35] as a special case if the source and all relays have only a single antenna.

3.3.3 AF–BF with Joint Power Constraint for Source and Relays

For the joint source–relay power constraint, problem (3.7a), (3.10) can be rewritten as

$$\max_{P_1, \mathbf{g}, \mathbf{B}_i, 1 \leq i \leq N_R} \frac{|\mathbf{f}^T \mathbf{B}_D \mathbf{u}|^2}{\|\mathbf{f}^T \mathbf{B}_D\|_2^2 \sigma_1^2 + \sigma_2^2} \quad (3.28a)$$

$$\text{s.t.} \quad \|\mathbf{g}\|_2^2 \leq P_1 \quad (3.28b)$$

$$\sum_{i=1}^{N_R} \|\mathbf{B}_i \mathbf{g}_i\|_2^2 + \sigma_1^2 \|\mathbf{B}_i\|_F^2 \leq P - P_1 . \quad (3.28c)$$

For given P_1 and \mathbf{g} , problem (3.28) is equivalent to the joint relay power constraint problem considered in Section 3.3.2. Thus, the optimal AF–BF matrix is given by (3.25)–(3.27) if we let $P_2 = P - P_1$. Using this result in (3.28) and assuming the direction of \mathbf{g} is fixed, the optimization problem reduces to a power allocation problem between the source and the relays, i.e.,

$$\max_{P_1} \sum_{i=1}^{N_R} \frac{P_1 (P - P_1) \Gamma_{1,i} \Gamma_{2,i}}{P_1 \Gamma_{1,i} + (P - P_1) \Gamma_{2,i} + 1} \quad (3.29a)$$

$$\text{s.t.} \quad 0 \leq P_1 \leq P , \quad (3.29b)$$

where we have introduced the equivalent source–relay SNR $\Gamma_{1,i} \triangleq \|\mathbf{u}_i\|^2 / (\sigma_1^2 \|\mathbf{g}\|^2)$ and the equivalent relay–destination SNR $\Gamma_{2,i} \triangleq \|\mathbf{f}_i\|^2 / \sigma_2^2$. It is easy to show that the second derivative of the objective function (SINR) in (3.29a) with respect to P_1 is always negative:

$$\frac{\partial^2 \text{SINR}}{\partial P_1^2} = - \sum_{i=1}^{N_R} \frac{2\Gamma_{1,i} \Gamma_{2,i} (P\Gamma_{1,i} + 1) (P\Gamma_{2,i} + 1)}{[P_1 \Gamma_{1,i} + (P - P_1) \Gamma_{2,i} + 1]^3} < 0 , \text{ when } 0 \leq P_1 \leq P. \quad (3.30)$$

Therefore, the objective function is concave and the optimum power allocation can be obtained with a simple bisectional search method based on [1]

$$\frac{\partial \text{SINR}}{\partial P_1} = \sum_{i=1}^{N_R} \frac{\Gamma_{1,i} \Gamma_{2,i} [-P_1^2 (\Gamma_{1,i} - \Gamma_{2,i}) - 2(P\Gamma_{2,i} + 1)P_1 + P(P\Gamma_{2,i} + 1)]}{[P_1 \Gamma_{1,i} + (P - P_1) \Gamma_{2,i} + 1]^2} = 0. \quad (3.31)$$

For the special case when there is only one relay in the cooperative network, a closed–form solution for the optimal P_1 is obtained as

$$P_1 = \begin{cases} \frac{\sqrt{(P\Gamma_{1,1}+1)(P\Gamma_{2,1}+1)} + (P\Gamma_{2,1}+1)}{\Gamma_{2,1} - \Gamma_{1,1}} & , \text{ if } \Gamma_{1,1} < \Gamma_{2,1}, \\ P/2 & , \text{ if } \Gamma_{1,1} = \Gamma_{2,1}, \\ \frac{\sqrt{(P\Gamma_{1,1}+1)(P\Gamma_{2,1}+1)} - (P\Gamma_{2,1}+1)}{\Gamma_{1,1} - \Gamma_{2,1}} & , \text{ if } \Gamma_{1,1} > \Gamma_{2,1}. \end{cases} \quad (3.32)$$

Eq. (3.32) shows that the optimal power allocation tries to balance the received SNRs of the source–relay and the relay–destination channels by allocating more power to the weaker channel. This result is intuitively pleasing since the performance of two–hop links is limited by the SNR of the weaker link.

3.3.4 Comparison of the Solutions for the Different Constraints

A comparison of (3.18) and (3.25) shows that the optimal AF–BF matrices for all power constraints can be expressed as $\mathbf{B}_i = c_i s_i \mathbf{f}_i^* \mathbf{u}_i^H$, $1 \leq i \leq N_R$, where $s_i = 1$, $1 \leq i \leq N_R$, and $c_i = c$, $1 \leq i \leq N_R$, for individual relay power constraints and joint relay/joint relay–source power constraints, respectively. The structure of the optimal \mathbf{B}_i reveals that for all three power constraints, eigenbeamforming with respect to the source–relay and the relay–destination channels is optimal. We note that although this result may have been intuitively expected, it was not obvious from (3.7). It is also interesting to observe that while for the joint relay and the joint source–relay power constraints the relays and the

source always utilize the full available transmit power, some relays may not utilize the maximum available power if individual relay power constraints are imposed on the relays, cf. (3.21).

3.4 Optimal BF Vector at the Source

We first note that for the case of $N_T = 1$ source antenna, $\mathbf{g}/\|\mathbf{g}\|_2 = 1$ is optimal and the optimal AF–BF matrices obtained in Section 3.3 constitute the solution to problem (3.7). In Subsections 3.4.1–3.4.3, we propose optimal and suboptimal solutions for the BF vector \mathbf{g} for the case $N_T > 1$ assuming that the optimal AF–BF matrices obtained in Subsections 3.3.1–3.3.3 are adopted at the relays, respectively. In Subsection 3.4.4, we discuss the feedback requirements of the proposed AF–BF scheme.

3.4.1 AF–BF with Individual Power Constraints for Relays

The degree to which the optimization problem for \mathbf{g} can be solved largely depends on the underlying power constraints. Thereby, individual power constraints for the relays lead to the most difficult and least tractable problem. Considering (3.19) and using $\mathbf{u}_i = \mathbf{H}_i \mathbf{g}$, the optimal \mathbf{g} is the solution to the following optimization problem

$$\max_{\mathbf{g}} \quad \text{SINR}(\mathbf{g}) = \frac{\left(\sum_{i=1}^{N_R} |c_i(\mathbf{g})| \|\mathbf{f}_i\|_2 \|\mathbf{H}_i \mathbf{g}\|_2 \right)^2}{\sigma_1^2 \sum_{i=1}^{N_R} |c_i(\mathbf{g})|^2 \|\mathbf{f}_i\|_2^2 + \sigma_2^2} \quad (3.33a)$$

$$\text{s.t.} \quad \|\mathbf{g}\|_2^2 = P_1, \quad (3.33b)$$

where we have made the dependence of c_i on \mathbf{g} explicit, cf. (3.21). Since $\text{SINR}(\mathbf{g})$ depends on \mathbf{g} in a complicated manner, it does not seem possible to obtain the globally optimal solution to problem (3.33). Hence, we propose two suboptimal methods for optimization

of \mathbf{g} .

1) *Ad hoc Method:* One suboptimal solution is to perform eigenbeamforming at the source with respect to the average source–relay channel. This means we choose \mathbf{g} as the dominant eigenvector of matrix $\sum_{i=1}^{N_R} \mathbf{H}_i^H \mathbf{H}_i$ and normalize it to $\|\mathbf{g}\|_2^2 = P_1$.

2) *Gradient Method:* The solution obtained with the ad hoc method can be improved using a gradient method. We note, however, that since problem (3.33) is not convex, the gradient method may not achieve the globally optimal solution. Since the derivative of $\text{SINR}(\mathbf{g})$ in (3.33a) with respect to \mathbf{g} is cumbersome, we express the SINR as a function of $\bar{\mathbf{g}} \triangleq [\Re\{\mathbf{g}\}^T \Im\{\mathbf{g}\}^T]^T$ and use a gradient estimate given by [79]

$$\nabla_{\bar{\mathbf{g}}} \text{SINR}(\bar{\mathbf{g}}) = \frac{1}{2\delta} \left[(\text{SINR}(\bar{\mathbf{g}} + \delta \mathbf{e}_1) - \text{SINR}(\bar{\mathbf{g}} - \delta \mathbf{e}_1)) \dots (\text{SINR}(\bar{\mathbf{g}} + \delta \mathbf{e}_{2N_T}) - \text{SINR}(\bar{\mathbf{g}} - \delta \mathbf{e}_{2N_T})) \right]^T \quad (3.34)$$

where δ is a small positive constant and \mathbf{e}_i has a one in position i , $1 \leq i \leq 2N_T$, and zeros in all other positions (i th unit norm vector). This leads to the gradient algorithm given in Table 3.1, where $\hat{\mathbf{g}}_k \triangleq \bar{\mathbf{g}}_k$ and $\text{grad}_k \triangleq \nabla_{\bar{\mathbf{g}}} \text{SINR}(\hat{\mathbf{g}}_k)$. The gradient algorithm is guaranteed to find a locally optimal solution that is not worse than the solution obtained with the ad hoc method, which is used for initialization, cf. Table 3.1. We note that for computation of the gradient estimate in (3.34), constants c_i , $1 \leq i \leq N_R$, have to be computed for all $4N_T$ vectors $\bar{\mathbf{g}}_k \pm \delta \mathbf{e}_i$, $1 \leq i \leq 2N_T$, using (3.19).

Table 3.1: Gradient algorithm for calculation of source BF vector $\hat{\mathbf{g}}$ for individual and joint relay power constraints. The definitions of $\hat{\mathbf{g}}$ and the gradient grad_k depend on the power constraint, cf. Section 3.4. Termination constant ϵ has a small value (e.g. $\epsilon = 10^{-5}$). k denotes the iteration index and a_k is the adaptation step size chosen through a backtracking line search [1].

1	Let $k = 0$ and initialize vector $\hat{\mathbf{g}}_0$ with solution of ad hoc method
2	Update the BF vector: $\tilde{\mathbf{g}}_{k+1} = \hat{\mathbf{g}}_k + a_k \text{grad}_k$
3	Rescale the BF vector: $\hat{\mathbf{g}}_{k+1} = \sqrt{P_1} \tilde{\mathbf{g}}_{k+1} / \ \tilde{\mathbf{g}}_{k+1}\ _2$
4	If $1 - \hat{\mathbf{g}}_{k+1}^H \hat{\mathbf{g}}_k / P_1 < \epsilon$, goto Step 5, otherwise increment counter k and goto Step 2
5	$\hat{\mathbf{g}}_{k+1}$ is the desired BF vector

3.4.2 AF–BF with Joint Power Constraint for Relays

In this case, applying (3.25)–(3.27) in (3.7) and (3.9), we obtain

$$\max_{\mathbf{g}} \quad \sum_{i=1}^{N_R} \frac{P_2 \|\mathbf{f}_i\|_2^2 \|\mathbf{H}_i \mathbf{g}\|_2^2}{P_2 \|\mathbf{f}_i\|_2^2 \sigma_1^2 + \|\mathbf{H}_i \mathbf{g}\|_2^2 \sigma_2^2 + \sigma_1^2 \sigma_2^2} \quad (3.35a)$$

$$\text{s.t.} \quad \|\mathbf{g}\|_2^2 \leq P_1. \quad (3.35b)$$

For the following it is convenient to rewrite the objective function in (3.35a) as

$$\text{SINR} = \frac{P_2}{\sigma_2^2} \sum_{i=1}^{N_R} \|\mathbf{f}_i\|_2^2 - \sum_{i=1}^{N_R} \frac{e_i}{\mathbf{g}^H \mathbf{A}_i \mathbf{g}}, \quad (3.36)$$

where $e_i \triangleq \sigma_1^2 \frac{P_2}{\sigma_2^2} \|\mathbf{f}_i\|_2^2 (P_2 \|\mathbf{f}_i\|_2^2 + \sigma_2^2)$ and $\mathbf{A}_i \triangleq \sigma_2^2 \mathbf{H}_i^H \mathbf{H}_i + \frac{\sigma_1^2}{P_1} (P_2 \|\mathbf{f}_i\|_2^2 + \sigma_2^2) \mathbf{I}_{N_T}$ are independent of \mathbf{g} . The first term in (3.36) is the SINR achieved with beamforming in point-to-point transmission without relaying where all the relay antennas are located at one transmitter. Thus, the second term in (3.36) may be interpreted as the penalty incurred because the considered system uses AF–BF with distributed relays and not BF for the relay–destination channel with co-located antennas. Consequently, maximization problem

(3.35) is equivalent to the following minimization problem

$$\min_{\mathbf{g}} \sum_{i=1}^{N_R} \frac{e_i}{\mathbf{g}^H \mathbf{A}_i \mathbf{g}} \quad (3.37a)$$

$$\text{s.t.} \quad \|\mathbf{g}\|_2^2 \leq P_1 . \quad (3.37b)$$

For the special case of $N_R = 1$ relay having M_1 antennas it is obvious from (3.37) that the optimal \mathbf{g} is simply the dominant eigenvector of matrix $\mathbf{H}_1^H \mathbf{H}_1$. This result is not new and has already been mentioned in [38]. However, here we are interested in the more difficult case of multiple relays, for which a solution has not been provided before. We note that for $N_R > 1$ (3.37) is a difficult non–convex optimization problem. In the following, we provide the optimal and three suboptimal solutions to problem (3.37) which differ in their complexity and performance.

1) *Transformation Method:* Problem (3.37) can be transformed into the following polynomial programming problem

$$\min_{\bar{\mathbf{g}}, t_i, 1 \leq i \leq N_R} \sum_{i=1}^{N_R} t_i \quad (3.38a)$$

$$\text{s.t.} \quad t_i \bar{\mathbf{g}}^T \begin{bmatrix} \Re\{\mathbf{A}_i\} & -\Im\{\mathbf{A}_i\} \\ \Im\{\mathbf{A}_i\} & \Re\{\mathbf{A}_i\} \end{bmatrix} \bar{\mathbf{g}} \geq e_i, \quad 1 \leq i \leq N_R \quad (3.38b)$$

$$\bar{\mathbf{g}}^T \bar{\mathbf{g}} \leq P_1 , \quad (3.38c)$$

where $\bar{\mathbf{g}} = [\Re\{\mathbf{g}\}^T \Im\{\mathbf{g}\}^T]^T$. Although the polynomial programming problem in (3.38) is still non–convex, for small N_T and small N_R (e.g., $N_T = 2$ and $N_R = 2$), it can be solved by using the GloptiPoly or SOSTOOLS software [75, 76]. In this case, we can indeed obtain the globally optimal solution to the AF–BF problem. However, for large N_T and N_R finding the globally optimal solution with the aforementioned software tools does not

seem feasible. Thus, it is desirable to provide suboptimal methods for optimization of \mathbf{g} having a lower complexity than the transformation method.

2) *Ad hoc Method:* Assuming that the relay–destination channels have a much *higher* SNR than the source–relay channels, i.e., $\frac{P_2}{\sigma_2^2} \|\mathbf{f}_i\|_2^2 \gg \frac{1}{\sigma_1^2} \|\mathbf{H}_i \mathbf{g}\|_2^2$, $1 \leq i \leq N_R$, it is easy to see from (3.35a) that the optimal BF vector \mathbf{g} is the dominant eigenvector of matrix $\sum_{i=1}^{N_R} \mathbf{H}_i^H \mathbf{H}_i$ normalized to $\|\mathbf{g}\|_2^2 = P_1$. This dominant eigenvector can also be considered as an ad hoc solution to the problem if the underlying condition on the SNRs of the subchannels is not fulfilled. We note that for the case where the relay–destination channels have a much *lower* SNR than the source–relay channels, the objective function in (3.35a) becomes independent of \mathbf{g} and optimization of the BF vector at the source is not necessary.

3) *Gradient Method:* Similar to the case of individual relay power constraints, we may use a gradient algorithm to improve the solution obtained with the ad hoc method. The corresponding algorithm is again given in Table 3.1 with $\hat{\mathbf{g}}_k \triangleq \mathbf{g}_k$ and $\text{grad}_k \triangleq \left[\sum_{i=1}^{N_R} e_i \mathbf{A}_i / (\hat{\mathbf{g}}_k^H \mathbf{A}_i \hat{\mathbf{g}}_k)^2 \right] \hat{\mathbf{g}}_k$. The gradient method will find that local optimum of the objective function which is closest to the solution provided by the ad hoc method. Since problem (3.37) is not convex, there is no guarantee that this local optimum coincides with the global optimum. Nevertheless, our simulation results in Section 3.5 suggest that the solution found with the gradient method achieves a performance comparable to that of the global optimum.

4) *Relaxation Method:* Considering (3.36) a “good” suboptimal strategy to achieving a high SINR is to maximize the minimum value of $\mathbf{g}^H \mathbf{A}_i \mathbf{g}$, $1 \leq i \leq N_R$. This results in a new (relaxed) optimization problem:

$$\max_{\mathbf{g}} \quad \min_{i, 1 \leq i \leq N_R} \quad \frac{1}{e_i} \mathbf{g}^H \mathbf{A}_i \mathbf{g} \quad (3.39a)$$

$$\text{s.t.} \quad \|\mathbf{g}\|_2^2 \leq P_1 . \quad (3.39b)$$

The max–min problem in (3.39) can be easily relaxed to a semidefinite programming (SDP) problem and efficiently solved using SeDuMi in Matlab [71].

3.4.3 AF–BF with Joint Power Constraint for Source and Relays

In this case, the optimal source BF vector \mathbf{g} and power P_1 that maximize the SINR in (3.28a) have to be found. This leads to the following problem:

$$\max_{\mathbf{g}} \sum_{i=1}^{N_R} \frac{(P - P_1) \|\mathbf{f}_i\|_2^2 \|\mathbf{H}_i \mathbf{g}\|_2^2}{(P - P_1) \|\mathbf{f}_i\|_2^2 \sigma_1^2 + \|\mathbf{H}_i \mathbf{g}\|_2^2 \sigma_2^2 + \sigma_1^2 \sigma_2^2} \quad (3.40a)$$

$$\text{s.t.} \quad \|\mathbf{g}\|_2^2 \leq P_1 \quad (3.40b)$$

$$0 \leq P_1 \leq P. \quad (3.40c)$$

Clearly, this non–convex problem is in general more difficult than the problem with the joint relay power constraint considered in Section 3.4.2. Nevertheless, we will show in the following that similar approaches as in Section 3.4.2 can also be applied to problem (3.40). For the special case of $N_R = 1$ relay, it can be observed from (3.40a) that the optimal direction $\mathbf{g}/\|\mathbf{g}\|_2$ of the source BF vector is given by the dominant eigenvector of matrix $\mathbf{H}_1^H \mathbf{H}_1$. The corresponding optimal power P_1 is given by (3.32), where $\Gamma_{1,1} = \lambda_{\max}(\mathbf{H}_1^H \mathbf{H}_1)/\sigma_1^2$ and $\Gamma_{2,1} = \|\mathbf{f}_1\|_2^2/\sigma_2^2$. For the general case of $N_R > 1$, a closed–form solution cannot be found. Nevertheless, in the following, we provide the globally optimal and two suboptimal solutions to problem (3.40).

1) *Transformation Method:* Problem (3.40) can be transformed into the following poly-

nomial programming problem

$$\bar{\mathbf{g}}, P_1, t_i, 1 \leq i \leq N_R \quad \max \quad \sum_{i=1}^{N_R} t_i \quad (3.41a)$$

$$\text{s.t.} \quad \left((P - P_1) \|\mathbf{f}_i\|_2^2 - t_i \sigma_2^2 \right) \bar{\mathbf{g}}^T \begin{bmatrix} \Re\{\mathbf{H}_i\} & -\Im\{\mathbf{H}_i\} \\ \Im\{\mathbf{H}_i\} & \Re\{\mathbf{H}_i\} \end{bmatrix} \bar{\mathbf{g}} \\ \geq t_i \sigma_1^2 \left((P - P_1) \|\mathbf{f}_i\|_2^2 - \sigma_2^2 \right), \quad 1 \leq i \leq N_R \quad (3.41b)$$

$$\bar{\mathbf{g}}^T \bar{\mathbf{g}} \leq P_1 \quad (3.41c)$$

$$0 \leq P_1 \leq P, \quad (3.41d)$$

where again $\bar{\mathbf{g}} = [\Re\{\mathbf{g}\}^T \Im\{\mathbf{g}\}^T]^T$ is used. Compared to problem (3.38), problem (3.41) has one additional optimization variable (P_1) and one additional constraint. Despite its non-convexity, for small scale networks (e.g. $N_T = 2$ and $N_R = 2$), the globally optimal solution for problem (3.41) can be readily obtained using the GloptiPoly or SOSTOOLS software [75, 76]. For large scale networks, we turn again to suboptimal solutions to reduce complexity.

2) *Ad hoc Method:* As an ad hoc solution, we may adopt the dominant eigenvector of $\sum_{i=1}^{N_R} \mathbf{H}_i^H \mathbf{H}_i$ for the direction of the BF vector \mathbf{g} , i.e., for $\mathbf{g}/\|\mathbf{g}\|_2$. The optimal power allocation for this direction can be found with (3.31).

3) *Gradient Method:* For both small-scale and large-scale networks the solution found with the ad hoc method can be improved with a gradient algorithm. In each iteration, the gradient algorithm first improves the direction of the BF vector and subsequently computes the power allocation for the new BF vector. The gradient algorithm is given in detail in Table 3.2.

Table 3.2: Gradient algorithm for calculation of source BF vector \mathbf{g} and power allocation for joint source–relay power constraint. Termination constant ϵ has a small value (e.g. $\epsilon = 10^{-5}$). k denotes the iteration index and a_k is the adaptation step size chosen through a backtracking line search [1].

1	Let $k = 0$ and initialize \mathbf{g}_0 , $P_{1,0}$, and $P_{2,0} = P - P_{1,0}$ with the solution obtained with the ad hoc method and calculate the corresponding SNR_0 (objective function in (3.40a))
2	Update the BF vector: $\tilde{\mathbf{g}}_{k+1} = \mathbf{g}_k + a_k \left[\sum_{i=1}^{N_R} e_i \mathbf{A}_i / (\mathbf{g}_k^H \mathbf{A}_i \mathbf{g}_k)^2 \right] \mathbf{g}_k$
3	Rescale the BF vector: $\mathbf{g}_{k+1} = \sqrt{P_{1,k}} \tilde{\mathbf{g}}_{k+1} / \ \tilde{\mathbf{g}}_{k+1}\ _2$
4	Find the optimal power allocation $P_{1,k+1}$ and $P_{2,k+1} = P - P_{1,k+1}$ for \mathbf{g}_{k+1} based on (3.31) using the bisectional search method and compute the corresponding SNR_{k+1}
5	If $ \text{SNR}_{k+1} - \text{SNR}_k < \epsilon$, goto Step 6, otherwise increment counter k and goto Step 2
6	\mathbf{g}_{k+1} and $P_{1,k+1}$ are the desired BF vector and power, respectively

3.4.4 Comparison of the Solutions and CSI Feedback

Requirements

Optimality: Our results in Sections 3.4.1–3.4.3 show that for the special case of $N_R = 1$ relay, the optimal source BF vector \mathbf{g} can be found in closed form for all three constraints (note that for $N_R = 1$ the individual power constraint is identical to the joint power constraint for the relays). In contrast for $N_R > 1$ numerical methods have to be used to obtain \mathbf{g} . While the globally optimal solution can be found in principle for the joint relay and the joint source and relay power constraints, this does not seem possible for the individual relay power constraints.

Feedback Requirements: We first consider the feedback necessary for computation of the source BF vector \mathbf{g} . We assume that in a first training phase the relays and the destination transmit suitable pilot symbols such that the source can estimate all source–

relay channels \mathbf{H}_i , $1 \leq i \leq N_R$, and each relay can estimate its own relay–destination channel \mathbf{f}_i . Subsequently, relay i feeds back real number $\|\mathbf{f}_i\|_2^2$ to the source. With the knowledge of \mathbf{H}_i and $\|\mathbf{f}_i\|_2^2$, $1 \leq i \leq N_R$, the source can compute the optimal BF vector \mathbf{g} for all three considered power constraints.

Now, we consider the feedback required for computation of the optimal BF matrices at the relays. We first recall from Section 3.3 that for all considered constraints the AF–BF matrix can be expressed as $\mathbf{B}_i = c_i s_i \mathbf{f}_i^* \mathbf{u}_i^H$, where c_i depends on the channel gains of all source–relay and all relay–destination links and s_i depends on the source–relay and relay–destination channels of relay i only. The specific values of c_i and s_i depend on the power constraint. We assume that after it has obtained the optimal BF vector \mathbf{g} , the source transmits in a second training phase pilot symbols such that each relay can estimate its (effective) source–relay channel $\mathbf{u}_i = \mathbf{H}_i \mathbf{g}$. Thus, relay i knows \mathbf{f}_i and \mathbf{u}_i and can compute s_i , while the source can compute c_i . The additional feedback requirements depend on the particular form of c_i and are slightly different for the three considered power constraints. For the individual relay power constraints, c_i depends on i and the source has to feedback one complex number c_i to each relay, cf. (3.18). For the joint relay power constraint, $c_i = c$, $1 \leq i \leq N_R$, and the source has to broadcast only one complex number c to all relays, cf. (3.27). For the joint source–relay power constraint, the source has to broadcast complex constant c and the power P_2 (which affects s_i in this case) to all relays.

Overall the feedback requirements for the proposed AF–BF scheme are considered to be moderate. In particular, we note that the source may need the CSI of all links in the network also for other purposes such as cross–layer resource allocation.

3.5 Simulation Results

In this section, we present simulation results for the SINR, the mutual information, and the BER of a cooperative network with AF–BF. For all mutual information and SINR results presented in this section we assume a cooperative network with $\sigma_1^2 = \sigma_2^2 = 0.1$. For the individual relay power constraints, the joint relay power constraint, and the joint source–relay power constraint, we use $(P_1 = 1, P_{2,i} = 1/N_R, 1 \leq i \leq N_R)$, $(P_1 = 1, P_2 = 1)$, and $P = 2$, respectively. The locations of the source, the destination, and the relays are shown in Fig. 3.2, where the numbers on top and beside the arrows indicate the normalized distance between the nodes. Potential relay locations are marked by (a)–(e). The normalized distance between the source and the destination is equal to 2 and the normalized horizontal distance between the source and the potential relay locations is d . The fading gains of all links are modeled as independent, identically distributed Rayleigh fading. Furthermore, a path–loss exponent of 3 is assumed and all results were averaged over 100,000 independent realizations of the fading channels unless specified otherwise. The optimal BF vectors at the source and the optimal AF–BF matrices at the relays were obtained with the algorithms introduced in Sections 3.3 and 3.4.

For a fair evaluation of the gain achievable with multi–relay BF, we compare the performance of the proposed schemes with relay selection [80], which has a lower implementation complexity. For relay selection, we compute the optimal source BF vector and the optimal AF–BF matrix for each relay in the network, and select subsequently the relay which achieves the highest SINR for transmission.

3.5.1 Comparison of Source BF Vector Optimization Methods

First, we compare the performance of the proposed suboptimal source BF vector optimization methods. For this purpose, we show in Figs. 3.3–3.5 cumulative distribution functions

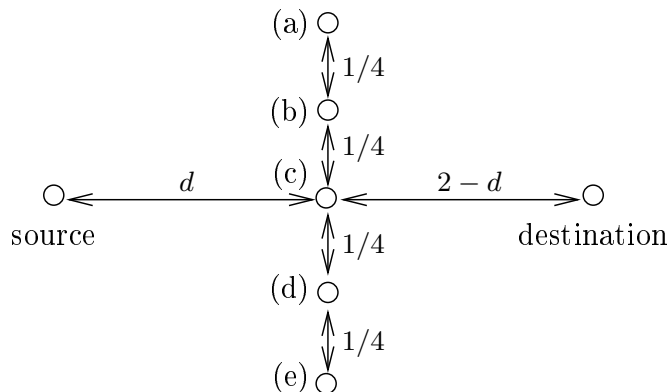


Figure 3.2: Locations of source, destination, and relays in simulation.

(CDFs) of the achieved SINR, i.e., the probability that the achieved SINR is smaller than the SINR value on the x-axis. Since the optimal source beamforming vectors can be computed with the proposed transformation methods only for joint relay and joint source-relay power constraints and $N_T = 2$ and $N_R = 2$, we also consider a gradient method with multiple random initializations. In particular, we run the gradient algorithms in Sections 3.4.2 and 3.4.3 for 100 random initializations and for the solution of the ad hoc method. Subsequently, we select the beamforming vector which yields the highest SINR among the 101 obtained solutions. Results for the gradient method with random initialization are shown in Figs. 3.4 and 3.5.

In Fig. 3.3, we compare the performances of the different source BF vector optimization methods proposed for the joint relay power constraint. There are $N_T = 2$ antennas at the source and one relay at locations (a) and (e), respectively. For the relays we consider the cases $M_1 = M_2 = 1$ and $M_1 = 2, M_2 = 3$, respectively. As can be observed, for both considered numbers of relay antennas the gradient method closely approaches the global optimal solution, which was found with the transformation method. The loss in performance suffered by the relaxation method and the ad hoc method is larger for $M_1 = M_2 = 1$ than for $M_1 = 2, M_2 = 3$. Relay selection suffers from a significant loss in

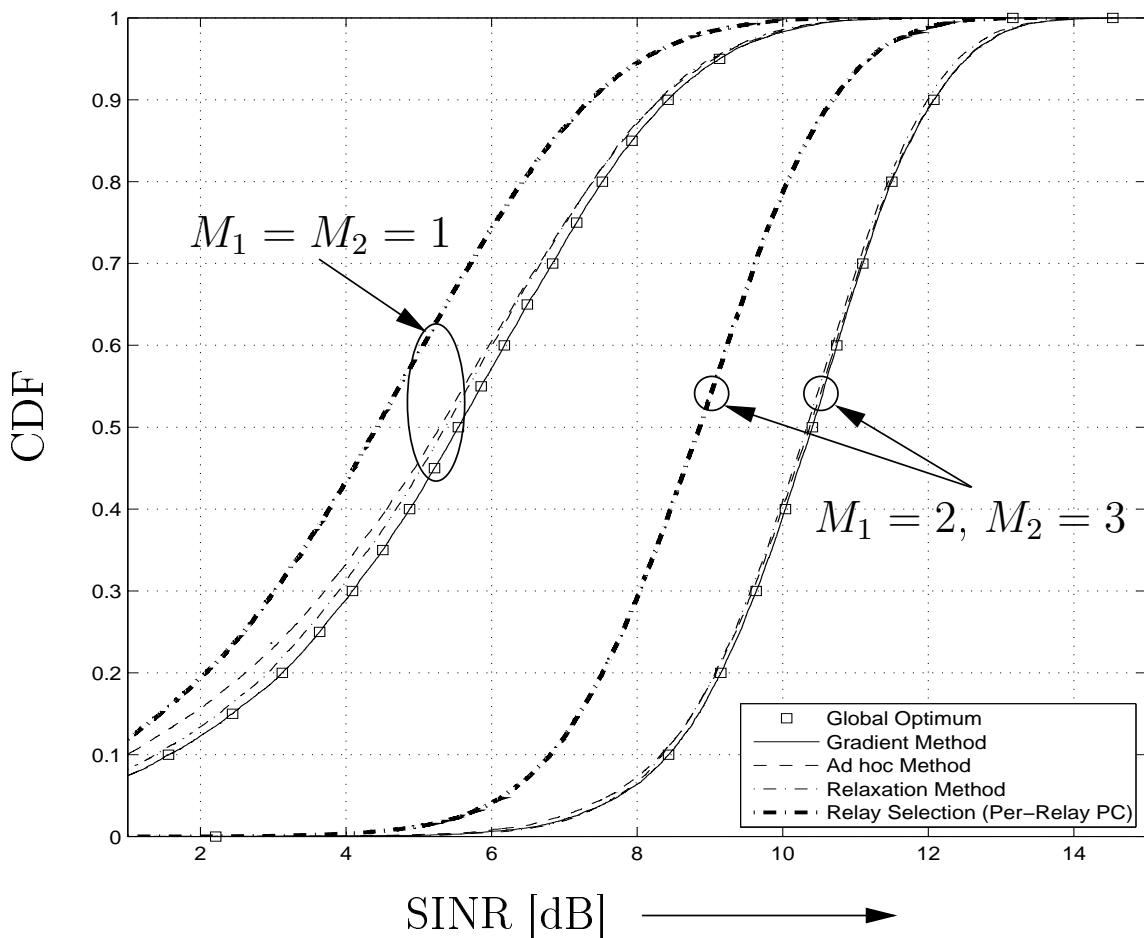


Figure 3.3: CDF of the instantaneous SINR for AF-BF with *joint relay power constraint (PC)* and one relay located at (a) and (e), respectively. Results for different optimization methods for the source BF vector for multiple relays are shown and compared with relay selection. A path-loss exponent of 3, $N_T = 2$, and $d = 1$ are assumed.

performance since it cannot exploit the BF gain across the relays.

In Fig. 3.4, we compare the performance of the proposed source BF vector optimization techniques for the joint source-relay power constraint for $N_T = 2$ antennas at the source and N_R single-antenna relays for $d = 1$. For $N_R = 2$ the gradient algorithm achieves practically the same performance as the optimal transformation method, which becomes too complex for $N_R = 5$ and $N_R = 10$. For $N_R = 5$ and $N_R = 10$, it can be observed

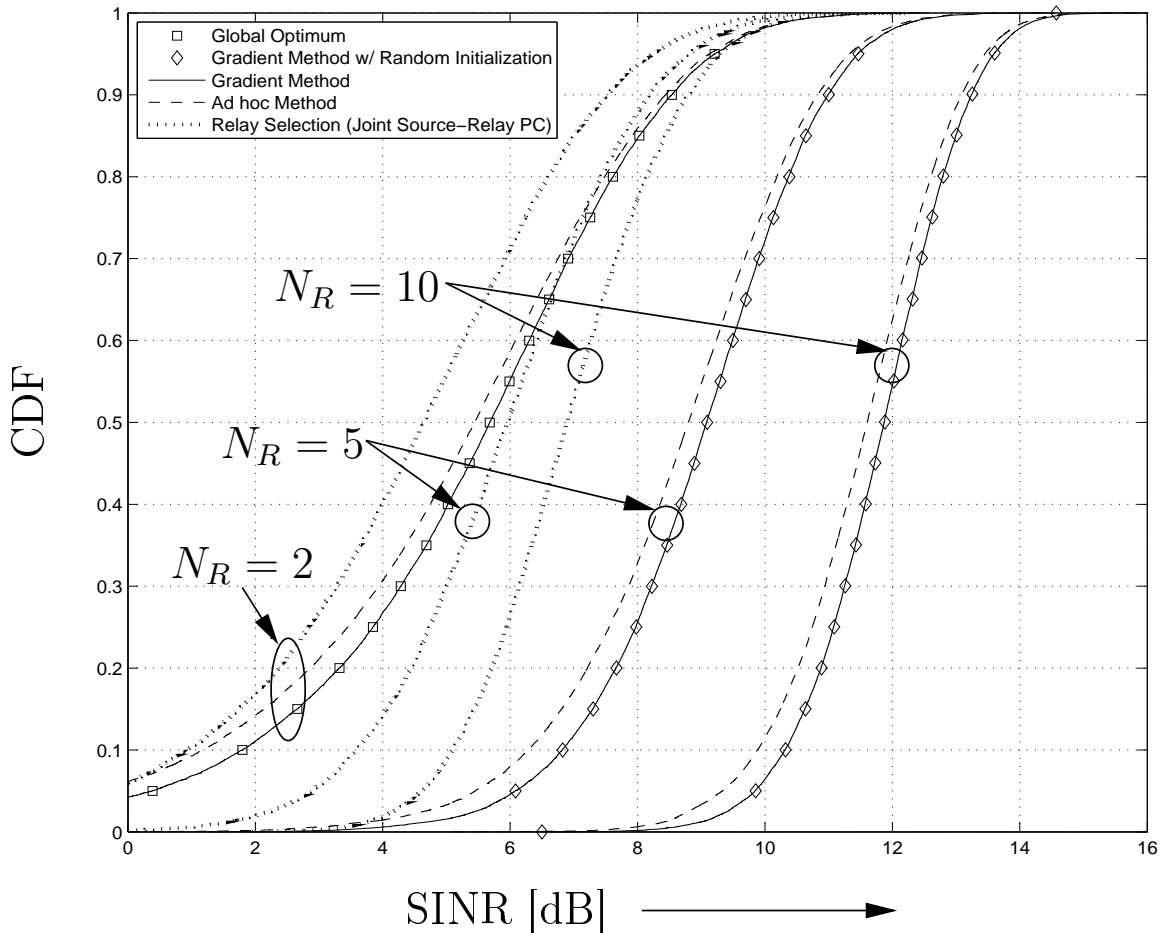


Figure 3.4: CDF of the instantaneous SINR for AF-BF with *joint source-relay power constraint (PC)* and N_R relays. Results for different optimization methods for the source BF vector for multiple relays are shown and compared with relay selection. A path-loss exponent of 3, $N_T = 2$, and $d = 1$ are assumed. The relays are located at (a) and (e) for $N_R = 2$, (a)-(e) for $N_R = 5$, and (a)-(e) with 2 relays at each location for $N_R = 10$.

that additional random initializations cannot significantly improve the performance of the gradient method, which suggests that the gradient method initialized with the solution of the ad hoc method is close-to-optimal also for large numbers of relays. The performance gap between the gradient method and the ad hoc method is practically independent of the number of relays. In contrast, the performance loss suffered by relay selection increases

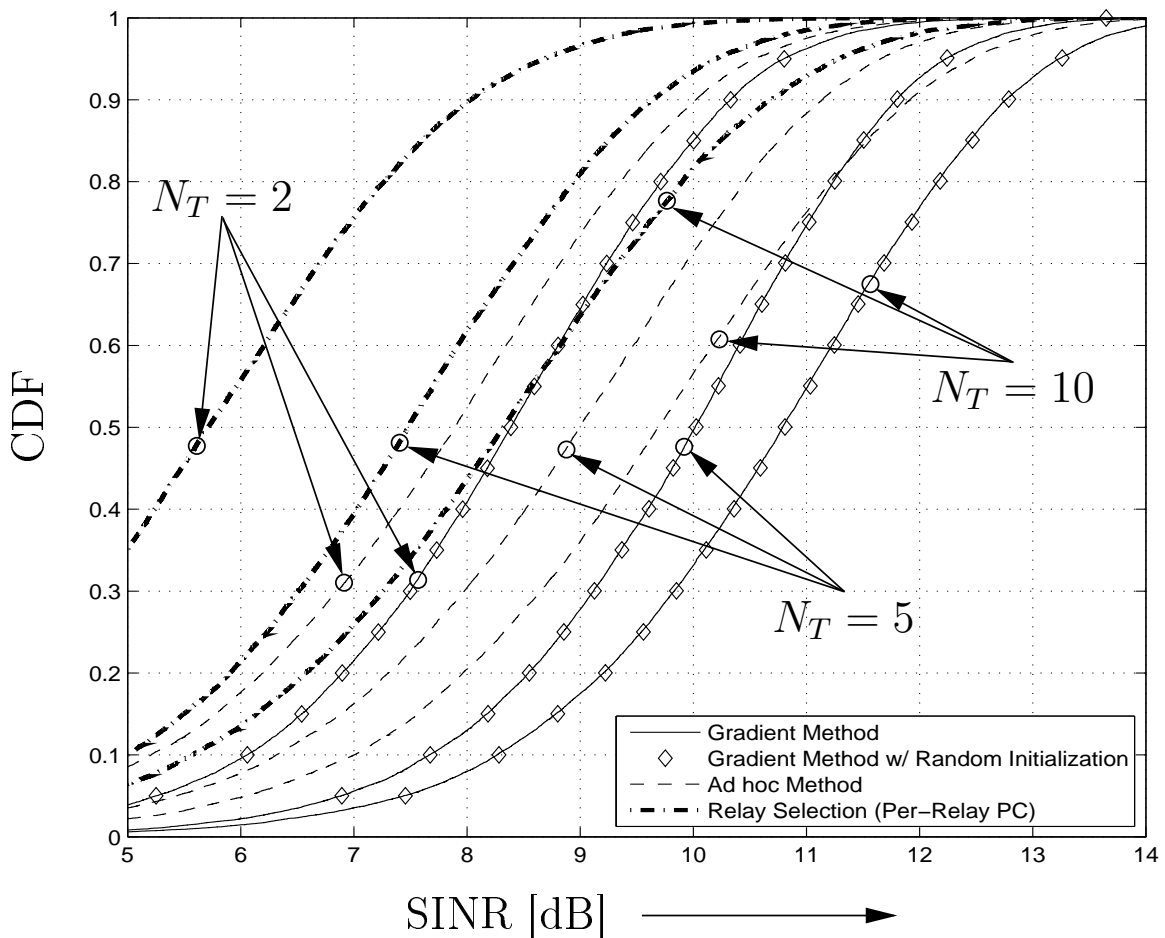


Figure 3.5: CDF of the instantaneous SINR for AF-BF with *individual relay power constraints (PCs)* and $N_R = 5$ single-antenna relays at locations (a)–(e). Results for different optimization methods for the source BF vector for multiple relays are shown and compared with relay selection. A path-loss exponent of 3 and $d = 1$ are assumed.

with increasing numbers of relays.

In Fig. 3.5, we consider the case of individual relay power constraints and show the CDFs achieved with the different source BF vector optimization methods for $N_R = 5$ single-antenna relays located at positions (a)–(e) in Fig. 3.2 for $d = 1$. For the gradient method, the performance gain achievable with additional random initializations is negligible even for $N_T = 10$ source antennas. However, the performance loss suffered by the ad hoc method

compared to the gradient method increases with increasing number of source antennas. For example, for a CDF value of 0.5, the performance difference between both schemes is 0.5 dB and 1.1 dB for $N_T = 2$ and $N_T = 10$, respectively.

3.5.2 Impact of Network Parameters on Performance

Figs. 3.6 and 3.7 show the average SINR vs. distance d for AF–BF with different numbers of transmit antennas for joint relay and individual relay power constraints, respectively. We assume $N_R = 2$ relays with one relay located in (a) and (e), respectively. For both considered constraints multi–relay AF–BF enables considerable performance gains compared to relay selection and direct transmission. Direct transmission is preferable only if the relay–destination SNR is poor because the relays are located close to the source (small d). The performance loss suffered by relay selection is between 1 and 2 dB. Increasing the number of source antennas is beneficial for both constraints unless the relays are located close to the source. In the latter case, the relay–destination channel is the performance bottleneck and more source antennas cannot improve performance. If only $N_T = 1$ source antenna is available, BF is not used at the source (i.e., $\mathbf{g}/\|\mathbf{g}\|_2 = 1$). For $N_T = 2$ and $N_T = 5$ source antennas the gradient methods achieve the highest SINRs in both figures. Fig. 3.6 shows that while the max–min relaxation method outperforms the ad hoc method for small d , the ad hoc method is preferable for large d (e.g. $d \geq 1.4$ for $N_T = 5$). In the latter case, the SINR of the source–relay channels is much lower than that of the relay–destination channels and the ad hoc method becomes optimal, cf. Section 3.4.2.

Next we investigate the impact of the number of relays and the number of relay antennas. In Fig. 3.8, we show the average SINR vs. distance d for AF–BF with $N_T = 5$ source antennas for the joint source–relay power constraint. For the case with two relays (in positions (a) and (e)) increasing the number of relay antennas from $M_1 = M_2 = 1$ to

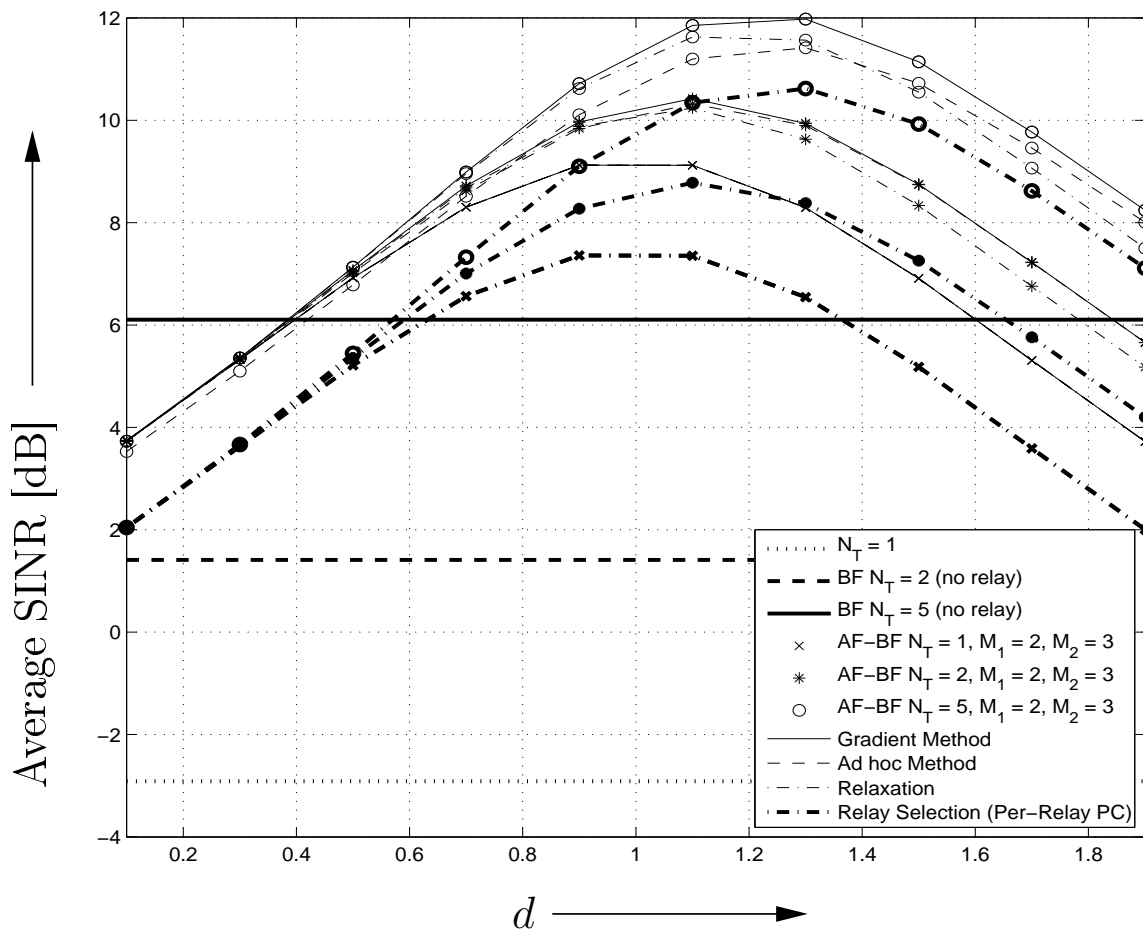


Figure 3.6: Average SINR vs. distance d for AF-BF with *joint relay power constraint (PC)* and different numbers of antennas N_T at the source. A path-loss exponent of 3 is assumed. For comparison the SINR without relaying for a source transmit power of $P = 2$ and the SINR for relay selection are also shown.

$M_1 = 2, M_2 = 3$ significantly improves performance. Furthermore, Fig. 3.8 shows that it is preferable to have the 5 relay antennas located in just two relays rather than having them distributed over five relays. This can be explained by the fact that in the former case the AF-BF matrices have $9 + 4 = 13$ elements that can be optimized whereas in the latter case they have only $5 \times 1 = 5$ elements. Similar to Fig. 3.3, we observe from Fig. 3.8 that the gradient algorithm yields larger gains over the ad hoc method for single-antenna

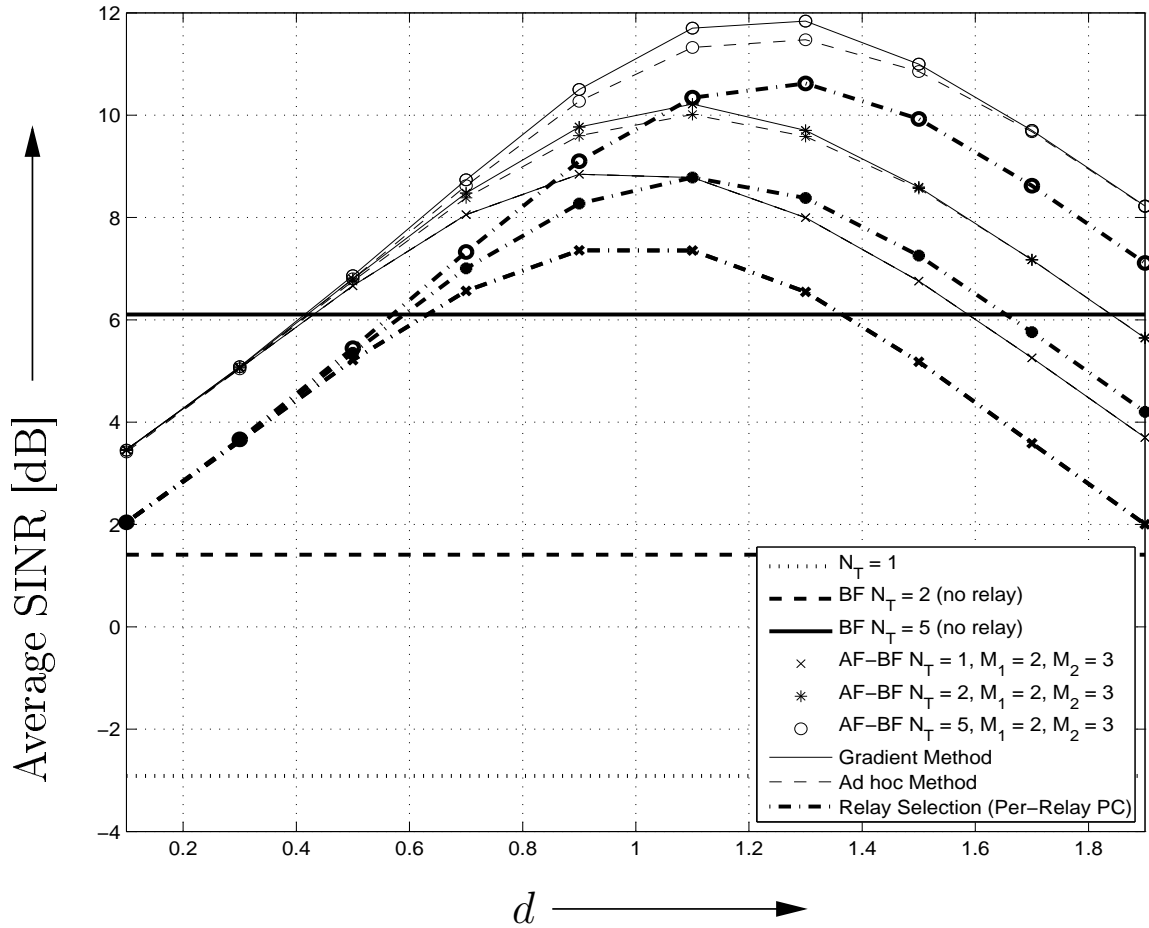


Figure 3.7: Average SINR vs. distance d for AF-BF with *individual relay power constraints (PCs)* and different numbers of antennas N_T at the source. A path-loss exponent of 3 is assumed. For comparison the SINR without relaying for a source transmit power of $P = 2$ and the SINR for relay selection are also shown.

relays than for multi-antenna relays.

3.5.3 Impact of Power Constraints on Performance

In Fig. 3.9, we compare the average mutual information of AF-BF for the three considered power constraints and different network setups. For $N_T = 2$ and $N_T = 5$ source antennas the respective gradient methods were used to find the optimal source BF vector. If the

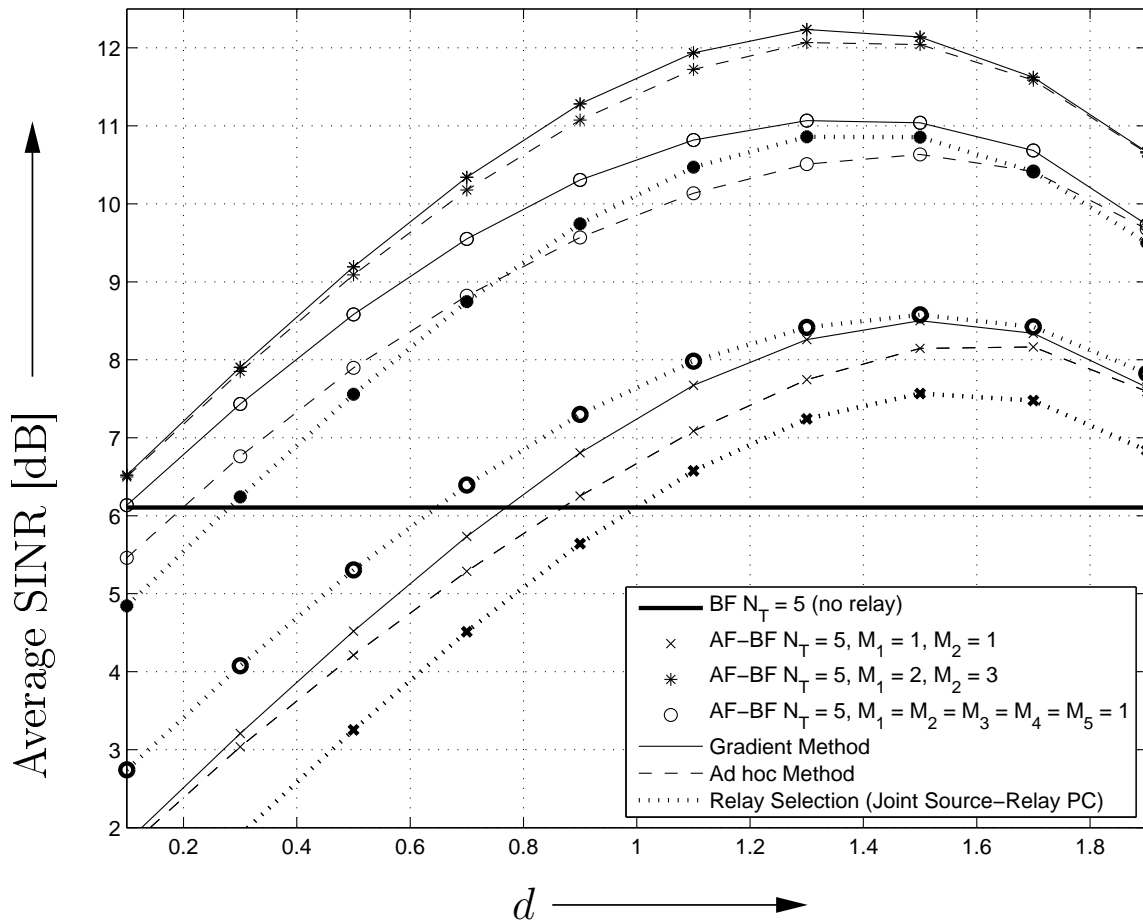


Figure 3.8: Average SINR vs. distance d for AF-BF with *joint source-relay power constraint (PC)* and different numbers of relays and different numbers of relay antennas. A path-loss exponent of 3 is assumed. For comparison the SNR without relaying for a source transmit power of $P = 2$ and the SINR for relay selection are also shown.

relays are located in the middle between the source and the destination (i.e., $d \approx 1$) all three constraints result in a comparable performance. Furthermore, because of the symmetry of the considered setups, the performance difference between the joint relay power constraint and the individual relay power constraints is comparatively small. In contrast, the joint source-relay power constraint can yield significant performance gains if the relays are close to the source or close to the destination, respectively, by flexibly allocating more or less

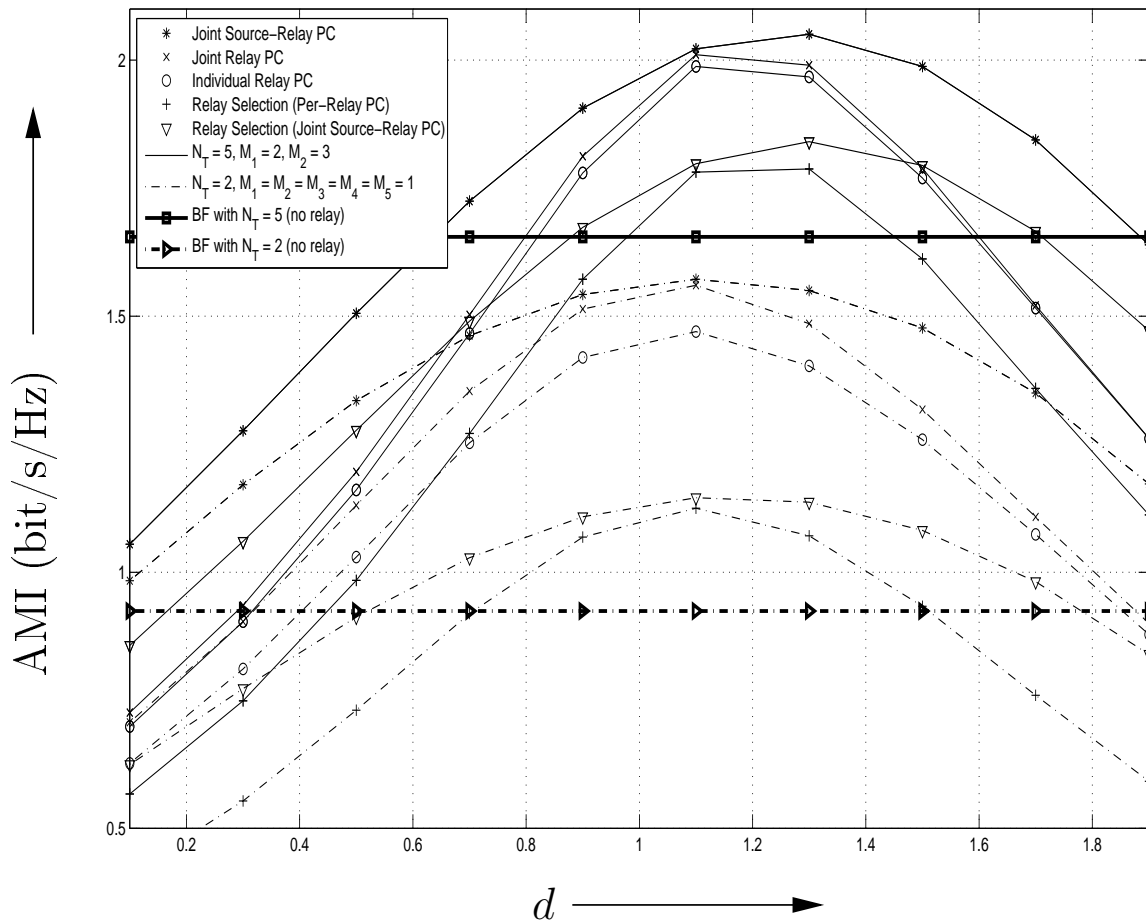


Figure 3.9: Average mutual information (AMI) in (bits/s/Hz) vs. distance d for two different network setups and different power constraints (PCs). The relays are in locations (a) and (e) for $N_R = 2$ and (a)–(e) for $N_R = 5$. The proposed gradient methods are used for computation of the source BF vector \mathbf{g} . A path-loss exponent of 4 is assumed. For comparison the average mutual information without relaying for a source transmit power of $P = 2$ and the average mutual information for relay selection are also shown.

power to the source.

Fig. 3.10 shows the BER of 16-ary quadrature amplitude modulation (16-QAM) for the three considered power constraints. For comparison we also show the BER for direct transmission with quaternary phase-shift keying (QPSK), i.e., the data rates for transmission with and without relaying are identical. Fig. 3.10 clearly shows that for the same number

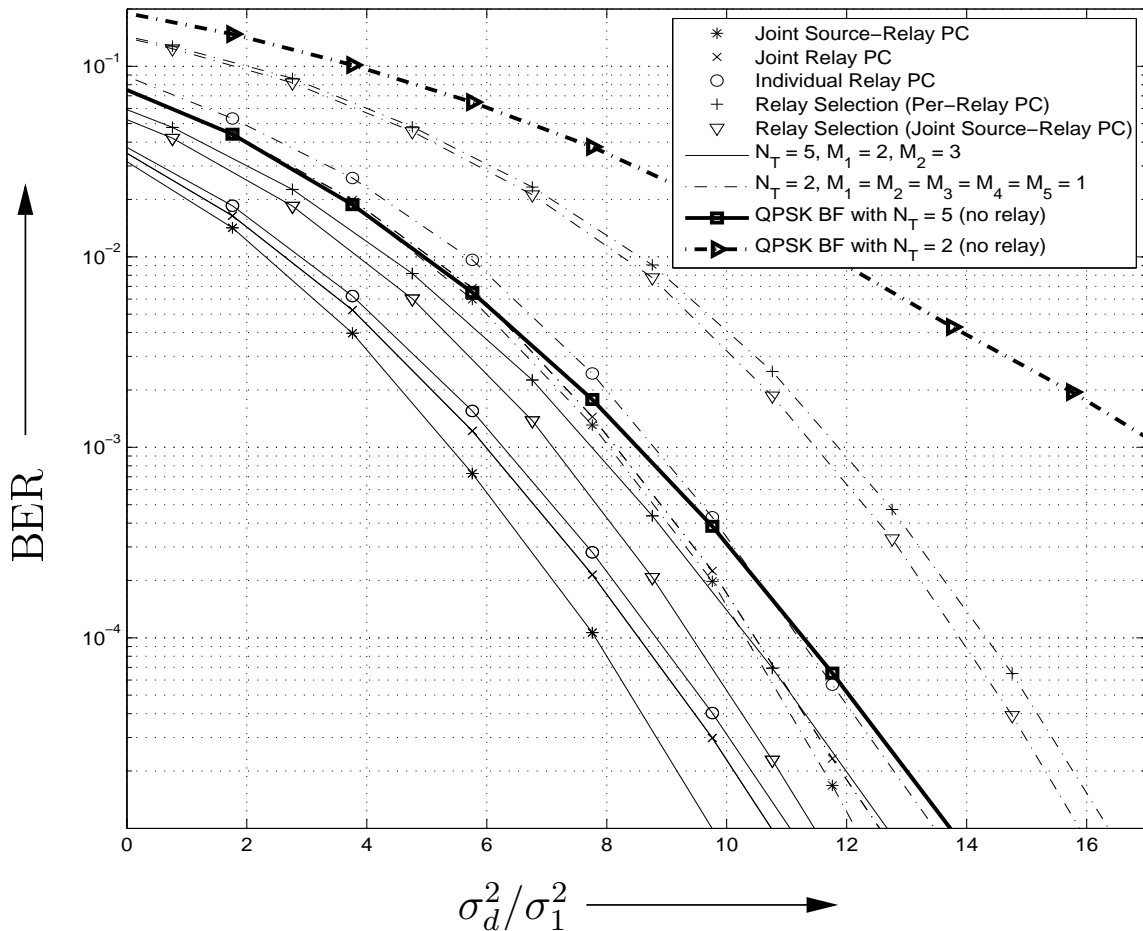


Figure 3.10: Average BER vs. σ_d^2/σ_n^2 for two different network setups and different power constraints. The relays are in locations (a) and (e) for $N_R = 2$ and (a)–(e) for $N_R = 5$. The proposed gradient methods are used for computation of the source BF vector \mathbf{g} . A path-loss exponent of 3 and $d = 1$ are assumed. AF-BF: 16-QAM. Direct transmission: QPSK, source transmit power $P = 2$.

of source transmit antennas, AF-BF yields significant performance gains in terms of the achievable BER compared to direct transmission and relay selection. Thereby, the achievable BER is the lower, the less restrictive the power constraints are, i.e., for a given SINR, the joint source-relay power constraint yields a lower BER than the joint relay power constraint and the joint relay power constraint yields a lower BER than the individual relay

power constraints.

3.6 Conclusions

In this chapter, we have considered AF–BF for cooperative networks with one multi–antenna source, multiple multi–antenna relays, and one single–antenna destination for three different power constraints. The obtained solutions show that while the source node requires the CSI of all channels in the network to compute the optimal BF vector, the relays only have to know their own source–relay and relay–destination channels for implementation of the optimal AF–BF matrices if the source can provide a small amount of feedback to each relay. For a given BF vector at the source, we have fully characterized the optimal AF–BF matrices for all three constraints. Furthermore, for small scale networks with joint relay or joint source–relay power constraints the optimal source BF vector can be found using polynomial programming. For large scale networks and networks with individual relay power constraints efficient suboptimal ad hoc and gradient methods for optimization of the source BF vectors have been provided. Simulation results confirm the close–to–optimal performance of the proposed gradient methods and show that the relative performance of the three considered power constraints significantly depends on the network topology. Furthermore, our results show that increasing the number of antennas at the source is particularly beneficial if the relays are located far away from the source. In contrast, increasing the number of antennas at the relays or the number of relays is always beneficial regardless of the location of the relays.

Chapter 4

Cooperative Filter-and-Forward Beamforming for Frequency-Selective Channels with Multiple Multi-Antenna Relays

4.1 Introduction

In the previous chapter, we have investigated BF for cooperative networks in frequency-nonselctive channels. Starting from this chapter, we will focus on BF schemes for cooperative networks in frequency-selective channels. Particularly, in this chapter, we consider one-way cooperative networks with one single-antenna source, one single-antenna destination, and multiple multi-antenna relay nodes. We assume single-carrier transmission and frequency-selective channels.

Relaying schemes for single-carrier transmission over frequency-selective channels have received little attention in the literature so far with [50, 81] being two notable exceptions. Specifically, a cooperative filter-and-forward (FF) BF technique was proposed and optimized under the assumptions that (1) there is no direct link between the source and the destination, (2) an equalizer is not available at the destination, and (3) full CSI of all links

is available [50]. We note that FF relaying for frequency–flat channels was also considered in [46]. For the frequency–selective case, distributed space–time block coding at the relays and equalization at the destination has been proposed in [81]. Distributed space–time coding does not require full CSI but has a worse performance than FF–BF.

In this chapter, we investigate cooperative FF–BF for frequency–selective channels for the case where the destination node has either (1) a simple slicer without equalization or (2) enough processing power to perform low–complexity equalization such as LE or DFE. Similar to [50] we assume that the central node, which computes the optimal FF–BF filters, has full CSI of all links. However, unlike [50], our model also includes multiple multi–antenna relays and equalization at the destination. This chapter makes the following contributions:

- For the simple slicer case, we optimize the FF–BF filters for maximization of the SINR under a transmit power constraint and for minimization of the transmit power under a QoS constraint, respectively. For both optimization criteria we find a closed–form solution for the optimal FIR FF–BF matrix filters at the relays.
- For the LE/DFE case, we assume FIR and IIR filters at the relays. We optimize FF–BF for maximization of the SINR at the output of LE and DFE as well as an idealized matched filter (MF) receiver ignoring any inter–symbol interference (ISI) in the filter output. The latter provides a natural performance upper bound for any equalization scheme [5] and allows us to bound possible performance gains achievable with more complex equalization schemes such as maximum likelihood sequence estimation (MLSE).
- For IIR FF–BF with equalization, we show that the frequency response vector of the optimal FF–BF filters can be decomposed into a unit–norm direction vector and a scalar power allocation factor across frequencies. We provide a unified closed–form

solution for the direction vector valid for all three considered equalization receiver structures and an efficient numerical method with guaranteed convergence for the power allocation.

- For FIR FF–BF with equalization, we show that the FF–BF filter optimization problem is related to a difficult mathematical problem for which an exact solution in closed form does not seem to exist. Therefore, we provide an efficient numerical method for recursive calculation of the optimum FIR FF–BF filters.
- Our simulation results show that (1) the performance of FF–BF without equalization at the destination crucially depends on the slicer decision delay, (2) with the same FF–BF filter length, the addition of simple LE and DFE equalizers at the destination node yields large performance gains compared to FF–BF with a slicer, (3) if long FIR FF–BF filters are employed, the simple slicer receiver with optimized decision delay closely approaches the same performance as equalizers, (4) relatively short FIR FF–BF filters with equalization suffice to closely approach the performance of IIR FF–BF filters, (5) the gap between FF–BF with LE and DFE, respectively, and the MF receiver is small implying that little can be gained by adopting more complex equalization schemes, and (6) if the total number of antennas at the relays is the same, it is preferable to have fewer relays with multiple antennas rather than more relays with less antennas each.

The remainder of this chapter is organized as follows. In Section 4.2, the adopted system model is presented. The optimization of FIR FF–BF filters when the destination employs only a simple slicer is discussed in Section 4.3, and the case where the destination employs LE/DFE is considered in Section 4.4. Simulation results are provided in Section 4.5, and some conclusions are drawn in Section 4.6.

4.2 System Model

We consider a relay network with one single–antenna source node, N_R multi–antenna relays, and one single–antenna destination node. A block diagram of the discrete–time overall transmission system in equivalent complex baseband representation is shown in Fig. 4.1. As usual, transmission is organized in two intervals. In the first interval, the source node transmits a data packet which is received by the relays. In the second interval, the relays filter the received packet and forward it to the destination node. We assume that there is no direct link between the source and the destination node (FF–BF for LE/DFE with direct link has been considered in our journal paper [82]). At the destination, the data packets received during the second interval are processed and detected.

In Fig. 4.1, the discrete–time CIRs between the source and the i th antenna of the z th relay, $g_{i,z}[k]$, $0 \leq k \leq L_g - 1$, and between the i th antenna of relay z and the destination, $h_{i,z}[k]$, $0 \leq k \leq L_h - 1$, contain the combined effects of transmit pulse shaping, the continuous–time channel, receive filtering, and sampling. Here, L_g and L_h denote the lengths of the source–relay and the relay–destination CIRs, respectively. Furthermore, we assume that relay z has M_z antennas and define $\mathbf{h}_z[k] \triangleq [h_{1,z}[k] \dots h_{M_z,z}[k]]^T$ and $\mathbf{g}_z[k] \triangleq [g_{1,z}[k] \dots g_{M_z,z}[k]]^T$. In the following, we describe the processing performed at the relays and the destination in detail.

4.2.1 FF–BF at Relays

The signal received at the i th antenna, $i = 1, \dots, M_z$, of the z th relay, $z = 1, \dots, N_R$, during the first time interval is given by

$$y_{i,z}[k] = g_{i,z}[k] * s[k] + n_{i,z}[k], \quad (4.1)$$

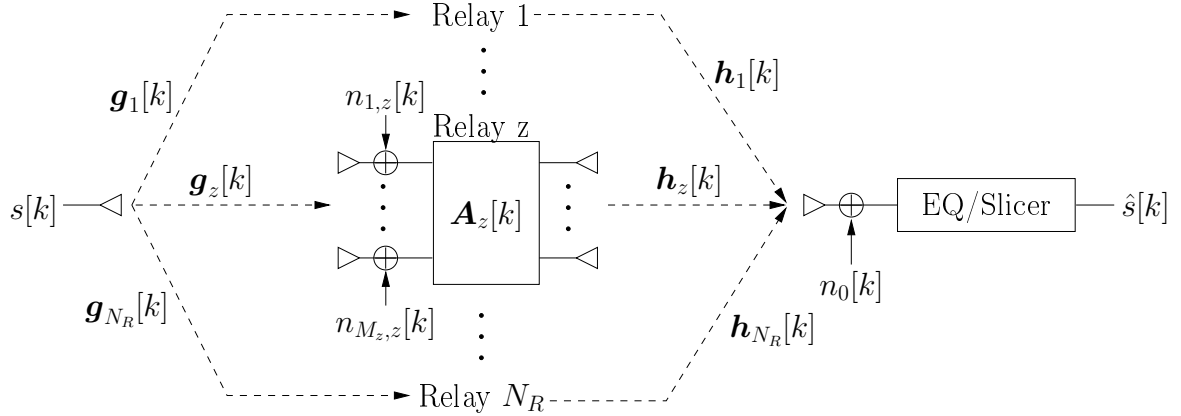


Figure 4.1: Cooperative network with one single–antenna source, multiple multi–antenna relay nodes, and one single–antenna destination. EQ is the equalizer at the destination. $\hat{s}[k]$ are estimated symbols after the equalizer or slicer.

where $s[k]$ are i.i.d. symbols taken from a scalar symbol alphabet \mathcal{A} such as PSK or QAM with variance $\sigma_s^2 \triangleq \mathcal{E}\{|s[k]|^2\}$, and $n_{i,z}[k]$ denotes the AWGN at the i th receive antenna of the z th relay with variance $\sigma_n^2 \triangleq \mathcal{E}\{|n_{i,z}[k]|^2\}$.

The FF–BF matrix filter impulse response coefficients of relay z are denoted by $M_z \times M_z$ matrix $\mathbf{A}_z[k]$, $-q_l \leq k \leq q_u$, with elements $a_{ji,z}[k]$ on row j and column i . For IIR FF–BF matrix filters $q_l \rightarrow \infty$ and $q_u \rightarrow \infty$ and for FIR FF–BF filters $q_l = 0$ and $q_u = L_a - 1$, where L_a is the FIR FF–BF matrix filter length. The signal transmitted by the j th antenna, $j = 1, \dots, M_z$, of the z th relay, $z = 1, \dots, N_R$, during the second time interval can be expressed as

$$t_{j,z}[k] = \sum_{i=1}^{M_z} a_{ji,z}[k] * y_{i,z}[k] = \sum_{i=1}^{M_z} a_{ji,z}[k] * g_{i,z}[k] * s[k] + \sum_{i=1}^{M_z} a_{ji,z}[k] * n_{i,z}[k]. \quad (4.2)$$

4.2.2 Processing at Destination

Since there is no direct link between the source and the destination, the signal received at the destination is given by

$$r[k] = \sum_{z=1}^{N_R} \sum_{j=1}^{M_z} h_{j,z}[k] * t_{j,z}[k] + n_0[k] = h_{eq}[k] * s[k] + n[k], \quad (4.3)$$

where $n_0[k]$ is AWGN with variance $\sigma_v^2 \triangleq \mathcal{E}\{|n_0[k]|^2\}$. The equivalent CIR $h_{eq}[k]$ between source and destination and the effective noise $n[k]$ are given by

$$h_{eq}[k] \triangleq \sum_{z=1}^{N_R} \sum_{j=1}^{M_z} h_{j,z}[k] * \sum_{i=1}^{M_z} a_{ji,z}[k] * g_{i,z}[k], \quad (4.4)$$

and

$$n[k] \triangleq \sum_{z=1}^{N_R} \sum_{j=1}^{M_z} h_{j,z}[k] * \sum_{i=1}^{M_z} a_{ji,z}[k] * n_{i,z}[k] + n_0[k], \quad (4.5)$$

respectively. Note that $n[k]$ is *colored* noise because of the filtering of $n_{i,z}[k]$ by $\mathbf{h}_z[k]$ and $\mathbf{A}_z[k]$. Eq. (4.3) shows that a cooperative relay network with FF–BF can be modeled as an equivalent SISO system. Therefore, as long as the destination knows the statistics of the colored noise $n[k]$, at the destination the same equalization, channel estimation, and channel tracking techniques as for point–to–point single–antenna transmission can be used. Here, we consider two cases: (1) The destination makes a decision based on $r[k]$ without equalization. (2) The destination first equalizes $r[k]$ using LE or DFE optimized under zero–forcing (ZF) and minimum mean–squared error (MMSE) criteria before making a decision [5]. The optimization of the corresponding FF–BF matrix filters will be discussed in Sections 4.3 and 4.4, respectively.

4.2.3 Feedback Channel

We assume that the destination estimates the relay–destination CIRs $h_{i,z}[k]$, $0 \leq k \leq L_h - 1$, $1 \leq i \leq N_R$ and $1 \leq z \leq N_R$, during a training phase. Similarly, relay i estimate its own source–relay CIR $g_{i,z}[k]$, $0 \leq k \leq L_g - 1$, and forwards the estimate to the destination node. Alternatively, the destination may directly estimate the combined CIR of the source–relay and relay–destination channels, $h_{i,z}[k] * g_{i,z}[k]$ if relay i retransmits the training signal received from the source. The destination can then extract $g_{i,z}[k]$ from $h_{i,z}[k] * g_{i,z}[k]$ and $h_{i,z}[k]$ via deconvolution. Subsequently, the destination node computes the FF–BF filters using the CSI of all links and feeds back the filter coefficients to the relays. Throughout this chapter we assume that the CSI and the feedback channel are perfect, which implies that the nodes in the network have limited mobility, and thus, all channels are slowly fading. We note that similar assumptions regarding the availability of CSI and the feedback channel are typically made in the distributed BF literature for both frequency–flat and frequency–selective channels, cf. e.g. [35, 39, 42, 44, 50].

4.3 FIR FF–BF without Equalization

In this section, we consider the case where the destination node cannot afford an equalizer due to size and/or power limitations. Therefore, we assume that a simple slicer is employed at the destination throughout this section. In the following, we will optimize FIR FF–BF matrix filters for maximization of the SINR at the slicer output under a power constraint and for minimization of the transmit power under a QoS constraint, respectively. We note that the results for multi–antenna relays in Sections 4.3.1 and 4.3.2 are extensions of the results for single–antenna relays given in [50]. Joint source–relay power constraints as considered in Sections 4.3.3 and 4.3.4 were not discussed in [50]. Also, for relaying with

single antenna relays a decision delay k_0 was not considered in [50], i.e., $k_0 = 0$. However, as will be shown in Section 4.5, the proper choice of decision delay k_0 is important for system performance.

The equivalent CIR $\mathbf{h}_{eq} \triangleq [h_{eq}[0] \ h_{eq}[1] \ \dots \ h_{eq}[L_a + L_g + L_h - 3]]^T$ between source and destination in Eq. (4.4) can be rewritten as

$$\mathbf{h}_{eq} = \sum_{z=1}^{N_R} \mathbf{H}_z \bar{\mathbf{G}}_z \bar{\mathbf{a}}_z \triangleq \mathcal{H} \mathcal{G}_D \mathbf{a}, \quad (4.6)$$

where $\mathcal{H} \triangleq [\mathbf{H}_1 \ \dots \ \mathbf{H}_{N_R}]$, $\mathcal{G}_D \triangleq \text{diag} \{ \bar{\mathbf{G}}_1, \dots, \bar{\mathbf{G}}_{N_R} \}$, and $\mathbf{a} \triangleq [\mathbf{a}_1^T \ \dots \ \mathbf{a}_{N_R}^T]^T$ with $(L_a + L_g + L_h - 2) \times (L_a + L_g - 1)M_z$ matrix $\mathbf{H}_z \triangleq [\mathbf{H}_{1,z} \ \mathbf{H}_{2,z} \ \dots \ \mathbf{H}_{M_z,z}]$, $(L_a + L_g - 1)M_z \times M_z^2 L_a$ matrix $\bar{\mathbf{G}}_z \triangleq \mathbf{I}_{M_z} \otimes [\bar{\mathbf{G}}_{1,z} \ \dots \ \bar{\mathbf{G}}_{M_z,z}]$, and $M_z^2 L_a \times 1$ vector $\mathbf{a}_z \triangleq [\mathbf{a}_{11,z}^T \ \mathbf{a}_{12,z}^T \ \dots \ \mathbf{a}_{1M_z,z}^T \ \mathbf{a}_{21,z}^T \ \dots \ \mathbf{a}_{M_z M_z,z}^T]^T$ with $\mathbf{a}_{ij,z} \triangleq [a_{ij,z}[0] \ a_{ij,z}[1] \ \dots \ a_{ij,z}[L_a - 1]]^T$. Moreover, $(L_a + L_g - 1) \times L_a$ matrix $\bar{\mathbf{G}}_{i,z}$ and $(L_a + L_g + L_h - 2) \times (L_a + L_g - 1)$ matrix $\mathbf{H}_{i,z}$ are column circular matrices with $[g_{i,z}[0] \ \dots \ g_{i,z}[L_g - 1] \ \mathbf{0}_{L_a-1}^T]^T$ and $[h_{i,z}[0] \ \dots \ h_{i,z}[L_h - 1] \ \mathbf{0}_{L_a+L_g-2}^T]^T$ in the first columns, respectively.

Matrix \mathcal{H} can be separated into one vector \mathbf{h}_{k_0} and one sub-matrix \mathcal{H}_{k_0} , i.e., length $(L_a + L_g - 1) \sum_{z=1}^{N_R} M_z$ vector $\mathbf{h}_{k_0}^T$ is the row k_0 of \mathcal{H}_{k_0} , and $\mathcal{H}_{k_0} \triangleq [\mathcal{H}]_{ij}$, $i \in \{1, \dots, k_0 - 1, k_0 + 1, \dots, (L_a + L_g + L_h - 2)\}$, $j \in \{1, \dots, (L_a + L_g - 1) \sum_{z=1}^{N_R} M_z\}$. Therefore, the first term in (4.3) can be decomposed into a signal part and an ISI part

$$\begin{aligned} h_{eq}[k] * s[k] &= h_{eq}[k_0]s[k - k_0] + \sum_{l=1, l \neq k_0}^{L_a+L_g+L_h-3} h_{eq}[l]s[k - l] \\ &= \underbrace{\mathbf{h}_{k_0}^T \mathcal{G}_D \mathbf{a} s[k - k_0]}_{\text{desired signal}} + \underbrace{\mathbf{s}^T[k] \mathcal{H}_{k_0} \mathcal{G}_D \mathbf{a}}_{\text{ISI}} \end{aligned} \quad (4.7)$$

with $\mathbf{s}[k] = [s[k] \ \dots \ s[k - k_0 + 1] \ s[k - k_0 - 1] \ \dots \ s_1[k - (L_a + L_g + L_h - 3)]]^T$, and k_0 is the slicer decision delay at the destination. Therefore, the power of the desired signal and

the ISI can be obtained as

$$\mathcal{E} \left\{ \left| \mathbf{h}_{k_0}^T \mathcal{G}_D \mathbf{a} s[k - k_0] \right|^2 \right\} = \sigma_s^2 \mathbf{a}^H \mathcal{G}_D^H \mathbf{h}_{k_0}^* \mathbf{h}_{k_0}^T \mathcal{G}_D \mathbf{a} \quad (4.8)$$

and

$$\mathcal{E} \left\{ \left| \mathbf{s}^T[k] \mathcal{H}_{k_0} \mathcal{G}_D \mathbf{a} \right|^2 \right\} = \sigma_s^2 \mathbf{a}^H \mathcal{G}_D^H \mathcal{H}_{k_0}^H \mathcal{H}_{k_0} \mathcal{G}_D \mathbf{a}, \quad (4.9)$$

respectively. Similarly, $n[k]$ in (4.5) can be rewritten as

$$n[k] = \sum_{z=1}^{N_R} \mathbf{n}_z[k] \check{\mathbf{H}}_z \bar{\mathbf{a}}_z + n_0[k] \triangleq \mathbf{N}[k] \check{\mathbf{H}} \mathbf{a} + n_0[k] \quad (4.10)$$

with length $\sum_{z=1}^{N_R} (L_a + L_h - 1) M_z$ row vector $\mathbf{n}[k] \triangleq [\mathbf{n}_1^T[k] \dots \mathbf{n}_{N_R}^T[k]]^T$ and $\sum_{z=1}^{N_R} (L_a + L_h - 1) M_z \times \sum_{z=1}^{N_R} M_z^2 L_a$ matrix $\check{\mathbf{H}} \triangleq \text{diag} \left\{ \check{\mathbf{H}}_1, \dots, \check{\mathbf{H}}_{N_R} \right\}$. Moreover, $\mathbf{n}_z[k] \triangleq [\mathbf{n}_{1,z}^T[k] \dots \mathbf{n}_{M_z,z}^T[k]]^T$ with $\mathbf{n}_{i,z}[k] \triangleq [n_{i,z}[k] \dots n_{i,z}[k - (L_a + L_h - 2)]]^T$, and $\check{\mathbf{H}}_z \triangleq [\mathbf{I}_{M_z} \otimes \bar{\mathbf{H}}_{1,z} \dots \mathbf{I}_{M_z} \otimes \bar{\mathbf{H}}_{M_z,z}]$, where $(L_a + L_h - 1) \times L_a$ matrix $\bar{\mathbf{H}}_{i,z}$ is column circular matrix with $[h_{i,z}[0] \dots h_{i,z}[L_h - 1] \mathbf{0}_{L_a-1}^T]^T$ in the first column. The noise power can be obtained as

$$\mathcal{E}\{|n[k]|^2\} = \sigma_n^2 \mathbf{a}^H \check{\mathbf{H}}^H \check{\mathbf{H}} \mathbf{a} + \sigma_v^2. \quad (4.11)$$

From (4.8), (4.9), and (4.11), the SINR at the destination can be obtained as

$$\begin{aligned} \text{SINR}(\mathbf{a}) &= \frac{\mathcal{E} \left\{ \left| \mathbf{h}_{k_0}^T \mathcal{G}_D \mathbf{a} s[k - k_0] \right|^2 \right\}}{\mathcal{E} \left\{ \left| \mathbf{s}^T[k] \mathcal{H}_{k_0} \mathcal{G}_D \mathbf{a} \right|^2 \right\} + \mathcal{E}\{|n[k]|^2\}} \\ &= \frac{\mathbf{a}^H \mathbf{W}_1 \mathbf{a}}{\mathbf{a}^H \mathbf{W}_2 \mathbf{a} + \mathbf{a}^H \mathbf{W}_3 \mathbf{a} + 1} \end{aligned} \quad (4.12)$$

with $\mathbf{W}_1 \triangleq \sigma_s^2 \mathcal{G}_D^H \mathbf{h}_{k_0}^* \mathbf{h}_{k_0}^T \mathcal{G}_D / \sigma_v^2$, $\mathbf{W}_2 \triangleq \sigma_s^2 \mathcal{G}_D^H \mathcal{H}_{k_0}^H \mathcal{H}_{k_0} \mathcal{G}_D / \sigma_v^2$, and $\mathbf{W}_3 \triangleq \sigma_n^2 \check{\mathbf{H}}^H \check{\mathbf{H}} / \sigma_v^2$.

From (4.2), the total transmit power, $P_R(\mathbf{a})$, of the relays can be obtained as

$$P_R(\mathbf{a}) = \sum_{z=1}^{N_R} \sum_{j=1}^{M_z} \mathcal{E} \{ |t_{j,z}[k]|^2 \} = \mathbf{a}^H \mathbf{D} \mathbf{a}, \quad (4.13)$$

with $\mathbf{D} \triangleq \sigma_s^2 \mathcal{G}_D^H \mathcal{G}_D + \sigma_n^2 \mathbf{I}_{L_a \sum_{z=1}^{N_R} M_z}$.

In the following, we will formulate various FF–BF filter optimization problems based on (4.12) and (4.13).

4.3.1 SINR Maximization Under Relay Power Constraint

First, we consider the optimization of the FF–BF matrix filters for maximization of the SINR subject to maximum relay power P [50]. In comparison to [50], we consider a more general case where relays have multiple antennas, and the resulting optimization problem is more involved. Accordingly, the optimization problem can be formulated as

$$\max_{\mathbf{a}} \quad \text{SINR}(\mathbf{a}) \quad (4.14a)$$

$$s.t. \quad \mathbf{a}^H \mathbf{D} \mathbf{a} \leq P. \quad (4.14b)$$

By letting $\mathbf{w} \triangleq \mathbf{D}^{1/2} \mathbf{a}$, where $\mathbf{D}^{1/2}$ is the Cholesky decomposition of \mathbf{D} , the optimization problem in (4.14) can be reformulated as a generalized eigenvalue problem. The optimum \mathbf{w} can be obtained as

$$\begin{aligned} \mathbf{w}_{\text{opt}} &= \sqrt{P} \mathbf{u} \left\{ \mathbf{Q}_1^{-1} \mathbf{D}^{-H/2} \mathbf{W}_1 \mathbf{D}^{-1/2} \right\} \\ &= \frac{\sqrt{P} \mathbf{Q}_1^{-1} \mathbf{D}^{-H/2} \mathcal{G}_D^H \mathbf{h}_{k_0}^*}{\sqrt{\mathbf{h}_{k_0}^T \mathcal{G}_D \mathbf{D}^{-1/2} \mathbf{Q}_1^{-2} \mathbf{D}^{-H/2} \mathcal{G}_D^H \mathbf{h}_{k_0}^*}}, \end{aligned} \quad (4.15)$$

where $\mathbf{Q}_1 \triangleq \mathbf{D}^{-H/2} (\mathbf{W}_2 + \mathbf{W}_3) \mathbf{D}^{-1/2} + \frac{1}{P} \mathbf{I}_{L_a \sum_{z=1}^{N_R} M_z^2}$ and $\mathbf{u}\{\mathbf{X}\}$ is the principle eigenvector of matrix \mathbf{X} . Therefore, the maximum SINR can be obtained as

$$\text{SINR}_{\max} = \frac{\sigma_s^2}{\sigma_v^2} \mathbf{h}_{k_0}^T \mathcal{G}_D \left(\mathbf{W}_2 + \mathbf{W}_3 + \frac{1}{P} \mathbf{D} \right)^{-1} \mathcal{G}_D^H \mathbf{h}_{k_0}^*, \quad (4.16)$$

and the corresponding optimum FF–BF matrix filter in vector form is given as

$$\mathbf{a}_{\text{opt}} = \frac{\sqrt{P} (\mathbf{W}_2 + \mathbf{W}_3 + \frac{1}{P} \mathbf{D})^{-1} \mathcal{G}_D^H \mathbf{h}_{k_0}^*}{\sqrt{\mathbf{h}_{k_0}^T \mathcal{G}_D \mathbf{D}^{-1/2} \mathbf{Q}_1^{-2} \mathbf{D}^{-H/2} \mathcal{G}_D^H \mathbf{h}_{k_0}^*}}. \quad (4.17)$$

4.3.2 Relay Power Minimization Under SINR Constraint

Here, we optimize the FF–BF matrix filters for minimization of the relay transmit power, $P_R(\mathbf{a})$, subject to an SINR constraint [50]. Again, we extend the results from [50] for single-antenna relays to multiple-antenna relays. The optimization problem can be formulated as

$$\min_{\mathbf{a}} \quad P_R(\mathbf{a}) = \mathbf{a}^H \mathbf{D} \mathbf{a} \quad (4.18a)$$

$$s.t. \quad \frac{\mathbf{a}^H \mathbf{W}_1 \mathbf{a}}{\mathbf{a}^H \mathbf{W}_2 \mathbf{a} + \mathbf{a}^H \mathbf{W}_3 \mathbf{a} + 1} \geq \gamma, \quad (4.18b)$$

where γ is the QoS requirement (minimal required SINR) at the destination. We let $\mathbf{w} = \mathbf{D}^{1/2} \mathbf{a}$ again and note that the above problem is infeasible when $\mathbf{Q}_2 \triangleq \mathbf{D}^{-H/2} (\mathbf{W}_1 - \gamma \mathbf{W}_2 - \gamma \mathbf{W}_3) \mathbf{D}^{-1/2}$, is negative semidefinite. If the problem is feasible, the optimum FF–BF matrix filter can be obtained as

$$\mathbf{a}_{\text{opt}} = \left(\frac{\gamma}{\lambda_{\max}\{\mathbf{Q}_2\}} \right)^{1/2} \mathbf{D}^{-1/2} \mathbf{u}\{\mathbf{Q}_2\} \quad (4.19)$$

and the corresponding minimum relay power is

$$P_{\min} = \frac{\gamma}{\lambda_{\max}\{\mathbf{Q}_2\}}. \quad (4.20)$$

4.3.3 SINR Maximization Under Source–Relay Power Constraint

Compared to the case with separate power constraints for the source and the relays, which was considered in Section 4.3.1, additional performance gains are possible with a joint source–relay transmit power constraint. We note that the joint source–relay transmit power constraint cases in Subsections 4.3.3 and 4.3.4 were not considered in [50]. The corresponding optimization problem can be formulated as

$$\max_{\mathbf{a}, \sigma_s^2} \frac{\mathbf{a}^H \mathbf{W}_1 \mathbf{a}}{\mathbf{a}^H \mathbf{W}_2 \mathbf{a} + \mathbf{a}^H \mathbf{W}_3 \mathbf{a} + 1} \quad (4.21a)$$

$$s.t. \quad \mathbf{a}^H \mathbf{D} \mathbf{a} + \sigma_s^2 \leq P \quad (4.21b)$$

The optimal solution can be found with a divide–and–conquer method. In particular, if we assume that σ_s^2 is fixed, problem (4.21) is identical to problem (4.14). The optimum FF–BF matrix filter is obtained as

$$\mathbf{a}_{\text{opt}} = \frac{\sqrt{P - \sigma_s^2} \left(\mathbf{W}_2(\sigma_s^2) + \mathbf{W}_3 + \frac{\mathbf{D}(\sigma_s^2)}{P - \sigma_s^2} \right)^{-1} \mathcal{G}_D^H \mathbf{h}_{k_0}^*}{\sqrt{\mathbf{h}_{k_0}^T \mathcal{G}_D \mathbf{D}^{-1/2}(\sigma_s^2) \mathbf{Q}_1^{-2}(\sigma_s^2) \mathbf{D}^{-H/2}(\sigma_s^2) \mathcal{G}_D^H \mathbf{h}_{k_0}^*}}, \quad (4.22)$$

and the corresponding maximum SINR is given by

$$\text{SINR}_{\max}(\sigma_s^2) = \frac{\sigma_s^2}{\sigma_v^2} \mathbf{h}_{k_0}^T \mathcal{G}_D \left(\mathbf{W}_2(\sigma_s^2) + \mathbf{W}_3 + \frac{\mathbf{D}(\sigma_s^2)}{P - \sigma_s^2} \right)^{-1} \mathcal{G}_D^H \mathbf{h}_{k_0}^* \quad (4.23)$$

where

$$\mathbf{Q}_1(\sigma_s^2) \triangleq \mathbf{D}^{-H/2}(\sigma_s^2) (\mathbf{W}_2(\sigma_s^2) + \mathbf{W}_3) \mathbf{D}^{-1/2}(\sigma_s^2) + \frac{1}{P - \sigma_s^2} \mathbf{I}_{L_a \sum_{z=1}^{N_R} M_z^2}. \quad (4.24)$$

Note that \mathbf{D} , \mathbf{W}_1 , and \mathbf{W}_2 defined earlier depend on σ_s^2 in this case. The remaining problem is to find the optimal σ_s^2 such that $\text{SINR}_{\max}(\sigma_s^2)$ is maximized, i.e.

$$\max_{\sigma_s^2, 0 \leq \sigma_s^2 \leq P} \text{SINR}_{\max}(\sigma_s^2). \quad (4.25)$$

Problem (4.25) can be easily solved by a grid search or other numerical methods given in [1].

4.3.4 Source–Relay Power Minimization Under SINR Constraint

In this case, the goal is to minimize the joint source–relay transmit power subject to a destination SINR constraint. The optimization problem can be formulated as

$$\min_{\mathbf{a}, \sigma_s^2} \quad \mathbf{a}^H \mathbf{D} \mathbf{a} + \sigma_s^2 \quad (4.26a)$$

$$s.t. \quad \frac{\mathbf{a}^H \mathbf{W}_1 \mathbf{a}}{\mathbf{a}^H \mathbf{W}_2 \mathbf{a} + \mathbf{a}^H \mathbf{W}_3 \mathbf{a} + 1} \geq \gamma \quad (4.26b)$$

Again, we assume that σ_s^2 is fixed, and the resulting problem is identical to problem (4.18).

If the problem is feasible, the optimum FF–BF matrix filter is given by

$$\mathbf{a}_{\text{opt}} = \left(\frac{\gamma}{\lambda_{\max}\{\mathbf{Q}_2(\sigma_s^2)\}} \right)^{1/2} \mathbf{D}^{-1/2}(\sigma_s^2) \mathbf{u}\{\mathbf{Q}_2(\sigma_s^2)\}, \quad (4.27)$$

where $\lambda_{\max}\{\cdot\}$ denotes maximum eigenvalue of a matrix, and the corresponding minimum joint source–relay transmit power is

$$P_{\min} = \frac{\gamma}{\lambda_{\max}\{\mathbf{Q}_2(\sigma_s^2)\}} + \sigma_s^2 \quad (4.28)$$

with $\mathbf{Q}_2(\sigma_s^2) \triangleq \mathbf{D}^{-H/2}(\sigma_s^2) (\mathbf{W}_1(\sigma_s^2) - \gamma \mathbf{W}_2(\sigma_s^2) - \gamma \mathbf{W}_3) \times \mathbf{D}^{-1/2}(\sigma_s^2)$. The remaining optimization problem is

$$\min_{\sigma_s^2} \frac{\gamma}{\lambda_{\max}\{\mathbf{Q}_2(\sigma_s^2)\}} + \sigma_s^2 \quad (4.29a)$$

$$s.t. \quad \lambda_{\max}\{\mathbf{Q}_2(\sigma_s^2)\} > 0. \quad (4.29b)$$

Note that $\lambda_{\max}\{\mathbf{Q}_2(\sigma_s^2)\} = 0$ when $\sigma_s^2 = 0$. Therefore, $\sigma_s^2 = 0$ has been ignored in problem (4.29) due to the fact that (4.29b) is satisfied only if $\sigma_s^2 > 0$. Problem (4.29) can be easily solved by numerical methods given in [1].

4.4 FF–BF with Equalization

Throughout this section we assume that the destination node employs LE or DFE with IIR equalization filters. In a practical implementation, FIR equalization filters are used, of course. However, sufficiently long FIR filters will approach the performance of IIR filters arbitrarily close. Assuming IIR equalization filters has the advantage that relatively simple and elegant expressions for the SINR at the equalizer output exist [83, 84].

4.4.1 Optimal IIR FF–BF with Equalization

In order to exploit the SINR expressions in [83, 84], we first have to whiten the noise impairing the signal received at the destination. The power spectral density of $n[k]$ in

(4.5) can be obtained as

$$\Phi_n(f) = \sigma_n^2 \sum_{z=1}^{N_R} \sum_{i=1}^{M_z} \left| \sum_{j=1}^{M_z} H_{j,z}(f) A_{ji,z}(f) \right|^2 + \sigma_v^2 = \sigma_n^2 \mathbf{a}^H(f) \mathbf{\Gamma}(f) \mathbf{a}(f) + \sigma_v^2 \quad (4.30)$$

with $\sum_{z=1}^{N_R} M_z^2 \times \sum_{z=1}^{N_R} M_z^2$ square matrix $\mathbf{\Gamma}(f) \triangleq \text{diag} \{ \mathbf{\Gamma}_1(f), \dots, \mathbf{\Gamma}_{N_R}(f) \}$, where $\mathbf{\Gamma}_z(f) \triangleq (\mathbf{h}_z^*(f) \mathbf{h}_z^T(f)) \otimes \mathbf{I}_{M_z}$ and $\mathbf{h}_z(f) \triangleq [H_{1,z}(f), \dots, H_{M_z,z}(f)]^T$. The frequency response of the relay–destination channel corresponding to the j th antenna of the z th relay is given by $H_{j,z}(f) \triangleq \mathcal{F}\{h_{j,z}[k]\}$. The frequency responses of the FF–BF matrix filters are collected in vector $\mathbf{a}(f) \triangleq [\mathbf{a}_1^T(f) \dots \mathbf{a}_{N_R}^T(f)]^T$ with $\mathbf{a}_z(f) \triangleq [A_{11,z}(f) \ A_{12,z}(f) \ \dots \ A_{M_z M_z,z}(f)]^T$, where $A_{ji,z}(f) \triangleq \mathcal{F}\{a_{ji,z}[k]\}$ denotes the frequency response of the FF–BF matrix filter at relay z corresponding to the i th receive antenna and the j th transmit antenna. The whitening filter $W(f)$ for $n[k]$ can be easily obtained as

$$\begin{aligned} W(f) &= \left(\sigma_n^2 \sum_{z=1}^{N_R} \sum_{i=1}^{M_z} \left| \sum_{j=1}^{M_z} H_{j,z}(f) A_{ji,z}(f) \right|^2 + \sigma_v^2 \right)^{-1/2} \\ &= (\sigma_n^2 \mathbf{a}^H(f) \mathbf{\Gamma}(f) \mathbf{a}(f) + \sigma_v^2)^{-1/2}, \end{aligned} \quad (4.31)$$

and we denote the output of the whitening filter by $r'[k]$. Taking into account the whitening, the frequency response of the equivalent overall channel can be obtained as

$$H'_{eq}(f) \triangleq W(f) \mathcal{F}\{h_{eq}[k]\} = (\sigma_n^2 \mathbf{a}^H(f) \mathbf{\Gamma}(f) \mathbf{a}(f) + \sigma_v^2)^{-1/2} \mathbf{q}^T(f) \mathbf{a}(f) \quad (4.32)$$

with $\mathbf{q}(f) \triangleq [\mathbf{q}_1^T(f) \dots \mathbf{q}_{N_R}^T(f)]^T$, $\mathbf{q}_z(f) \triangleq \mathbf{h}_z(f) \otimes \mathbf{g}_z(f)$, $\mathbf{g}_z(f) \triangleq [G_{1,z}(f) \ G_{2,z}(f) \ \dots \ G_{M_z,z}(f)]^T$, $G_{i,z}(f) \triangleq \mathcal{F}\{g_{i,z}[k]\}$, and $\mathbf{h}_z(f) \triangleq [H_{1,z}(f) \ H_{2,z}(f) \ \dots \ H_{M_z,z}(f)]^T$. The power spectral density of the noise component, $n'[k]$, of $r'[k]$ is $\Phi_{n'}(f) = 1$.

In the remainder of this section, we formulate and solve the IIR FF–BF filter opti-

mization problems for LE, DFE, and an idealized matched filter (MF) receiver in a unified manner. After introducing

$$Z(\mathbf{a}(f)) \triangleq |H'_{eq}(f)|^2 = \frac{\mathbf{a}^H(f)\mathbf{q}^*(f)\mathbf{q}^T(f)\mathbf{a}(f)}{\sigma_n^2\mathbf{a}^H(f)\mathbf{\Gamma}(f)\mathbf{a}(f) + \sigma_v^2}, \quad (4.33)$$

we can express the SINRs at the outputs of a decision feedback and a linear equalizer as [83, 84]

$$\text{SINR}_{\text{DFE}}(\mathbf{a}(f)) = \sigma_s^2 \exp \left\{ \int_{-1/2}^{1/2} \ln(Z(\mathbf{a}(f)) + \xi) \, df \right\} - \chi \quad (4.34)$$

and

$$\text{SINR}_{\text{LE}}(\mathbf{a}(f)) = \sigma_s^2 \left(\int_{-1/2}^{1/2} (Z(\mathbf{a}(f)) + \xi)^{-1} \, df \right)^{-1} - \chi, \quad (4.35)$$

respectively. In (4.34) and (4.35), we have $\chi = 0$, $\xi = 0$ and $\chi = 1$, $\xi = 1/\sigma_s^2$ if the equalization filters are optimized based on a ZF and an MMSE criterion, respectively. Similarly, if only a single, isolated symbol $s[k]$ is transmitted, the SINR at the output of an MF is given by [5]

$$\text{SINR}_{\text{MF}}(\mathbf{a}(f)) = \sigma_s^2 \int_{-1/2}^{1/2} Z(\mathbf{a}(f)) \, df. \quad (4.36)$$

It is not difficult to show that regardless of how the FF–BF filter frequency responses $\mathbf{a}(f)$ are chosen, we always have [84]

$$\text{SINR}_{\text{MF}}(\mathbf{a}(f)) \geq \text{SINR}_{\text{DFE}}(\mathbf{a}(f)) \geq \text{SINR}_{\text{LE}}(\mathbf{a}(f)). \quad (4.37)$$

Thus, the MF receiver constitutes a performance upper bound for DFE and LE with

continuous transmission of symbols $s[k]$. In fact, it can be shown that the MF receiver provides a performance upper bound for any realizable equalization structure including optimal MLSE [5]. Note, however, that the MF receiver generally has a poor performance for continuous symbol transmission since it does not combat ISI.

In this section, our goal is to optimize the FF–BF matrix filters for maximization of the SINRs at the output of the considered equalizers. To make the problem well defined, we constrain the relay transmit power, P_R , which is given by

$$P_R = \sum_{z=1}^{N_R} \sum_{j=1}^{M_z} \int_{-1/2}^{1/2} \Phi_{t_{j,z}}(f) df = \int_{-1/2}^{1/2} \mathbf{a}^H(f) \mathbf{D}(f) \mathbf{a}(f) df \quad (4.38)$$

where $\Phi_{t_{j,z}}(f) \triangleq \sigma_s^2 |\sum_{i=1}^{M_z} A_{ji,z}(f) G_{i,z}(f)|^2 + \sigma_n^2 \sum_{i=1}^{M_z} |A_{ji,z}(f)|^2$, $z = 1, \dots, N_R$, $j = 1, \dots, M_z$, is the power spectral density of the transmit signal $t_{j,z}[k]$ at the j th antenna of the z th relay, $\mathbf{D}(f) \triangleq \sigma_s^2 \mathbf{G}^H(f) \mathbf{G}(f) + \sigma_n^2 \mathbf{I}_{\sum_{z=1}^{N_R} M_z^2}$, $\mathbf{G}(f) \triangleq \text{diag} \{ \mathbf{G}_1(f), \dots, \mathbf{G}_{N_R}(f) \}$, and $\mathbf{G}_z(f) \triangleq \mathbf{I}_{M_z} \otimes \mathbf{g}_z^T(f)$.

Formally, the IIR FF–BF filter optimization problem can now be stated as

$$\max_{\mathbf{a}(f)} \quad \text{SINR}_X(\mathbf{a}(f)) \quad (4.39a)$$

$$\text{s.t.} \quad \int_{-1/2}^{1/2} \mathbf{a}^H(f) \mathbf{D}(f) \mathbf{a}(f) df \leq P, \quad (4.39b)$$

where P denotes the maximum relay transmit power, and $X = \text{DFE}$, $X = \text{LE}$, and $X = \text{MF}$ for DFE, LE, and an MF receiver, respectively. It is convenient to introduce vector $\mathbf{v}(f) \triangleq \mathbf{D}^{1/2}(f) \mathbf{a}(f)$, which can be expressed as $\mathbf{v}(f) = \sqrt{p(f)} \mathbf{u}(f)$ without loss of generality, where $p(f)$ denotes the power of $\mathbf{v}(f)$ and $\mathbf{u}(f)$ has unit norm, $\|\mathbf{u}(f)\|^2 = 1$. Furthermore,

we introduce $\bar{Z}(\mathbf{v}(f)) = \bar{Z}(\sqrt{p(f)}\mathbf{u}(f)) \triangleq Z(\mathbf{a}(f))$, which is given by

$$\bar{Z}(\mathbf{v}(f)) = \frac{\mathbf{a}^H(f)\mathbf{q}^*(f)\mathbf{q}^T(f)\mathbf{a}(f)}{\sigma_n^2\mathbf{a}^H(f)\mathbf{\Gamma}(f)\mathbf{a}(f) + \sigma_v^2} = \frac{\mathbf{u}^H(f)\mathbf{J}(f)\mathbf{u}(f)}{\mathbf{u}^H(f)\mathbf{X}(f)\mathbf{u}(f)} \quad (4.40)$$

with rank one, positive semi-definite matrix

$$\mathbf{J}(f) = p(f)\mathbf{D}^{-1/2}(f)\mathbf{q}^*(f)\mathbf{q}^T(f)\mathbf{D}^{-1/2}(f) \quad (4.41)$$

and full rank, positive definite matrix

$$\mathbf{X}(f) = \sigma_n^2 p(f)\mathbf{D}^{-1/2}(f)\mathbf{\Gamma}(f)\mathbf{D}^{-1/2}(f) + \sigma_v^2\mathbf{I}_{N_R}. \quad (4.42)$$

Introducing $\overline{\text{SINR}}_X(\mathbf{v}(f)) = \overline{\text{SINR}}_X\left(\sqrt{p(f)}\mathbf{u}(f)\right) \triangleq \text{SINR}_X(\mathbf{a}(f))$, we can restate problem (4.39) in equivalent form as

$$\max_{p(f), \mathbf{u}(f)} \overline{\text{SINR}}_X\left(\sqrt{p(f)}\mathbf{u}(f)\right) \quad (4.43a)$$

$$\text{s.t.} \quad \int_{-1/2}^{1/2} p(f) \, df \leq P \quad (4.43b)$$

$$p(f) \geq 0. \quad (4.43c)$$

In the following, we provide a unified solution to problem (4.43) valid for all three considered equalization schemes.

- 1) *Optimum IIR FF-BF Filters*: We observe from (4.43) that the constraints of the considered optimization problem do not depend on $\mathbf{u}(f)$. Thus, without loss of generality, we can find the globally optimal solution of problem (4.43) by first maximizing the SINR with respect to $\mathbf{u}(f)$ for a given power allocation $p(f)$ and by subsequently

optimizing the resulting SINR expression with respect to $p(f)$.

Furthermore, for all three considered receiver structures, the SINR $\overline{\text{SINR}}_{\mathbf{X}}(\mathbf{v}(f))$ is monotonically increasing in $\bar{Z}(\sqrt{p(f)}\mathbf{u}(f))$. Thus, for any given power allocation $p(f)$, we can maximize the SINR $\overline{\text{SINR}}_{\mathbf{X}}(\mathbf{v}(f))$ by maximizing $\bar{Z}(\sqrt{p(f)}\mathbf{u}(f))$ with respect to $\mathbf{u}(f)$ for all frequencies f . Hence, the optimal FF–BF direction vector, $\mathbf{u}_{\text{opt}}(f)$, can be found from the following optimization problem

$$\max_{\mathbf{u}(f)} \bar{Z}(\sqrt{p(f)}\mathbf{u}) = \frac{\mathbf{u}^H(f)\mathbf{J}(f)\mathbf{u}(f)}{\mathbf{u}^H(f)\mathbf{X}(f)\mathbf{u}(f)}. \quad (4.44)$$

Problem (4.44) is a generalized eigenvalue problem for which a closed–form solution exists since matrix $\mathbf{J}(f)$ has rank one and matrix $\mathbf{X}(f)$ has full rank. The solution of problem (4.44) can be easily obtained as

$$\mathbf{u}_{\text{opt}}(f) = c(f)\mathbf{X}^{-1}(f)\mathbf{D}^{-1/2}(f)\mathbf{q}^*(f), \quad (4.45)$$

where $c(f)$ is a real–valued scaling factor which is given by

$$c(f) = \frac{1}{\sqrt{\mathbf{q}^T(f)\mathbf{D}^{-1/2}(f)\mathbf{X}^{-2}(f)\mathbf{D}^{-1/2}(f)\mathbf{q}^*(f)}}. \quad (4.46)$$

The maximum $\bar{Z}(\sqrt{p(f)}\mathbf{u}(f))$ achievable with $\mathbf{u}_{\text{opt}}(f)$ is

$$\begin{aligned} \bar{Z}(\sqrt{p(f)}\mathbf{u}_{\text{opt}}(f)) &= p(f)\mathbf{q}^T(f)\mathbf{D}^{-1/2}(f)\mathbf{X}^{-1}(f)\mathbf{D}^{-1/2}(f)\mathbf{q}^*(f) \\ &= p(f)\mathbf{q}^T(f)(\sigma_n^2 p(f)\mathbf{\Gamma}(f) + \sigma_v^2 \mathbf{D}(f))^{-1}\mathbf{q}^*(f). \end{aligned} \quad (4.47)$$

Now, we can express the optimal FF–BF filter frequency response vector (for a given

power allocation), $\mathbf{a}_{\text{opt}}(f)$, as

$$\mathbf{a}_{\text{opt}}(f) = \sqrt{p(f)}c(f) (\sigma_n^2 p(f)\mathbf{\Gamma}(f) + \sigma_v^2 \mathbf{D}(f))^{-1} \mathbf{q}^*(f). \quad (4.48)$$

From (4.48), the optimum individual FF–BF filter of relay z , $\mathbf{a}_z^{\text{opt}}(f)$, can be simplified as

$$\begin{aligned} \mathbf{a}_z^{\text{opt}}(f) &= \sqrt{p(f)}c(f) \left(\sigma_n^2 p(f)\mathbf{\Gamma}_z(f) + \sigma_v^2 \sigma_s^2 \mathbf{G}_z^H(f)\mathbf{G}_z(f) + \sigma_n^2 \sigma_v^2 \mathbf{I}_{M_z} \right)^{-1} \mathbf{q}_z^*(f) \\ &= \sqrt{p(f)}c(f) \left(\sigma_n^2 p(f) [\mathbf{h}_z^*(f)\mathbf{h}_z^T(f)] \oplus [\sigma_v^2 \sigma_s^2 \mathbf{g}_z^*(f)\mathbf{g}_z^T(f) + \sigma_n^2 \sigma_v^2 \mathbf{I}_{M_z}] \right)^{-1} \\ &\quad \times (\mathbf{h}_z^*(f) \otimes \mathbf{g}_z^*(f)) \end{aligned} \quad (4.49)$$

$$= \frac{\sqrt{p(f)}c(f) (\mathbf{h}_z^*(f) \otimes \mathbf{g}_z^*(f))}{\sigma_n^2 p(f) \|\mathbf{h}_z(f)\|^2 + \sigma_v^2 \sigma_s^2 \|\mathbf{g}_z(f)\|^2 + \sigma_n^2 \sigma_v^2}. \quad (4.50)$$

The transformation from (4.49) to (4.50) is accomplished by exploiting the relation [78]

$$(\mathbf{M} \oplus \mathbf{N})^{-1} = \sum_{i=1}^N \sum_{j=1}^N \frac{(\mathbf{m}_i \otimes \mathbf{n}_j) (\bar{\mathbf{m}}_i \otimes \bar{\mathbf{n}}_j)^H}{\lambda_i(\mathbf{M}) + \lambda_j(\mathbf{N})}, \quad (4.51)$$

where \mathbf{m}_i , \mathbf{n}_i , $\bar{\mathbf{m}}_i$, and $\bar{\mathbf{n}}_i$ denote the eigenvectors of $N \times N$ matrices \mathbf{M} , \mathbf{N} , \mathbf{M}^H , and \mathbf{N}^H , respectively. Therefore, the optimum beamforming matrix filter $\mathbf{A}_z^{\text{opt}}(f)$ of relay z is obtained as

$$\mathbf{A}_z^{\text{opt}}(f) = \frac{\sqrt{p(f)}c(f)}{\sigma_n^2 p(f) \|\mathbf{h}_z(f)\|^2 + \sigma_v^2 \sigma_s^2 \|\mathbf{g}_z(f)\|^2 + \sigma_n^2 \sigma_v^2} \mathbf{h}_z^*(f) \mathbf{g}_z^H(f), \quad z = 1, \dots, N_R. \quad (4.52)$$

Eq. (4.52) reveals that the optimal IIR FF–BF matrix filters for all considered receiver structures can be interpreted as the concatenation of a filter matched to the source–relay and the relay–destination link with frequency response $\mathbf{h}_z^*(f)\mathbf{g}_z^H(f)$ and a second filter whose frequency response $\sqrt{p(f)}c(f)/(\sigma_n^2 p(f) \|\mathbf{h}_z(f)\|^2 + \sigma_v^2 \sigma_s^2 \|\mathbf{g}_z(f)\|^2 + \sigma_n^2 \sigma_v^2)$

depends on the power allocation, and thus on the particular equalizer used at the destination. Note that $A_z^{\text{opt}}(f)$ of relay z depends on the CIRs of all source–relay, all relay–destination, and the source–destination channels via power allocation factor $p(f)$.

2) *Optimum Power Allocation*: Before we formulate the power allocation problem for the three considered receiver structures in a unified way, we first introduce the following definitions:

$$S_{\text{DFE}}(f) \triangleq \ln(M(f)), \quad S_{\text{LE}}(f) \triangleq -1/M(f), \quad \text{and} \quad S_{\text{MF}}(f) \triangleq M(f), \quad (4.53)$$

with

$$M(f) \triangleq \mathbf{q}^T(f)(\sigma_n^2 \mathbf{\Gamma}(f) + \sigma_v^2 \mathbf{D}(f)/p(f))^{-1} \mathbf{q}^*(f) + \xi, \quad (4.54)$$

where for DFE and LE ξ is defined after (4.35) and $\xi = 0$ for the MF receiver. Based on these definitions, the equalizer output SINRs (4.34)–(4.36), the original optimization problem (4.43), and the optimal frequency response direction in (4.45), we can formulate the power allocation problem as

$$\max_{p(f)} \int_{-1/2}^{1/2} S_X(f) \, df \quad (4.55a)$$

$$\text{s.t.} \quad \int_{-1/2}^{1/2} p(f) \, df \leq P \quad (4.55b)$$

$$p(f) \geq 0, \quad (4.55c)$$

where $X = \text{DFE}$, $X = \text{LE}$, and $X = \text{MF}$ for DFE, LE, and an MF at the receiver, respectively. Since $\partial M(f)/\partial p(f) < 0$ and $\partial S_X(f)/\partial M(f) > 0$ for $M(f) > 0$ and $X \in$

{DFE, LE, MF}, the power allocation problem is convex for all considered equalizer structures. The Lagrangian of problem (4.55) is given by

$$\mathcal{L}(p(f), \mu) = \int_{-1/2}^{1/2} S_X(f) df - \mu \int_{-1/2}^{1/2} p(f) df, \quad (4.56)$$

where $\mu \geq 0$ is the Lagrangian multiplier. The corresponding Lagrange dual function is

$$\begin{aligned} \mathcal{D}(\mu) &= \max_{p(f)} \mathcal{L}(p(f), \mu) = \max_{p(f)} \int_{-1/2}^{1/2} (S_X(f) - \mu p(f)) df \\ &= \int_{-1/2}^{1/2} \max_{p(f)} (S_X(f) - \mu p(f)) df. \end{aligned} \quad (4.57)$$

The last step in (4.57) can be established because the total power constraint (4.55b) is implicitly captured by the dual variable μ and the maximization over $p(f)$ can be moved inside the integration. Therefore, for a given μ , $p(f)$ can be obtained from

$$\max_{p(f)} \mathcal{S}_X(p(f)) = S_X(f) - \mu p(f) \quad (4.58)$$

or equivalently

$$S'_X(f) \triangleq \frac{\partial S_X(f)}{\partial p(f)} = \mu. \quad (4.59)$$

$S'_X(f)$ can be easily computed for all considered equalization schemes. In particular, we obtain

$$S'_{\text{DFE}}(f) \triangleq M'(f)/M(f), \quad S'_{\text{LE}}(f) \triangleq M'(f)/M^2(f), \quad \text{and} \quad S'_{\text{MF}}(f) \triangleq M'(f), \quad (4.60)$$

where

$$M'(f) \triangleq \frac{\partial M(f)}{\partial p(f)} = \mathbf{q}^T(f) \mathbf{D}(f) (\sigma_n^2 p(f) \mathbf{\Gamma}(f) + \sigma_v^2 \mathbf{D}(f))^{-2} \mathbf{q}^*(f). \quad (4.61)$$

Note that constraint (4.55c), which has been ignored in (4.57), can be taken into account by evaluating $S'_X(f) \triangleq \partial S_X(f)/\partial p(f)$ for $p(f) \rightarrow 0^+$. In particular, since $S'_X(f)$ is a monotonic decreasing function of $p(f)$ for all considered equalization schemes, for a given μ , $S'_X(f) = \mu$ does not have a positive solution if $\lim_{p(f) \rightarrow 0^+} S'_X(f) < \mu$, and we set $p(f) = 0$ in this case. Otherwise, we find $p(f)$ from (4.59) by using e.g. the bisection search method [1]³. On the other hand, the optimal value $\mu = \mu_{\text{opt}}$ that ensures the power constraint is satisfied can be found iteratively by another bisection search. More specifically, if the corresponding total power $P_R = \int_{-1/2}^{1/2} p(f) df$ is less than the maximum power P for a given μ , the Lagrange multiplier μ has to be decreased, whereas it is increased if $P_R > P$.

We note that since the frequency axis is real valued, in practice, f has to be discretized in $-1/2 \leq f \leq 1/2$ to make the problem computationally tractable. A summary of the numerical algorithm for finding the optimal power allocation, $p_{\text{opt}}(f)$, for discrete frequency points for the three considered equalization schemes is given in Table 4.1. Applying $p_{\text{opt}}(f)$ found with the algorithm in Table 4.1 in (4.52), yields the optimal FF–BF filter frequency response $A_z^{\text{opt}}(f)$ for relay z , $1 \leq z \leq N_R$.

Although we concentrate in this section on the case where the direct source–destination link is not exploited for detection, with a minor modification our equalization results are valid if the source–destination link is also used. In particular, for the latter case, our journal paper [82] provides the details.

³Note that algorithms with faster convergence, e.g. Newton’s method, can be used as long as the condition $p(f) \geq 0$ is satisfied.

Table 4.1: Numerical algorithm for finding the optimum power allocation $p(f)$ for IIR FF–BF filters at the relays. $X = \text{DFE}$, $X = \text{LE}$, and $X = \text{MF}$ for DFE, LE, and an MF receiver, respectively. Termination constant ϵ and frequency spacing Δf have small values (e.g. $\epsilon = 10^{-5}$, $\Delta f = 10^{-5}$). i denotes the iteration index.

1	Let $i = 0$, $N = \lceil 1/\Delta f \rceil$, and $f_n = -1/2 + (n - 1)\Delta f$, $1 \leq n \leq N$. Initialize $l = 0$ and $u = \max_f \lim_{p(f) \rightarrow 0^+} S'_X(f)$.
2	Update μ by $\mu = (l + u)/2$.
3	For $n = 1$ to N If $\lim_{p(f_n) \rightarrow 0^+} (S'_X(f_n) - \mu) < 0$, set $p(f_n) = 0$, otherwise compute $p(f_n)$ by solving $S'_X(f_n) = \mu$ with the bisectional search method [1].
4	If $\sum_{n=1}^N p(f_n)\Delta f > P$, $l = \mu$, else $u = \mu$.
5	If $u - l > \epsilon$, goto Step 2; else $p(f_n)$, $1 \leq n \leq N$, are the optimal power allocation parameters, and μ is the optimum Lagrange multiplier μ_{opt} .

4.4.2 Optimal FIR FF–BF with Equalization

In practice, it is not possible to implement the IIR FF–BF filters discussed in the previous section since they would require the feedback of an infinite number of filter coefficients from the destination to the relays. However, the performance achievable with these IIR FF–BF filters provides a useful upper bound for the FIR FF–BF filters considered in this section. In particular, the performance of the IIR solution can be used for optimizing the FIR BF–FF length to achieve a desired trade–off between the amount of feedback and performance. We note that although FIR FF–BF filters are considered in this section, in order to be able to exploit the simple SINR expressions in (4.34)–(4.36), we still assume that the equalizers at the destination employ IIR filters.

With FIR FF–BF filters of length L_a at the relays, the length of the equivalent CIR $h_{\text{eq}}[k]$ (4.4) is given by $L_{\text{eq}} = L_a + L_g + L_h - 2$. In this case, the Fourier transform of $h_{\text{eq}}[k]$ can be expressed as

$$H_{\text{eq}}(f) = \mathbf{d}^H(f) \mathcal{H} \mathcal{G}_D \mathbf{a} \quad (4.62)$$

with $\mathbf{d}(f) \triangleq [1 e^{j2\pi f} \dots e^{j2\pi f(L_{\text{eq}}-1)}]^T$. FIR FF–BF coefficient vector \mathbf{a} , \mathcal{H} , and \mathcal{G}_D are defined in Section 4.3 after (4.6), respectively.

The noise whitening filter in the FIR case is given by

$$W(f) = (\sigma_n^2 \mathbf{a}^H \bar{\Gamma}(f) \mathbf{a} + \sigma_v^2)^{-1/2} \quad (4.63)$$

with $\sum_{z=1}^{N_R} M_z^2 L_a \times \sum_{z=1}^{N_R} M_z^2 L_a$ block diagonal matrix $\bar{\Gamma}(f) \triangleq \text{diag} \{ \bar{\Gamma}_1(f), \dots, \bar{\Gamma}_{N_R}(f) \}$ of rank $\sum_{z=1}^{N_R} M_z$, where $\bar{\Gamma}_z(f) \triangleq \check{\mathbf{H}}_z^H (\mathbf{I}_{M_z} \otimes \bar{\mathbf{d}}(f)) (\mathbf{I}_{M_z} \otimes \bar{\mathbf{d}}(f))^H \check{\mathbf{H}}_z$ is an $M_z^2 L_a \times M_z^2 L_a$ matrix of rank M_z . $\check{\mathbf{H}}_z$ is defined after (4.10), and $\bar{\mathbf{d}}(f) \triangleq [1 e^{j2\pi f} \dots e^{j2\pi f(L_h+L_a-2)}]^T$. Therefore, after noise whitening, the frequency response of the overall channel is

$$H'_{\text{eq}}(f) = \mathbf{d}^H(f) \mathcal{H} \mathcal{G}_D \mathbf{a} (\sigma_n^2 \mathbf{a}^H \bar{\Gamma}(f) \mathbf{a} + \sigma_v^2)^{-1/2}. \quad (4.64)$$

We note that for a practical implementation, the noise whitening filter does not have to be implemented. Instead, the noise correlation can be directly taken into account for equalizer filter design [83]. However, in order to be able to exploit the simple existing expressions for the SINR of the equalizer output given in [83, 84], it is advantageous to assume the presence of a whitening filter for FIR BF–FF filter design.

Similar to the IIR case in (4.33), also for the FIR case it is convenient to introduce the definition

$$Z(\mathbf{a}) \triangleq |H'_{\text{eq}}(f)|^2 = \frac{\mathbf{a}^H \mathcal{G}_D^H \mathcal{H}^H \mathbf{d}(f) \mathbf{d}^H(f) \mathcal{H} \mathcal{G}_D \mathbf{a}}{\sigma_n^2 \mathbf{a}^H \bar{\Gamma}(f) \mathbf{a} + \sigma_v^2}. \quad (4.65)$$

Note, however, that this is a slight abuse of notation since while the argument of $Z(\mathbf{a}(f))$ in (4.33) is a vector containing all frequency responses of the IIR FF–BF filters, the argument of $Z(\mathbf{a})$ in (4.65) is a vector containing all FIR FF–BF coefficients. Replacing $Z(\mathbf{a}(f))$ now in the SINR expressions in (4.34)–(4.36) by $Z(\mathbf{a})$ from (4.65), we obtain the SINRs $\text{SINR}_X(\mathbf{a})$, where $X = \text{DFE}$, $X = \text{LE}$, and $X = \text{MF}$ for DFE, LE, and an MF receiver,

respectively. This allows us to formulate the FIR FF–BF filter optimization problem in a unified manner:

$$\max_{\mathbf{a}} \text{SINR}_X(\mathbf{a}) \quad (4.66a)$$

$$\text{s.t. } \mathbf{a}^H \mathbf{D} \mathbf{a} \leq P, \quad (4.66b)$$

where the power constraint (4.66b) is the same as in (4.14b). Although problem (4.66) formally looks very similar to problem (4.39), it is substantially more difficult to solve. The main reason for this lies in the fact that the optimization variable $\mathbf{a}(f)$ in (4.39) can be chosen freely for each frequency f , whereas the coefficient vector \mathbf{a} in (4.66) is fixed for all frequencies.

To simplify the power constraint, we introduce $\mathbf{v} \triangleq \mathbf{D}^{1/2} \mathbf{a}$. Furthermore, it is not difficult to see that at optimality, the power constraint in (4.66b) is fulfilled with equality, i.e., $\mathbf{a}^H \mathbf{D} \mathbf{a} = \mathbf{v}^H \mathbf{v} = P$. With this identity, we obtain

$$M(\mathbf{v}, f) \triangleq Z(\mathbf{a}) + \xi \triangleq \frac{\mathbf{v}^H \bar{\mathbf{J}}(f) \mathbf{v}}{\mathbf{v}^H \bar{\mathbf{X}}(f) \mathbf{v}} \quad (4.67)$$

where

$$\bar{\mathbf{J}}(f) \triangleq \mathbf{D}^{-H/2} \bar{\Phi}(f) \mathbf{D}^{-1/2} + \frac{\xi \sigma_v^2}{P} \mathbf{I}_{N_R L_a}, \quad (4.68)$$

$$\bar{\mathbf{X}}(f) \triangleq \sigma_n^2 \mathbf{D}^{-H/2} \bar{\Gamma}(f) \mathbf{D}^{-1/2} + \frac{\sigma_v^2}{P} \mathbf{I}_{N_R L_a}, \quad (4.69)$$

$$\bar{\Phi}(f) \triangleq \mathcal{G}_D^H \mathcal{H}^H \mathbf{d}(f) \mathbf{d}^H(f) \mathcal{H} \mathcal{G}_D + \xi \sigma_n^2 \bar{\Gamma}(f). \quad (4.70)$$

Now, we can rewrite optimization problem (4.66) in equivalent form as

$$\max_{\mathbf{v}} \int_{-1/2}^{1/2} S_X(\mathbf{v}, f) df \quad (4.71a)$$

$$\text{s.t. } \mathbf{v}^H \mathbf{v} = P, \quad (4.71b)$$

where

$$S_{\text{DFE}}(\mathbf{v}, f) \triangleq \ln(M(\mathbf{v}, f)), \quad S_{\text{LE}}(\mathbf{v}, f) \triangleq -1/M(\mathbf{v}, f), \quad \text{and } S_{\text{MF}}(\mathbf{v}, f) \triangleq M(\mathbf{v}, f). \quad (4.72)$$

The FIR FF–BF optimization problem in (4.71) is a difficult non–convex optimization problem. To substantiate this claim, we consider the special case of DFE and discretize the integral in (4.71a). This leads to the new equivalent problem

$$\max_{\mathbf{v}^H \mathbf{v} = P} \prod_{i=1}^N \frac{\mathbf{v}^H \bar{\mathbf{J}}(f_i) \mathbf{v}}{\mathbf{v}^H \bar{\mathbf{X}}(f_i) \mathbf{v}}, \quad (4.73)$$

where $f_i \triangleq -1/2 + (i-1)/N$ and N denotes the number of sampling points. The objective function in (4.73) is a product of generalized Rayleigh quotients. Unfortunately, it is well known that the maximization of a product of generalized Rayleigh quotients is a difficult mathematical problem which is not well understood and a solution is not known except for the trivial case $N = 1$, cf. e.g. [67, 68]. Therefore, we also do not expect to find a simple solution for optimization problem (4.71). Similar statements apply for the optimization problems resulting for LE and an MF receiver.

In order to obtain a practical and simple method for finding a locally optimal solution for the FIR BF–FF coefficient vectors, we propose a gradient algorithm (GA). In iteration

Table 4.2: Gradient algorithm (GA) for calculation of near-optimal FIR FF–BF filter vector \mathbf{a} . Termination constant ϵ has a small value (e.g. $\epsilon = 10^{-5}$). i denotes the iteration index and δ_i is the adaptation step size chosen through a backtracking line search [1].

1	Let $i = 0$ and initialize vector \mathbf{v} with some \mathbf{v}_0 fulfilling $\mathbf{v}_0^H \mathbf{v}_0 = P$.
2	Update the vector \mathbf{v} : DFE: $\mathbf{v}_{i+1} = \mathbf{v}_i + \delta_i \left[\int_{-1/2}^{1/2} \left(\frac{\bar{\mathbf{J}}(f)}{\mathbf{v}_i^H \bar{\mathbf{J}}(f) \mathbf{v}_i} - \frac{\bar{\mathbf{X}}(f)}{\mathbf{v}_i^H \bar{\mathbf{X}}(f) \mathbf{v}_i} \right) df \right] \mathbf{v}_i$; LE: $\mathbf{v}_{i+1} = \mathbf{v}_i - \delta_i \left[\int_{-1/2}^{1/2} \frac{\mathbf{v}_i^H \bar{\mathbf{J}}(f) \mathbf{v}_i \bar{\mathbf{X}}(f) - \mathbf{v}_i^H \bar{\mathbf{X}}(f) \mathbf{v}_i \bar{\mathbf{J}}(f)}{(\mathbf{v}_i^H \bar{\mathbf{J}}(f) \mathbf{v}_i)^2} df \right] \mathbf{v}_i$; MF: $\mathbf{v}_{i+1} = \mathbf{v}_i + \delta_i \left[\int_{-1/2}^{1/2} \frac{\mathbf{v}_i^H \bar{\mathbf{X}}(f) \mathbf{v}_i \bar{\mathbf{J}}(f) - \mathbf{v}_i^H \bar{\mathbf{J}}(f) \mathbf{v}_i \bar{\mathbf{X}}(f)}{(\mathbf{v}_i^H \bar{\mathbf{X}}(f) \mathbf{v}_i)^2} df \right] \mathbf{v}_i$. (Note that normalization of vector \mathbf{v}_{i+1} is not necessary since $\mathbf{v}_{i+1}^H \mathbf{v}_{i+1} = P$.)
3	Compute $\text{SINR}_X(\mathbf{v}_{i+1})$ based on (4.34)–(4.36).
4	If $ \text{SINR}_X(\mathbf{v}_{i+1}) - \text{SINR}_X(\mathbf{v}_i) < \epsilon$, goto Step 5, otherwise increment $i \rightarrow i + 1$ and goto Step 2.
5	\mathbf{v}_{i+1} is the desired vector, and the corresponding optimum FF–BF filter is $\mathbf{a} = \mathbf{D}^{-1/2} \mathbf{v}_{i+1}$.

$i + 1$, the GA improves vector \mathbf{v}_i from iteration i in the direction of the steepest ascent [1]

$$\int_{-1/2}^{1/2} \frac{\partial S_X(\mathbf{v}, f)}{\partial \mathbf{v}} df \quad (4.74)$$

of the objective function in (4.71a). The GA for the three considered equalization schemes is summarized in Table 4.2. Although, in principle, the GA may not be able to find the globally optimal solution, extensive simulations have shown that for the problem at hand the performance achievable with GA is practically independent of the initialization \mathbf{v}_0 . More importantly, for sufficiently large FIR filter lengths L_a , the solution found with the GA closely approaches the performance of the optimal IIR FF–BF filter. This suggests that the solution found by the GA is at least near optimal. Exemplary simulation results confirming these claims are provided and discussed in the next section.

We note that we can again accommodate the case where the source–destination channel is exploited for detection, please refer to our journal paper [82] for details.

4.5 Simulation Results

In this section, we present simulation results for the SINR and the BER of a cooperative network with FF–BF. Throughout this section we assume $\sigma_n^2 = \sigma_v^2 = 1$ and $P = 1$. This allows us to decompose the CIRs as $h_{i,z}[k] = \sqrt{\gamma_h} \bar{h}_{i,z}[k]$ and $g_{i,z}[k] = \sqrt{\gamma_g} \bar{g}_{i,z}[k]$, where γ_h and γ_g denote the transmitter SNRs of the relay–destination and the source–relay links, respectively. The normalized CIRs $\bar{h}_i[k]$ and $\bar{g}_i[k]$ include the effects of multipath fading and path–loss. All IIR and FIR FF–BF filters were obtained using the methods introduced in Sections 4.3 and 4.4.

The locations of the source, the destination, and the relays are shown in Fig. 4.2, where the numbers on top and beside the arrows indicate the normalized distance between the nodes. We consider the following three cooperative relay network setups: 1) $N_R = 1$ relays with $M_1 = 5$ at location (c); 2) $N_R = 2$ relays with $M_1 = 2$ and $M_2 = 3$ at locations (a) and (e), respectively; and 3) $N_R = 5$ relays with $M_z = 1$, $1 \leq z \leq N_R$, at locations (a)–(e), respectively. The normalized distance between the source and the destination is equal to 2 and the normalized horizontal distance between the source and the relays is d . A path–loss exponent of 3 with reference distance $d_{\text{ref}} = 1$ is assumed. The CIR coefficients of all links are modeled as independent quasi–static Rayleigh fading with $L_g = L_h = 5$ and following an exponential power delay profile

$$p[k] = \frac{1}{\sigma_t} \sum_{l=0}^{L_x-1} e^{-k/\sigma_t} \delta[k-l], \quad (4.75)$$

where $L_x \in \{L_g, L_h\}$ and σ_t characterizes the delay spread [85]. All results shown were

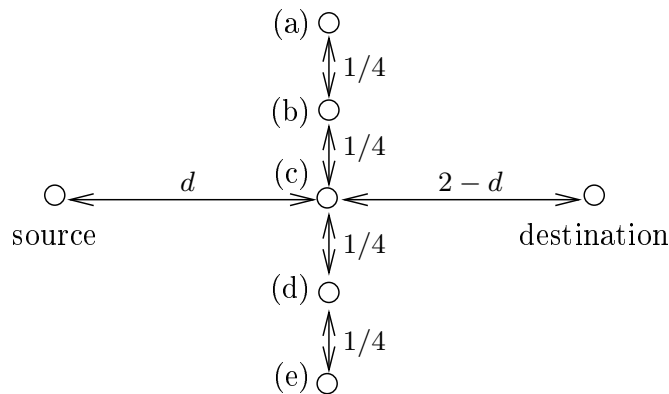


Figure 4.2: Locations of source, destination, and relays in simulation.

averaged over 100,000 independent realizations of the fading channels.

4.5.1 FF-BF without Equalization

Optimal Decision Delay: First, we consider the optimal decision delay for FF-BF without equalization. In theory, the decision delay parameter k_0 can be optimized for each channel realization. However, it is not practical to search for the optimal delay k_0 for every channel realization. In practice, it is preferable to find a value for k_0 which works well for given channel statistics. Fig. 4.3 shows the average SINR vs. decision delay k_0 for FIR FF-BF without equalization for $\sigma_t = 2$ and $\sigma_t = 7$. The FIR FF-BF filters were optimized for the *SINR Maximization Under Relay Power Constraint* criterion in Section 4.3.1. We assume network setup 3), $d = 1$, and $\gamma_g = \gamma_h = 10$ dB. As can be observed, for $\sigma_t = 2$, the optimal k_0 is equal to 2, 3, and 6 for filter length $L_a = 1, 3$, and 7, respectively. In comparison, for $\sigma_t = 7$, the optimal k_0 is equal to 5, 5, and 7 for $L_a = 1, 3$, and 7, respectively. In other words, the larger the channel delay spread σ_t , i.e., the more frequency selective the channel, the larger the optimal delay k_0 . Fig. 4.3 also shows that increasing the FF-BF filter length is highly beneficial for the achievable maximum average SINR. For the remaining results presented in this section, we will adopt the optimal values for k_0 .

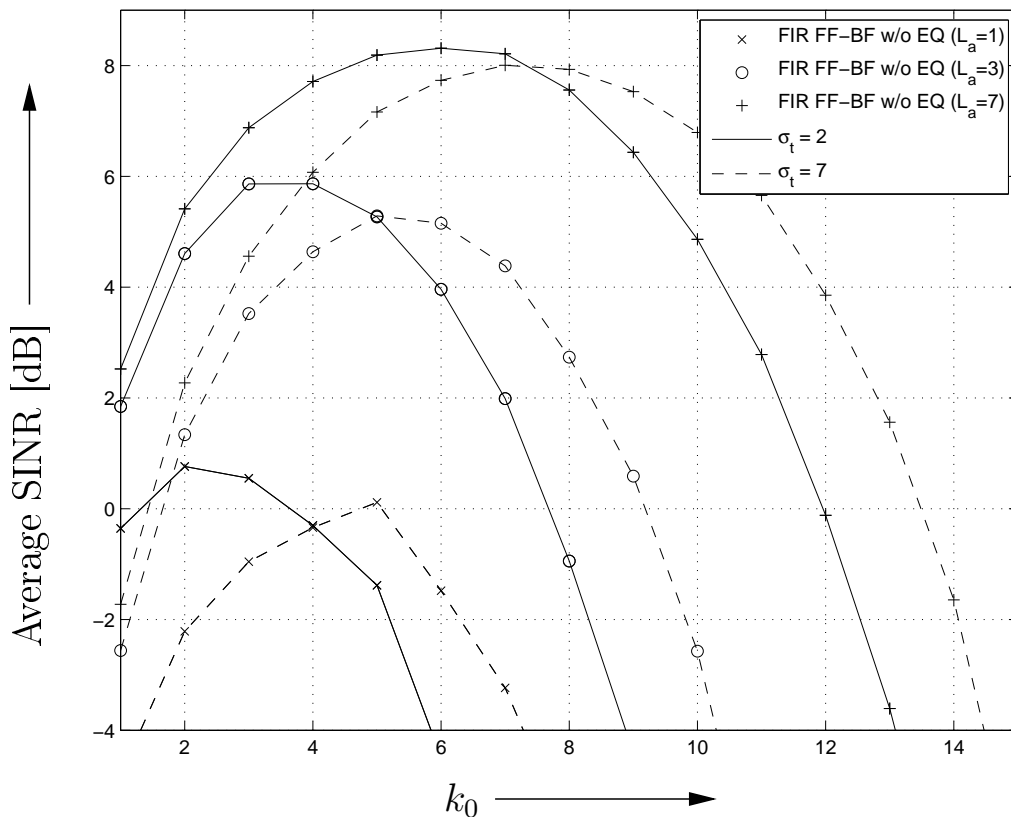


Figure 4.3: Average SINR vs. decision delay k_0 for FIR FF–BF without equalization (EQ) at the destination. The FF–BF filters were optimized for SINR maximization under *joint relay power constraint*. Exponentially decaying channel power delay profile with $L_g = L_h = 5$, $d = 1$, $N_R = 5$, $M_z = 1$, $z \in \{1, 2, \dots, 5\}$ and $\gamma_g = \gamma_h = 10$ dB.

SINR Optimization: Figs. 4.4 and 4.5 show the average SINR vs. distance d for FF–BF for joint relay and joint source–relay power constraints, respectively. Relay network setups 1) – 3) were adopted. The FF–BF matrix filters were generated using the results in Section 4.3.1 and 4.3.3, respectively. For both considered constraints FF–BF relaying enables considerable performance gains compared to direct transmission except for the case with $L_a = 1$, $N_R = 5$, and $M_z = 1$, $z \in \{1, 2, \dots, 5\}$. Direct transmission is preferable only if the relay is located either closed to the source or the destination (small d or large d). The joint source–relay power constraint can yield significant performance gains if the relays are

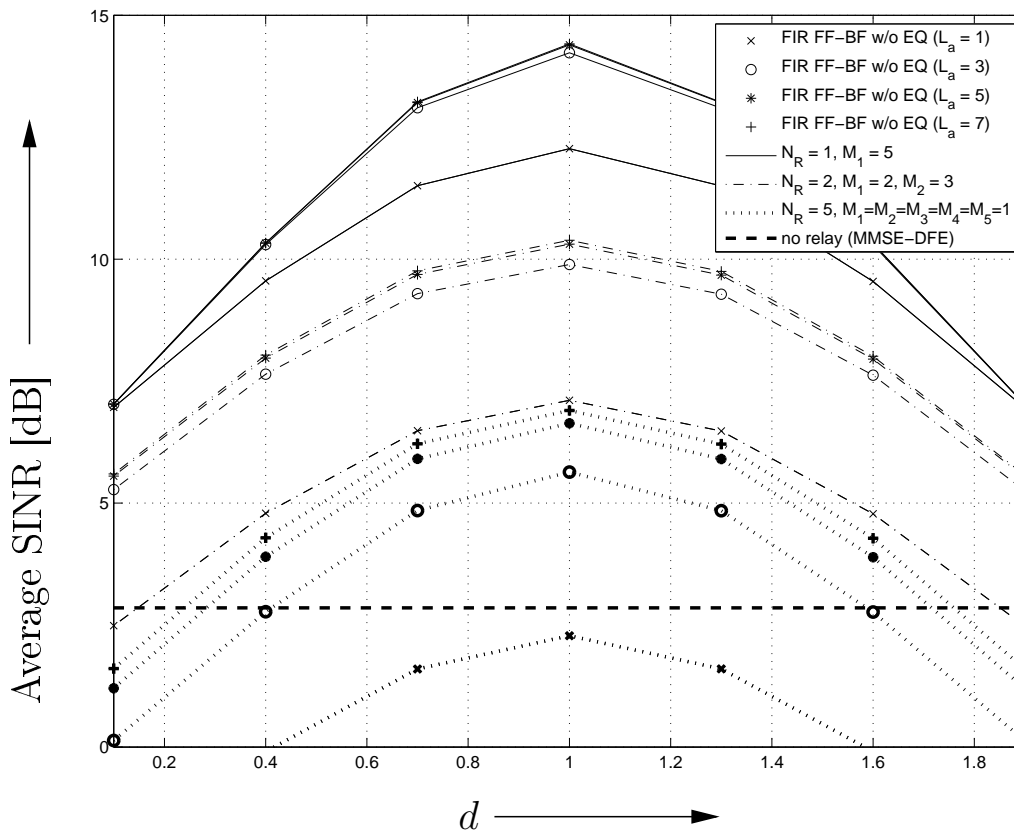


Figure 4.4: Average SINR vs. distance d for FIR FF-BF without equalization (EQ) at the destination. The FF-BF matrix filters were optimized for a *joint relay power constraint*. Exponentially decaying channel power delay profile with $\sigma_t = 2$ and $L_g = L_h = 5$, and $\gamma_g = \gamma_h = 10$ dB. Results for direct transmission with transmit power $P = 2$ at the source are also included.

close to the source or close to the destination, respectively, by flexibly allocating more or less power to the source. Furthermore, Figs. 4.4 and 4.5 also show that it is preferable to have fewer relays with more antennas than more relays with fewer antennas.

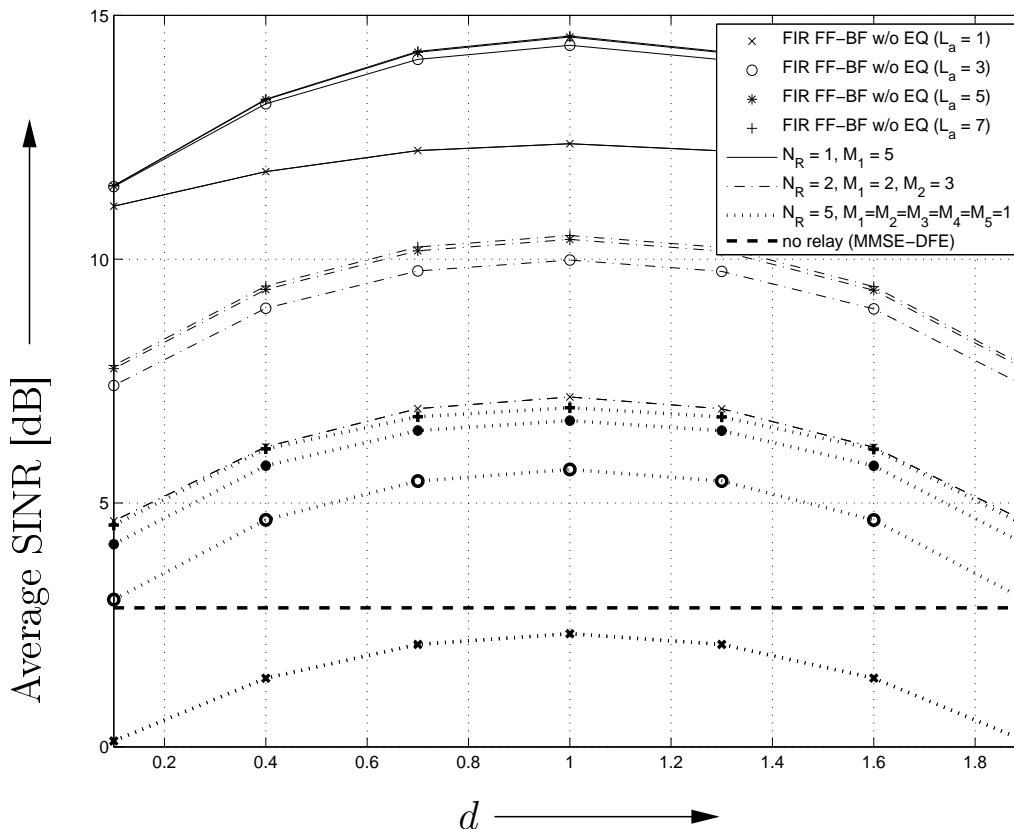


Figure 4.5: Average SINR vs. distance d for FIR FF-BF without equalization (EQ) at the destination. The FF-BF matrix filters were optimized for a *joint source-relay power constraint*. Exponentially decaying channel power delay profile with $\sigma_t = 2$ and $L_g = L_h = 5$, and $\gamma_g = \gamma_h = 10$ dB. Results for direct transmission with transmit power $P = 2$ at the source are also included.

Power Minimization: Fig. 4.6 shows the total source and relay transmit power, $P_R + \sigma_s^2$, vs. the minimum required SINR γ at the destination for different relay network setups. The FF-BF matrix filters are generated based on the results in Sections 4.3.2 and 4.3.4, respectively. Similar to [50], we have only included simulation points which guarantee feasibility of the optimization problem for more than 50 % of the channels. The total source and relay transmit power is computed by averaging over the feasible runs. The probability that this problem is feasible is shown in Fig. 4.7. From Figs. 4.6 and

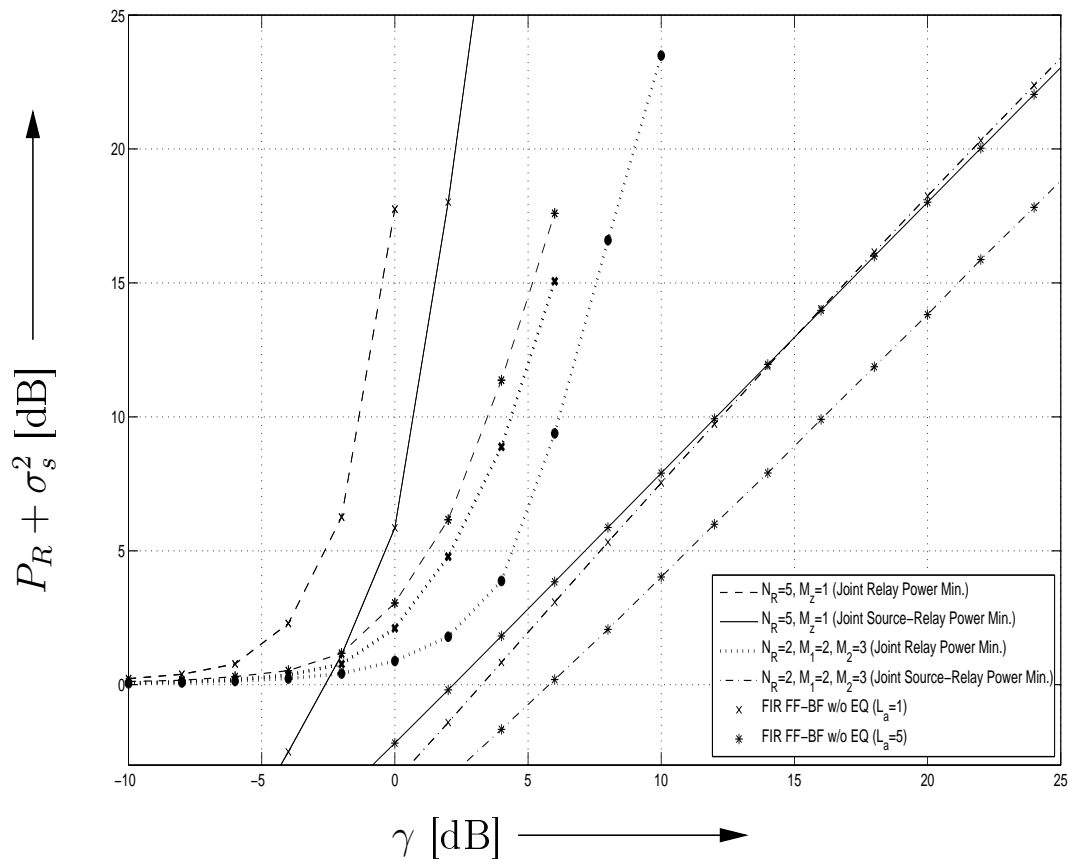


Figure 4.6: Total average source and relay transmit power vs. required SINR γ for FIR FF-BF without equalization (EQ) at the destination for *relay power minimization* and *joint source-relay power minimization*. Exponentially decaying power delay profile with $\sigma_t = 2$ and $L_g = L_h = 5$, $d = 1$, and $\gamma_g = \gamma_h = 10$ dB.

4.7, we observe that joint source-relay transmit power minimization and multiple-antenna relays can lead to significant power savings. Fig. 4.6 also reveals that increasing L_a can substantially reduce the total source and relay transmit power.

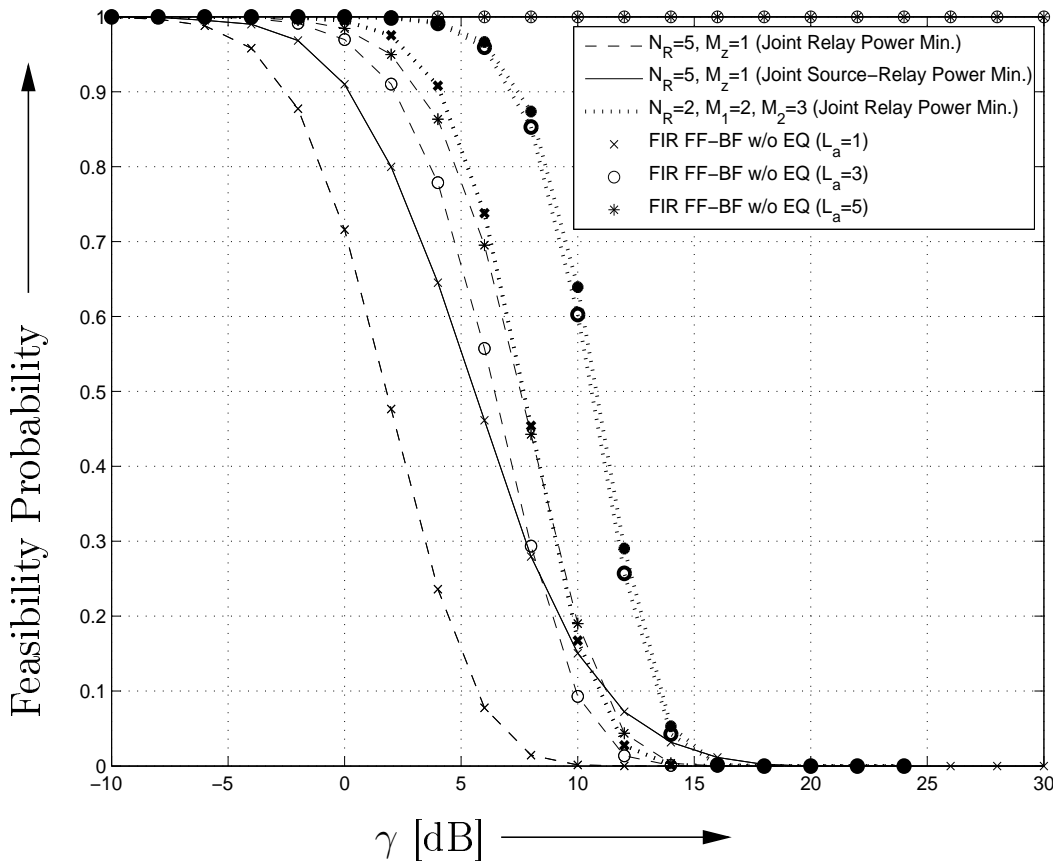


Figure 4.7: Feasibility probability vs. required SINR γ for FIR FF-BF without equalization (EQ) at the destination for *relay power minimization* and *joint source-relay power minimization*. Exponentially decaying power delay profile with $\sigma_t = 2$ and $L_g = L_h = 5$, $d = 1$, and $\gamma_g = \gamma_h = 10$ dB.

4.5.2 FF-BF with Equalization

Convergence of the GA: We first investigate the convergence of the proposed GA for optimization of the FIR FF-BF filters. We assume MMSE-DFE at the destination and relay network setup 3) (i.e., $N_R = 5$ relays with $M_z = 1$, $1 \leq z \leq N_R$, at locations (a)–(e), respectively). The CIRs of all involved channels are given by $\bar{g}_{1,z}[k] = \bar{h}_{1,z}[k] = 1/\sqrt{5}$, $0 \leq k < 5$, $1 \leq z \leq 5$, with $L_g = L_h = 5$ and $\gamma_g = \gamma_h = 10$ dB. Fig. 4.8 shows the achievable

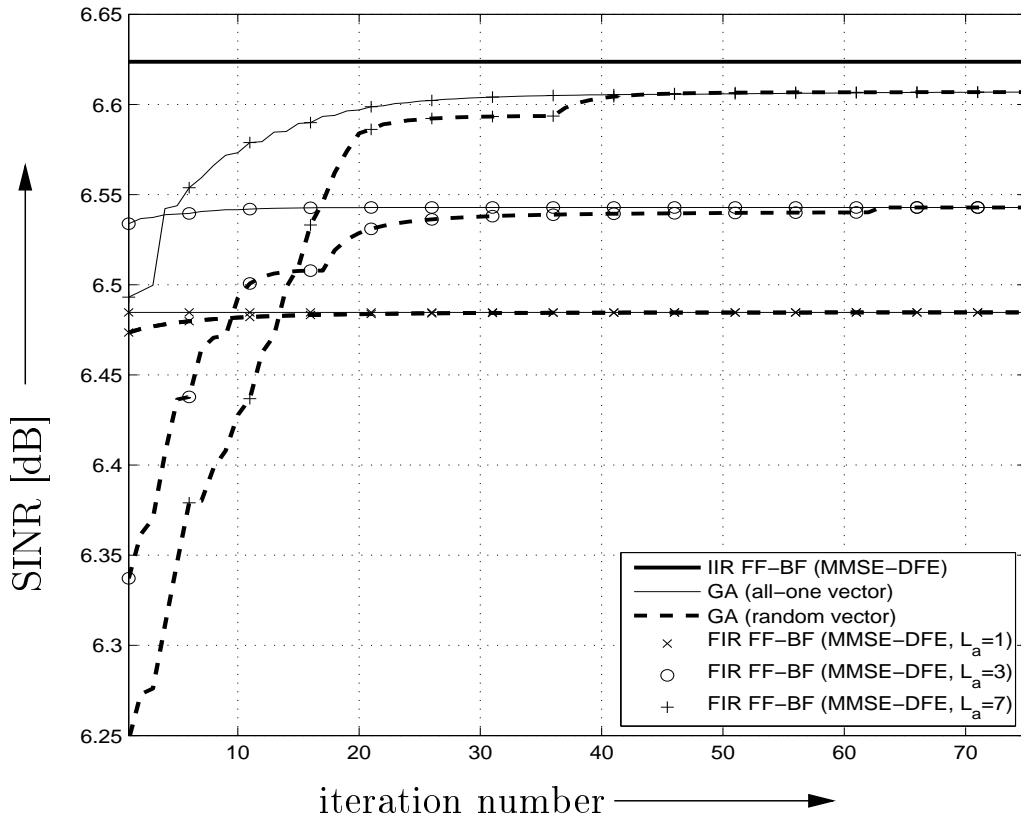


Figure 4.8: SINR vs. iteration number i of GA given in Table 4.2 for FIR FF-BF with MMSE-DFE at the destination. $\gamma_g = \gamma_h = 10$ dB, $L_g = L_h = 5$, and $\bar{g}_{1,z}[k] = \bar{h}_{1,z}[k] = 1/\sqrt{5}$, $0 \leq k < 5$, $1 \leq z \leq 5$. $N_R = 5$ relays with $M_z = 1$, $1 \leq z \leq N_R$, at locations (a)–(e), respectively. For comparison the SINR for IIR FF-BF is also shown.

SINR vs. iteration number i for initialization of the GA with a normalized random vector and a normalized all-one vector for different FIR filter lengths L_a , respectively. Note that the adaptation step size, δ_i , is obtained from a backtracking line search, cf. Table 4.2. After a sufficiently large number of iterations, the SINR converges to the same constant value for both initializations. The steady-state SINR increases with increasing L_a and for sufficiently large FIR filter lengths L_a , the steady-state SINR approaches the SINR of IIR FF-BF. Similar observations were made for other random and deterministic initializations of the proposed GA. Thus, for all results shown in the remaining figures, the GA in Table

4.2 was initialized with a normalized all–one vector.

Filter Design for a Fixed Test Channel: In order to get some insight into the effect that different equalization schemes have on the IIR and FIR FF–BF filter design, we consider next a cooperative network with $N_R = 1$ single antenna relay and assume a simplified test channel with $L_g = L_h = 2$ and $\bar{g}_{1,1}[k] = \bar{h}_{1,1}[k] = 1/\sqrt{2}$, $k \in \{0, 1\}$, i.e., all involved channels are identical and their frequency response has a zero at frequency $f = 1/2$, cf. Fig. 4.9. We also choose identical transmitter SINRs $\gamma_g = \gamma_h = 10$ dB for all channels.

In Fig. 4.9, we show the magnitude of the optimal IIR FF–BF filter frequency response $|A_1^{\text{opt}}(f)|$ vs. frequency f . We consider the cases where the destination is equipped with ZF–DFE, MMSE–DFE, ZF–LE, MMSE–LE, and an MF receiver. Interestingly, although the frequency responses for all equalization schemes have the same structure, cf. (4.52), due to differences in the optimal relay power allocation, $p(f)$, the FF–BF filter frequency response for the ZF–LE case exhibits a completely different behavior than the frequency responses for the other equalization schemes. In particular, since a zero in the frequency response of the overall channel, consisting of the source–relay channel, the FF–BF filter, and the relay–destination channel, would lead to infinite noise enhancement in a linear zero–forcing equalizer at the destination, the FF–BF filter design tries to avoid this problem by enhancing frequencies around $f = 1/2$. Note that the resulting scheme would still have a very poor performance since most of the relay power is allocated to frequencies where the overall channel is poor. In contrast, the other considered equalization strategies inherently avoid infinite noise enhancement at the destination even if the overall channel has zeros. Thus, in these cases, the optimal FF–BF filters avoid allocating significant amounts of power to frequencies around $f = 1/2$. This is particularly true for the MMSE equalizers and the MF receiver. The former allocate the power such that there is an optimal tradeoff

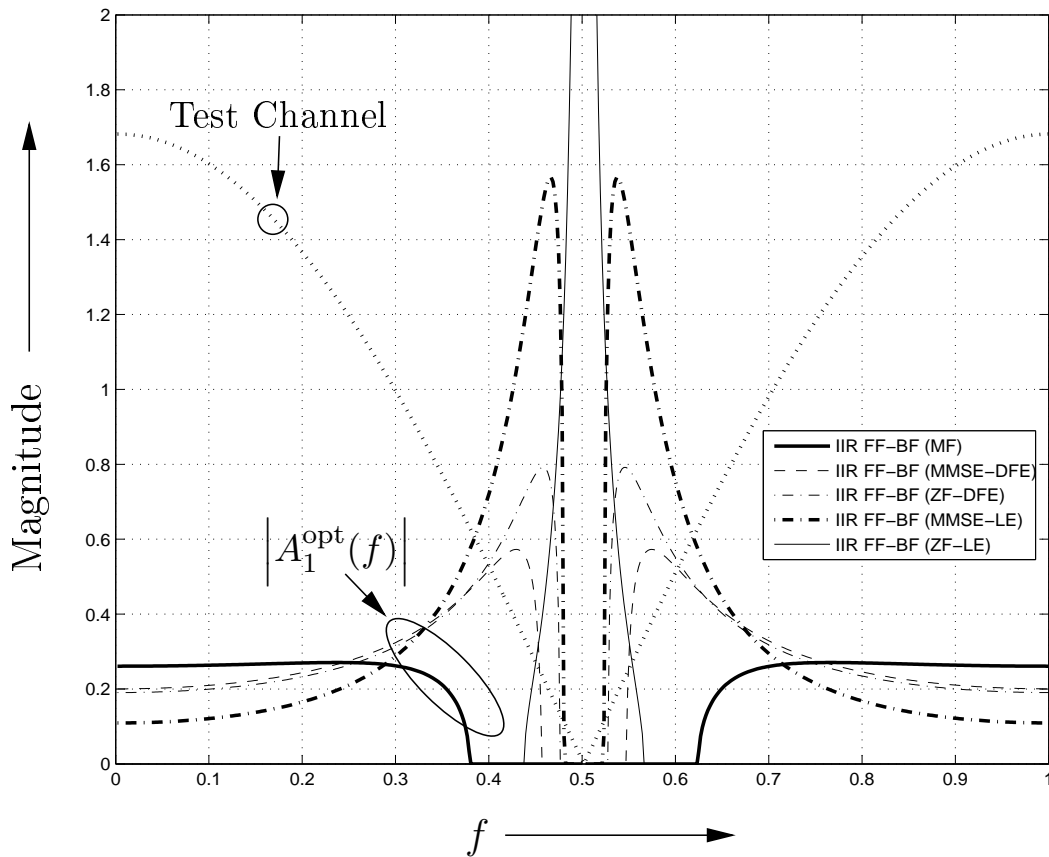


Figure 4.9: Frequency responses of IIR FF-BF filters for $\gamma_g = \gamma_h = 10$ dB, $N_R = 1$ single antenna relay, $L_g = L_h = 2$, and $\bar{g}_{1,1}[k] = \bar{h}_{1,1}[k] = 1/\sqrt{2}$, $k \in \{0, 1\}$. For comparison the frequency response of the test channel is also shown.

between residual ISI and noise enhancement in the equalizer output signal, whereas the latter, idealized receiver is not affected by residual ISI.

Fig. 4.10 compares the frequency responses of the IIR FF-BF filter and FIR FF-BF filters of various lengths assuming MMSE-DFE at the receiver. As expected, as the FIR FF-BF filter length L_a increases, the degree to which the FIR frequency response approximates the IIR frequency response increases. Although Fig. 4.10 suggests that relatively long FIR FF-BF filters are required to closely approximate the IIR filters, subsequent results

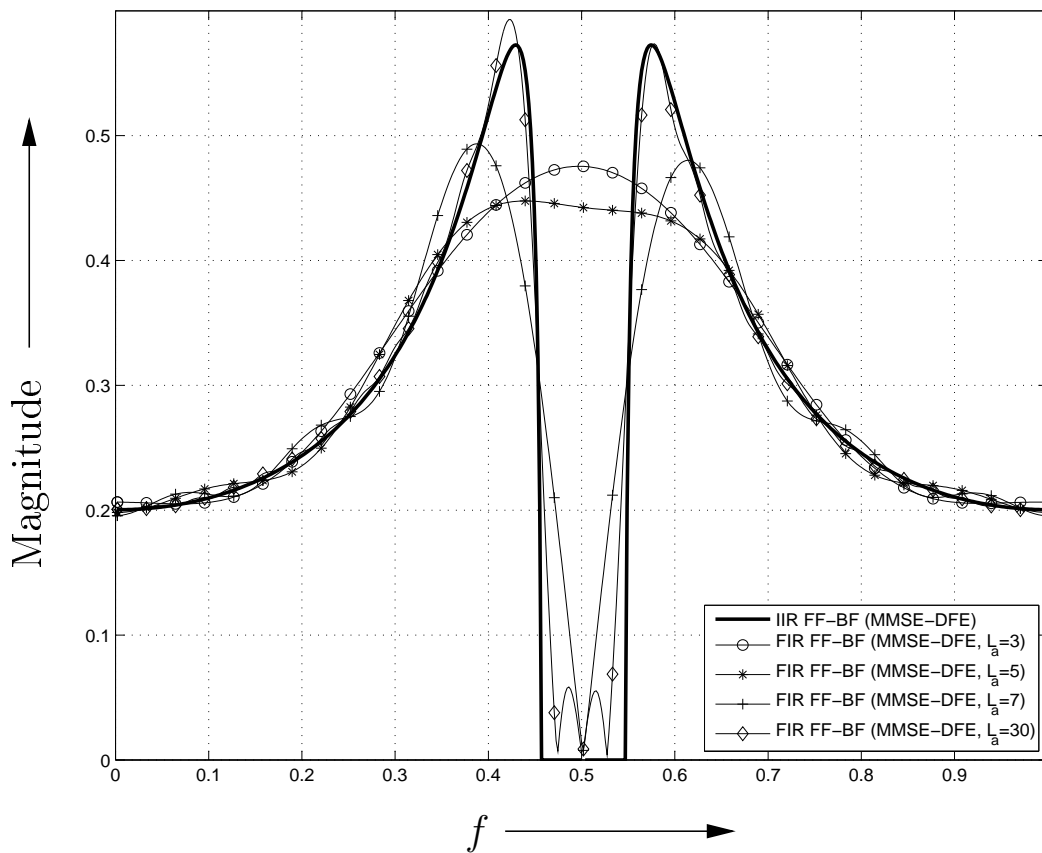


Figure 4.10: Frequency responses of IIR FF-BF filter and FIR FF-BF filters of various lengths for MMSE-DFE at the receiver. All channel parameters are identical to those in Fig. 4.9.

will show that short FIR FF-BF filters suffice to closely approach the SINR performance of IIR FF-BF filters.

SINR Performance for Fading Channels: In Fig. 4.11, we show the average SINR vs. distance d for various FF-BF filter and equalization designs for relay network setup 2) (i.e., $N_R = 2$, $M_1 = 2$, and $M_2 = 3$). We compare the performance of the proposed FF-BF matrix filter design with MMSE-DFE and without equalizer at the destination. Interestingly, while for short FIR FF-BF filters equalization at the transceivers results

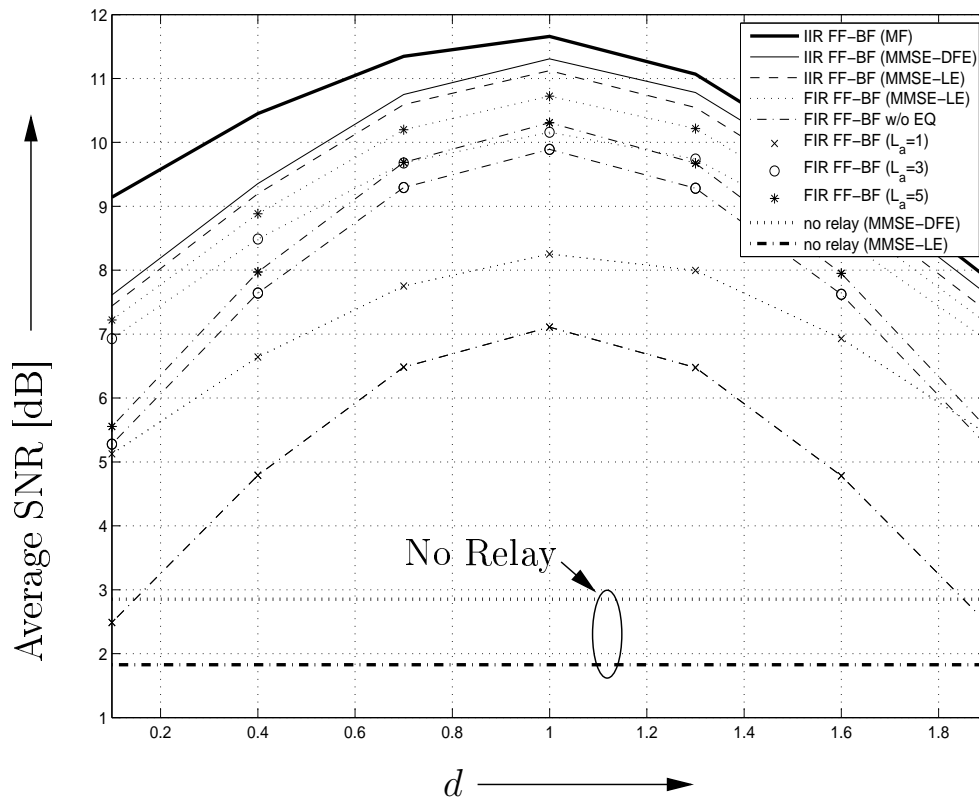


Figure 4.11: Average SINR vs. distance d for FF-BF with MMSE-LE, MMSE-DFE, and an MF receiver at the destination. $N_R = 2$ relays with $M_1 = 2$ and $M_2 = 3$, exponentially decaying power delay profile with $\sigma_t = 2$ and $L_g = L_h = 5$, and $\gamma_g = \gamma_h = 10$ dB. For comparison the SINRs of FF-BF without (w/o) equalization (EQ) at the destination and without relaying are also shown, respectively.

in large performance gains, FIR FF-BF without equalization with large L_a approaches the same performance as FIR FF-BF with equalization. We note that for a given filter length L_a the feedback requirements and the relay complexity for the proposed FIR FF-BF schemes with or without equalization are identical. Fig. 4.11 also shows that as L_a increases, the performance of FIR FF-BF approaches the performance of IIR FF-BF with MMSE-DFE at the destination. For IIR FF-BF filters, Fig. 4.11 shows that the loss of MMSE-DFE compared to an idealized MF receiver, which is the ultimate performance bound for any equalizer architecture, exceeds 1 dB only for $d < 0.4$.

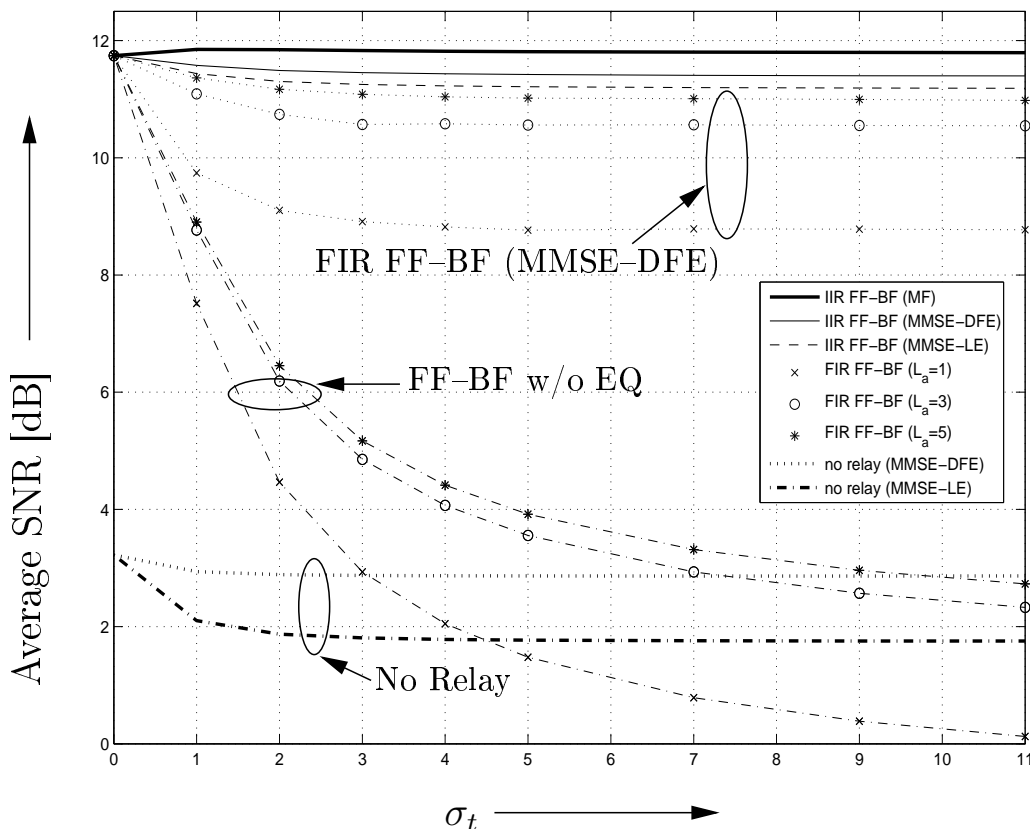


Figure 4.12: Average SINR vs. decay parameter σ_t for FF-BF with MMSE-LE, MMSE-DFE, and an MF receiver at the destination. $N_R = 2$ relays with $M_1 = 2$ and $M_2 = 3$, distance $d = 1$, exponentially decaying power delay profile with $L_g = L_h = 5$, and $\gamma_g = \gamma_h = 10$ dB. For comparison the SINRs of FF-BF without (w/o) equalization (EQ) at the destination and without relaying are also shown, respectively.

Impact of Decay Parameter σ_t : In Fig. 4.12, we investigate the impact of decay parameter σ_t on the performance of FF-BF for $d = 1$ and $\gamma_g = \gamma_h = 10$ dB. We note that the CIR coefficients of the test channel decay the faster (i.e., the channel is less frequency selective), the smaller σ_t is. As a special case, the channel becomes frequency flat when $\sigma_t = 0$. Fig. 4.12 shows that when the channel becomes frequency flat, i.e., $\sigma_t = 0$, all relaying schemes provide the same average SINR performance. We also observe that the performance of sufficiently long FF-BF filters is practically not affected by the

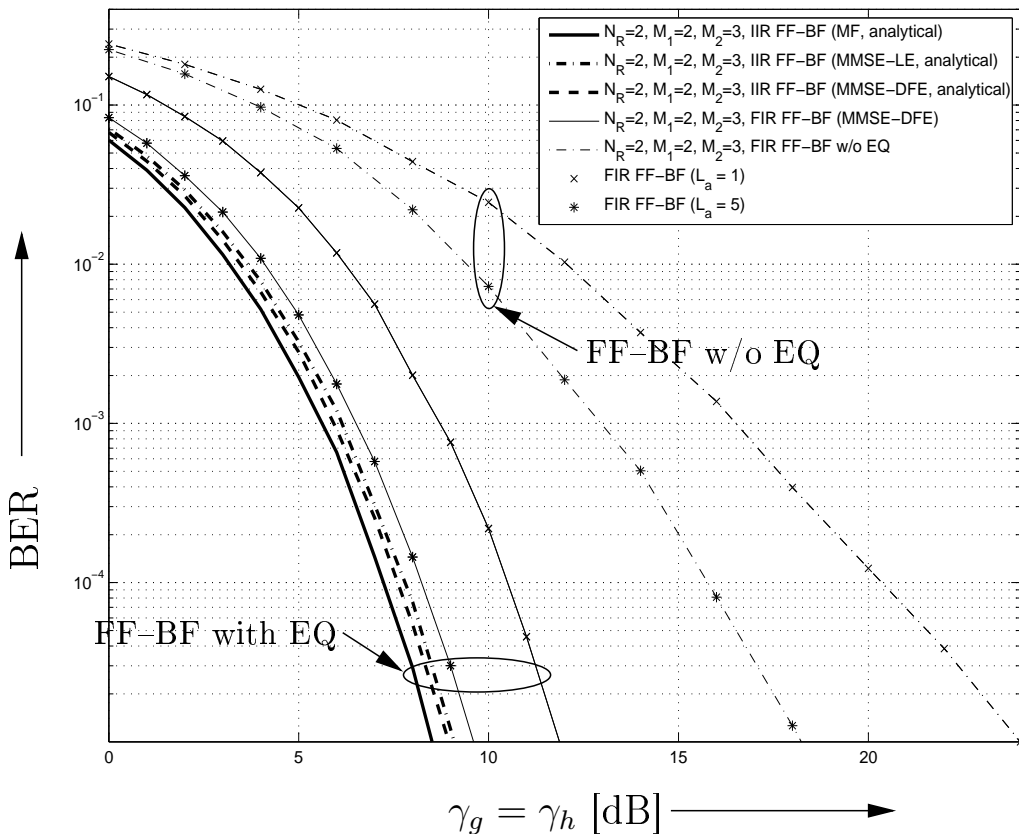


Figure 4.13: Average BER of BPSK vs. transmit SNR γ for FF-BF with MMSE-LE, MMSE-DFE, and an MF receiver at the destination. Exponentially decaying power delay profile with $\sigma_t = 2$ and $L_g = L_h = 5$. For comparison the BER of FF-BF without (w/o) equalization (EQ) at the destination is also shown.

frequency selectivity of the channel if MMSE-LE or MMSE-DFE are employed at the destination. The idealized MF receiver with IIR FF-BF benefits even slightly from more frequency selectivity (larger σ_t) because of the additional diversity offered by the channel. In contrast, FF-BF without equalization at the receiver is adversely affected by increased frequency selectivity and is even outperformed by direct transmission without relay (but with equalization at the destination) for $\sigma_t > 11$.

BER Performance for Fading Channels: Fig. 4.13 shows BERs of BPSK modulation vs. transmit SNR, $\gamma = \gamma_g = \gamma_h$, for FIR and IIR FF-BF matrix filters. We adopt

cooperative relay network setup 2), and assume $\sigma_t = 2$ and $d = 1$. The BERs for FIR FF–BF matrix filters were simulated by implementing MMSE–DFE with FIR equalization filters of lengths $4 \times L_{\text{eq}}$, which caused negligible performance degradation compared to IIR equalization filters. The BERs for IIR FF–BF were obtained by approximating the BER of BPSK transmission by $\text{BER}_X = Q(\sqrt{2\text{SINR}_X})$ [84], where $X = \text{DFE}$, $X = \text{LE}$, and $X = \text{MF}$ for DFE, LE, and an MF receiver at the destination, respectively. Fig. 4.13 shows that equalization at the destination is very beneficial in terms of the achievable BER and large performance gains are realized compared to FF–BF without equalization. Also, for IIR FF–BF matrix filters MMSE–LE and MMSE–DFE receivers achieve practically identical BERs and the gap to the idealized MF receiver is less than 0.6 dB. This gap could potentially be closed by trellis–based equalizers, such as decision–feedback sequence estimation, at the expense of an increase in complexity.

4.6 Conclusions

In this chapter, we considered FF–BF for frequency–selective cooperative relay networks with one source, multiple multi–antenna relays, and one destination. In contrast to prior work, we assumed that the destination is equipped with either a slicer or a simple equalizer such as a linear or a decision feedback equalizer. For both cases, the FF–BF filters at the relays were optimized for maximization of the SINR at the equalizer output under a joint relay power constraint. Additionally, for the simple slicer case we also considered the optimization of the FF–BF filters for minimization of the total transmit power subject to a QoS constraint to guarantee a certain level of performance.

For the slicer case, we obtained closed–form solutions and efficient numerical methods for computation of the optimal FIR FF–BF matrix filters. For IIR FF–BF filters, we found a unified expression for the frequency response of the optimal filters valid for LE, DFE, and

an idealized MF receiver. We proposed a simple algorithm with guaranteed convergence for optimization of the power allocation factor included in the optimal frequency response. For FIR FF–BF filters, we showed that a difficult non–convex optimization problem results and proposed a simple and efficient gradient algorithm to find near–optimal filter coefficients.

Our simulation results confirmed that (1) the performance gap between FF–BF filters with LE/DFE and FF–BF filters with an idealized MF receiver is relatively small implying that little can be gained by employing more complex trellis–based equalization schemes at the destination, (2) relatively short FIR FF–BF filters closely approach the performance of IIR FF–BF filters for all considered receiver structures confirming the near–optimal performance of the proposed gradient algorithm for FIR filter optimization, (3) for a given total number of antennas it is preferable to have the antennas concentrated in few relays rather than having many relays with few antennas, (4) if short FIR FF–BF filters are used and/or few relays are employed, equalization at the destination is beneficial; 5) if long FIR FF–BF filters are employed, the simple slicer destination with optimized decision delay closely approaches the same performance as destinations with equalizers.

Chapter 5

Two-Way Filter-and-Forward

Beamforming for Frequency-Selective

Channels with Multiple Single Antenna

Relays

5.1 Introduction

Drawing from the findings on one-way relaying in the previous chapter, we investigate FF-BF for two-way cooperative relay networks in this chapters. Particularly, we consider FF-BF for two-way cooperative networks with two transceivers communicating with each other over frequency-selective channels via multiple single-antenna relays using the so-called MABC protocol. Thereby, we consider two cases for the receive processing at the transceivers: (1) a simple slicer is used without equalization and (2) LE or DFE is performed. The resulting FF-BF filter design problems are substantially more challenging than those for one-way relaying in the previous chapter and [50, 82], since one filter at the relay has to be optimized to achieve a certain level of performance at two receivers. In particular, we consider the following design problems. For both case (1) and case (2), we optimize the FF-BF filters at the relays for a SINR balancing objective under a relay transmit power

constraint, i.e., maximization of the worst transceiver SINR. Additionally, for case (1) we also consider the optimization of the FF-BF filters for minimization of the total transmit power subject to two QoS constraints to guarantee a certain level of performance. For case (1), we convert the resulting optimization problems into convex SOCP problems for which efficient off-the-self interior point algorithms are available for finding global optimal solutions. For case (2), it does not seem possible to find an exact solution to the problem. However, we provide an upper bound and an achievable lower bound for the optimization problem, and our results show that the gap between both bounds is small. In addition, for case (2), we also consider the problem of minimizing the sum of the MSEs of the outputs of the equalizers, which allows for an exact solution.

Our simulation results show that while transceivers with equalizers always achieve a superior performance, the gap to transceivers employing simple slicers decreases with increasing FF-BF filter length and increasing number of relays. Furthermore, for sufficiently long FF-BF filters and a sufficiently large number of relays, transceivers with and without equalizers lead to an SINR loss of less than one decibel compared to an idealized matched filter receiver, which constitutes a performance upper bound for all receiver structures.

The remainder of this chapter is organized as follows. In Section 5.2, the adopted system model is presented. The optimization of FIR FF-BF filters for transceivers without and with equalization is presented in Sections 5.3 and 5.4, respectively. Simulation results are provided in Section 5.5, and some conclusions are drawn in Section 5.6.

5.2 System Model

We consider a relay network with two transceiver nodes and N_R relay nodes. All network nodes have a single antenna. A block diagram of the discrete-time overall transmission system in equivalent complex baseband representation is depicted in Fig. 5.1. The adopted

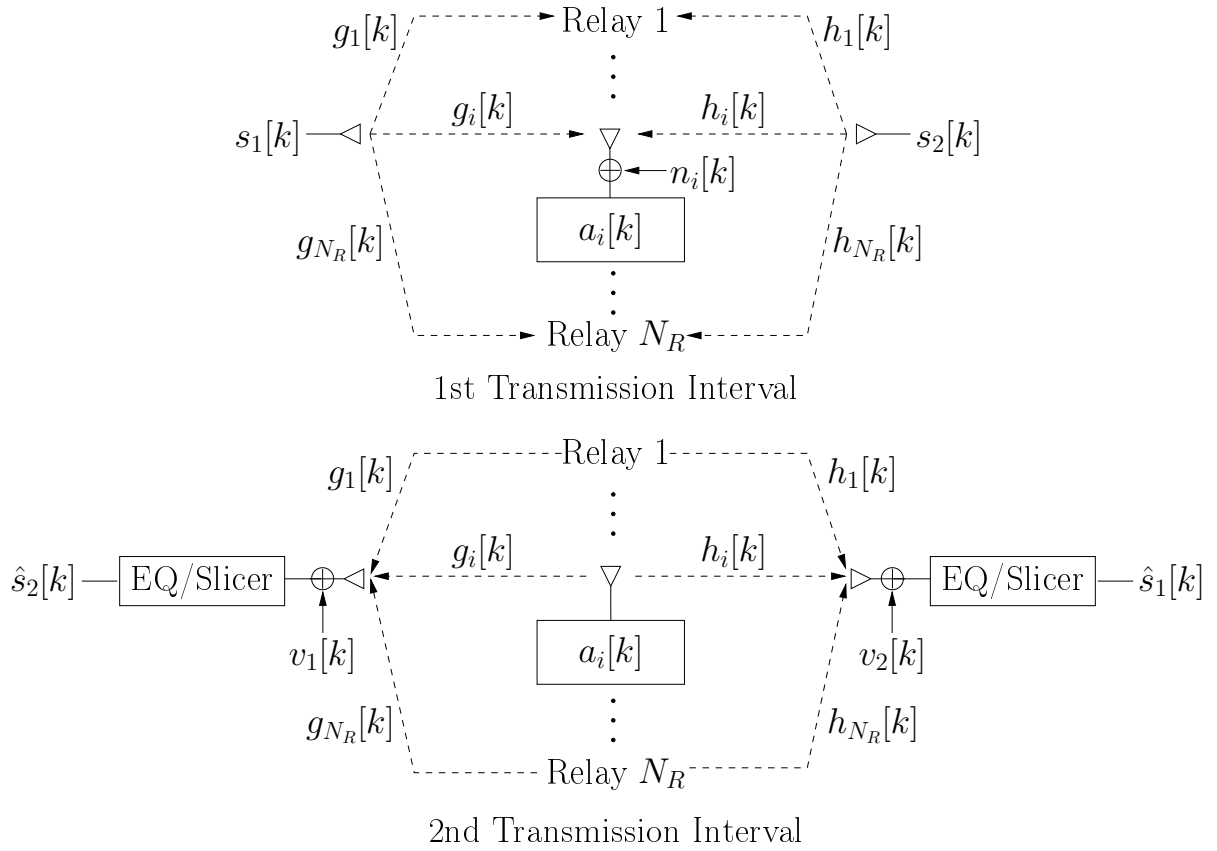


Figure 5.1: Cooperative two-way network with two transceiver nodes and N_R relay nodes. EQ is the equalizer at the transceivers. $\hat{s}_1[k]$ and $\hat{s}_2[k]$ are estimated received symbols at TC2 and TC1, respectively.

two-way MABC relay protocol involves only two transmission intervals. In the first interval, the two transceivers transmit their packets simultaneously to the relays, and in the second interval, the relays process the packets and broadcast them to the two transceiver nodes.

The discrete-time CIRs between transceiver 1 (TC1) and relay i , $g_i[k]$, $0 \leq k \leq L_g - 1$, and between transceiver 2 (TC2) and relay i , $h_i[k]$, $0 \leq k \leq L_h - 1$, contain the combined effects of transmit pulse shaping, the continuous-time channel, receive filtering, and sampling. Here, L_g and L_h denote the lengths of the TC1-relay and the TC2-relay channels, respectively.

Similar to [50, 57, 58], we assume in this chapter that both transceivers have perfect knowledge of all channels in the network. This can be accomplished by having separate training phases for all involved nodes, where they transmit training symbols. In this way, both transceivers can estimate their respective CIRs to the relays and the over all channels $h_i[k] * g_i[k]$ to the other transceiver. TC1 can then obtain the channel between TC2 and relay i from $h_i[k] * g_i[k]$ and $g_i[k]$, $i = 1, \dots, N_R$, via deconvolution or via a low rate feedback channel from TC2. TC2 can obtain $h_i[k]$, $i = 1, \dots, N_R$, in a similar manner. Subsequently, one of the two transceivers computes the optimal FF-BF filters adopting the algorithms proposed in Sections 5.3 and 5.4 and broadcasts the filter coefficients $a_i[k]$ to relay i and the other transceiver via an error-free and zero-delay feedback channel.

5.2.1 FF-BF at Relays

In the first phase of transmission, TC j transmits the i.i.d. symbols $s_j[k]$, $j \in \{1, 2\}$, which are taken from a scalar symbol alphabet \mathcal{A} such as phase-shift keying (PSK) or quadrature amplitude modulation (QAM), and have variance $\sigma_{s_j}^2 \triangleq \mathcal{E}\{|s_j[k]|^2\}$, $j \in \{1, 2\}$. The signal received at the i th relay, $i = 1, \dots, N_R$, is given by

$$y_i[k] = g_i[k] * s_1[k] + h_i[k] * s_2[k] + n_i[k], \quad (5.1)$$

where $n_i[k]$ denotes AWGN with variance $\sigma_n^2 \triangleq \mathcal{E}\{|n_i[k]|^2\}$.

The FF-BF filter impulse response coefficients of relay i for the second transmission interval are denoted by $a_i[k]$, $-q_l \leq k \leq q_u$. For IIR FF-BF filters $q_l \rightarrow \infty$ and $q_u \rightarrow \infty$ and for FIR FF-BF filters $q_l = 0$ and $q_u = L_a - 1$, where L_a is the FIR BF filter length.

The signal transmitted from the i th relay during the second interval can be expressed as

$$\begin{aligned} t_i[k] &= a_i[k] * y_i[k] \\ &= a_i[k] * g_i[k] * s_1[k] + a_i[k] * h_i[k] * s_2[k] + a_i[k] * n_i[k], \quad i = 1, \dots, N_R. \end{aligned} \quad (5.2)$$

5.2.2 Transceiver Processing

The signal received at TC2 during the second time interval is given by⁴

$$\begin{aligned} \tilde{r}_2[k] &= \sum_{i=1}^{N_R} h_i[k] * t_i[k] + v_2[k] \\ &= \sum_{i=1}^{N_R} h_i[k] * a_i[k] * g_i[k] * s_1[k] + \sum_{i=1}^{N_R} h_i[k] * a_i[k] * h_i[k] * s_2[k] \\ &\quad + \sum_{i=1}^{N_R} h_i[k] * a_i[k] * n_i[k] + v_2[k], \end{aligned} \quad (5.3)$$

where $v_j[k]$ denotes AWGN with variance $\sigma_{v_j}^2$, $j \in \{1, 2\}$. It is noteworthy that since $s_2[k]$, $h_i[k]$, and $a_i[k]$, $i = 1, \dots, N_R$, are known at TC2, the second term on the right hand side of (5.3) can be subtracted from $\tilde{r}_2[k]$ before the residual signal $r_2[k]$ is further processed to extract the information symbols $s_1[k]$. Similar considerations hold for TC1. Thus, the residual received signal at TC j can be expressed as

$$r_j[k] = h_{\text{eq}}[k] * s_i[k] + v'_j[k], \quad j \in \{1, 2\}, \quad (5.4)$$

where $i = 1$ if $j = 2$ and $i = 2$ if $j = 1$ and we introduced the equivalent CIR between TC1 and TC2

$$h_{\text{eq}}[k] \triangleq \sum_{i=1}^{N_R} h_i[k] * a_i[k] * g_i[k], \quad (5.5)$$

⁴Note that during the first time interval the two transceivers do not receive any signal, since we assumed that there is no direct link between them.

and the effective noise

$$v'_1[k] \triangleq \sum_{i=1}^{N_R} g_i[k] * a_i[k] * n_i[k] + v_1[k], \quad (5.6)$$

$$v'_2[k] \triangleq \sum_{i=1}^{N_R} h_i[k] * a_i[k] * n_i[k] + v_2[k]. \quad (5.7)$$

We note that $v'_j[k]$, $j \in \{1, 2\}$, is colored noise because of the filtering with the TC-relay CIRs and the FF-BF filters.

5.3 FIR FF-BF without Equalization

In practice, it is conceivable that the transceiver nodes cannot afford an equalizer due to size and/or power limitation. This may be valid for applications such as sensor networks with battery powered sensors. This case is considered in this section and the transceivers are assumed to apply only simple slicers for detection. We note that FF-BF filter optimization for transmit power minimization in two-way relaying networks has been considered independently in [86]. In particular, [86] deals with FF-BF for two-way relaying without equalization at the transceiver and is closely related to this Section 5.3.2, where relay power minimization under SINR constraints are considered. However, [86] only considers the case of power minimization under SINR constraints but not the case of max-min SINR maximization under a power constraint, which will be discussed in Section 5.3.1. Furthermore, a decision delay was not considered in [86]. As has been shown in Chapter 4 for one-way relaying, such decision delay parameter leads to significant performance improvements.

The vector containing the coefficients of the equivalent CIR between TC1 and TC2,

$\mathbf{h}_{\text{eq}} \triangleq [h_{\text{eq},2}[0] \ h_{\text{eq},2}[1] \ \dots \ h_{\text{eq},2}[L_a + L_g + L_h - 3]]^T$, can be rewritten as

$$\mathbf{h}_{\text{eq}} = \sum_{i=1}^{N_R} \mathbf{H}_i \bar{\mathbf{G}}_i \mathbf{a}_i \triangleq \mathcal{H} \mathcal{G}_D \mathbf{a} \quad (5.8)$$

where $\mathcal{H} \triangleq [\mathbf{H}_1 \ \dots \ \mathbf{H}_{N_R}]$, $\mathcal{G}_D \triangleq \text{diag} \{ \bar{\mathbf{G}}_1, \dots, \bar{\mathbf{G}}_{N_R} \}$, and $\mathbf{a} \triangleq [\mathbf{a}_1^T \ \dots \ \mathbf{a}_{N_R}^T]^T$. $(L_a + L_g + L_h - 2) \times (L_a + L_g - 1)$ matrix \mathbf{H}_i and $(L_a + L_g - 1) \times L_a$ matrix $\bar{\mathbf{G}}_i$ are column-circulant matrices with $[h_i[0] \ \dots \ h_i[L_h - 1] \ \mathbf{0}_{L_a + L_g - 2}^T]^T$ and $[g_i[0] \ \dots \ g_i[L_g - 1] \ \mathbf{0}_{L_a - 1}^T]^T$ in the first columns, respectively, and $\mathbf{a}_i \triangleq [a_i[0] \ a_i[1] \ \dots \ a_i[L_a - 1]]^T$.

Matrix \mathcal{H} can be separated into a vector \mathbf{h}_{k_0} and a sub-matrix \mathcal{H}_{k_0} , i.e., vector $\mathbf{h}_{k_0}^T$ of length $(L_a + L_g - 1)N_R$ is the k_0 th row of matrix \mathcal{H} , and $\mathcal{H}_{k_0} \triangleq [\mathcal{H}]_{ij}$, $i \in \{1, \dots, k_0 - 1, k_0 + 1, \dots, (L_a + L_g + L_h - 2)\}$, $j \in \{1, \dots, (L_a + L_g - 1)N_R\}$. Therefore, for $j = 2$ and $i = 1$, the first term in (5.4) can be decomposed into a signal part and an ISI part

$$\begin{aligned} h_{\text{eq}}[k] * s_1[k] &= h_{\text{eq}}[k_0] s_1[k - k_0] + \sum_{l=0, l \neq k_0}^{L_a + L_g + L_h - 3} h_{\text{eq}}[l] s_1[k - l] \\ &= \underbrace{\mathbf{h}_{k_0}^T \mathcal{G}_D \mathbf{a} s_1[k - k_0]}_{\text{desired signal}} + \underbrace{\mathbf{s}_1^T[k] \mathcal{H}_{k_0} \mathcal{G}_D \mathbf{a}}_{\text{ISI}} \end{aligned} \quad (5.9)$$

where $\mathbf{s}_1[k] = [s_1[k] \ \dots \ s_1[k - k_0 + 1] \ s_1[k - k_0 - 1] \ \dots \ s_1[k - (L_a + L_g + L_h - 3)]]^T$, and k_0 is the slicer decision delay at the transceiver. We note that for one-way relaying such a decision delay was not introduced in [50]. However, as will be shown in Section 5.5, for two-way relaying a decision delay is highly beneficial. The power of the desired signal and the ISI can be obtained as

$$\mathcal{E} \left\{ \left| \mathbf{h}_{k_0}^T \mathcal{G}_D \mathbf{a} s_1[k - k_0] \right|^2 \right\} = \sigma_{s_1}^2 \mathbf{a}^H \mathcal{G}_D^H \mathbf{h}_{k_0}^* \mathbf{h}_{k_0}^T \mathcal{G}_D \mathbf{a} \quad (5.10)$$

and

$$\mathcal{E} \left\{ \left| \mathbf{s}_1^T[k] \mathcal{H}_{k_0} \mathcal{G}_D \mathbf{a} \right|^2 \right\} = \sigma_{s_1}^2 \mathbf{a}^H \mathcal{G}_D^H \mathcal{H}_{k_0}^H \mathcal{H}_{k_0} \mathcal{G}_D \mathbf{a}, \quad (5.11)$$

respectively. Similarly, $v'_2[k]$ in (5.7) can be rewritten as

$$v'_2[k] = \sum_{i=1}^{N_R} \mathbf{n}_i^T[k] \mathbf{H}_i \mathbf{a}_i + v_2[k] \triangleq \mathbf{n}^T[k] \mathcal{H}_D \mathbf{a} + v_2[k] \quad (5.12)$$

with row vector $\mathbf{n}[k] \triangleq [\mathbf{n}_1^T[k] \ \dots \ \mathbf{n}_{N_R}^T[k]]^T$ of length $(L_a + L_h - 1)N_R$ and $(L_a + L_h - 1)N_R \times N_R L_a$ matrix $\mathcal{H}_D \triangleq \text{diag} \{ \bar{\mathbf{H}}_1, \dots, \bar{\mathbf{H}}_{N_R} \}$, where $\mathbf{n}_i[k] \triangleq [n_i[k] \ \dots \ n_i[k - (L_a + L_h - 2)]]^T$ and $\bar{\mathbf{H}}_i$ is a $(L_a + L_h - 1) \times L_a$ column-circulant matrix with vector $[h_i[0] \ \dots \ h_i[L_h - 1] \ \mathbf{0}_{L_a - 1}^T]^T$ in the first column. The noise power is obtained as

$$\mathcal{E} \{ |v'_2[k]|^2 \} = \sigma_n^2 \mathbf{a}^H \mathcal{H}_D^H \mathcal{H}_D \mathbf{a} + \sigma_{v_2}^2. \quad (5.13)$$

The SINR at TC2 can be obtained by combining (5.9)–(5.11), and (5.13) and is given by

$$\begin{aligned} \text{SINR}_{\text{slicer}, 2}(\mathbf{a}) &\triangleq \frac{\mathcal{E} \left\{ \left| \mathbf{h}_{k_0}^T \mathcal{G}_D \mathbf{a}_{s_1}[k - k_0] \right|^2 \right\}}{\mathcal{E} \left\{ \left| \mathbf{s}_1^T[k] \mathcal{H}_{k_0} \mathcal{G}_D \mathbf{a} \right|^2 \right\} + \mathcal{E} \{ |v'_2[k]|^2 \}} \\ &= \frac{\sigma_{s_1}^2 \mathbf{a}^H \mathcal{G}_D^H \mathbf{h}_{k_0}^* \mathbf{h}_{k_0}^T \mathcal{G}_D \mathbf{a}}{\sigma_{s_1}^2 \mathbf{a}^H \mathcal{G}_D^H \mathcal{H}_{k_0}^H \mathcal{H}_{k_0} \mathcal{G}_D \mathbf{a} + \sigma_n^2 \mathbf{a}^H \mathcal{H}_D^H \mathcal{H}_D \mathbf{a} + \sigma_{v_2}^2}. \end{aligned} \quad (5.14)$$

Similarly, the SINR at TC1 is given by

$$\text{SINR}_{\text{slicer}, 1}(\mathbf{a}) = \frac{\sigma_{s_2}^2 \mathbf{a}^H \mathcal{H}_D^H \mathbf{g}_{k_0}^* \mathbf{g}_{k_0}^T \mathcal{H}_D \mathbf{a}}{\sigma_{s_2}^2 \mathbf{a}^H \mathcal{H}_D^H \mathcal{G}_{k_0}^H \mathcal{G}_{k_0} \mathcal{H}_D \mathbf{a} + \sigma_n^2 \mathbf{a}^H \mathcal{G}_D^H \mathcal{G}_D \mathbf{a} + \sigma_{v_1}^2}, \quad (5.15)$$

where $\mathbf{g}_{k_0}^T$ is the k_0 th row of matrix \mathcal{G} and matrix \mathcal{G}_{k_0} is matrix \mathcal{G} without the k_0 th row. Here, $\mathcal{G} \triangleq [\mathbf{G}_1 \ \dots \ \mathbf{G}_{N_R}]$ with $(L_a + L_g + L_h - 2) \times (L_a + L_h - 1)$ column-circulant matrix

\mathbf{G}_i which has vector $[g_i[0] \dots g_i[L_g - 1] \mathbf{0}_{L_a+L_h-2}^T]^T$ in the first column.

From (5.2), the total relay transmit power, $P_R(\mathbf{a})$, in the second transmission interval is given by

$$P_R(\mathbf{a}) = \sum_{i=1}^{N_R} \mathcal{E} \{ |t_i[k]|^2 \} = \mathbf{a}^H \mathbf{D} \mathbf{a} \quad (5.16)$$

with $\mathbf{D} \triangleq \sigma_{s_1}^2 \mathcal{G}_D^H \mathcal{G}_D + \sigma_{s_2}^2 \mathcal{H}_D^H \mathcal{H}_D + \sigma_n^2 \mathbf{I}_{L_a N_R}$.

In the following two subsections, we will optimize the FIR FF-BF filters for (a) maximization of the minimum transceiver SINR at the slicer output under a relay transmit power constraint and (b) minimization of the transmit power under individual transceiver SINR constraints, respectively. The decision delay k_0 is assumed to be fixed for filter optimization. We will show in Section 5.5 that the choice of k_0 can have a substantial impact on performance.

5.3.1 Max-min Criterion Under Relay Power Constraint

First, we consider the optimization of the FF-BF filters for maximization of the worst transceiver SINR subject to a maximum relay power of P . This problem is of interest when the power available at the relays is limited and the aim is to maximize the QoS given this strict system restriction [50, 58, 87]. The corresponding optimization problem can be formulated as

$$\max_{\mathbf{a}} \min \{ \text{SINR}_{\text{slicer},1}(\mathbf{a}), \text{SINR}_{\text{slicer},2}(\mathbf{a}) \} \quad (5.17a)$$

$$\text{s.t. } \mathbf{a}^H \mathbf{D} \mathbf{a} \leq P. \quad (5.17b)$$

Equivalently, problem (5.17) can be rewritten as

$$\max_{\mathbf{a}} t \quad (5.18a)$$

$$\text{s.t. } \text{SINR}_{\text{ slicer, 1}}(\mathbf{a}) \geq t \quad (5.18b)$$

$$\text{SINR}_{\text{ slicer, 2}}(\mathbf{a}) \geq t \quad (5.18c)$$

$$\mathbf{a}^H \mathbf{D} \mathbf{a} \leq P. \quad (5.18d)$$

Realizing that $\mathcal{H}_D^H \mathbf{g}_{k_0}^* = \mathcal{G}_D^H \mathbf{h}_{k_0}^*$, we let $\mathbf{q} \triangleq \mathcal{H}_D^H \mathbf{g}_{k_0}^*$, and reformulate problem (5.18) as

$$\max_{\mathbf{c}} t \quad (5.19a)$$

$$\text{s.t. } \mathbf{c}^H \bar{\mathbf{V}}(t) \mathbf{c} \leq \mathbf{c}^H \bar{\mathbf{q}} \bar{\mathbf{q}}^H \mathbf{c} \quad (5.19b)$$

$$\mathbf{c}^H \bar{\mathbf{W}}(t) \mathbf{c} \leq \mathbf{c}^H \bar{\mathbf{q}} \bar{\mathbf{q}}^H \mathbf{c} \quad (5.19c)$$

$$\mathbf{c}^H \mathbf{c} \leq P + 1 \quad (5.19d)$$

$$[\mathbf{c}]_{N_R L_a + 1} = 1, \quad (5.19e)$$

where $\mathbf{c} \triangleq [(\mathbf{D}^{1/2} \mathbf{a})^T \ 1]^T$, $\bar{\mathbf{q}} \triangleq [(\mathbf{D}^{-H/2} \mathbf{q})^T \ 0]^T$, $\bar{\mathbf{V}}(t) \triangleq \frac{t\sigma_{v_1}^2}{\sigma_{s_2}^2} \text{diag} \{ \mathbf{D}^{-H/2} \mathbf{V} \mathbf{D}^{-1/2}, 1 \}$ with $\mathbf{V} \triangleq \frac{\sigma_{s_2}^2}{\sigma_{v_1}^2} \mathcal{H}_D^H \mathcal{G}_{k_0}^H \mathcal{G}_{k_0} \mathcal{H}_D + \frac{\sigma_n^2}{\sigma_{v_1}^2} \mathcal{G}_D^H \mathcal{G}_D$, and $\bar{\mathbf{W}}(t) \triangleq \frac{t\sigma_{v_2}^2}{\sigma_{s_1}^2} \text{diag} \{ \mathbf{D}^{-H/2} \mathbf{W} \mathbf{D}^{-1/2}, 1 \}$ with $\mathbf{W} \triangleq \frac{\sigma_{s_1}^2}{\sigma_{v_2}^2} \mathcal{G}_D^H \mathcal{H}_{k_0}^H \mathcal{H}_{k_0} \mathcal{G}_D + \frac{\sigma_n^2}{\sigma_{v_2}^2} \mathcal{H}_D^H \mathcal{H}_D$.

Note that multiplying the optimal \mathbf{c} by $e^{j\theta}$, where θ is an arbitrary phase, does not affect the objective function or the constraints for problem (5.19). Therefore, we can assume that $\bar{\mathbf{q}}^H \mathbf{c}$ is a real number without loss of generality. Thus, for a given t , problem (5.19) can be

transformed into the convex SOCP feasibility problem

$$\min_{\mathbf{c}} \quad -t \quad (5.20a)$$

$$\text{s.t.} \quad \left\| \bar{\mathbf{V}}^{1/2}(t)\mathbf{c} \right\| \leq \bar{\mathbf{q}}^H \mathbf{c} \quad (5.20b)$$

$$\left\| \bar{\mathbf{W}}^{1/2}(t)\mathbf{c} \right\| \leq \bar{\mathbf{q}}^H \mathbf{c} \quad (5.20c)$$

$$\|\mathbf{c}\| \leq \sqrt{P+1} \quad (5.20d)$$

$$[\mathbf{c}]_{N_R L_a + 1} = 1. \quad (5.20e)$$

Consequently, for a given t , problem (5.20) can be efficiently solved using interior point methods [88] and a bisectional search can be used to find the optimal t [1]. Since the optimal FF-BF filter vector \mathbf{a}_{opt} can be directly obtained from the solution of (5.20), we have provided an efficient procedure for computation of the optimal FF-BF filter vector.

5.3.2 Relay Power Minimization Under SINR Constraints

Another relevant problem is the minimization of the relay transmit power under SINR constraints. This problem is of interest when we want to satisfy a required QoS with minimum relay transmitted power [50, 58, 89]. The corresponding optimization problem can be formulated as

$$\min_{\mathbf{a}} \quad \mathbf{a}^H \mathbf{D} \mathbf{a} \quad (5.21a)$$

$$\text{s.t.} \quad \text{SINR}_{\text{ slicer,1}}(\mathbf{a}) \geq \gamma_1 \quad (5.21b)$$

$$\text{SINR}_{\text{ slicer,2}}(\mathbf{a}) \geq \gamma_2. \quad (5.21c)$$

Equivalently, problem (5.21) can be reformulated as

$$\min_{\mathbf{c}} \quad \mathbf{c}^H \mathbf{c} - 1 \quad (5.22a)$$

$$\text{s.t.} \quad \mathbf{c}^H \bar{\mathbf{q}} \bar{\mathbf{q}}^H \mathbf{c} \geq \mathbf{c}^H \bar{\mathbf{V}}(\gamma_1) \mathbf{c} \quad (5.22b)$$

$$\mathbf{c}^H \bar{\mathbf{q}} \bar{\mathbf{q}}^H \mathbf{c} \geq \mathbf{c}^H \bar{\mathbf{W}}(\gamma_2) \mathbf{c}, \quad (5.22c)$$

where \mathbf{c} , $\bar{\mathbf{V}}(\cdot)$, $\bar{\mathbf{W}}(\cdot)$, and $\bar{\mathbf{q}}$ are defined after (5.19). By exploiting again the fact that multiplying the optimal \mathbf{c} by $e^{j\theta}$ does not affect the objective function or the constraints of problem (5.22), we can assume $\bar{\mathbf{q}}^H \mathbf{c}$ is a real number without loss of generality and transform problem (5.22) into an SOCP problem

$$\min_{\mathbf{c}} \quad \tau \quad (5.23a)$$

$$\text{s.t.} \quad \left\| \tilde{\mathbf{V}}^{1/2} \mathbf{c} \right\| \leq \bar{\mathbf{q}}^H \mathbf{c} \quad (5.23b)$$

$$\left\| \tilde{\mathbf{W}}^{1/2} \mathbf{c} \right\| \leq \bar{\mathbf{q}}^H \mathbf{c} \quad (5.23c)$$

$$\|\mathbf{c}\| \leq \tau \quad (5.23d)$$

$$[\mathbf{c}]_{N_R L_a + 1} = 1. \quad (5.23e)$$

The SOCP problem (5.23) can again be efficiently solved using interior point methods [88].

5.4 FF-BF with Equalization

If only a simple slicer is employed at the transceivers, the FF-BF filters at the relays are burdened with equalizing both TC-relay channels. By implementing equalizers at the transceivers some of the processing burden is shifted from the relays to the transceivers, which leads to better performance at the expense of an increase in complexity. However,

for some applications, such as the GSM and EDGE communication network, the increased complexity at the transceivers is acceptable, since these systems also use equalizers if relaying is not applied.

From (5.4) we observe that a cooperative two-way relay network with FF-BF can be modeled as an equivalent SISO system. Therefore, as long as the transceivers know the CIRs of all involved channels and the coefficients of the FF-BF filter, the same equalization techniques as for point-to-point single-antenna transmission can be used [83]. Here, we consider LE and DFE optimized according to the conventional ZF and MMSE criteria [84, 90].

Throughout this section we assume that the transceivers employ LE or DFE with IIR equalization filters. In a practical implementation, FIR equalization filters are used, of course. However, sufficiently long FIR filters will approach the performance of IIR filters arbitrarily close. Assuming IIR equalization filters has the advantage that relatively simple and elegant expressions for the SINR at the equalizer output exist [83, 84]. For FF-BF, we consider both IIR filters, which provide performance bounds, and FIR filters, which are required for practical implementation.

5.4.1 Optimal IIR FF-BF with Equalization

In order to be able to exploit the SINR expressions in [83, 84], we first whiten the noise impairing the signal received at the transceivers. The power spectral densities of the noises $v'_1[k]$ and $v'_2[k]$ at the two transceivers are given by

$$\Phi_{v'_j}(f) = \sigma_n^2 \mathbf{a}^H(f) \mathbf{\Gamma}_j(f) \mathbf{a}(f) + \sigma_{v_j}^2, \quad j \in \{1, 2\}, \quad (5.24)$$

where $\mathbf{\Gamma}_1(f) \triangleq \text{diag}\{|G_1(f)|^2, \dots, |G_{N_R}(f)|^2\}$, $\mathbf{\Gamma}_2(f) \triangleq \text{diag}\{|H_1(f)|^2, \dots, |H_{N_R}(f)|^2\}$, and $\mathbf{a}(f) \triangleq [A_1(f), \dots, A_{N_R}(f)]^T$. $G_i(f) \triangleq \mathcal{F}\{g_i[k]\}$, $H_i(f) \triangleq \mathcal{F}\{h_i[k]\}$, and $A_i(f) \triangleq \mathcal{F}\{a_i[k]\}$

denote the frequency responses of the TC1- i th relay channel, TC2- i th relay channel, and the FF-BF filter at the i th relay, respectively. Therefore, the whitening filter for $v'_j[k]$ is given by

$$W_j(f) = \left(\sigma_n^2 \mathbf{a}^H(f) \mathbf{\Gamma}_j(f) \mathbf{a}(f) + \sigma_{v_j}^2 \right)^{-1/2}. \quad (5.25)$$

After whitening, the frequency response of the equivalent overall channel at transceiver j can be obtained as

$$\begin{aligned} H'_{\text{eq},j}(f) &\triangleq W_j(f) \mathcal{F}\{h_{\text{eq},j}[k]\} \\ &= \mathbf{q}^T(f) \mathbf{a}(f) \left(\sigma_n^2 \mathbf{a}^H(f) \mathbf{\Gamma}_j(f) \mathbf{a}(f) + \sigma_{v_j}^2 \right)^{-1/2}, \quad j \in \{1, 2\}, \end{aligned} \quad (5.26)$$

where $h_{\text{eq},j}[k] \triangleq h_j[k] * a_j[k] * g_j[k]$, $\mathbf{q}(f) \triangleq [Q_1(f) \dots Q_{N_R}(f)]^T$ and $Q_i(f) \triangleq H_i(f)G_i(f)$. Note that, after whitening, the power spectral density of the noise at the output of the whitening filter at TC j , $n'_j[k]$, is $\Phi_{n'_j}(f) = 1$.

For TC j , we can express the SINRs at the outputs of a decision feedback and a linear equalizer as [83, 84]

$$\text{SINR}_{\text{DFE},j}(\mathbf{a}(f)) = P_{s_j} \exp \left\{ \int_{-1/2}^{1/2} \ln (|H'_{\text{eq},j}(f)|^2 + \xi_j) \, df \right\} - \chi, \quad (5.27)$$

and

$$\text{SINR}_{\text{LE},j}(\mathbf{a}(f)) = P_{s_j} \left(\int_{-1/2}^{1/2} (|H'_{\text{eq},j}(f)|^2 + \xi_j)^{-1} \, df \right)^{-1} - \chi, \quad (5.28)$$

respectively, where

$$|H'_{\text{eq},j}(f)|^2 = \frac{\mathbf{a}^H(f)\mathbf{q}^*(f)\mathbf{q}^T(f)\mathbf{a}(f)}{\sigma_n^2\mathbf{a}^H(f)\mathbf{\Gamma}_j(f)\mathbf{a}(f) + \sigma_{v_j}^2}. \quad (5.29)$$

In (5.27) and (5.28), we have $\chi = 0$, $\xi_1 = \xi_2 = 0$ and $\chi = 1$, $\xi_1 = 1/\sigma_{s_2}^2$, $\xi_2 = 1/\sigma_{s_1}^2$ if the equalization filters are optimized based on a ZF and an MMSE criterion, respectively. Also, we define $P_{s_1} \triangleq \sigma_{s_2}^2$ and $P_{s_2} \triangleq \sigma_{s_1}^2$. Similarly, if only a single isolated symbol is transmitted, the SINR at the output of an MF is given by [5]

$$\text{SINR}_{\text{MF},j}(\mathbf{a}(f)) = P_{s_j} \int_{-1/2}^{1/2} |H'_{\text{eq},j}(f)|^2 df. \quad (5.30)$$

The MF SINR, $\text{SINR}_{\text{MF},j}(\mathbf{a}(f))$, constitutes an upper bound for the SINR achievable with any realizable receiver structure [5] and can be used to quantify the suboptimality of simple equalizers such as LE and DFE.

From (5.2), the total relay transmit power, $P_R(\mathbf{a}(f))$, is given by

$$P_R(\mathbf{a}(f)) = \sum_{i=1}^{N_R} \int_{-1/2}^{1/2} \Phi_{t_i}(f) df = \int_{-1/2}^{1/2} \mathbf{a}^H(f)\mathbf{D}(f)\mathbf{a}(f) df, \quad (5.31)$$

where $\Phi_{t_i}(f) \triangleq |A_i(f)|^2 (\sigma_{s_1}^2 |G_i(f)|^2 + \sigma_{s_2}^2 |H_i(f)|^2 + \sigma_n^2)$ is the power spectral density of the transmit signal $t_i[k]$ at the i th relay, and $\mathbf{D}(f) \triangleq \sigma_{s_1}^2 \text{diag}\{|G_1(f)|^2, \dots, |G_{N_R}(f)|^2\} + \sigma_{s_2}^2 \text{diag}\{|H_1(f)|^2, \dots, |H_{N_R}(f)|^2\} + \sigma_n^2 \mathbf{I}_{N_R}$.

Max-min Criterion Under Relay Power Constraint

In analogy to Section 5.3.1, we consider first the optimization of the FF-BF filters $\mathbf{a}(f)$ at the relays for maximization of the minimum transceiver SINR at the output of DFE/LE/MF receivers under a relay transmit power constraint. Formally, the resulting optimization

problem can be formulated as

$$\max_{\mathbf{a}(f)} \quad \min \{ \text{SINR}_{X,1}(\mathbf{a}(f)), \text{SINR}_{X,2}(\mathbf{a}(f)) \} \quad (5.32a)$$

$$\text{s.t.} \quad \int_{-1/2}^{1/2} \mathbf{a}^H(f) \mathbf{D}(f) \mathbf{a}(f) df \leq P, \quad (5.32b)$$

where $X = \text{DFE}$, $X = \text{LE}$, and $X = \text{MF}$ for DFE, LE, and an MF receiver, respectively. Unfortunately, problem (5.32) is very difficult to solve because of the structure of the SINR expressions in (5.27), (5.29), and (5.30) and the fact that $\mathbf{\Gamma}_1(f) \neq \mathbf{\Gamma}_2(f)$ in (5.29). Here, we provide a tight upper bound and tight achievable lower bound for the solution of (5.32).

The basic idea of the proposed bounds is to compute two beamformers where each one maximizes the SINR at one transceiver under the power constraint. In other words, we consider the problem

$$\max_{\mathbf{a}_j(f)} \quad \text{SINR}_{X,j}(\mathbf{a}_j(f)) \quad (5.33a)$$

$$\text{s.t.} \quad \int_{-1/2}^{1/2} \mathbf{a}_j^H(f) \mathbf{D}(f) \mathbf{a}_j(f) df \leq P, \quad (5.33b)$$

where $j \in \{1, 2\}$. Let $\mathbf{a}_j^{\text{opt}}(f)$ denote the optimum solution for problem (5.33). Since (5.33) is equivalent to the optimization of the FF-BF filters for two one-way relaying systems, we can draw from the results in Chapter 4 and [82]. In particular, $\mathbf{a}_j^{\text{opt}}(f)$, $j \in \{1, 2\}$, can be efficiently obtained with the algorithm summarized in Table 4.1. Based on these FF-BF filters we are able provide upper and lower bounds for the optimal solution of problem (5.32). In particular, the performance upper bound is given by

$$\text{SINR}_{\text{up}} \triangleq \min \{ \text{SINR}_{X,1}(\mathbf{a}_1^{\text{opt}}(f)), \text{SINR}_{X,2}(\mathbf{a}_2^{\text{opt}}(f)) \} \quad (5.34)$$

and the achievable lower bound is

$$\begin{aligned} \text{SINR}_{\text{low}} \triangleq & \max \left\{ \min \left\{ \text{SINR}_{\text{X},1}(\mathbf{a}_1^{\text{opt}}(f)), \text{SINR}_{\text{X},2}(\mathbf{a}_1^{\text{opt}}(f)) \right\}, \right. \\ & \left. \min \left\{ \text{SINR}_{\text{X},1}(\mathbf{a}_2^{\text{opt}}(f)), \text{SINR}_{\text{X},2}(\mathbf{a}_2^{\text{opt}}(f)) \right\} \right\}, \end{aligned} \quad (5.35)$$

where the (in general) suboptimal solution to problem (5.32) is given by the argument of the SINR on the right hand side of (5.35) after the max and min operations. If $\text{SINR}_{\text{X},1}(\mathbf{a}_1^{\text{opt}}(f)) \leq \text{SINR}_{\text{X},2}(\mathbf{a}_1^{\text{opt}}(f))$ or $\text{SINR}_{\text{X},2}(\mathbf{a}_2^{\text{opt}}(f)) \leq \text{SINR}_{\text{X},1}(\mathbf{a}_2^{\text{opt}}(f))$, which typically occurs if the relays are closer to one transceiver than the other, cf. Section 5.5, $\text{SINR}_{\text{up}} = \text{SINR}_{\text{low}}$ and the optimal solution for problem (5.32) is obtained. Otherwise, $\text{SINR}_{\text{up}} \neq \text{SINR}_{\text{low}}$ and the obtained solution is suboptimal. However, even in this case the gap between the upper and the lower bounds is typically only a fraction of a decibel. Thus, we have provided a close-to-optimal solution to problem (5.32). The small gap between both bounds can be explained by the fact that the only difference between the equivalent TC1-TC2 and TC2-TC1 channels is the noise correlation in (5.24), which has a minor impact on the design of the FF-BF filters.

Minimization of the Sum of MSEs

As an alternative FF-BF filter optimization criterion we consider the minimization of the sum of the MSEs (error variances) at the output of the equalizers at the two transceivers. This criterion allows for an exact solution for ZF-LE but not for the other considered equalization schemes. Thus, we concentrate on the ZF-LE case in the following. For ZF-LE, the MSE at the output of the equalizer at TC j is given by

$$\sigma_{\text{LE},j}^2(\mathbf{a}(f)) = \int_{-1/2}^{1/2} |H'_{\text{eq},j}(f)|^{-2} df. \quad (5.36)$$

i.e., $\text{SINR}_{\text{LE},j}(\mathbf{a}(f)) = P_{s_j}/\sigma_{\text{LE},j}^2(\mathbf{a}(f))$. The considered optimization problem can be expressed as

$$\min_{\mathbf{a}(f)} \mathcal{J}_{\text{LE}}(\mathbf{a}(f)) = \sum_{j=1}^2 \sigma_{\text{LE},j}^2(\mathbf{a}(f)) \quad (5.37a)$$

$$\text{s.t.} \quad \int_{-1/2}^{1/2} \mathbf{a}^H(f) \mathbf{D}(f) \mathbf{a}(f) df \leq P. \quad (5.37b)$$

Exploiting (5.29) the objective function (5.37a) can be expressed as

$$\mathcal{J}_{\text{LE}}(\mathbf{a}(f)) = \int_{-1/2}^{1/2} \frac{\sigma_n^2 \mathbf{a}^H(f) (\mathbf{\Gamma}_1(f) + \mathbf{\Gamma}_2(f)) \mathbf{a}(f) + \sigma_{v_1}^2 + \sigma_{v_2}^2}{\mathbf{a}^H(f) \mathbf{q}^*(f) \mathbf{q}^T(f) \mathbf{a}(f)} df. \quad (5.38)$$

Next, we introduce matrix $\mathbf{\Gamma}(f) \triangleq \frac{\sigma_n^2}{\sigma_{v_1}^2 + \sigma_{v_2}^2} (\mathbf{\Gamma}_1(f) + \mathbf{\Gamma}_2(f))$ and restate problem (5.37) in equivalent form as

$$\max_{\mathbf{a}(f)} \left(\int_{-1/2}^{1/2} \left(\frac{\mathbf{a}^H(f) \mathbf{q}^*(f) \mathbf{q}^T(f) \mathbf{a}(f)}{\mathbf{a}^H(f) \mathbf{\Gamma}(f) \mathbf{a}(f) + 1} \right)^{-1} df \right)^{-1} \quad (5.39a)$$

$$\text{s.t.} \quad \int_{-1/2}^{1/2} \mathbf{a}^H(f) \mathbf{D}(f) \mathbf{a}(f) df \leq P. \quad (5.39b)$$

Since $\mathbf{\Gamma}(f)$ is a diagonal matrix, problem (5.37) is of the same form as the ZF-LE SINR maximization problem for one-way relaying considered in Chapter 4 and [82]. Thus, the exact solution to (5.37) can be computed with the algorithm provided in Table 4.1.

5.4.2 FIR FF-BF Filter Optimization

Since the IIR FF-BF filters would require an infinite amount of feedback, they are mostly useful to establish performance bounds for practical FIR FF-BF filters. We emphasize that although FIR FF-BF filters are considered in this section, the equalizers at the transceivers are still assumed to employ IIR filters.

Assuming FIR FF-BF filters of length L_a at the relays the length of the equivalent CIR $h_{\text{eq}}[k]$ is given by $L_{\text{eq}} = L_a + L_g + L_h - 2$ and its Fourier transform can be expressed as

$$H_{\text{eq}}(f) = \mathbf{d}^H(f) \mathbf{Q} \mathbf{a} \quad (5.40)$$

with $\mathbf{d}(f) \triangleq [1 \ e^{j2\pi f} \ \dots \ e^{j2\pi f(L_{\text{eq}}-1)}]^T$, FIR FF-BF coefficient vector $\mathbf{a} \triangleq [a_1[0] \ a_1[1] \ \dots \ a_1[L_a - 1] \ a_2[0] \ \dots \ a_{N_R}[L_a - 1]]^T$, and $L_{\text{eq}} \times N_R L_a$ matrix $\mathbf{Q} \triangleq [\mathbf{Q}_1 \ \dots \ \mathbf{Q}_{N_R}]$, where \mathbf{Q}_i is an $L_{\text{eq}} \times L_a$ column-circulant matrix with vector $[(\tilde{\mathbf{H}}_i \tilde{\mathbf{g}}_i)^T \ \mathbf{0}_{L_a-1}^T]^T$ in the first column. Here, $\tilde{\mathbf{H}}_i$ is an $(L_h + L_g - 1) \times L_g$ column-circulant matrix with vector $[h_i[0] \ \dots \ h_i[L_h - 1] \ \mathbf{0}_{L_g-1}^T]^T$ in the first column and $\tilde{\mathbf{g}}_i \triangleq [g_i[0] \ \dots \ g_i[L_g - 1]]^T$.

We apply again noise whitening which transforms $H_{\text{eq}}(f)$ into the equivalent frequency responses of TC1 and TC2:

$$H'_{\text{eq},j}(f) = \mathbf{d}^H(f) \mathbf{Q} \mathbf{a} \left(\sigma_n^2 \mathbf{a}^H \tilde{\mathbf{\Gamma}}_j(f) \mathbf{a} + \sigma_{v_j}^2 \right)^{-1/2}, \quad j \in \{1, 2\}, \quad (5.41)$$

with $L_a N_R \times L_a N_R$ block diagonal matrices $\tilde{\mathbf{\Gamma}}_j(f) \triangleq \text{diag} \left\{ \tilde{\mathbf{\Gamma}}_{j,1}(f), \dots, \tilde{\mathbf{\Gamma}}_{j,N_R}(f) \right\}$, $j \in \{1, 2\}$, where $\tilde{\mathbf{\Gamma}}_{1,i}(f) \triangleq \tilde{\mathbf{G}}_i^H \tilde{\mathbf{d}}(f) \tilde{\mathbf{d}}^H(f) \tilde{\mathbf{G}}_i$ and $\tilde{\mathbf{\Gamma}}_{2,i}(f) \triangleq \tilde{\mathbf{H}}_i^H \tilde{\mathbf{d}}(f) \tilde{\mathbf{d}}^H(f) \tilde{\mathbf{H}}_i$ are $L_a \times L_a$ matrices of rank 1. Here, $\tilde{\mathbf{G}}_i$ and $\tilde{\mathbf{H}}_i$ are $(L_g + L_a - 1) \times L_a$ and $(L_h + L_a - 1) \times L_a$ column-circulant matrices with vectors $[g_i[0] \ \dots \ g_i[L_g - 1] \ \mathbf{0}_{L_a-1}^T]^T$ and $[h_i[0] \ \dots \ h_i[L_h - 1] \ \mathbf{0}_{L_a-1}^T]^T$ in the first columns, respectively, and $\tilde{\mathbf{d}}(f) \triangleq [1 \ e^{j2\pi f} \ \dots \ e^{j2\pi f(L_h + L_a - 2)}]^T$. The noise power spectral density at the output of the noise whitening filter is again equal to one.

In the following, we will discuss the optimization of the FF-BF coefficient vector \mathbf{a} for the two criteria considered in Section 5.4.1.

Max-min criterion under relay power constraint: Similar to the IIR case, an exact solution of the max-min FIR FF-BF filter optimization problem does not seem possible. Instead, we use the same approach as in Section 5.4.1 and compute the FIR filters for two one-way relaying setups having equivalent channel frequency responses $H'_{\text{eq},1}(f)$ and $H'_{\text{eq},2}(f)$, respectively.

Comparing the equivalent frequency response in (5.41) with the corresponding frequency response for the one-way relaying case in (4.64) or [82, Eq. (38)], we conclude that optimal FIR FF-BF coefficient vectors $\mathbf{a}_1^{\text{opt}}$ and $\mathbf{a}_2^{\text{opt}}$ required for evaluation of the upper and lower bounds in (5.34) and (5.35) can be computed with the algorithm given in Table 4.2. Thus, a close-to-optimal solution for max-min optimization of the FIR FF-BF filters for the two-way relaying is available.

Minimization of the sum of MSEs: For FIR BF-FF with ZF-LE receivers, the sum MSE can be written as

$$\mathcal{J}_{\text{LE}}(\mathbf{a}) = (\sigma_{v_1}^2 + \sigma_{v_2}^2) \int_{-1/2}^{1/2} \left(\frac{\mathbf{a}^H \mathbf{Q}^H \mathbf{d}(f) \mathbf{d}^H(f) \mathbf{Q} \mathbf{a}}{\mathbf{a}^H \tilde{\mathbf{\Gamma}}(f) \mathbf{a} + 1} \right)^{-1} df, \quad (5.42)$$

where $\tilde{\mathbf{\Gamma}} \triangleq \frac{\sigma_n^2}{\sigma_{v_1}^2 + \sigma_{v_2}^2} (\tilde{\mathbf{\Gamma}}_1(f) + \tilde{\mathbf{\Gamma}}_2(f))$. Now, the FIR FF-BF filter optimization problem can be written as

$$\max_{\mathbf{a}} \quad 1/\mathcal{J}_{\text{LE}}(\mathbf{a}) \quad (5.43a)$$

$$\text{s.t.} \quad \mathbf{a}^H \mathbf{D} \mathbf{a} \leq P, \quad (5.43b)$$

where \mathbf{D} is defined after (5.16). Problem (5.43) is of the same form as the FIR FF-BF

filter optimization problem for one-way relaying with ZF-LE at the receiver. Thus, we can again use the algorithm given in Table 4.2 to find the optimal vector \mathbf{a}_{opt} .

5.5 Simulations

In this section, we present simulation results for the SINR and the BER of a cooperative two-way relay network with FF-BF. Throughout this section we assume $\sigma_n^2 = \sigma_{v_1}^2 = \sigma_{v_2}^2 = 1$ and $P = 1$. This allows us to decompose the CIRs as $g_i[k] = \sqrt{\gamma_g} \bar{g}_i[k]$ and $h_i[k] = \sqrt{\gamma_h} \bar{h}_i[k]$, where γ_g and γ_h denote the transmitter SNRs of the TC1-relay and TC2-relay links, respectively. The normalized CIRs $\bar{h}_i[k]$ and $\bar{g}_i[k]$ include the effects of multipath fading and path-loss. All IIR and FIR FF-BF filters were obtained using the methods developed in Sections 5.3 and 5.4, respectively. In this section, unless stated otherwise, we consider the cooperative relay network shown in Fig. 5.2 with $N_R = 5$ relays at locations (a)–(e). The normalized distance between the two transceivers is equal to 2 and the normalized horizontal distance between TC1 and the relays is d . A path-loss exponent of 3 with reference distance $d_{\text{ref}} = 1$ is assumed. The CIR coefficients of all links are modeled as independent quasi-static Rayleigh fading with $L_g = L_h = 5$ and following an exponential power delay profile $p[k] = \frac{1}{\sigma_t} \sum_{l=0}^{L_x-1} e^{-k/\sigma_t} \delta[k-l]$, where $L_x \in \{L_g, L_h\}$ and σ_t characterizes the delay spread [85].

5.5.1 Relay Power Minimization for FF-BF without Equalization

Fig. 5.3 shows the total relay transmit power, $P_R(\mathbf{a})$, vs. the minimum required SINR γ_1 and γ_2 at the transceivers for $\gamma_1 = \gamma_2$. We adopted $\sigma_t = 2$, $d = 1$, $N_R = 5$, and $\gamma_g = \gamma_h = 10$ dB. Similar to [50], we have only included simulation points which guarantee feasibility of the optimization problem for more than 50 % of the channels. The total relay transmit power is computed by averaging over the feasible runs. The probability that the problem

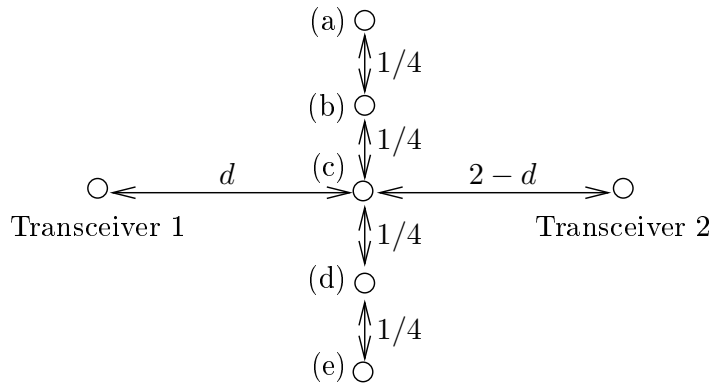


Figure 5.2: Locations of TC1, TC2, and the relays in the simulations.

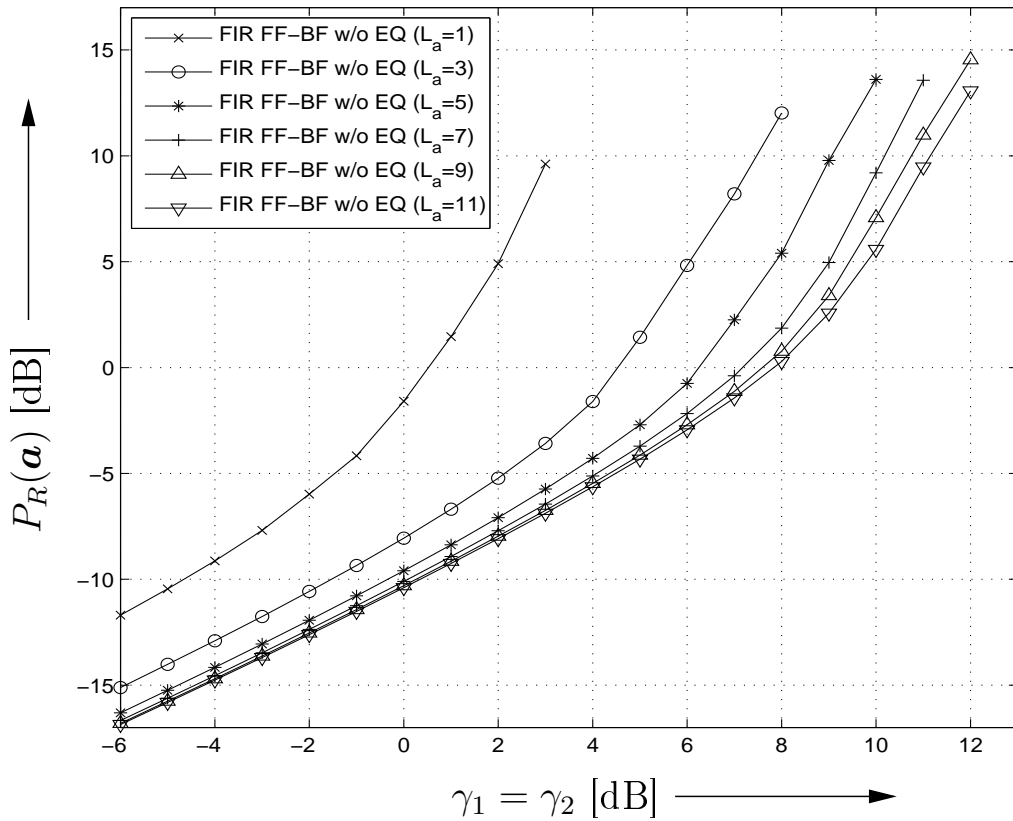


Figure 5.3: Total average relay transmit power vs. required SINRs γ_1 and γ_2 for FIR FF-BF without equalization at the transceivers. The FF-BF filters were optimized for minimization of the relay transmit power. Exponentially decaying power delay profile with $\sigma_t = 2$, $L_g = L_h = 5$, $d = 1$, $N_R = 5$, and $\gamma_g = \gamma_h = 10$ dB.

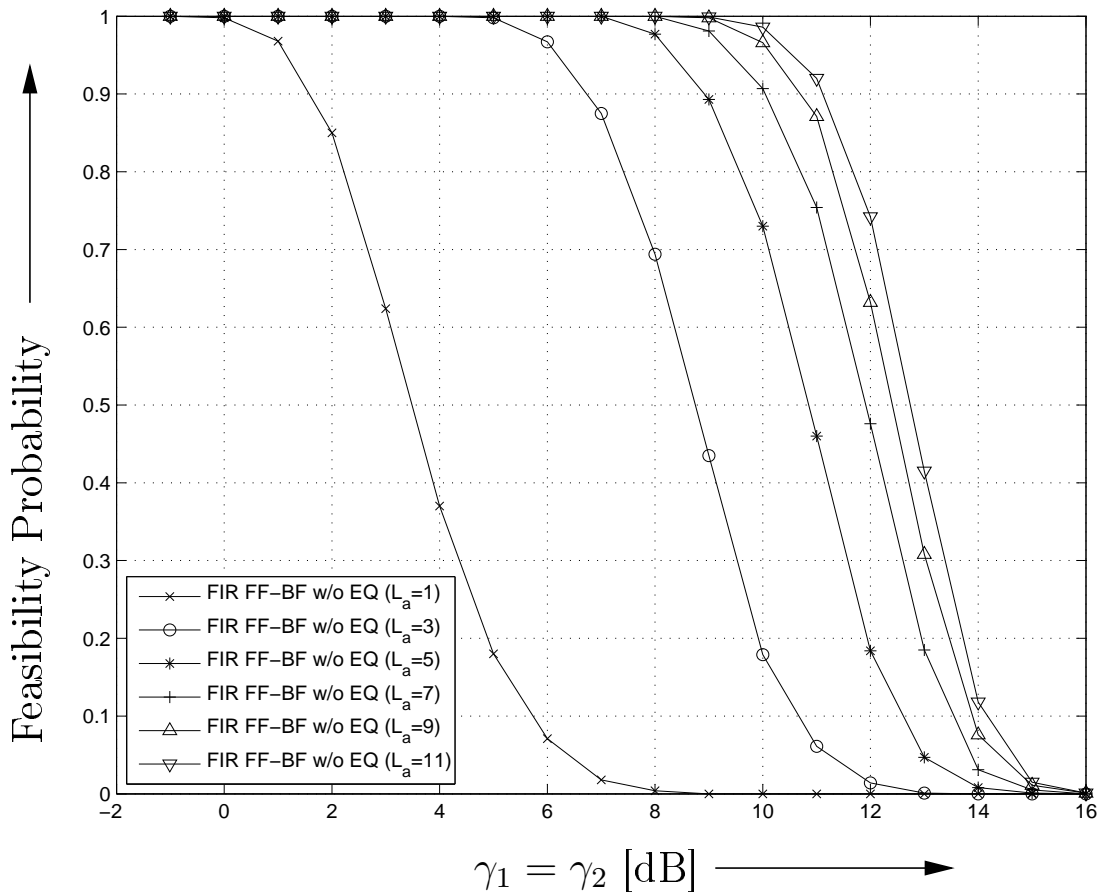


Figure 5.4: Feasibility probability vs. required SINRs γ_1 and γ_2 for FIR FF-BF without equalization at the transceivers. The FF-BF filters were optimized for minimization of the relay transmit power. Exponentially decaying power delay profile with $\sigma_t = 2$, $L_g = L_h = 5$, $d = 1$, $N_R = 5$, and $\gamma_g = \gamma_h = 10$ dB.

is feasible is shown in Fig. 5.4. From Figs. 5.3 and 5.4, we observe that increasing L_a substantially reduces the total required relay transmit power and increases the probability that the problem is feasible especially for higher SINR requirements.

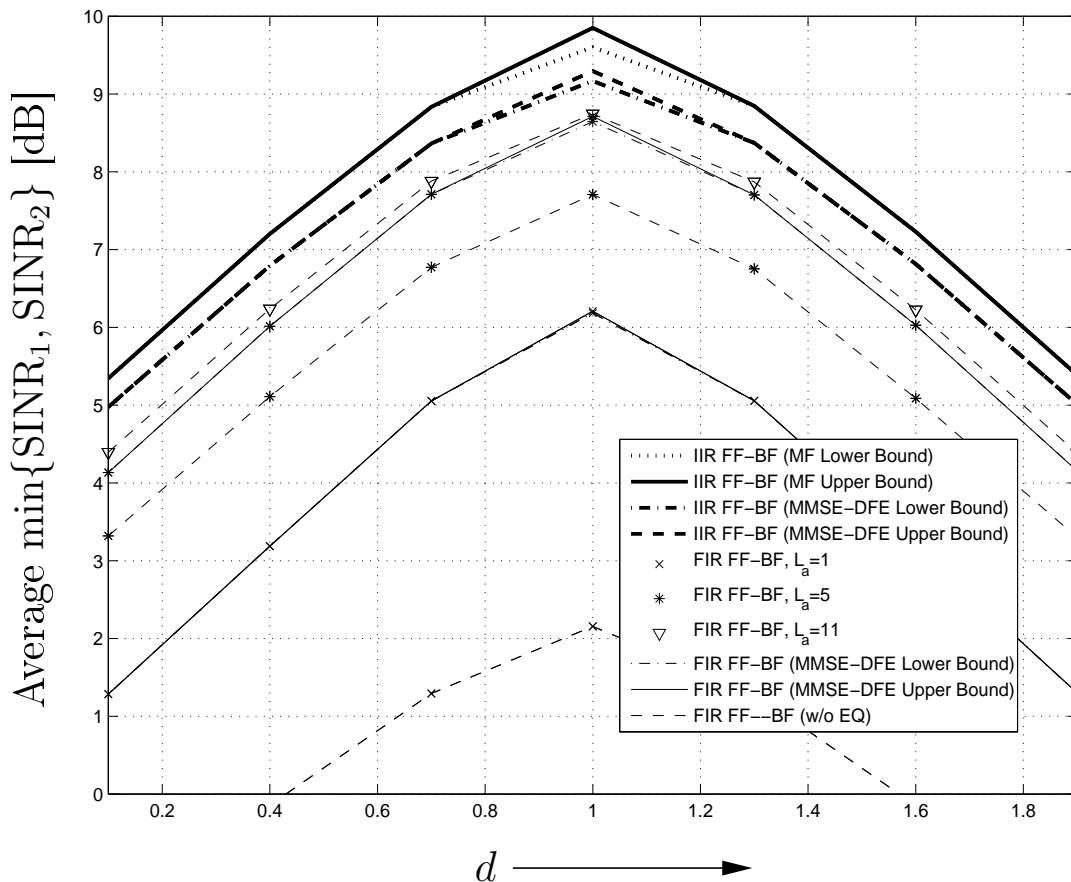


Figure 5.5: Average worst-case SINR at the transceivers vs. distance d for FF-BF with/without equalization at the transceivers. The FF-BF filters were optimized for maximization of the minimum transceiver SINR. Exponentially decaying channel power delay profile with $\sigma_t = 2$, $L_g = L_h = 5$, $d = 1$, $N_R = 5$, and $\gamma_g = \gamma_h = 10$ dB.

5.5.2 Max-min SINR Optimization for FF-BF with and without Equalization

In Figs. 5.5 and 5.6, we show the average SINR at the transceivers vs. distance d for various FF-BF filter designs at the relays and various transceiver structures. We adopted $\sigma_t = 2$, $N_R = 5$, and $\gamma_g = \gamma_h = 10$ dB. The FF-BF filters were optimized for maximization of the minimum transceiver SINR.

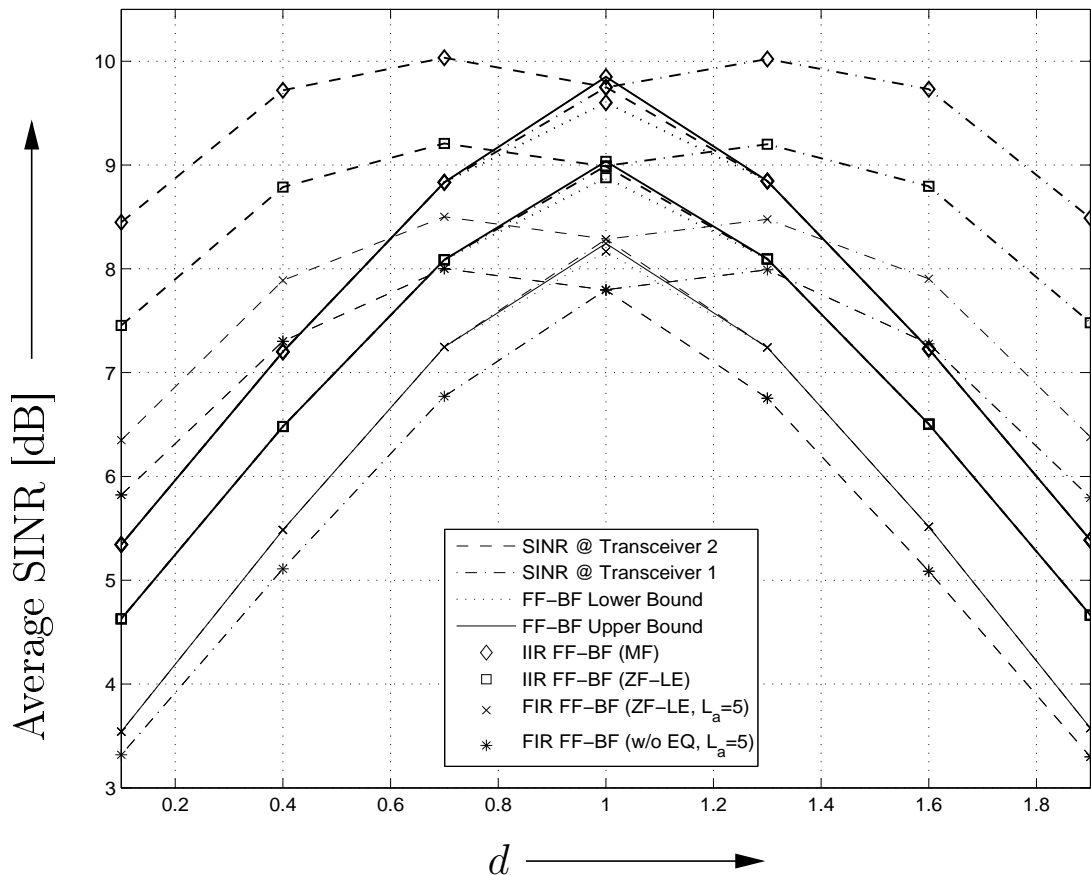


Figure 5.6: Average SINR at transceivers vs. distance d for FF-BF with/without equalization (EQ) at the transceivers. The FF-BF filters were optimized for maximization of the minimum transceiver SINR. Exponentially decaying channel power delay profile with $\sigma_t = 2$, $L_g = L_h = 5$, $d = 1$, $N_R = 5$, and $\gamma_g = \gamma_h = 10$ dB.

In Fig. 5.5, we show the minimum transceiver SINR and observe that the performance gap between the upper and lower bounds for FF-BF with equalization is very small for both IIR and FIR FF-BF filters. The performance gap is largest for $d = 1$ and IIR filters. However, even in this case the gap is less than 0.3 dB suggesting that the filters obtained from the achievable lower bound are close-to-optimal. Furthermore, Fig. 5.5 shows that transceivers employing MMSE-DFE closely approach the performance of idealized MF receivers if IIR FF-BF filters are adopted implying that little can be gained by employing

more complex trellis-based receivers compared to MMSE-DFE. Also, as the length of the FIR FF-BF filters increases, FIR FF-BF approaches the performance of IIR FF-BF. For $L_a = 5$ and MMSE-DFE receivers, the gap between both schemes is less than 0.6 dB over considered range of distances d . Interestingly, while for short FIR FF-BF filters equalization at the transceivers results in large performance gains, FIR FF-BF without equalization with $L_a = 11$ achieves practically the same performance as FIR FF-BF with MMSE-DFE with $L_a = 5$. We note that FF-BF with MMSE-DFE with $L_a = 11$ slightly outperforms FIR FF-BF without equalization with $L_a = 11$ but the corresponding curve is not shown in Fig. 5.5 for clarity.

Fig. 5.6 shows the average SINRs at both transceivers with and without equalization and also the performance upper and lower bounds for the case of equalization. Note that since we show average SINRs, for a given d , the minimum transceiver SINR in Fig. 5.6 does not necessarily coincide with the (average) performance lower bound. For example, at $d = 1$, the probability that TC1 or TC2 contributes to the minimum SINR is half and half. As expected, TC2 enjoys a higher SINR than TC1 when the relays are close to TC1, and vice versa. We also note that even simple ZF-LE at the transceivers can approach the performance of an idealized MF receiver up to less than one decibel.

5.5.3 Max-min SINR vs. Minimum Sum MSE Optimization for FF-BF with ZF-LE

In Fig. 5.7, we compare the average SINRs at both transceivers for ZF-LE at the transceivers with max-min and minimum sum MSE FF-BF optimization. We adopted $\sigma_t = 2$, $N_R = 5$, and $\gamma_g = \gamma_h = 10$ dB. For the max-min criterion, Fig. 5.7 shows the SINRs obtained from the achievable lower bound. As can be observed, both criteria achieve very similar SINRs at both transceivers for both IIR and FIR equalizers. Since the minimum sum MSE opti-

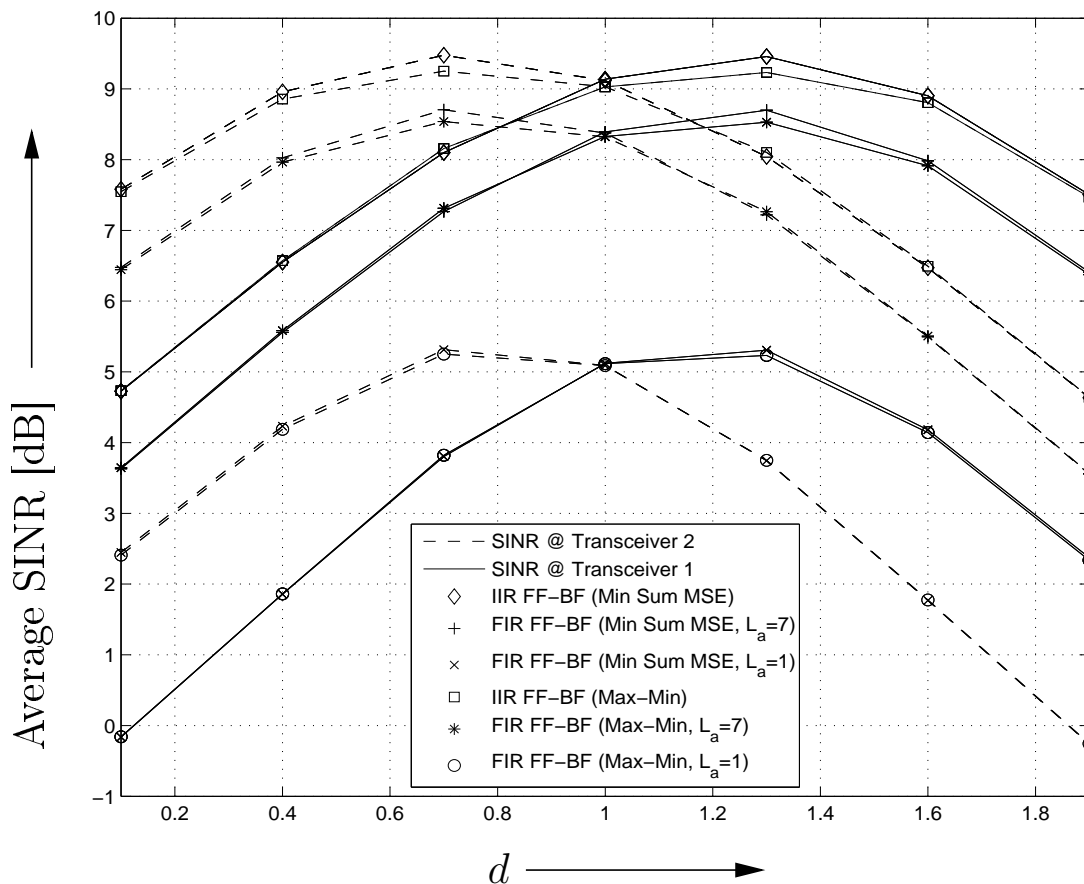


Figure 5.7: Average SINR at transceivers vs. distance d for FF-BF with ZF-LE at the transceivers. Exponentially decaying channel power delay profile with $\sigma_t = 2$, $L_g = L_h = 5$, $d = 1$, $N_R = 5$, and $\gamma_g = \gamma_h = 10$ dB.

mization requires only the computation of one FF-BF filter, its complexity is roughly half of that of the max-min optimization. Thus, in practice, the minimum sum MSE criterion may be preferable if ZF-LE is employed at the transceivers.

5.5.4 Impact of Number of Relays N_R

In Fig. 5.8, we investigate the impact of the number of relays N_R on the performance of various FF-BF and equalizer designs for $\sigma_t = 2$, $d = 1$, and $\gamma_g = \gamma_h = 10$ dB. We assume

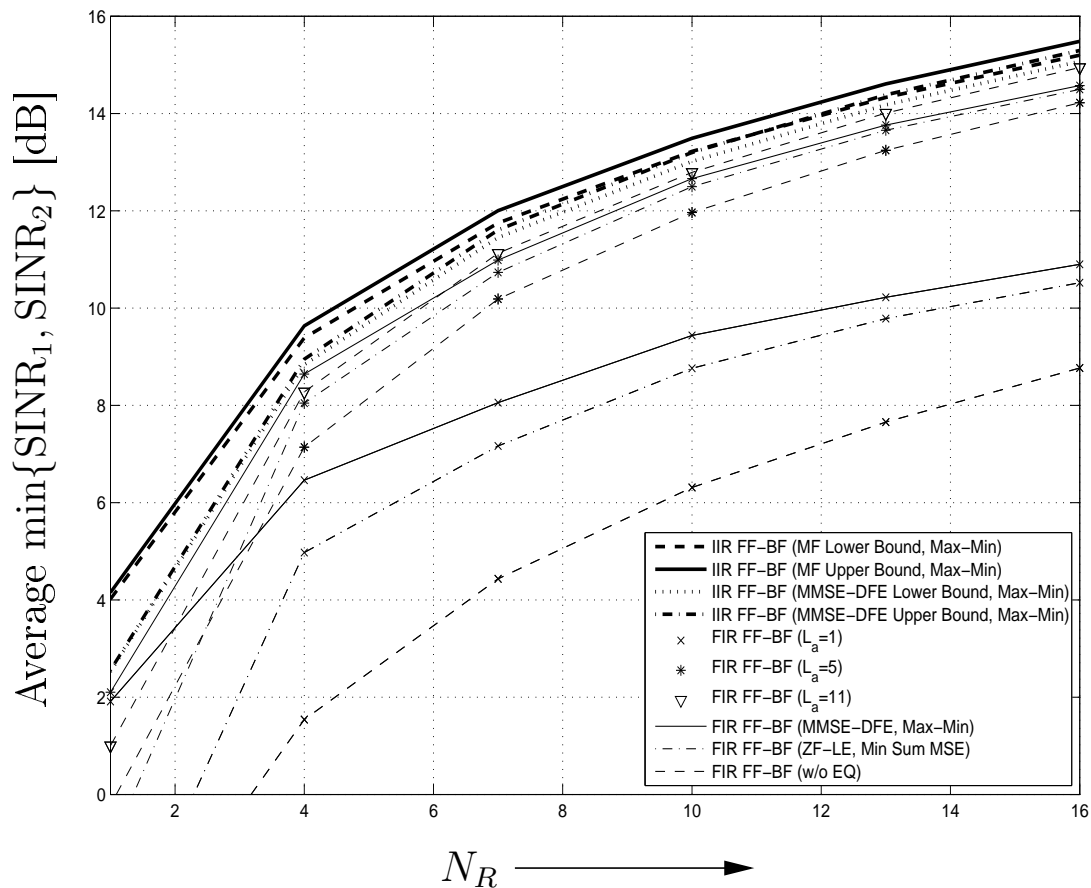


Figure 5.8: Average SINR vs. number of relays N_R for FF-BF with MMSE-DFE, ZF-LE, MF, and slicer (no equalizer) receivers at the transceivers. Exponentially decaying power delay profile with $\sigma_t = 2$, $L_g = L_h = 5$, $d = 1$, and $\gamma_g = \gamma_h = 10$ dB.

all the relays are located at location (c) of Fig. 5.2. We show results for MMSE-DFE, MF, and slicer (no equalizer) receivers with the FF-BF filters optimized for maximization of the minimum transceiver SINR. For MMSE-DFE and MF receivers with IIR FF-BF filter the performance upper and lower bounds introduced in Section 5.4.1 are shown. For the FIR case only the achievable lower bound is shown for clarity. In addition, we show the average SINR for ZF-LE with FF-BF filters optimized under the sum MSE criterion. We observe from Fig. 5.8 that for all values of N_R the gap between the upper and lower bound

for max-min FF-BF filter optimization with equalization is very small. As N_R increases the gap between the simple slicer receiver and the MMSE-DFE receiver diminishes. In fact, the slicer receiver with FIR FF-BF filters of length $L_a = 11$ closely approaches the performance of MMSE-DFE with IIR FF-BF filter and FIR FF-BF filters of length $L_a = 11$ (which is not shown for clarity), but outperforms MMSE-DFE with FIR FF-BF filters of length $L_a = 5$.

5.5.5 BER Performance for Fading Channels

Figs. 5.9 and 5.10 show BERs of BPSK modulation vs. transmit SNR, $\gamma = \gamma_g = \gamma_h$, for FIR and IIR FF-BF filters. The BERs for FIR FF-BF filters were simulated by implementing ZF-LE and MMSE-DFE receivers with FIR equalization filters of lengths $4 \times L_{\text{eq}}$, which caused negligible performance degradation compared to IIR equalization filters. The BERs for IIR FF-BF were obtained by approximating the BER of BPSK transmission by $\text{BER}_X = Q(\sqrt{2\text{SINR}_X})$, where $X = \text{DFE}$, $X = \text{LE}$, and $X = \text{MF}$ for DFE, LE, and MF receivers at the transceivers, respectively. The BERs for FIR FF-BF with equalization and max-min criterion were generated by using the FF-BF filters from the achievable lower bound. Here, the BER is averaged over 100,000 channel realizations. We consider a network with $\sigma_t = 2$, $N_R = 5$, and $d = 1$.

Fig. 5.9 shows that MMSE-DFE with IIR FF-BF at the relays closely approaches the performance of a MF receiver with IIR-BF. Furthermore, FIR FF-BF filters of moderate length ($L_a = 5$) approach the performance of IIR FF-BF filters up to less than one decibel if MMSE-DFE is employed at the transceivers. The same performance can also be achieved without equalization at the transceivers but with longer FF-BF filters ($L_a = 11$). At $\text{BER} = 10^{-5}$, slicer (no equalizer) receivers with $L_a = 11$ achieve only 0.4 dB performance lost comparing with the performance of the MMSE-DFE receivers with FIR FF-BF and

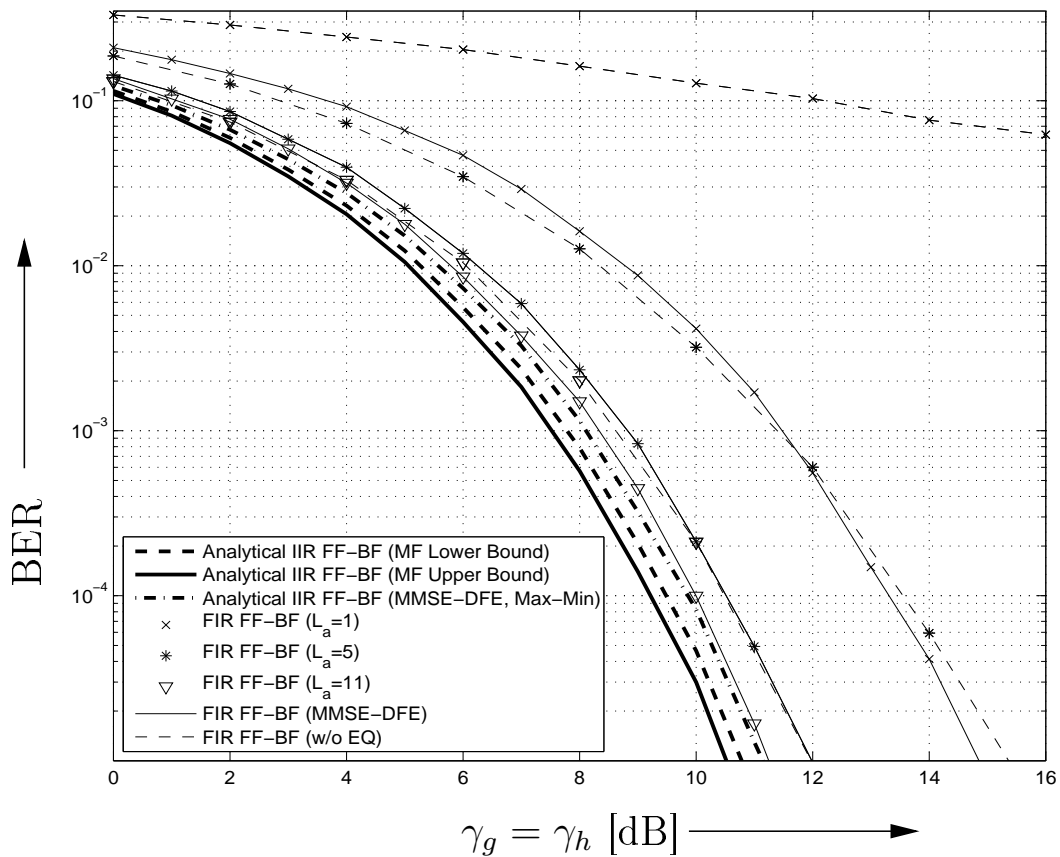


Figure 5.9: Average BER of BPSK vs. transmit SINR γ for FF-BF with MMSE-DFE, MF, and slicer receiver at the transceivers. BERs for FIR FF-BF with EQ and IIR FF-BF with MMSE-DFE were generated using the FF-BF filters from the achievable lower bound of the max-min criterion. Exponentially decaying power delay profile with $\sigma_t = 2$, $L_g = L_h = 5$, $N_R = 5$, and $d = 1$.

$L_a = 11$.

Fig. 5.10 reveals that for ZF-LE at the transceivers, FF-BF filters according to the max-min and sum MSE criteria achieve a similar BER performance. Furthermore, the performance gap between the MF receiver and the simple ZF-LE receiver with IIR FF-BF filters is less than one decibel which suggests again that simple LE and DFE equalizers are sufficient to achieve a close-to-optimal performance.

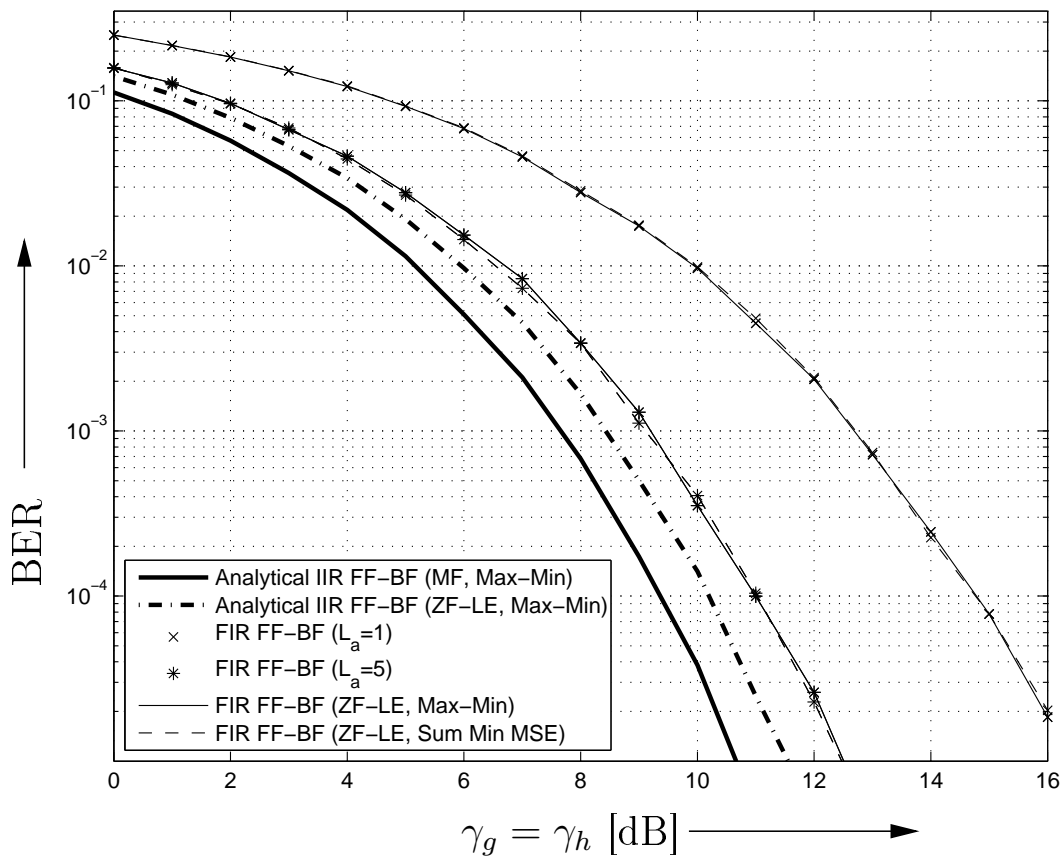


Figure 5.10: Average BER of BPSK vs. transmit SINR γ for FF-BF with ZF-LE and MF receiver at the transceivers. For the min-max criterion, BERs were generated using the FF-BF filters from the achievable lower bound. Exponentially decaying power delay profile with $\sigma_t = 2$, $L_g = L_h = 5$, $N_R = 5$, and $d = 1$.

5.6 Conclusions

In this chapter, we have investigated FF-BF for two-way relaying networks employing single-carrier transmission over frequency-selective channels. For the processing at the transceivers, we considered two different cases: (1) a simple slicer without equalization and (2) LE or DFE. For the first case, we optimized FIR FF-BF filters at the relays for maximization of the minimum transceiver SINR subject to a relay power constraint and for minimization of the total relay transmit power subject to two QoS constraints.

Both problems can be transformed into convex SOCP problems, which can be efficiently solved with standard numerical methods. For the second case, we optimized FIR and IIR FF-BF filters for maximization of the minimum transceiver SINR and, in case of ZF-LE, also for minimization of the sum MSE at the equalizer outputs of both transceivers. For the max-min criterion, we established an upper and an achievable lower bound for the original problem. Both optimization problems were solved by transforming them into one-way relay problems and leveraging corresponding results from Chapter 4. From our simulation results, we can draw the following conclusions: for max-min optimization with equalization, the gap between the upper bound and the achievable lower bound is very small rendering the obtained solution close-to-optimal; and for ZF-LE the max-min and the minimum sum MSE criteria lead to as similar performance.

Thus, the two proposed architectures allow us to trade relay complexity and transceiver complexity. For networks with powerful relays and low-complexity transceivers, long FF-BF filters and a simple slicer may be implemented at the relays and the transceivers, respectively. In contrast, for networks with powerful transceivers and simple relays, it is preferable to implement short FF-BF filters and equalizers at the relay and the transceivers, respectively.

Chapter 6

Summary of Thesis and Future Research Topics

In this final chapter, we summarize our results and highlight the contributions of this thesis in Section 6.1. In Section 6.2, we also propose ideas for future related research.

6.1 Summary of Results

This thesis as a whole has focused on beamforming design for next generation wireless communication systems, namely: (1) a novel TD transmit beamforming scheme for MIMO-OFDM systems; (2) cooperative AF-BF schemes with multiple multi-antenna relays and multi-antenna source; (3) one-way cooperative FF-BF schemes for frequency-selective channels with multiple multi-antenna relays; (4) two-way cooperative FF-BF schemes for frequency-selective channels with multiple single-antenna relays. In the following, we briefly review the main results of each chapter.

In Chapter 2, we have proposed a novel TD approach to BF in MIMO-OFDM systems. The C-BFFs have been optimized for maximization of the AMI and minimization of the BER, respectively, and efficient algorithms for recursive calculation of the optimum C-BFFs have been provided for both criteria. For the case of a finite-rate feedback channel a GVQ algorithm has been introduced for codebook design. Simulation results for the IEEE 802.11n Channel Model B have confirmed the excellent performance of TD-BF and have

shown that TD-BF achieves a more favorable performance/feedback rate trade-off than traditional FD-BF.

In Chapter 3, we have considered AF-BF for cooperative networks with one multi-antenna source, multiple multi-antenna relays, and one single-antenna destination for three different power constraints. In particular, we have considered the cases of individual relay power constraints, a joint power constraint for all relays, and a joint source-relay power constraint. For a given BF vector at the source, we have fully characterized the optimal AF-BF matrices for all three constraints. Furthermore, optimal and sub-optimal methods for optimization of the source BF vectors have been provided. Simulation results show that increasing the number of antennas at the source is particularly beneficial if the relays are located far away from the source. In contrast, increasing the number of antennas at the relays or the number of relays is always beneficial regardless of the location of the relays.

In Chapter 4, we investigated FF-BF for one-way relay networks with multiple multi-antenna relays and single-carrier transmission over frequency-selective channels. The FF-BF matrix filters at the relays were optimized for the cases where (1) a simple slicer without equalization and (2) LE/DFE were employed at the destination. For the first case, we obtained closed-form solutions and efficient numerical methods for computation of the optimal FIR FF-BF matrix filters. For the second case, we obtained an elegant method for calculation of the optimal IIR FF-BF matrix filters and an efficient numerical algorithm for calculation of near-optimal FIR FF-BF matrix filters.

In Chapter 5, we have investigated FF-BF for two-way relay networks employing single-carrier transmission over frequency-selective channels. Multiple single antenna relays are assumed in the network. For the processing at the transceivers, we again considered two different cases: (1) a simple slicer without equalization and (2) LE or DFE. For the

first case, we optimized FIR FF–BF filters at the relays for maximization of the minimum transceiver SINR subject to a relay power constraint and for minimization of the total relay transmit power subject to two QoS constraints. Both problems can be transformed into convex SOCP problems, which can be efficiently solved with standard numerical methods. For the second case, we optimized FIR and IIR FF–BF filters for maximization of the minimum transceiver SINR and, in case of ZF–LE, also for minimization of the sum MSE at the equalizer outputs of both transceivers. For the max–min criterion, we established an upper and an achievable lower bound for the original problem. Both optimization problems were solved by transforming them into one–way relay problems and leveraging corresponding results from Chapter 4.

6.2 Future Work

Future wireless communication networks will have to strive for higher data rates and more reliable communication, and at the same time, cope with a tremendous growth in the number of users. This brings about several technical problems such as a higher interference level as well as a major decrease in available bandwidth per user. The above issues have raised serious concerns on whether existing network topologies are able to cope with the challenges introduced by future applications. In Chapters 3–5, we have considered beamforming for cooperative networks, and proposed several innovative beamforming schemes for such networks. However, cooperative communication system design is a vast research area and many problems are still unsolved.

Cooperative communications may also be combined with the cognitive radio concept [91]. Since the wireless spectrum is a scarce and costly resource, the difficulty in obtaining spectrum allocations is becoming a hindrance to innovation. This problem has prompted regulatory bodies to allow unlicensed terminals, known as cognitive radios, to use previ-

ously allocated spectrum if they can avoid causing interference to the incumbent licensees. The combination of cognitive radios and cooperative communications has the potential to revolutionize the wireless industry. In the following, we propose some ideas for further research that are similar to or can be based on the results of this thesis.

6.2.1 Two-way Relaying with Multiple Multi-antenna Relays

One immediate extension of the current work is on beamforming schemes for two-way MABC relaying with multiple multi-antenna relays. As a matter of fact, we have already made preliminary but encouraging progress on such topic. In [92], we assume single-carrier transmission and frequency-selective channels. The relays are equipped with FF-BF *matrix* filters in contrast with FF-BF filters in Chapter 5. As shown in Chapter 5, the performance of a simple slicer with optimized decision delay can closely approach the performance of transceivers with equalizers. Therefore, we assume that a simple slicer is employed at each of the transceivers in [92]. We optimize the FF-BF matrix filters at the relays for (1) a SINR balancing objective under a relay transmit power constraint, i.e. maximization of the worst transceiver SINR, and (2) minimization of the total relay transmit power subject to two QoS constraints to guarantee a certain level of performance. We show that the optimization problems are difficult to solve in general. However, by relaxing the rank constraints, we convert the optimization problems to semidefinite programming (SDP) problems, which provide certified numerical upper bounds for the original problems. Subsequently, we show that the original problems can be approximated as convex SOCP problems by strengthening the constraints. It is noteworthy that the SOCP approximation method does not impose any rank relaxations. Simulations reveal that the close-to-optimal SOCP approximation method provides practically the same performance as the SDP rank relaxation method. In future work, we can leverage the finding for slicer transceiver in [92]

and conduct research on transceivers equipped with equalizers.

6.2.2 Cooperative Communications for Multi-user Systems

Next generation mobile communication systems have to be able to provide reliable communications for a large number of users within a cell and on cell edges. Multi-user MIMO schemes can provide a substantial gain in network downlink throughput by allowing multiple users to communicate in the same frequency (or OFDM subcarrier) and time slots [93]. The combination of multi-user MIMO-OFDM beamforming and relaying is a promising technique for performance enhancement for next generation wireless communications. Although some preliminary research has been already conducted on MIMO-OFDM relaying system [94, 95] and multi-user MIMO relaying systems [96], there are still many interesting open problems such as resource allocation and protocol design. Since different users interfere with each other in a multi-user MIMO relaying systems, maximizing the performance of a particular user may degrade the performance of the other users. To deal with this problem in a systematic way, a constraint optimization framework for the design of multi-user cooperative beamforming communications should be developed. This will optimally allocate system resources (time, frequency, and beamforming direction) to all the users, permit the maximization of the performance of certain (preferred) users while guaranteeing a certain minimum performance for other (secondary) users. For example, preferred users may be those who have an ongoing call, whereas secondary users are those who are just in the process of establishing a connection.

6.2.3 Synchronization for Cooperative Communications

Perfect timing is assumed in most of the literature, e.g. [28]–[31], for analyzing the performance of cooperative communications. However, in practices, perfect timing is an unrealis-

tic assumption due to the distributed nature of the cooperative networks. Therefore, time synchronization is a critical issue for any cooperative network. Since cooperative network usually consists of two transmission phases, it is difficult to provide a precise clock reference for all the signal coming from distributed users with different perspectives. Literature on synchronization for cooperative networks is very sparse. Recent publication [97] considered frequency offset estimation and correction for AF and DF cooperative networks, and [98] proposed timing resynchronization algorithms for AF cooperative networks. However, both paper considered single antenna equipped relays in flat fading channels, and many open questions are still unanswered, e.g. the impact of synchronization error in frequency-selective channels. Thus, time synchronization problem should be investigated and special attention should be given to signaling schemes which are robust against synchronization errors.

6.2.4 Cooperative Communications for Cognitive Radio

Beamforming for cognitive radio has attracted considerable attention recently, cf. e.g. [99, 100] and references therein. The combination of cooperative communications with cognitive radio would allow for relaying retransmissions to occur in temporarily idle licensed frequency bands, hence considerably reducing the inherent overhead per channel use. This novel approach entails several interesting design challenges such as (a) methods for relays to detect the presence of interfering signals from incumbent systems, (b) transmit adaptation techniques for relays, and (c) time synchronization for each node. The results from this thesis on cooperative communications could be extended to cooperative communications for cognitive radio.

Bibliography

- [1] S. Boyd and L. Vandenberghe. *Convex Optimization*. Cambridge University Press, 2004.
- [2] J. Choi and R. Heath. Interpolation Based Transmit Beamforming for MIMO–OFDM with Limited Feedback. *IEEE Trans. Signal Processing*, 53:4125–4135, November 2005.
- [3] T. Pande, D. Love, and J. Krogmeier. Reduced Feedback MIMO–OFDM Precoding and Antenna Selection. *IEEE Trans. Signal Processing*, 55:2284–2293, May 2007.
- [4] D. Love. Tables of Complex Grassmannian Packings. [Online]. Available: <http://www.ece.purdue.edu/djlove/grass.html>.
- [5] J.G. Proakis. *Digital Communications*. McGraw–Hill, New York, forth edition, 2000.
- [6] J. Winters. On the Capacity of Radio Communication Systems with Diversity in a Rayleigh Fading Environment. *IEEE J. Select. Areas Commun.*, 5(5):871–878, June 1987.
- [7] G. J. Foschini and M. J. Gans. On limits of Wireless Communications in a Fading Environment When Using Multiple Antennas. *Wireless Personal Communications*, 6:311–335, 1998.
- [8] I. E. Telatar. Capacity of Multi–Antenna Gaussian Channels. *Technical Report (BL0112170-950615-07TM)*, AT & T Bell Laboratories, 1995.
- [9] S.M. Alamouti. A Simple Transmit Diversity Technique for Wireless Communications . *IEEE J. Select. Areas Commun.*, 16(8):1451–1458, October 1998.
- [10] V. Tarokh, H. Jafarkhani, and A.R. Calderbank. Space–Time Block Codes from Orthogonal Designs. *IEEE Trans. Inform. Theory*, 45(5):1456–1467, July 1999.
- [11] V. Tarokh, H. Jafarkhani, and A.R. Calderbank. Space–Time Codes for High Data Rate Wireless Communication: Performance Criterion and Code Construction. *IEEE Trans. Inform. Theory*, 44(2):744–765, March 1998.
- [12] G.J. Foschini, G.D. Golden, R.A. Valenzuela, and P.W. Wolniansky. Simplified Processing for High Spectral Efficiency Wireless Communication Employing Multi–Element Arrays. *IEEE J. Select. Areas Commun.*, 17(11):1841–1852, November 1999.

- [13] G.J. Foschini. Layered Space–Time Architecture for Wireless Communication in a Fading Environment When Using Multi–Element Antennas. *Bell Labs Tech. J.*, pages 41–59, 1996.
- [14] P. Dighe, R. Mallik, and S. Jamuar. Analysis of Transmit–Receive Diversity in Rayleigh Fading. *IEEE Trans. Commun.*, 51:694–703, April 2003.
- [15] K. Mukkavilli, A. Sabharwal, E. Erkip, and B. Aazhang. Beamforming with Finite Rate Feedback in Multiple Antenna Systems. *IEEE Trans. Inform. Theory*, 49:2562–2579, October 2003.
- [16] D. Love, R. Heath, and T. Strohmer. Grassmannian Beamforming for Multiple–Input Multiple–Output Wireless Systems. *IEEE Trans. Inform. Theory*, 49:2735–2747, October 2003.
- [17] P. Xia and G. Giannakis. Design and Analysis of Transmit–Beamforming based on Limited–Rate Feedback. In *Proceedings of IEEE Veh. Techn. Conf. (VTC)*, September 2004.
- [18] J. Roh and B. Rao. Transmit Beamforming in Multiple Antenna Systems with Finite Rate Feedback: A VQ-based Approach. *IEEE Trans. Inform. Theory*, 52:1101–1112, March 2006.
- [19] J. Zheng, E. Duni, and B. Rao. Analysis of Multiple-Antenna Systems With Finite–Rate Feedback Using High–Resolution Quantization Theory. *IEEE Trans. Signal Processing*, 55:1461–1476, April 2007.
- [20] H. Bölcskei. MIMO–OFDM Wireless Systems: Basics, Perspectives, and Challenges. *IEEE Wireless Commun.*, 13:31–37, August 2006.
- [21] Wireless LAN Medium Access Control(MAC) and Physical Layer (PHY) Specifications. *IEEE Std 802.11p-2010*, 2010.
- [22] Air Interface for Fixed and Mobile Broadband Wireless Access Systems, Amendment 1: Physical and Medium Access Control Layer for Combined Fixed and Mobile Operation in Licensed Bands. *IEEE Std 802.16e-2005*, 2005.
- [23] 3GPP LTE Specifications. [Online] <http://www.3gpp.org/ftp/Specs/html-info/36-series.htm>.
- [24] D. Palomar, J. Cioffi, and M. Lagunas. Joint Tx–Rx Beamforming Design for Multicarrier MIMO Channels: A Unified Framework for Convex Optimization. *IEEE Trans. Signal Processing*, 51:2381–2401, September 2003.
- [25] E. Akay, E. Sengul, and E. Ayanoglu. Bit Interleaved Coded Multiple Beamforming. *IEEE Trans. Commun.*, 55:1802–1811, September 2007.

- [26] S. Zhou, B. Li, and P. Willett. Recursive and Trellis-Based Feedback Reduction for MIMO-OFDM with Rate-Limited Feedback. *IEEE Trans. Wireless Commun.*, 5:3400–3405, December 2006.
- [27] T. Pande, D. Love, and J. Krogmeier. A Weighted Least Squares Approach to Precoding With Pilots for MIMO-OFDM. *IEEE Trans. Signal Processing*, 54:4067–4073, October 2006.
- [28] M. Gastpar and M. Vetterli. On the Capacity of Wireless Networks: the Relay Case. In *Proceedings of INFOCOM*, volume 3, pages 1577–1586, 2002.
- [29] J.N. Laneman and G.W. Wornell. Distributed Space-Time Block Coded Protocols for Exploiting Cooperative Diversity in Wireless Networks. *IEEE Trans. Inform. Theory*, 49:2415–2425, October 2003.
- [30] R.U. Nabar, H. Bölcskei, and F.W. Kneubühler. Fading Relay Channels: Performance Limits and Space-Time Signal Design. *IEEE J. Select. Areas Commun.*, SAC-22:1099–1109, August 2004.
- [31] J. Laneman, D. Tse, and G. Wornell. Cooperative Diversity in Wireless Networks: Efficient Protocols and Outage Behavior. *IEEE Trans. Inform. Theory*, 50:3062–3080, December 2004.
- [32] B. Wang, J. Zhang, and A. Host-Madsen. On the Capacity of MIMO Relay Channels. *IEEE Trans. Inform. Theory*, 51(1):29–43, January 2005.
- [33] T. Kang and V. Rodoplu. Algorithms for the MIMO Single Relay Channel. *IEEE Trans. Wireless Commun.*, 6(5):1596–1600, May 2007.
- [34] X. Tang and Y. Hua. Optimal Design of Non-Regenerative MIMO Wireless Relays. *IEEE Trans. Wireless Commun.*, 6(4):1398–1407, April 2007.
- [35] P. Larsson. Large-Scale Cooperative Relaying Network with Optimal Combining Under Aggregate Relay Power Constraint. December 2003.
- [36] Y. Zhao, R. Adve, and T. J. Lim. Beamforming with Limited Feedback in Amplify-and-Forward Cooperative Networks. *IEEE Trans. Wireless Commun.*, 7(12):5145–5149, December 2008.
- [37] B. Khoshnevis, W. Yu, and R. Adve. Grassmannian Beamforming for MIMO Amplify-and-Forward Relaying. *IEEE J. Select. Areas Commun.*, 26(8):1397–1407, October 2008.
- [38] Y. Fan and J. Thompson. MIMO Configurations for Relay Channels: Theory and Practice. *IEEE Trans. Wireless Commun.*, 6(5):1774–1786, 2007.

- [39] Y. Jing and H. Jafarkhani. Network Beamforming Using Relays With Perfect Channel Information. *IEEE Trans. Inform. Theory*, 55(6):2499–2517, June 2009.
- [40] M. Abdallah and H. Papadopoulos. Beamforming Algorithms for Information Relaying in Wireless Sensor Networks. *IEEE Trans. Signal Processing*, 56:4772–4784, October 2008.
- [41] G. Zheng, K.-K. Wong, A. Paulraj, and B. Ottersten. Robust Collaborative–Relay Beamforming. *IEEE Trans. Signal Processing*, 57:3130–3143, August 2009.
- [42] G. Zheng, K.-K. Wong, A. Paulraj, and B. Ottersten. Collaborative–Relay Beamforming with Perfect CSI: Optimum and Distributed Implementation. *IEEE Signal Processing Letters*, 16:257–260, April 2009.
- [43] D. Costa and S. Aissa. Cooperative Dual–Hop Relaying Systems with Beamforming over Nakagami-m Fading Channels. *IEEE Trans. Wireless Commun.*, 8:3950–3954, August 2009.
- [44] R. Louie, Y. Li, H. Suraweera, and B. Vucetic. Performance Analysis of Beamforming in Two Hop Amplify and Forward Relay Networks with Antenna Correlation. *IEEE Trans. Wireless Commun.*, 8:3132–3141, June 2009.
- [45] I. Hammerstrom and A. Wittneben. Power Allocation Schemes for Amplify–and–Forward MIMO–OFDM Relay Links. *IEEE Trans. Wireless Commun.*, 6(8):2798–2802, August 2007.
- [46] O. Munoz-Medina, J. Vidal, and A. Agustin. Linear Transceiver Design in Nonregenerative Relays With Channel State Information. *IEEE Trans. Signal Processing*, 55(6):2593–2604, June 2007.
- [47] T. Ng and W. Yu. Joint Optimization of Relay Strategies and Resource Allocations in Cooperative Cellular Networks. *IEEE J. Select. Areas Commun.*, 25(2):328–339, February 2007.
- [48] Y. Ma, N. Yi, and R. Tafazolli. Bit and Power Loading for OFDM–Based Three–Node Relaying Communications. *IEEE Trans. Signal Processing*, 56(7):3236–3247, July 2008.
- [49] Y. Liang and R. Schober. Cooperative Amplify–and–Forward Beamforming for OFDM Systems with Multiple Relays. In *Proceedings of the IEEE International Conference on Communications*, June 2009.
- [50] H. Chen, A. Gershman, and S. Shahbazpanahi. Filter–And–Forward Distributed Beamforming in Relay Networks with Frequency Selective Fading. *IEEE Trans. Signal Processing*, 58:1251–1262, March 2010.

- [51] IEEE Standard for Local and metropolitan area networks Part 16: Air Interface for Broadband Wireless Access Systems Amendment 1: Multiple Relay Specification. *IEEE Std 802.16j-2009 (Amendment to IEEE Std 802.16-2009)*, 12 2009.
- [52] 3GPP Technical Report 36.806, Evolved Universal Terrestrial Radio Access (E-UTRA); Relay architectures for E-UTRA (LTE-Advanced). *www.3gpp.org*, 2011.
- [53] Y. Wu, P. A. Chou, and S. Y. Kung. Information Exchange in Wireless Networks with Network Coding and Physical-Layer Broadcast. March 2005.
- [54] P. Larsson, N. Johansson, and K. E. Sunell. Coded Bi-Directional Relaying. In *Proceedings of IEEE Veh. Techn. Conf. (VTC)*, May 2006.
- [55] R. Vaze and R. Heath. Capacity Scaling for MIMO Two-Way Relaying. In *Proceedings of IEEE International Symposium on Information Theory*, pages 1451–1455, June 2007.
- [56] J. K. Sang, N. Devroye, P. Mitran, and V. Tarokh. Comparison of Bi-Directional Relaying Protocols. In *Proceedings of IEEE Sarnoff Symposium*, April 2008.
- [57] R. Zhang, C. C. Chai, and Y. C. Liang. Joint Beamforming and Power Control for Multiantenna Relay Broadcast Channel With QoS Constraints. *IEEE Trans. Signal Processing*, 57:726–737, February 2009.
- [58] V. Havary-Nassab, S. Shahbazpanahi, and A. Grami. Optimal Distributed Beamforming for Two-Way Relay Networks. *IEEE Trans. Signal Processing*, 58(3):1238–1250, March 2010.
- [59] C. Yuen, W. Chin, Y. Guan, W. Chen, and T. Tee. Bi-Directional Multi-Antenna Relay Communications with Wireless Network Coding. In *Proceedings of IEEE Veh. Techn. Conf. (VTC)*, pages 1385–1388, May 2008.
- [60] T. Cui and J. Kliewer. Memoryless Relay Strategies for Two-Way Relay Channels: Performance Analysis and Optimization. In *Proceedings of IEEE International Communications Conference*, pages 1139–1143, May 2008.
- [61] A. Likas, N. Vlassis, and J. Verbeek. The Global K-means Clustering Algorithm. *Pattern Recognition*, 36:451–561, 2003.
- [62] Y. Liang, R. Schober, and W. Gerstacker. Transmit Beamforming for Frequency-Selective Channels with Decision-Feedback Equalization. *IEEE Trans. Wireless Commun.*, 6:4401–4411, December 2007.
- [63] S. Li, D. Huang, K. Letaief, and Z. Zhou. Multi-Stage Beamforming for Coded OFDM with Multiple Transmit and Multiple Receive Antennas. *IEEE Trans. Wireless Commun.*, 6(3):959–969, March 2007.

- [64] A. Dammann and S. Kaiser. Standard Conformable Antenna Diversity Techniques for OFDM Systems and Its Application to the DVB-T System. In *Proceedings of the IEEE Global Telecommun. Conf.*, December 2001.
- [65] G. Bauch and J. Malik. Cyclic Delay Diversity with Bit-Interleaved Coded Modulation in Orthogonal Frequency Division Multiple Access. *IEEE Trans. Wireless Commun.*, 5:2092–2100, August 2006.
- [66] D. Tse and P. Viswanath. *Fundamentals of Wireless Communication*. Cambridge University Press, 2005.
- [67] R. Cameron. Minimizing the Product of Two Raleigh Quotients. *Linear and Multilinear Algebra*, 13:177–178, 1983.
- [68] R. Martin, K. Vanbleu, M. Ding, G. Ysebaert, M. Milosevic, B. Evans, M. Moonen, and R. Johnson. Unification and Evaluation of Equalization Structures and Design Algorithms for Discrete Multitone Modulation Systems. *IEEE Trans. Signal Processing*, 53:3880–3894, October 2005.
- [69] J. Nocedal and S. J. Wright. *Numerical Optimization*. Springer, 2006.
- [70] A. Goldsmith. *Wireless Communications*. Cambridge University Press, 2005.
- [71] N. Sidiropoulos, T. Davidson, and Z. Luo. Transmit Beamforming for Physical-Layer Multicasting. *IEEE Trans. Signal Processing*, 54:2239–2251, June 2006.
- [72] V. Erceg et al. *IEEE 802.11-0/940r4, TGn Indoor MIMO WLAN Channel Models*, May 2004.
- [73] Z. Yi and I.-M. Kim. Joint Optimization of Relay-Precoders and Decoders with Partial Channel Side Information in Cooperative Networks. *IEEE J. Select. Areas Commun.*, 25:447–458, February 2007.
- [74] A. Talebi and W. Krzymien. Multiple-Antenna Multiple-Relay Cooperative Communication System with Beamforming. *IEEE Veh. Techn. Conf. (VTC)*, May 2008.
- [75] D. Henrion and J. B. Lasserre. GloptiPoly: Global Optimization over Polynomials with Matlab and SeDuMi. *ACM Trans. Math. Soft*, 29:165–194, 2002.
- [76] S. Prajna, A. Papachristodoulou, and P. A. Parrilo. SOSTOOLS: Sum of Squares Optimization Toolbox for Matlab. *available from <http://www.cds.caltech.edu/sostools>*, 2002–04.
- [77] T. Moon and W. Stirling. *Mathematical Methods and Algorithms for Signal Processing*. Prentice Hall, New York, 2000.

- [78] J. Brewer. Kronecker Products and Matrix Calculus in System Theory. *IEEE Tran. on Circuits and Systems*, 25(9):772–781, September 1978.
- [79] D. Bertsekas. *Nonlinear Programming*. Athena Scientific, 2008.
- [80] A. Bletsas, A. Khisti, D. Reed, and A. Lippman. A Simple Cooperative Diversity Method Based on Network Path Selection. *IEEE J. Select. Areas Commun.*, 24:659–672, March 2006.
- [81] H. Mheidat, M. Uysal, and N. Al-Dhahir. Equalization Techniques for Distributed Space–Time Block Codes With Amplify–and–Forward Relaying. *IEEE Trans. Signal Processing*, 55(5):1839–1852, May 2007.
- [82] Y. Liang, A. Ikhlef, W. Gerstacker, and R. Schober. Cooperative Filter–and–Forward Beamforming for Frequency–Selective Channels with Equalization. *IEEE Trans. Wireless Commun.*, 10(1):228–239, January 2011.
- [83] K.E. Baddour and P.J. McLane. Analysis of Optimum Diversity Combining and Decision Feedback Equalization in Dispersive Rayleigh Fading. In *Proceedings of IEEE International Communications Conference*, pages 21–26, June 1999.
- [84] J. Cioffi, G. Dudevoir, M. Eyuboglu, and G. Forney Jr. MMSE Decision–Feedback Equalizers and Coding – Part I: Equalization Results. *IEEE Trans. Commun.*, 43:2582–2594, October 1995.
- [85] T. S. Rappaport. *Wireless communications : principles and practice*. Prentice Hall, New York, 2002.
- [86] H. Chen, A. B. Gershman, and S. Shahbazpanahi. Filter–and–Forward Distributed Beamforming for Two–Way Relay Networks with Frequency Selective Channels. In *Proceedings of the IEEE Global Telecommunications Conference (GLOBECOM)*, December 2010.
- [87] M. Schubert and H. Boche. Solution of the Multiuser Downlink Beamforming Problem with Individual SINR Constraints. *IEEE Trans. Veh. Technol.*, 53(1):18–28, January 2004.
- [88] Z. Q. Luo and W. Yu. An Introduction to Convex Optimization for Communications and Signal Processing. *IEEE J. Select. Areas Commun.*, 24(8):1426–1438, August 2006.
- [89] D. P. Palomar, M. A. Lagunas, and J. M. Cioffi. Optimum Linear Joint Transmit–Receive Processing for MIMO Channels with QoS Constraints. *IEEE Trans. Signal Processing*, 52(5):1179–1197, May 2004.

- [90] M.V. Clark, L.J. Greenstein, W.K. Kennedy, and M. Shafi. Optimum Linear Diversity Receivers for Mobile Communications. *IEEE Trans. Veh. Technol.*, 43:47–56, February 1994.
- [91] S. Haykin. Cognitive Radio: Brain-Empowered Wireless Communications. *IEEE J. Select. Areas Commun.*, 23(2):201–220, February 2005.
- [92] Y. Liang, A. Ikhlef, W. Gerstacker, and R. Schober. Two-Way Filter-and-Forward Beamforming with Multiple Multi-Antenna Relays for Frequency-Selective Channels. In preparation for the *IEEE Trans. Veh. Technol.*
- [93] K. K. Wong, R. D. Murch, and K. B. Letaief. Performance Enhancement of Multiuser MIMO Wireless Communication Systems. *IEEE Trans. Commun.*, 50(12):1960–1970, December 2002.
- [94] T. C. Ng and W. Yu. Joint Optimization of Relay Strategies and Resource Allocations in Cooperative Cellular Networks. *IEEE J. Select. Areas Commun.*, 25(2):328–339, February 2007.
- [95] S. J. Kim, X. Wang, and M. Madhian. Optimal Resource Allocation in Multi-Hop OFDMA Wireless Networks with Cooperative Relay. *IEEE Trans. Wireless Commun.*, 7(5):1833–1838, May 2008.
- [96] T. Tang, C. Chae, R. Heath, and S. Cho. On Achievable Sum Rates of A Multiuser MIMO Relay Channel. In *Proceedings of IEEE International Symposium on Information Theory*, pages 1026–1030, July 2006.
- [97] H. Mehrpouyan and S. D. Blostein. Bounds and Algorithms for Multiple Frequency Offset Estimation in Cooperative Networks. *IEEE Trans. Wireless Commun.*, 10(4):1300–1311, April 2011.
- [98] X. Li, C. Xing, Y. Wu, and S.C. Chan. Timing Estimation and Resynchronization for Amplify-and-Forward Communication Systems. *IEEE Trans. Signal Processing*, 58(4):2218–2229, April 2010.
- [99] L. Zhang, Y. C. Liang, Y. Xin, R. Zhang, and H. V. Poor. On Gaussian MIMO BC-MAC Duality with Multiple Transmit Covariance Constraints. In *Proceedings of the IEEE International Symposium on Information Theory*, pages 2502–2506, June 2009.
- [100] G. Zheng, K. K. Wong, and B. Ottersten. Robust Cognitive Beamforming With Bounded Channel Uncertainties. *IEEE Trans. Signal Processing*, 57(12):4871–4881, December 2009.